Topics in Current Chemistry

Fortschritte der
chemischen Forschung

61

Physical and Chemical Applications of

Dyestuffs

F. P. Schäfer
Organic Dyes in Laser Technology

H. Gerischer · F. Willig
Reaction of Excited Dye Molecules
at Electrodes

H. Meier
Semiconductor Properties of Dyes

H. Jahnke · M. Schönborn
G. Zimmermann
Organic Dyestuffs as Catalysts
for Fuel Cells

Volume 17: W. DEMTRÖDER
Laser Spectroscopy
2nd., enlarged edition. 16 figures. 3 tables.
III, 106 pages. 1973. Cloth DM 36,–; US $14.80
ISBN 3-540-06334-X

Contents: Spectroscopy with Lasers: Introduction.
Characteristic Features of Lasers as Spectroscopic Light
Sources. Spectroscopic Applications of Lasers. High-
Resolution Spectroscopy Based on Saturation Effects.
Spectroscopy of Laser Media. Conclusion. Zusammen-
fassung. (418 references).

Volume 21: L. EBERSON and H. SCHÄFER
Organic Electrochemistry
10 figures. IV, 182 pages. 1971. DM 68,–; US $27.90
ISBN 3-540-05463-4

Contents: Classification of Electro-Organic Reactions.
Electrolytic Reactions and Their Use in Organic
Synthesis. Methods for the Study of Electro-Organic
Reactions. Experimental Factors.Experimental Procedures.
General Mechanistic Considerations. Conversions of a
Functional Group into another Functional Group.
Electrochemical Substitution. Electrochemical Addition.
Electrochemical Coupling. Electrochemical Cleavage.
Electron Transfer. Indirect Electrochemical Process.
Electropolymerization. Organometallics.

Volume 34: A.J. FRY and G. DRYHURST
Organic Electrochemistry
20 figures. III, 85 pages. 1972. DM 38,–; US $15.60
ISBN 3-540-06074-X

Contents: Stereochemistry of Electrochemical Reductions.
Electrochemical Oxidation of Biologically-Important
Purines at the Pyrolytic Graphite Electrode. Relationship
to the Biological Oxidation of Purines.

Volume 37: K.L. KOMPA
Chemical Lasers
31 figures. III, 92 pages. 1973. DM 44,–; US $18.10
ISBN 3-540-06099-5

Contents: Population Inversion and Molecular Amplifica-
tion. Energy-partitioning in Elementary Chemical
Reactions: Vibrational Relaxation. Requirements for
Laser Oscillation. Design Parameters of Pulsed Chemical
Lasers. Specific Chemical Laser Systems. Future Chemical
Lasers. Present Perspectives of High-Power Chemical
Lasers. Kinetic Information through Chemical Laser
Studies.

Prices are subject to change without notice.

Volume 1: J. TSUJI

Organic Synthesis by Means of Transition Metal Complexes

A Systematic Approach. IX, 199 pages. 1975
Cloth DM 68,–; US $27.90   ISBN 3-540-07227-6

This book is the first in a new series, REACTIVITY AND STRUCTURE: CONCEPTS IN ORGANIC CHEMISTRY, designed to treat topical themes in organic chemistry in a critical manner. A high standard is assured by the composition of the editorial board, which consists of scientists of international repute. This volume deals with the currently fashionable theme of complexes of transition-metal compounds. Not only are these intermediates becoming increasingly important in the synthesis of substances of scientific appeal, but they have already acquired great significance in large-scale chemical manufacturing. The new potentialities for synthesis are discussed with examples.. The 618 references bear witness to the author's extensive coverage of the literature. This book is intended to stimulate organic chemists to undertake further research and to make coordination chemists aware of the unforeseen development of this research field.

Volume 2: K. FUKUI

Theory of Orientation and Stereoselection

72 figures. 2 tables. VII, 134 pages. 1975
Cloth DM 44,–; US $18.10   ISBN 3-540-07426-0

The' electronic theory' has long been insufficient to interpret various modern organic chemical facts, in particular those of reactivity. The time has come for a book which shows clearly what is within, and what is beyond, the reach of quantum-chemical methods. Graduate students and young researchers in chemistry, both theoretical and experimental, will find this book an invaluable aid in helping them to become accustomed to the quantum-chemical way of thinking. Theory produces new experimental ideas, and, conversely, a host of experimental data opens new theoretical fields. A book such as the present one will constantly maintain its value, although the quantum-chemical approach to the theory of reactivity is, of course, still in the developmental stage.

Prices are subject to change without notice

Physical and
Chemical Applications of

Dyestuffs

This series presents critical reviews of the present position and future trends in modern chemical research. It is addressed to all research and industrial chemists who wish to keep abreast of advances in their subject.

As a rule, contributions are specially commissioned. The editors and publishers will, however, always be pleased to receive suggestions and supplementary information. Papers are accepted for "Topics in Current Chemistry" in either German or English.

Contents

Organic Dyes in Laser Technology

Prof. Dr. Fritz Peter Schäfer

Max-Planck-Institut für Biophysikalische Chemie, Abt. Laserphysik, D-3400 Göttingen, Postfach 968

Contents

Introduction

In the years since 1964, when the first passive Q-switching with organic dyes was accomplished, the use of organic dyes in laser technology has become increasingly important. Some of the most important developments in the laser field would not have been possible without organic dyes, and one can foresee even further possibilities for the use of dyes in laser technology which could be realized in the near future.

There are several reasons for the usefulness of organic dyes in the laser field. A physical reason can be seen in the very large cross-sections of dyes for the interaction with light, not only for a few lines but for broad bands in the visible part of the electromagnetic spectrum, including some extensions to the near ultraviolet and infrared. As a chemical reason one can give the almost infinite variety of dyes (with the resultingly large variation of their properties) which can be synthesized using the methods of organic chemistry. Finally, one should not forget to mention the inexpensiveness of organic dyes, an obvious advantage in many applications.

This short review will discuss all of the different applications of organic dyes in the laser field which have been reported up to the present, emphasizing a unified treatment of basic principles and leaving a discussion of the details to special reviews and monographs of the different applications. Within the limited space available it is not possible to give a complete list of references. Therefore, only a selection of the most important literature references will be presented here to enable the interested reader to acquire the complete literature of this field from the secondary references cited in these papers. Two review papers on organic dyes in laser technology appeared in 1970 [1,2].

Applications making use of the nonlinear absorption of dyes are passive Q-switching in solid-state lasers, pulse shaping, pulse intensity measurements of high-power ultrashort pulses, optical isolation between amplifier stages of high power solid-state lasers, and pulse width measurements of ultrashort pulses by the two-photon-fluorescence (TPF) method.

Dye lasers are presently the most important application of organic dyes in laser technology, making use of the fluorescence of dyes.

Finally, the nonlinear polarizability of dyes is used for frequency tripling the output of high-power lasers.

The nonlinear absorption of dyes will be treated first, followed by a description of the various applications making use of this property. Dye lasers will be examined next, but only briefly, since a monograph on dye lasers has recently been published [3]. Finally, frequency tripling in dyes will be considered.

It should be stated here that the term "dye" is used in this context in its broadest meaning, and is meant to include all organic compounds with conjugated double bonds since the mechanism of their interaction with light always involve the excitation or deactivation of π-electrons.

Nonlinear Absorption

A simplified energy level diagram of an organic dye is given in Fig. 1. It shows the singlet levels S_0, S_1, S_2, ... and the triplet levels T_1, T_2, ... with some rovibronic sublevels indicated. The absorption (upward) and emission (downward) arrows are drawn as sharp single lines as are the energy levels. Actually, however, the energy levels are smeared out considerably by solvent-solute interactions, and the huge number of possible transitions between the sublevels of the higher and lower levels form a quasi-continuum with a broad envelope, generally several thousand wavenumbers wide. Only at low temperatures (< 20 K), when the environment of the dye molecules cannot change significantly, is it possible to observe sharp, linelike spectra, when the fluorescence is excited with a laser of small spectral width as has been demonstrated only recently [4]. We will come back to this problem of the superposition of many sharp spectra to form a broad band in the discussion of "spectral hole-burning".

The radiationless transitions are indicated by wavy lines with the corresponding rate constants or lifetimes. The rates of thermalization of a dye molecule after an absorptive or emissive transition, namely k' in the excited singlet state S_1 and k'' in the ground state S_0, are so fast that they have not yet been reliably measured. From indirect evidence they are believed to be $k' \approx k'' \approx 10^{12} - 10^{13}$ sec^{-1}. The rate k_{21} of radiationless internal conversion from S_2 to S_1 has recently been measured for several dyes and was found to be in the range $k_{21} \approx 10^{11} - 10^{12}$ sec^{-1} [5,6]. While k_{TT} has not yet been measured directly, there is no reason to believe that it should be much different from k_{21}, and indirect evidence seems to
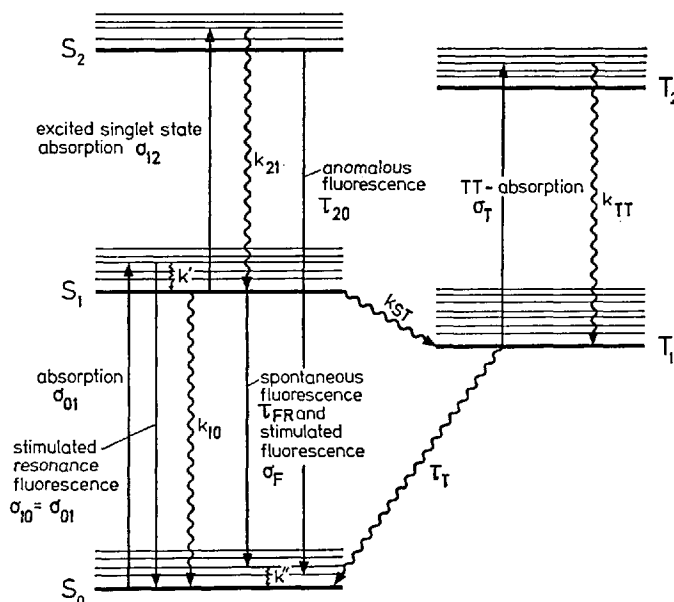

Fig. 1. Generalized energy level scheme of an organic dye molecule. Straight arrows: radiative transitions, wavy arrows: non-radiative transitions. The sigmas, kays, and taus are the corresponding cross-sections, transition rates, and lifetimes, respectively

confirm this assumption. The triplet lifetime τ_T is many orders of magnitude longer than the fluorescent decay time τ_F since the transition $T_1 \to S_0$ is spin-forbidden. The triplet lifetime approaches the radiative lifetime at very low temperatures and is then found to be several seconds for many dyes [7]. At room temperature, in liquid solution, τ_T is markedly reduced by spin-orbit coupling with triplet-quenching agents, such as O_2 or solvents with heavy atoms, and can be less than 100 nsec. The sum of $k_{10} + k_{ST}$ can easily be obtained when the fluorescence decay time τ_F is known by comparing with the radiative lifetime τ_{FR} — obtained from the absorption spectrum with the help of the Strickler-Berg formula [8] — since $1/\tau_F = 1/\tau_{FR} + k_{10} + k_{ST}$. The two rates can also be distinguished if the quantum yield of triplet production η_T is known, for example from flash-photolysis data, since $\eta_T = k_{ST} \cdot \tau_F$. The relative importance of k_{10}, the internal conversion rate, and k_{ST}, the intersystem crossing rate, on the radiationless deactivation of dye molecules differs greatly for different dyes, even within the same class of dyes, when the structure is slightly changed, and it depends very much on the environment.

The spontaneous fluorescent decay time τ_F is connected with the radiative lifetime τ_{FR} and the quantum yield of fluorescence η_F by $\eta_F = \tau_F/\tau_{FR}$. Since the radiative lifetime is of the order of a few nanoseconds in most dyes, the spontaneous fluorescent decay time is about the same for quantum yields of fluorescence near unity (i.e., $k_{10} \approx k_{ST} \approx 0$) and decreases to a few picoseconds for quantum yields of the order of 10^{-3}.

A large amount of information has been accumulated on T–T-absorption spectra [9] although the excited singlet state absorption spectra are much less well known [10].

With the above facts in mind we can now proceed to discuss the characteristics of light absorption in organic dyes at high light intensities.

Let m_0, m_1, m_2, m_{T1}, m_{T2} be the populations of the lowest rovibronic sublevels of S_0, S_1, S_2, T_1, and T_2, respectively, with $m = m_0 + m_1 + m_2 + m_{T1}$ the total dye population [molecules/cm³]. For simplicity the populations of higher rovibronic states are assumed to be negligibly small, which means that k' and k'' are assumed to be much greater than all other rates involved and that the temperature is low enough so that the Boltzmann distribution leaves higher sublevels empty.

Let us first consider the simplest case of a dye which has no excited singlet state absorption in the spectral region of the longest wavelenght absorption band corresponding to the transition $S_0 \to S_1$, and has a time of irradiation that is long compared to τ_F and short compared to $1/k_{ST}$. The latter condition means that we can forget about the triplet state in this simple case. A dye fulfilling these conditions would, for instance, be a xanthene dye with a quantum yield near unity and an irradiation time of around 20 nsec. This could be produced using a giant-pulse laser, such as a frequency-doubled neodymium laser, which would irradiate the dye at a wavelength of 532 nm and which should be absorbed by the particular dye. Now the rate equations for the populations in this simple case are the following:

$$\frac{\partial m_0}{\partial t} = - m_0 \sigma_{01} nc + m_1/\tau_F, \tag{1}$$

$$\frac{\partial m_1}{\partial t} = m_0\, \sigma_{01} nc - m_1/\tau_{\mathrm{F}}\, , \tag{2}$$

$$m_1 + m_0 = m\, . \tag{3}$$

Here n is the photon density [photons/cm^3] and c is the velocity of light in the medium, so that nc is the intensity of the laser light expressed in photons/cm$^2 \cdot$sec.

For an optically thin sample we can neglect the variation of nc over the distance x traveled by the light in the dye solution. Then, combining (1), (2), and (3) results in

$$T_{\mathrm{N}} = 1 - \frac{A}{A_0} = 1 - \frac{m_0}{m} = \frac{nc\sigma_{01}\tau_{\mathrm{F}}}{1 + nc\sigma_{01}\tau_{\mathrm{F}}}\, , \tag{4}$$

where T_{N} is the normalized transmission, A the absorption of the sample at a laser intensity nc, and A_0 the transmission of the sample at low light levels, since the absorption of the sample is proportional to the population density m_0 of the ground state S_0. If we call the laser intensity at which the normalized transmission equals 1/2 the saturation intensity $(nc)_{\mathrm{S}}$, then

$$(nc)_{\mathrm{S}} = 1/(\sigma_{01}\tau_{\mathrm{F}})\, , \tag{5}$$

and (4) becomes

$$T_{\mathrm{N}} = \frac{nc/(nc)_{\mathrm{S}}}{1 + nc/(nc)_{\mathrm{S}}}\, . \tag{6}$$

A plot of the relative transmission T_{N} of the dye sample versus the normalized laser intensity $nc/(nc)_{\mathrm{S}}$, according to (6), is shown in Fig. 2. It is seen that the absorption is completely bleached at very high light levels.
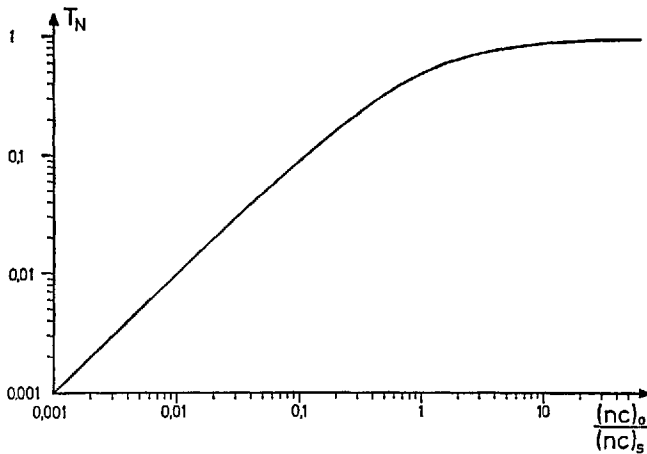
Fig. 2. Normalized transmission T_{N} versus the normalized laser intensity $nc/(nc)_{\mathrm{S}}$, according to Eq. (6)

For optically thick samples, which is the more interesting case applicable to the majority of experiments, Eqs. (1) − (3) have to be combined with the photon-transport equation:

$$\frac{\partial n}{\partial t} + c\frac{\partial n}{\partial x} = -m_0\sigma_{01}nc .$$ (7)

Since τ_F is assumed to be much smaller than the width of the laser pulse we may treat this problem as a stationary one and set all partial time derivatives equal to zero so that one differential equation remains:

$$c\frac{\partial n}{\partial x} = -nc\sigma_{01}m\,\frac{1}{1+nc\sigma_{01}\tau_F} .$$ (8)

Integrating (8) from $x = 0$ to $x = L$, the depth of the sample, we get

$$\ln\frac{(nc)_E}{(nc)_0} + \sigma_{01}\tau_F[(nc)_E - (nc)_0] = -\sigma_{01}mL ,$$ (9)

where $(nc)_0$ is the laser intensity entering the sample and $(nc)_E$ the intensity at the exit. For small light intensities this relation reduces to Beer's law,

$$\ln T_0 = \ln\frac{(nc)_E}{(nc)_0} = -\sigma_{01}mL ,$$ (10)

with T_0 being the low-intensity transmission. Using the intensity dependent transmission $T = (nc)_E/(nc)_0$, (9) can be rewritten as

$$T = T_0\exp\left[\sigma_{01}\tau_F(nc)_0(1-T)\right]$$ (11)

or

$$\frac{\ln T/T_0}{1-T} = \frac{(nc)_0}{(nc)_S} .$$ (12)

This relation [11] gives the sample transmission T as a function of the normalized intensity $(nc)_0/(nc)_S$. Figure 3 shows the saturation characteristics, according to (12), for several values of T_0. These curves approach complete bleaching of the sample at very high light levels, as in Fig. 2., but the point where the absorption of the sample is half of the initial value $A_0 = 1 - T_0$ is not reached at $(nc)_0/(nc)_S = 1$, but rather at higher light levels: the greater is A_0, the higher is the light level at half-absorption.

Unfortunately there are no experimental results which could be compared with these theoretical curves. All experiments reported in the literature are either made with cyanine dyes showing some excited state absorption or with phthalocyanine dyes which have an extremely high intersystem crossing rate so that triplet populations cannot be neglected.
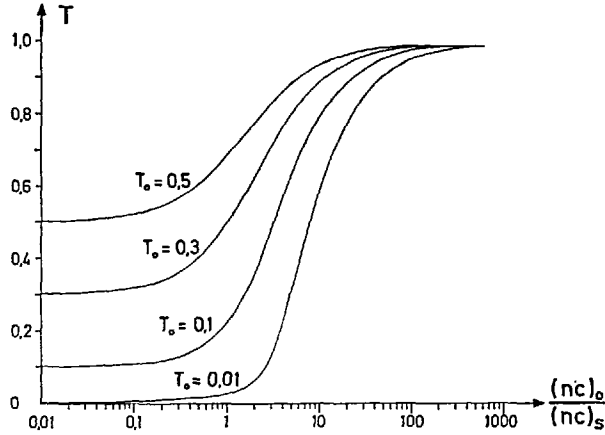
Fig. 3. Transmission T versus normalized laser intensity $nc/(nc)_S$ with low-level transmission T_0 as a parameter

To include excited-state absorption into the above model, Eqs. (1)—(3), and (7) have to be rewritten and another rate equation for the population m_2 of the singlet level S_2 has to be included:

$$\frac{\partial m_0}{\partial t} = -m_0 \sigma_{01} nc + m_1/\tau_F \tag{1a}$$

$$\frac{\partial m_1}{\partial t} = (m_0 \sigma_{01} - m_1 \sigma_{12}) nc + m_2 k_{21} - m_1/\tau_F \tag{2a}$$

$$\frac{\partial m_2}{\partial t} = m_1 \sigma_{12} nc - m_2 k_{21} \tag{13}$$

$$m_0 + m_1 + m_2 = m \tag{3a}$$

$$\frac{\partial n}{\partial t} + c\frac{\partial n}{\partial x} = -(\sigma_{01} m_0 + \sigma_{12} m_2) nc \tag{7a}$$

reducing again to a single differential equation,

$$c\frac{\partial n}{\partial x} = -nc\sigma_{01}m \frac{1 + \sigma_{12}\tau_F nc}{1 + \sigma_{01}\tau_F nc (1 + \sigma_{12}nc/k_{21})}$$

with the solution [12],

$$\ln\left(\frac{T}{T_0}\right) + \sigma_{01}\tau_F (nc)_0 (T-1) + \left(\frac{\sigma_{01}}{\sigma_{12}} - 1 - \frac{\sigma_{01}}{\sigma_{12}\tau_F k_{21}}\right) \ln\left[\frac{1 + \sigma_{12}\tau_F T(nc)_0}{1 + \sigma_{12}\tau_F (nc)_0}\right] = 0 \tag{11a}$$

7

For low intensities $((nc)_0 < (nc)_S)$ this reduces to (11); for high light intensities $((nc)_0 > k_{21}/\sigma_{12})$, however, to

$$T \approx T_0 \left[(\sigma_{12}/\sigma_{01})/(1 + (nc)_0 \cdot \sigma_{12}/k_{21}) \right] , \tag{14}$$

which shows that for very large values of k_{21} there should be a residual absorption at high light intensities:

$$T \approx T_0^{(\sigma_{12}/\sigma_{01})} . \tag{15}$$

This latter result has already been derived by Hercher [11].

To test this model, the nonlinear absorption of cryptocyanine solutions has been investigated by several authors [13-15]. The most conclusive results were obtained by Schüller and Puell [12] who used a ruby laser which, when focussed, produced an intensity of nearly 10^{10} W/cm^2 during a pulse width of 8 nsec. Their results for cryptocyanine dissolved in glycerol or alternatively in methanol are shown in Fig. 4. The solid lines in this figure, drawn through the experimental points, show the best fit to the relation (11a). The fitted parameters for glycerol solutions were σ_{12}, τ_F, and k_{21} which were fitted at the points indicated by arrows and resulted in the following values: $\sigma_{12} = 10^{-16}$ cm^2, $\tau_F = 0{,}83$ nsec, and $k_{21} = 0{,}83 \cdot 10^{12}$ sec^{-1}. The value of $\sigma_{01} = 5 \cdot 10^{-16}$ cm^2 was taken from the recorded absorption spectrum. For methanol it is known that τ_F is much shorter [16], while

Fig. 4. Measured transmission versus incident light intensity for solutions of cryptocyanine in glycerol and methanol at room temperature. Initial dye transmission $T_0 = 1\%$. Theoretical curves (—) according to Eq. (11a) were obtained from matching theory and experiment at points indicated by arrows. (From Ref. [12])

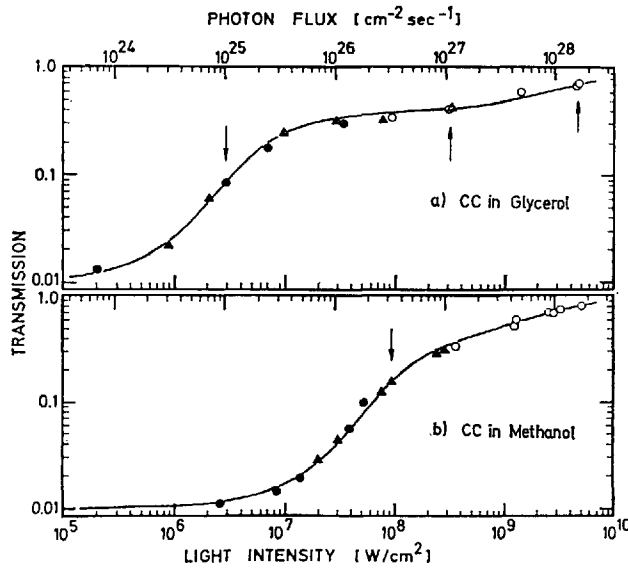one should expect the ratio σ_{12}/σ_{01} and the value of k_{21} should remain unaffected. Hence the only parameter that had to be readjusted was τ_F. This was done at the point indicated by the arrow resulting in $\tau_F = 25$ psec for this solvent. The agreement between the theoretical curve and the experimental data is seen to be excellent. The molecular data obtained by the curve-fitting must be regarded with some reservations, however, because of the neglect of stimulated emission which acts in two ways. First, the stimulated emission at the ruby laser wavelength would become noticeable at the highest pump powers, affecting the value of σ_{12} and/or k_{21}. Second, spontaneous emission is amplified at the wavelength of the peak of the fluorescence spectrum when it passes through the excited parts of the sample, thus effectively shortening the fluorescence decay time τ_F at high intensities. The values of τ_F found in these experiments are already shortened by stimulated emission and can only be considered a lower bound for the true spontaneous fluorescence decay time τ_F as measured at low light levels. The excitation of the second excited singlet state S_2 in these experiments is also substantiated by similar experiments by Müller and Pflüger [17] who found an anomalous blue fluorescence in ruby-laser-excited solutions of cryptocyanine, the kinetics of which also confirmed it as a two-step population of S_2 by the ruby laser excitation.

The situation is quite different with dyes like the phthalocyanines which have very high intersystem crossing rates k_{ST} (e.g. vanadiumphthalocyanine, $k_{ST} > 6 \cdot 10^9$ [14]). In addition, the triplet lifetime τ_T is usually in the microsecond region [7] for air-equilibrated samples and even longer in degassed solutions. This means that a laser pulse of a few nsec duration will increase the transmission of the sample by bringing many molecules into the triplet state T_1 via the excited singlet state S_1. How much the transmission is increased no longer depends on the peak intensity but rather on the energy density of the laser pulse $J = c \int_0^t n(t)\,dt$.

We therefore define an energy transmission [11]

$$T_J = \frac{\text{(transmitted energy density)}}{\text{(incident energy density)}} = \frac{J}{J_0}$$

with J_0 being the energy density of the incident laser pulse. Neglecting excited singlet and/or triplet state absorption, which is justified in the case of the phthalocyanines, and assuming that the internal conversion rate k_{10} can be neglected in comparison with k_{ST}, which means that $\eta_F = \dfrac{1/\tau_{FR}}{1/\tau_{FR} + k_{ST}}$, we obtain the following rate equation for m_0 in an optically thin sample:

$$dm_0/dt = -m_0 \sigma_{01}(1 - \eta_F)nc . \tag{16}$$

For every molecule which absorbs, η_F molecules return directly to the ground state, while $1 - \eta_F$ are transferred into the long-lived triplet state. Integrating (16) gives

$$\frac{m_0(t)}{m_0(t = 0)} = e^{-\sigma_{01}(1-\eta_F)nct} \tag{17}$$

9

or a normalized energy transmission T_{NJ} of

$$T_{NJ} = 1 - e^{-\sigma_0(1-\eta_F)J} . \qquad (18)$$

which becomes with $J_S = 1/[\sigma_0(1 - \eta_F)]$,

$$T_{NJ} = 1 - e^{J/J_S} . \qquad (18a)$$

This result shows that J_S is the energy density that is needed to reduce the sample absorption by a factor of $1/e$. Similarly, for an optically thick sample one finds[14]

$$T_J = (J_S/J_0)\ln[1 + T_0(e^{J_0/J_S} - 1)] . \qquad (19)$$

Plotted curves illustrating this relation, Fig. 5, resemble very much the curves of Fig. 3. Consequently, one cannot infer from a measured intensity or energy saturation curve reliable values of molecular data without additional information, as for instance an independent measurement of k_{ST}. Another possibility is a measurement of the temporal characteristics of the bleaching as demonstrated in an experiment by Hercher et al. [14]. These authors bleached a thoroughly degassed solution of metal-free phthalocyanine in 1-chloronaphthalene by a ruby laser pulse (694.3 nm) of about 59 nsec pulse width. At the same time they measured the absorption at 632.8 nm using a He-Ne-laser, and the result of this measurement is shown in Fig. 6. It clearly demonstrates that the sample was almost completely bleached even before the laser pulse reached its maximum intensity, and that almost all of the molecules were stored in the triplet state because the transmission did not decrease with the fall of the laser intensity for at least 100 nsec. A small residual absorption indicates triplet–triplet absorption.

For the general case, when neither the steady state approximation nor approximations regarding relaxation rates are valid, one has to use computer solutions of a set of rate equations, analogous to those above, including the triplet population.
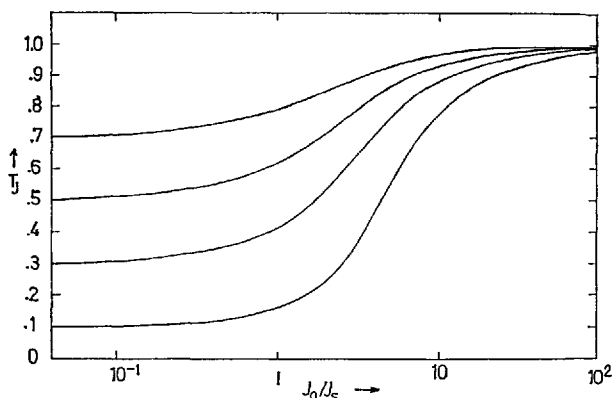
Fig. 5. Energy transmission T_J versus normalized energy density J_0/J_S. (From Ref. [14])
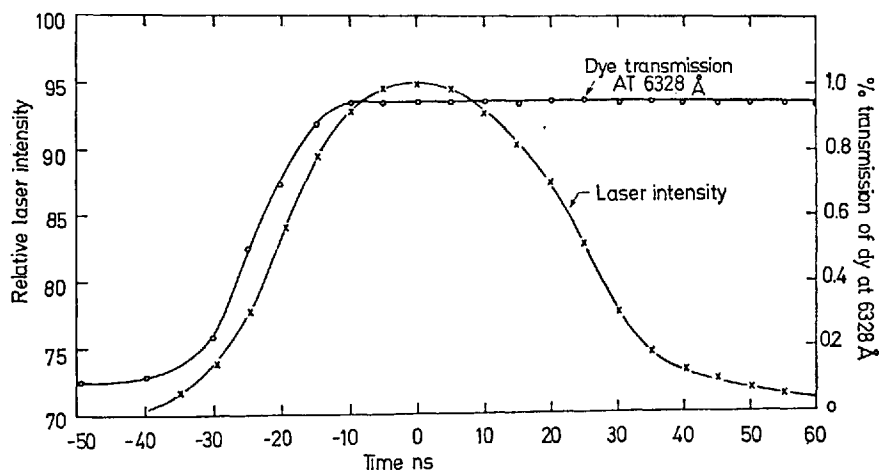
Fig. 6. Relative laser pulse intensity versus time of a ruby giant pulse laser that was used to bleach a solution of metal-free phthalocyanine and transmission of the dye solution at the wavelength of the He—Ne—laser. (From Ref. [14])

Noteworthy is the behaviour of some dyes, for example indanthrone dyes, which become opaque with high-power laser irradiation in contrast to the normal saturation of absorption discussed above [15]. It could be shown that in these cases photochemical processes are operative, creating species which exhibit a higher absorption coefficient at the laser wavelength [18].

Q-Switching of Solid-State Lasers

The most important application of the nonlinear absorption characteristics of dye solutions is the so-called passive Q-switching of solid-state lasers, in particular ruby lasers emitting at 694.3 nm and neodymium lasers emitting at 1.064 μm.

To explain this application, we consider the schematic drawing of a giant pulse laser, shown in Fig. 7. Such a laser consists essentially of (1) a rod of active material AM (for example a ruby or neodymium glass or neodymium-doped rod of yttrium-aluminum garnet) excited by the light pulse from a flashlamp F,
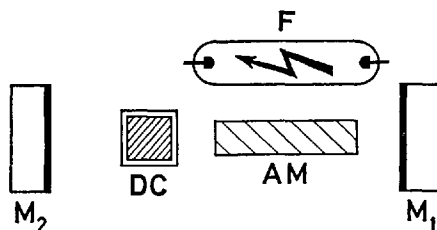
Fig. 7. Experimental arrangement of a giant-pulse laser (Q-switching by dye solution). AM, active material (e.g. ruby crystal rod), F, flashlamp, M_1, M_2, resonator mirrors, DC, dye cell

11

which is generally focussed onto the axis of the rod by an elliptic cylinder (not shown in the drawing) which surrounds both the rod and the flashlamp, each being positioned at one focal line of the elliptic cylinder, (2) two mirrors M_1 and M_2 with reflectivities R_1 and R_2, respectively, which are aligned parallel to each other and normal to the axis of the rod, and (3) a dye cell DC, containing a dye solution of low-level transmission T_0 at the laser wavelength, the faces of the cell often being antireflection coated for smaller reflection losses.

If the flashlamp is fired, the active material is excited and an inversion $i = M_U - M_L$ builds up, M_U and M_L being the population density of the upper and lower laser levels in the active medium. As the inversion increases, the amplification $V(t)$ by stimulated emission in the active medium rises accordingly:

$$V(t) = e^{\sigma F i L} . \tag{20}$$

Laser oscillation will start when $V(t)$ has increased to such a value that the overall amplification in one round trip of a photon through the laser resonator is greater than unity, resulting in the oscillation condition

$$V^2 \cdot T_0^2 \cdot R_1 \cdot R_2 > 1 . \tag{21}$$

As soon as the laser oscillation starts and the laser light level nc increases, the absorption of the dye solution decreases. The decreased attenuation of the laser light in the dye cell is equivalent to an increase in the overall amplification resulting in a much faster rise of the laser intensity. This again will have the effect that the transmission of the dye cell is increased at an even faster rate, and so on, in a fast regenerative process, until the absorption is completely bleached (or at least until only the absorption is left) and a so-called "giant laser pulse" is emitted. The width of such a giant pulse can vary from a few nsec to about 100 nsec, depending mainly on the initial transmission T_0 but also on the inversion and the mirror reflectivities.

A quantitative description of giant pulse generation is again given by a set of rate equations; in the simplest case one for the inversion, another for the population density m_0 of the dye in the ground state S_0 and a third for the laser light intensity nc. If excited state absorption has to be taken into account, additional rate equations would have to be added as described above in the section on nonlinear absorption.

The result of a computer solution of the rate equations is shown in Fig. 8 for a typical example, in this case the cyanine dye 3,3'-diethylthiadicarbocyanine bromide (DTDC) in methanol solution as a Q-switch for a ruby laser, with $T_0 = 0.36$. Peak laser powers of over 500 MW/cm^2 are easily obtained with dye solutions as passive Q-switches.

Until recently a general drawback of this passive Q-switching scheme was the difficulty of obtaining an exact synchronization of the giant pulse with other events in more complex experiments. This difficulty does not exist with active Q-switching in which an electro-optic device, *e.g.* a Kerr-cell or Pockels-cell, is used instead of a dye cell, and one is able to determine exactly the time at which
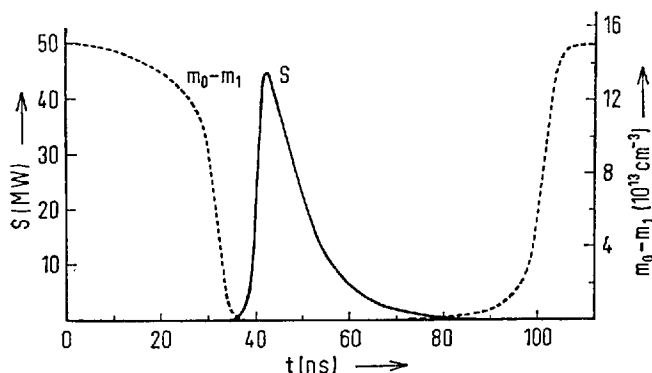
Fig. 8. Laser intensity S and dye population density difference between ground state and excited state, m_0-m_1, versus time for a typical example of a Q-switched ruby laser. (From Ref. [1])

the attenuation is switched off and the laser pulse starts. This can be done at any time during a period of usually 100 μs to several msec during which the inversion in the active material is kept at a sufficiently high level. On the other hand, with passive Q-switching one can never be quite sure at exactly which time the slowly rising inversion will reach the level at which the oscillation condition is fulfilled and the laser pulse is generated because small variations of the flashlamp light intensity from shot to shot give rise to large uncertainties in this respect.

This difficulty has now been resolved [19] in the following way. The inversion in the active material is built up to slightly below threshold level by using a slightly lower than usual voltage of the energy storage capacitor that is discharged through the flashlamp. At the suitable moment a second capacitor, much smaller than the first one and thus being capable of a much faster risetime, is discharged through the flashlamp bringing the inversion above threshold in less than a μsec and resulting in an exact timing of the laser pulse.

If a giant pulse from some other laser is available, part of its intensity can be directed at the dye cell of another giant pulse laser whose inversion is slightly below threshold. The sudden increase of the dye transmission by the absorption of energy from the master laser reduces the threshold of the slave laser, and a second giant pulse is generated [20,14,21]. This method is also important for the understanding of the so-called hole-burning in dyes, which will be discussed below.

Q-Switch Dyes

The above discussion of the Q-switching process immediately gives some requirements for a good Q-switching dye. First, this dye must exhibit a saturable absorption at the laser wavelength. Second, the residual losses by excited state absorption should be as low as possible. Third, the photochemical stability (and, of course, also the chemical stability in the dark) should be as high as possible. Fourth, the

dye should be highly soluble in solvents that are compatible with use inside a high power laser resonator such as water, methanol, ethanol, dimethylsulfoxide, dichloroethane, benzene, and others, that neither exhibit significant absorption at the laser wavelength nor are very susceptible to self-focussing, stimulated Raman- or Brillouin-emission and similar undesirable phenomena. The solvents should also have a low viscosity so that thermal gradients which are either generated accidentally or as a consequence of the laser operation, and which degrade the optical quality of the laser beam, will quickly disappear. If only dyes of a limited photochemical stability are available, one should use a flow cell in the laser resonator and a relatively large reservoir for the dye recirculation system if one wants a long uninterrupted period of laser operation.

There are many dyes which fulfill the above requirements, few of which have been used until now. The first dyes used with a ruby laser were phthalocyanines; the free base as well as chloro-aluminum- and vanadium-phthalocyanine in 1-chloronaphthalene or nitrobenzene [22]. While these dyes show little residual absorption [14] and good photochemical stability, the solubility is relatively low and the solvents are not well suited to operation in a laser resonator.

Other dyes which were used very early are some cyanines, such as crypto-cyanine and DTDC [23,24]. There is one insteresting difference between the latter two dyes. While cryptocyanine has an absorption spectrum with a peak wavelength (in methanol) of 707 nm, which practically coincides with the ruby laser wavelength of 694.3 nm, DTDC has a peak absorption wavelength of 652 nm, and the extinction coefficient is less than the peak value by roughly a factor of 30 at the ruby laser wavelength, which in this case practically coincides with the peak of the fluorescence spectrum. Nevertheless, DTDC is an efficient Q-switching dye, in fact even better than cryptocyanine because of its higher chemical and photochemical stability. This behaviour is explained by the energy level diagram of this dye which is shown together with absorption and fluorescence spectra in Fig. 9. The fact that the ruby laser wavelength lies at the extreme long-wavelength end of the absorption band, far beyond the wavelength of the O-O-transition, implies that at the ruby laser wavelength there can only be transitions from higher rovibronic sublevels of the ground state S_0 to the lowest sublevel of S_1, and that there is the possibility of stimulated emission by ruby laser photons, since these absorptive transitions (indicated by upward arrows) coincides with the peak of the spontaneous fluorescence emission. In this way the bleaching of the dye's absorption is already reached when 50% of the molecules are in S_1 and 50% in S_0, neglecting the intersystem crossing rate which is supposed to be relatively low in this dye since in similar cyanine dyes the radiationless deactivation was found to be mainly through internal conversion from S_1 to S_0 [25]. In addition, almost all of the photons absorbed by the dye at the beginning of the bleaching process are recovered through stimulated emission during the laser pulse resulting in a higher overall efficiency.

An essentially incomplete list of other dyes suitable for operation at the ruby laser wavelength can be found in [1]. Some merocyanine dyes were investigated as Q-switches in [26].

Q-switch dyes for neodymium lasers are not so numerous since there are only relatively few dyes known which exhibit absorption due to an electronic transition
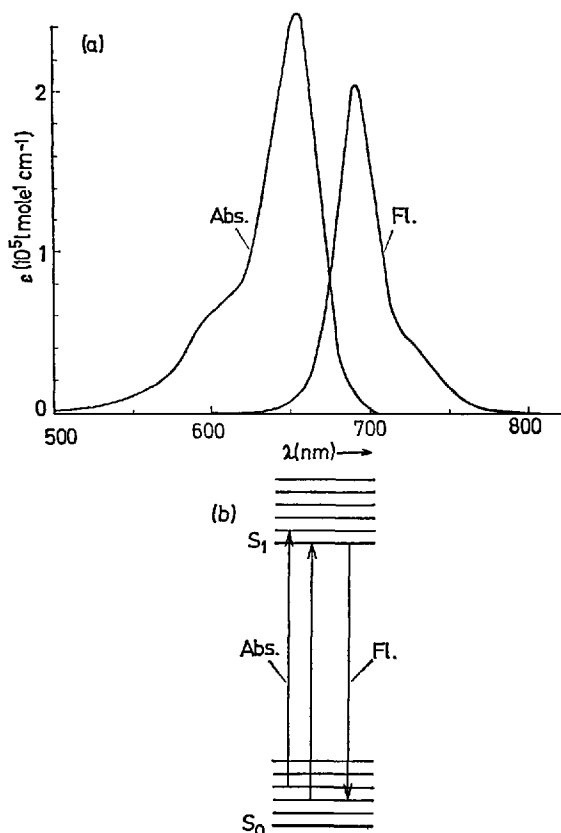
Fig. 9. a) Absorption and fluorescence spectra of 3,3'-diethylthiadicarbocyanine in methanol b) Corresponding energy level diagram. The lengths of the absorption and fluorescence arrows correspond to the energy of a ruby photon. (From Ref. [1])

at 1.064 μm. The first dyes for this applications were long-chain rigidized thia-cyanines [27] and pyrylocyanines [28]. These dyes are all relatively unstable in solutions, when kept in the dark, and rapidly deteriorate in diffuse daylight.

Recently, a new Q-switch for neodymium lasers has become available [29] which is extremely stable and shows energy-dependent Q-switching similar to the phthalocyanines by a rapid intersystem crossing into the triplet state [30]. This "dye" is a nickel-complex, bis-[p-dimethylamino]-dithiobenzylnickel, and has a strong absorption band around 1 μm in several solvents.

Mode-Locking

Another application which is very similar to Q-switching is the mode-locking in solid-state lasers. This application differs from Q-switching in the following experimental details. First, instead of a cell length of 1 cm, which is most often used in giant pulse lasers, only cell lengths of 1 mm or less are applied. Second, the

cell must be placed as near as possible to one of the resonator mirrors, the best position being when the dye solution is in direct contact with the reflective layer of the resonator mirror. Third, the dye's spontaneous fluorescence decay time τ_F should be as short as possible. Fourth, there must not be any reflecting surfaces parallel to each other apart from the resonator mirrors. This last condition is easily fulfilled using either wedged ($\approx 1°-5°$) compoments or Brewster-angle surfaces which give no reflection for the linearly polarized laser light.

If all of these conditions are fulfilled the laser operates in the following way. As the inversion in the active medium slowly increases with increasing excitation, the spontaneous emission increases proportionally, fluctuating statistically. These statistical fluctuations contain frequency components up to the inverse spectral bandwidth, i.e., to at least 10 THz. In due course of time one of these statistical fluctuations will be so high that it brings the laser above threshold for the short duration of its pulse width. Now this short pulse is traveling back and forth between the resonator mirrors, growing as long as there is sufficient inversion in the active medium. Consider, however, what will happen to a somewhat lower statistical fluctuation which happens to occur, say, 100 psec after the first successful spike. If $\tau_F \ll 100$ psec, it will experience a higher attenuation in the dye than the stronger spike since it will not be able to bleach the dye to the same extent because of its smaller energy. Consequently, the smaller spike experiences a smaller amplification in every round trip between the mirrors, and thus the first spike will soon have grown to a far greater intensity than the smaller one. Since this strong spike uses up the stored inversion of the active material as it travels back and forth, the inversion rapidly decreases, and any strong spike which comes long after the first strong spike will not find enough amplification in the active material left over to grow significantly. In this way there usually remains only one strong pulse in the resonator and, since part of it is coupled out every time the pulse is reflected from the partially transmitting resonator mirror, the laser beam consists of a train of short pulses as shown in the oscillogram of Fig. 10.

The build-up of the laser pulse from the statistical fluctuation is beautifully demonstrated in [31], where a short period of statistical fluctuations was registered with a streak camera while they were traveling back and forth in the resonator. A detailed theoretical treatment of this process is given in [32] for the case of solid-state lasers and in [33] for the case of dye lasers in which the saturation of the active medium plays an important rôle. The halfwidth of the pulse which is finally reached in this "mode-locking" process is theoretically determined by the inverse spectral bandwidth of the active medium provided that the dye relaxation time τ_F is sufficiently short.

This effective dye relaxation time τ_F is the spontaneous fluorescence decay time shortened by stimulated emission which is more severe the higher the excitation and therefore the higher the population density m_1. The dependence of fluorescence decay time on excitation intensity was shown in [34,35]. Thus, fluorescence decay times measured with high intensity laser excitation [36][37] are often not the true molecular constants of the spontaneous emission rate which can only be measured under low excitation conditions. At the short time scale of mode-locking the reorientation of the solvent cage after absorption has occurred plays a certain rôle [38] as well as the rotational reorientation of the dye molecules [39,40]
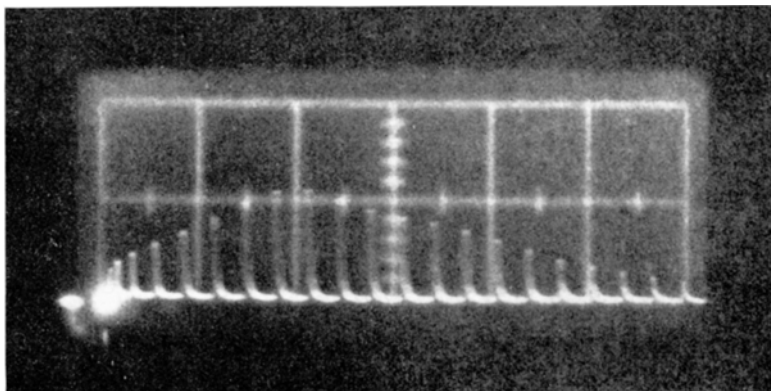
Fig. 10. Oscillogram of a typical mode-locked pulse train. Sweep speed 20 nsec per major division

which brings those ground-state molecules which were not excited by the transmitted pulse, because of an orthogonal orientation between their transition moment and the pulse polarization, into a position allowing excitation by the next pulse. The often-measured recovery times of dyes used for mode-locking [41]–[43], the lowest one of 7 psec, give always a superposition of these effects.

Intensity Measurement of Ultrashort Pulses

As described in the section on nonlinear absorption, the transmission of a pulse which is short compared to the various molecular relaxation times is determined by its energy content. A measurement of the energy transmission ratio will then give the peak intensity of the pulse when its pulse shape is known [44]. In fact, the temporal and spatial pulse shape is of relatively little importance. Fig. 11 gives the energy transmission T_E as a function of the peak intensity I [W/cm^2] for the saturable dye Kodak 9860 with the pulse halfwidth as a parameter. It is seen that this method is useful in the intensity region between 10^8 and 10^{10} MW/cm^2 for pulses with halfwidths greater than 5 to 10 psec. Since one can easily manipulate the cross-section and hence the intensity of a laser beam with a telescope, this method is almost universally applicable.

Pulse Shaping

Since the transmission of a nonlinear absorber is lower in the low-intensity wings of a laser pulse traveling through the absorber than in the peak of the pulse, the pulse shape is generally distorted in such a way that the pulse width is decreased. The front wing of the laser pulse is especially steepened since more energy is used up in the first portion of the pulse to excite dye molecules.

This effect can be used to produce shorter pulses than are obtainable by mode-locking alone. Using five transits through a saturable absorber cell (and 4 ampli-

17
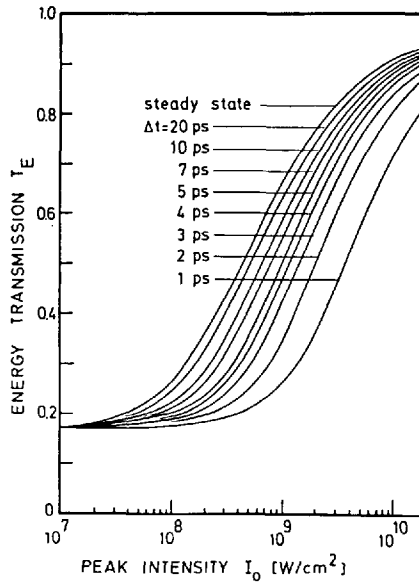
Fig. 11. Calculated energy transmission T_J versus peak laser intensity I_0 for several values of the laser pulse durations Δt, and the dye parameters $T_0 = 0{,}173$, $\sigma = 1{,}84 \cdot 10^{-16} cm^2$, and $\tau_F = 9.1$ psec. (From Ref. [44])

fying stages between them to restore the energy lost to the dye molecules) it was possible to reduce the incident pulse width of 8 psec to a transmitted pulse width of 0.7 psec [45].

Optical Isolators

For the generation of very high peak powers it is necessary to use many amplifier stages in which the pulse from the laser oscillator is amplified to the necessary peak power. The high overall amplification factor of such an amplifier chain could cause it to break into spurious oscillations long before the peak power of the laser pulse from the oscillator stage is reached. This must be prevented by intensity dependent optical isolators between the stages, which transmit high intensities practically unattenuated and reduce the transmitted low intensity light to an insignificant level.

Much simpler than the use of active isolators, such as rotators making use of the Faraday effect, is again a saturable absorber cell which can easily be adjusted in length, dye composition and concentration to give the desired low light level attenuation and high light level transmission [46].

Two-Photon Absorption

Another nonlinear absorption mechanism in dye molecules that becomes important at high light intensities is the "simultaneous" absorption of two photons of energy $E = h\nu$ to reach a stationary energy level, situated at $2E$, in the dye. This effect

is generally termed "two-photon absorption" and should be clearly distinguished from the successive absorption of two photons via an intermediate stationary energy level of the dye molecules, as for instance described in the section on nonlinear absorption to explain excited state absorption. A quantum-mechanical description of two-photon absorption was first given by Goeppert-Mayer many years ago [47]. This theory is difficult to apply for large molecules since it entails a fair knowledge of many excited states of the molecule which are not known in general.

For a numerical calculation of the two-photon absorption one can employ a simple phenomenological theory which describes very well the experimental facts at least in the case of an excitation of the lowest lying excited singlet state S_1 [48].

One starts with the postulate that two photons of wavelength λ_0 striking the molecule simultaneously are absorbed by it, in the same way as one photon of wavelength $\lambda_0/2$. It must be specified what is meant here by "simultaneously". The transit time of the photons (which are regarded as corpuscular) when they travel with the velocity of light c through the π-electron cloud of the molecule with thickness w and maximum cross section σ_{max} is $T = w/c$. If two photons fall within this time interval on the area covered by the π-electron cloud of the molecule, this may be described as simultaneous incidence. If nc photons/cm²sec (wavelength λ_0) fall on a thin layer of dye solution having thickness dl, the steady-state number of molecules m^* through whose π-electron clouds a photon is just passing is given by

$$m^* = (m/3)\, \sigma_{max} ncw/c \tag{22}$$

where the factor 1/3 arises from the averaging of the random orientation of the molecules. As was mentioned earlier, σ_{max} can be found from the absorption spectrum of the dye: $\sigma_{max} = 3\sigma$. According to the postulate mentioned above, the effective cross section σ_1 of any one of these m^* molecules for a second photon of wavelength λ_0 is the same as the effective cross section of the molecule for the absorption of a single photon of wavelength $\lambda_0/2$. The attenuation of the laser light in this layer is therefore

$$-dnc = 2\sigma_1 m^* ncdl \tag{23}$$

The factor of 2 takes into account the fact that two photons disappear in each act of absorption. Integration over the length L of the cell gives the absorption law for the two-quantum absorption:

$$\frac{1}{(nc)_1} - \frac{1}{nc} = \frac{2}{3}\, m\, \frac{w}{c}\, \sigma_{max} \sigma L \tag{24}$$

where nc_1 is the photon flux at the rear and of the cell. Even at very high irradiation intensities, the absorption is so weak that we can write $nc(nc)_1 \approx n^2 c^2$. Introduction of the cross section F of the beam gives, to a good approximation, the number m_{abs} of molecules excited per unit time, and multiplication of m_{abs} by the

fluorescence quantum yield η_F gives the number $(nc)_F$ of fluorescence photons emitted per unit time:

$$(nc)_F = \eta_F m_{abs} = (2/3)\eta_F m \,(w/c)\, \sigma_{max}\, \sigma_1\, FLn^2c^2. \tag{25}$$

As can be seen from Eq. (25), $(nc)_F$ is proportional to the square of the photon flux nc. It should also be proportional to the product of the maximum absorption cross section σ_{max} and the cross section σ_1 at wavelength λ_0. This relation has been checked experimentally in [48]. The relation between the fluorescence output $(nc)_F$ and the excitation power nc for an aqueous solution of rhodamine B resulted in a straight line in a double-logarithmic plot with a slope of 2.05 ± 0.1, thus verifying the square law of two-photon absorption.

A check of the dependence of $(nc)_F$ on $\sigma_{max}\sigma_1$ gave an agreement within an order of magnitude, with a relatively large scatter. Examination of these values suggested that fw/c should be used for the transit time instead of w/c, where f is the oscillator strength of the absorption band in question for one-photon absorption. The oscillator strength is generally a measure of the resonance of the electrons in the field of the stimulating light wave. Improvement of Eq. (25) to Eq. (25a)

$$(nc)_F = (2/3)\,\eta_F m f\,(w/c)\, \sigma_{max}\, \sigma_1\, FL\,(nc)^2 \tag{25a}$$

and comparison of the experimental results with (25a) shows not only the required linear dependence of fluorescence intensity $(nc)_F$ on $f\sigma_{max}\sigma_1$, but also an excellent agreement with the absolute calculated values if the only remaining free parameter w is assumed to have a value of 1.5 Å. This value approximately corresponds to the thickness of the π-electron cloud normal to the plane of the molecule. It is especially noteworthy that this relation not only holds for one particular dye or class of dyes but was found to be valid for dyes from different classes, including aromatic hydrocarbons. A recent critique of this theory [49] remarked that it does not give results in agreement with the experiment in some cases. Upon a closer examination all these cases were of such a nature that the excitation leaves the molecule in the second excited state S_2.

A theoretically well-founded theory of two-photon absorption using the free electron-gas model of dye molecules [50] is to be found in [49].

Pulse width Measurement by Two-Photon Fluorescence

To use the two-photon fluorescence (TPF), *i.e.*, the fluorescence excited by two-photon absorption, for the measurement of the halfwidth of ultrashort pulses from mode-locked lasers, the laser beam containing the train of pulses is split into two beams by a beam splitter B (Fig. 12) which are then redirected by two mirrors M_1 and M_2 so that they are collinear and completely overlap in the dye cell DC which is situated in the center between the two mirrors. In the selection of the dye, it need only be remembered that it should, as far as possible, be free from absorption at the laser wavelength, have a strong absorption band at half the wavelength, and have the highest possible fluorescence quantum yield η. Thus a
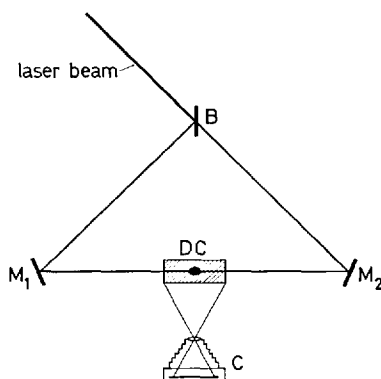
Fig. 12. Experimental arrangement for the measurement of pulse widths of ultrashort pulses by the two-photon fluorescence method. B, beam splitter, M_1, M_2, mirrors, DC, dye cell containing fluorescing dye solution that absorbs at half the laser wavelength, C, camera

solution of rhodamine 6G is generally used for neodymium glass laser pulses and, as an example, 9, 10-diphenylanthracene in benzene or 6-acetylaminopyrene-1, 3, 8-trisulfonic acid in water for ruby lasers. Now the fluorescence excited by each incoming pulse of peak intensity I is proportional to I^2. Let $F_{\rightarrow}$ be the intensity of the fluorescence trace generated by the pulses traveling from left to right and $F_{\leftarrow}$ that created by the pulses traveling in the opposite direction. Then the total fluorescence intensity in the trace recorded by the camera C is

$$F_{\rightarrow} + F_{\leftarrow} = 2 \cdot \text{const. } I^2 , \tag{26}$$

while at the points where the pulses traveling in the opposite directions overlap, the exciting intensity is $2I$ and thus

$$F_{\overset{\rightarrow}{\leftarrow}} = \text{const. } (2I)^2 . \tag{27}$$

This means that the fluorescence intensity at the point is twice as bright as at neighboring points of the trace. The width of this bright area divided by the velocity of light in the dye solution then gives the time halfwidth of the pulses.

This is a simplified description of the measurement principle. For a complete description and for limitations of the method at very high pulse intensities, see [51].

The above-mentioned "hole-burning" in dyes refers to the following effect. A laser beam incident on an absorbing dye solution only excites those molecules which have such a solvent configuration that their sharp absorption lines [4] of less than one wave number width are exactly coincident with the laser frequency. Since only a small fraction of the total number of molecules fulfills this condition, the absorption by these molecules is bleached even at low laser intensities. However, the energy levels of all molecules are constantly perturbed by thermal motion of the solvent molecules and the dye molecules themselves. Thus, the "hole burned" into the absorption spectrum is continuously filled up with molecules which then can absorb and make a transition of the excited state. At room temperature this spectral diffusion process is very fast and the spectral "hole" must be very small except at the highest laser intensities. Nevertheless, this phenomenon must be the cause for the frequency-locking of several giant pulse lasers as discussed above. A more detailed discussion of spectral hole-burning is to be found in [11] and [14].

Dye Lasers

Since a monograph on dye lasers has been published very recently [3], in this section a brief treatment of only the principles of dye laser operation and the main differences between solid-state and dye lasers will be presented. In addition, the latest progress in the field will be reported.

If the fluorescence band of a dye solution is utilized in a dye laser, the allowed transition from the lowest vibronic level of the first excited singlet state to some higher vibronic level of the ground state will give a high amplification factor even at low dye concentrations. The main complication in these systems is the existence of the lower-lying triplet states. The intersystem crossing rate to the lowest triplet state is high enough in most molecules to reduce the quantum yield of fluorescence to values substantially below unity. This has a twofold consequence: Firstly, it reduces the population of the excited singlet state, and hence the amplification factor; and secondly, it enhances the triplet–triplet absorption losses by increasing the population of the lowest triplet state. Assume a light-flux density which slowly rises to a level nc, a total molecular absorbing cross section σ, a quantum yield ϕ_T of triplet formation, a triplet lifetime τ_T, populations of the triplet and ground state of m_T and m_0, respectively, and, neglecting the small population of the excited singlet state, a total concentration of dye molecules of $m = m_0 + m_T$. A steady state is reached when the rate of triplet formation equals the rate of deactivation:

$$nc\sigma m_0 \phi_T = m_T/\tau_T . \tag{28}$$

Thus, the fraction of molecules in the triplet state is given by

$$m_T/m = nc\sigma\phi_T\tau_T/ \left(1 + nc\sigma\phi_T\tau_T\right) . \tag{29}$$

Assuming some typical values for a dye, $\sigma = 10^{-16}$ cm^2, $\phi_T = 0.1$ (corresponding to a 90% quantum yield of fluorescence), and $\tau_T = 10^{-4}$ sec, the power to maintain half of the molecules in the triplet state is $(nc)_{1/2} = 10^{21}$ photons sec^{-1} cm^{-2}, or an irradiation of only 1/2 kW cm^{-2} in the visible part of the spectrum. This is much less than the threshold pump power calculated below. Hence a slowly rising pump light pulse would transfer most of the molecules to the triplet state and deplete the ground state correspondingly. On the other hand, the population of the triplet level can be held arbitrarily small if the exciting light flux density rises fast enough, i.e., if it reaches threshold in a time t_R which is small compared to the reciprocal of the intersystem crossing rate $t_R \ll 1/k_{ST}$. Here t_R is the risetime of the pump light power, during which it rises from zero to the threshold level. For a typical value of $k_{ST} = 10^7$ sec^{-1}, the risetime should be less than 100 nsec. This is easily achieved, for example with a giant pulse laser as pump light source, since giant pulses usually have risetimes of 5—20 nsec. In such laser-pumped dye-laser systems one may neglect all triplet effects in a first approximation.

We thus can restrict our discussion to the singlet states. Molecules that take part in dye-laser operation have to fulfill the following cycle (Fig. 13): Absorption
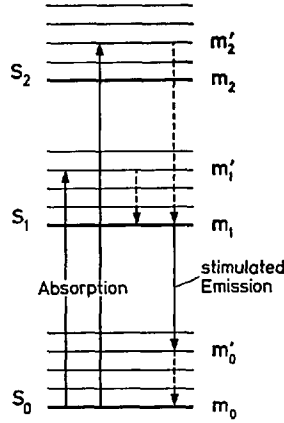
Fig. 13. Pump cycle of dye molecules. (From Ref. [3])

of pump radiation at λ_P, and with cross-section σ_P, lifts the molecule from the ground state with population m_0 into a higher vibronic level of the first (or second) excited singlet state S_1 (or S_2) with a population m_1' (or m_2'). Since the radiationless deactivation to the lowest level of S_1 is so fast, the steady-state population m_1' is negligibly small, provided the temperature is not so high that this vibronic level is already thermally populated by the Boltzmann distribution of the molecules in S_1. At room temperature $kT = 200$ cm^{-1}, so that this is not the case. Stimulated emission then occurs from the lowest vibronic level of S_1 to higher vibronic levels of S_0. Again the population m_0' of this vibronic level is negligible since the molecules quickly relax to the lowest vibronic levels of S_0.

It is easy then to write down the oscillation condition for a dye laser. In its simplest form a dye laser consists of a cuvette of length L [cm], with dye solution of concentration m [cm^{-3}], and of two parallel end windows carrying a reflective layer, each of reflectivity R, which form the laser resonator. With m_1 molecules/cm^3 excited to the first singlet state, the dye laser will start oscillating at a wavelength λ if the overall gain is equal to or greater than one:

$$\exp\left[-\sigma_A(\lambda)m_0L\right]R\exp\left[+\sigma_F(\lambda)m_1L\right] \geqq 1 . \tag{30}$$

Here $\sigma_A(\lambda)$ and $\sigma_F(\lambda)$ are the cross-sections for absorption and stimulated fluorescence at λ, respectively, and m_0 is the population of the ground state. The first exponential term gives the attenuation due to reabsorption of the fluorescence by the long-wavelength tail of the absorption band. The attenuation becomes more important, the greater the overlap between the absorption and fluorescence bands. The cross-section for stimulated fluorescence is related to the Einstein coefficient B by

$$\sigma_F(\lambda) = g(\lambda)Bh/\lambda \int\limits_{\substack{\text{fluorescence}\\\text{band}}} g(\lambda)d\lambda = 1 . \tag{31}$$

23

Substituting the Einstein coefficient A for spontaneous emission according to

$$B = \frac{\lambda^2}{8\pi} A \, \frac{\lambda}{h} \tag{32}$$

and realizing that $g(\lambda) A \cdot \phi_F = Q(\lambda)$, the number of fluorescence quanta per wavelength interval, one obtains

$$\sigma_F(\lambda) \frac{\lambda^2}{8\pi} \cdot \frac{Q(\lambda)}{\phi_F} \, . \tag{33}$$

Since the fluorescence band usually is a mirror image of the absorption band, the maximum values of the cross-sections in absorption and emission are found to be equal:

$$\sigma_{F, \max} = \sigma_{A, \max} \, . \tag{34}$$

Taking the logarithm of (30) and rearranging it leads to a form of the oscillation condition which makes it easier to discuss the influence of the various parameters:

$$\frac{S/m + \sigma_A(\lambda)}{\sigma_F(\lambda)} \frac{}{\sigma_A(\lambda)} \leqq \gamma(\lambda) \, , \tag{35}$$

where $S = (1/L) \ln (1/R)$ and $\gamma(\lambda) = m_1/m$.

The constant S on the left-hand side of (35) contains only parameters of the resonator, *i.e.*, the active length L, and reflectivity R. Other types of losses, like scattering, diffraction, etc., may be accounted for by an effective reflectivity, $R_{\rm eff}$. The value $\gamma(\lambda)$ is the minimum fraction of the molecules that must be raised to the first singlet state to reach the threshold of oscillation. One may then calculate the function $\gamma(\lambda)$ from the absorption and fluorescence spectra for any concentration m of the dye and value S of the cavity. In this way one finds the frequency for the minimum of this function.

Figure 14 represents a plot of the laser wavelength λ (*i.e.*, the wavelength at which the minimum of $\gamma(\lambda)$ occurs) versus the concentration with S a fixed
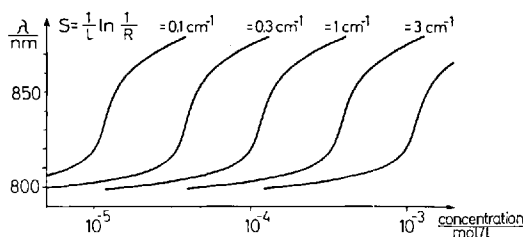

Fig. 14. Calculated laser wavelength versus concentration of the laser dye 3,3'-diethylthiatricarbocyanine bromide, with S as a parameter. (From Ref. [3])
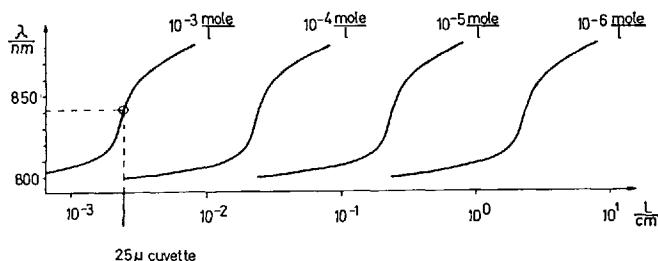
Fig. 15. Calculated laser wavelength versus active length of the laser cuvette, with the concentration of the solution of the dye 3,3'-diethylthiatricarbocyanine bromide as a parameter. From Ref. [3])

parameter. Similarly, Fig. 15 shows the laser wavelength versus the active length L of the cuvette with dye solution, with the concentration of the dye as a parameter. Both figures apply to the dye 3,3'-diethylthiatricarbocyanine (DTTC). These diagrams demonstrate the wide tunability range of dye lasers which can be induced by changing the concentration of the dye solution, or length, or Q of the resonating cavity. They also show the high gain which permits the use of extremely small active lengths.

The wide tunability of the laser emission and the very high gain are the two most prominent features of dye lasers that are not found in other lasers (with the exception, perhaps, of semiconductor lasers which, however, only reach peak powers that are many orders of magnitude lower than those of dye lasers).

The absorbed power density W necessary to maintain a fraction γ of the molecular concentration m in the excited state is

$$W = \gamma m h c / (\tau_F \lambda_P) \tag{36}$$

and the power flux, assuming the incident radiation is completely absorbed in the dye sample,

$$(nc)_P = W/m\sigma = \gamma h c / (\tau_F \sigma_P \lambda_P) \tag{37}$$

where λ_P is the wavelength of the absorbed pump radiation. If the radiation is not completely absorbed, the relation between the incident power W_{in} and the absorbed power is $W = W_{in}[1 - \exp(-\sigma_P m_0 L)]$. Since in most cases $m \approx m_0$, this reduces, for optically thin samples, to $W = W_{in}\sigma_P m L$. The threshold incident power flux, $(nc)_{in}$, then is

$$(nc)_{in} = (\gamma h c)/(\tau_F m \sigma^2 L \lambda_P) . \tag{38}$$

In the above derivation of the oscillation condition and concentration dependence of the laser wavelength, broad-band reflectors have been assumed. The extension to the case of wavelength-selective reflectors and/or dispersive elements in the cavity is straightforward and will not be treated here.

The necessary pump powers can be achieved either by other lasers (*e.g.* nitrogen lasers, solid-state lasers or even focussed He–Ne- or Ar^+-gas lasers) or by flashlamps. The simplest practical arrangement is a square spectrophotometer cell, polished on all sides, containing the dye solution which is pumped by a nitrogen laser whose beam is focussed into a line parallel to and directly behind one of the cell windows. Then the Fresnel reflection from the two adjacent windows gives enough feedback in most cases, so that no additional resonator mirrors are needed and the dye laser oscillation starts.

For only slowly rising or even continuous pumplight sources like slow flashlamps and continuous argon-ion lasers, one has to take care of the triplet problem. One way to solve this problem is by adding some agent to the dye solution that reduces the triplet lifetime by increasing the radiationless intersystem crossing rate $1/\tau_T$ between the triplet state T_1 and the ground state S_0. Such agents are, *e.g.*, paramagnetic molecules like oxygen or substances that have low-lying triplet states, like cyclooctatetraen (COT), and thus are able to take the energy from the dye molecule by energy transfer whenever the distance between the dye and the COT is lower than about 10 Å. In this way the triplet lifetime τ_T can often be reduced to less than 100 nsec, and the steady-state triplet population can thus be reduced so far that one can easily reach the threshold of laser action with generally available pumplight sources.

One drawback of dye lasers as compared to solid-state lasers is the short fluorescence lifetime τ_F or energy storage time, which implies a quick inversion decay when pumping stops. For this reason one cannot Q-switch a dye laser. On the other hand, dye lasers can be mode-locked by saturable absorbers [52] in much the same way as solid-state lasers, and many investigations have shown that one can obtain psec pulse in this way over a wide spectral region [53,54].

While dye lasers are usually operated in liquid solutions, it was shown very early that one could also use solid solutions of dyes either in plastic materials or as a dopant in crystals [55–56]. Very recently a vapor phase dye laser was operated for the first time [57–61]. This was achieved by heating an evacuated cell containing a small amount of the scintillator dye POPOP to about 400 °C, giving a vapour pressure of about 40 Torr and hence a concentration of dye molecules similar to that generally used in nitrogen laser pumped dye lasers. When the cell containing the dye vapor was pumped by a nitrogen laser, in the same way as a cell containing a dye solution, dye laser emission was observed with practically the same efficiency as in dye solution lasers. The efficiency did not decrease noticeably when a buffer gas such as argon or helium was added, with pressures of up to 1 atm.

The relevance of these experimental findings for the problem of direct electrical excitation is clear: one now can hope that it might be possible in one way or the other to avoid the inefficient optical pumping with flashlamps, or even with other lasers, and use a direct electrical excitation of dye vapors. The concomitant problem of the cracking of molecules in a discharge could perhaps be circumvented by employing electron beam excitation with monoenergetic electrons of optimal energy.

Another problem that remains to be solved is how to increase the photochemical stability of laser dyes. The most useful dyes, namely those of the xanthene

family, such as rhodamine 6G, were found to have a photochemical stability under normal operating conditions of 10^5 to 10^6 absorption and fluorescence acts per molecule [62,63]. With increased ultraviolet content of the pumping light, the photochemical stability was found to decrease considerably [1]. It was also evident in this case that the photodegradation went via the triplet state of the dye molecule, since the rate decreased with an increased content of triplet quencher, like COT.

The measured rate of photodegradation would be tolerable (one could make up for the loss of molecules by continuously adding new, concentrated solution) were it not for the fact that most of the products of the photodegradation process have an absorption band in the spectral region of the laser emission, resulting in unbearable absorption losses. This was nicely demonstrated very recently with a coumarin dye [64]. The authors demonstrated that five photooxydation products resulted in normal dye laser operation and that one of these, a carboxylic acid, had a relatively strong absorption band covering the whole of the fluorescence band. It was also shown that this product was preferentially adsorbed on an alumina filter and that the lifetime of the dye solution could be increased by a factor of 3 when the filter was included in the dye solution recirculation system. Much further progress is needed in this direction before large-scale industrial applications of dye lasers (*e.g.*, for laser-isotope separation) become possible.

Frequency Tripling

When a light wave with an electrical field amplitude E is incident on a dye solution which is non-absorbing in the spectral region of this light wave, a dipole moment μ is induced in each dye molecule:

$$\mu = \alpha E + \gamma E^3 + \cdots, \tag{39}$$

with α being the polarizability of the molecule and γ its third-order polarizability. Because of the smallness of γ, its contribution to the induced dipole moment μ is only noticed at high field strenghts as for instance in a laser beam.

A quantum-mechanical calculation of γ for a number of dyes has been carried through by several authors [65,66]. The value of γ was found to increase very fast with the extension of the π-electron gas. Thus long polyenes or cyanine dyes are especially useful for applications relying on the third-order polarizability. If the exciting light wave is a pure sine wave, the induced dipole moment $\mu(t)$ is a distorted sine wave because of the contribution of the third order polarizability. Performing a Fourier analysis of $\mu(t)$ (*i.e.*, experimentally, putting the light radiated by the induced dipole moment through a spectrometer) reveals a component of three times the fundamental frequency. As this third harmonic light travels through the dye solution at a speed that is generally different from that of the exciting light wave (since the refractive index $n(\omega_0)$ of the solution at the fundamental frequency ω_0 is in general different from the refractive index $n(3\omega_0)$ at the third harmonic frequency), the exciting light wave and the third harmonic wave get out of phase after some length traveled in the medium. Finally, the third

harmonic waves from one part of the solution and from the adjacent part are 180° out of phase and cancel each other by interference, so that in the general case only a small remaining amount of third harmonic light will leave the dye solution. For high-efficiency frequency tripling one can avoid this detrimental situation by "phase-matching", *i.e.*, matching the refractive index (and hence the speed of light) at the fundamental and third harmonic frequencies. This can be done by applying the effect of anomalous dispersion. One chooses a dye that has a strong absorption band near twice the fundamental frequency which will result in a negative contribution of the dye molecules to the refractive index at the third harmonic frequency and a positive contribution to the refractive index at the fundamental frequency. By judicious adjustment of the dye concentration these contributions which are added up to the normal dispersion curve of the solvent can be made just high enough to equalize the refractive index at the third harmonic and fundamental frequencies. Now both light waves are always in phase and the frequency tripled light output is maximized. One obvious condition is, of course, that the absorption at the fundamental and third harmonic frequencies should be as low as possible.

This scheme of frequency tripling was successfully tested with fuchsin in hexafluorisopropanol (a solvent selected for its low index of refraction and relatively flat dispersion curve) to frequency-triple the output of a neodymium laser [67,68]. With an input power of 10 MW/cm^2 a third-harmonic output of 0.2 mW/cm^2 was measured. This low value was mainly due to the relatively high absorption of fuchsin at 355 nm. An improvement of the efficiency by a factor of 80 was found with hexamethylindocarbocyanine iodide in hexafluorisopropanol because of the much lower absorption of this dye at 355 nm. Since the absorption minimum of this dye is at 383 nm, one could expect an additional efficiency increase by a factor of 70 for a fundamental laser wavelength of 1.15 μm [69]. Other cyanine dyes have been used for frequency tripling a fundamental wavelength of 1.89 μm [70].

A further improvement and more freedom in the choice of laser wavelengths can be expected with the use of dye vapors. In liquids, the phase-matching concentration is set by the requirement that the anomalous dispersion of the dye compensates for the normal dispersion of the solvent. The latter is a new parameter that can be varied at will in the gas phase by changing the nature and partial pressure of the buffer gas. The broader resonances of dyes as opposed to metal vapors, which are sometimes used for this purpose, is an advantage for tunable frequency tripling of dye lasers. Another advantage results from the possibility of working at much lower temperatures than with metal vapors.

References

1) Schäfer, F. P.: Angew. Chem., Intern. Ed. Engl. *9*, 9 (1970).
2) Leupold, D., König, R., Dähne, S.: Z. Chem. *10*, 409 (1970).
3) Schäfer, F. P. (ed.): Dye lasers. Berlin–Heidelberg–New York: Springer 1973.
4) Bykovskaya, L. A., Personov, R. I., Kharlamov, B. M.: Chem. Phys. Letters *27*, 80 (1974).
5) Ricard, D., Lowdermilk, W. H., Ducuing, J.: Chem. Phys. Letters *16*, 617 (1972).
6) Lin, C., Dienes, A.: Opt. Commun. *9*, 21 (1973).
7) Parker, C. A.: Photoluminescence of solutions. Amsterdam–London–New York: Elsevier Publ. Co. 1968.
8) Strickler, S. J., Berg, R. A.: J. Chem. Phys. *37*, 814 (1962).
9) Labhart, H., Heinzelmann, W.: Triplet-triplet absorption spectra of organic molecules. In: Birks, J. B., Organic photophysics, Vol. 1. London–New York–Toronto–Sydney: J. Wiley and Sons 1973.
10) Müller, A.: Z. Naturforsch. *23a*, 946 (1968).
11) Hercher, M.: Appl. Opt. *6*, 947 (1967).
12) Schüller, H., Puell, H.: Opt. Commun. *3*, 352 (1971).
13) Huff, L., DeShazer, L. G.: J. Opt. Soc. Am. *60*, 157 (1970).
14) Hercher, M., Chu, W., Stockman, D. L.: IEEE J. Quantum Electron. *QE-4*, 954 (1968).
15) Giuliano, C. R., Hess, L. D.: IEEE J. Quantum Electron. *QE-3*, 358 (1967).
16) Spaeth, M. L., Bortfeld, D. P.: Appl. Phys. Letters *9*, 179 (1966).
17) Müller, A., Pflüger, E.: Chem. Phys. Letters *2*, 155 (1968).
18) Huff, L., DeShazer, L. G.: J. Appl. Phys. *40*, 4836 (1969).
19) Müller, A., Willenbring, G. R.: Appl. Phys. *4*, 47 (1974).
20) Soffer, B. H., McFarland, B. B.: Appl. Phys. Letters *8*, 166 (1966).
21) Opower, H., Kaiser, W.: Phys. Letters *21*, 638 (1966).
22) Sorokin, P. P., Luzzi, J. J., Lankard, Pettit, J. R.: IBM J. Res. Dev. *8*, 182 (1964).
23) Kafalas, P., Masters, J. L., Murray, E. M. E.: J. Appl. Phys. *35*, 2349 (1964).
24) Schäfer, F. P., Schmidt, W.: Z. Naturforsch. *19a*, 1019 (1964).
25) Buettner, A. V.: J. Chem. Phys. *46*, 1398 (1967).
26) Klose, E., Dähne, S., Dürr, H.: Sov. J. Quantum Electron. *3*, 279 (1974).
27) Soffer, B. H., Hoskins, R. H.: Nature *204*, 276 (1964).
28) Ammons, J. W., Maurer, P. B., Reynolds, G. A., Allan, J. A.: US-Patent 3,462,706.
29) Drexhage, K. H., Müller-Westerhoff, U. T.: IEEE J. Quantum Electron. *QE-8*, 759 (1972).
30) Drexhage, K. H.: private communication.
31) Arthurs, E. G., Bradley, D. J., Glynn, T. J.: Opt. Commun. *12*, 136 (1974).
32) Chekalin, S. V., Krinkov, P. G., Matveetz, Yu. A., Shatberashvili, O. B.: Opto-Electronics *6*, 249 (1974).
33) New, G. H. C.: IEEE J. Quantum Electron. *QE-10*, 115 (1974).
34) Mourou, G., Busca, G., Denariez-Roberge, M. M.: Opt. Commun. *4*, 40 (1971).
35) Lessing, H. E., Lippert, E., Rapp, W.: Chem. Phys. Letters *7*, 227 (1970).
36) Duguay, M. A., Hansen, J. W.: Opt. Commun. *1*, 254 (1969).
37) Mack, M. E.: J. Appl. Phys. *39*, 2483 (1968).
38) Mourou, G., Drouin, B., Bergeron, M., Denariez-Roberge, M. M.: IEEE J. Quantum Electron. *QE-9*, 745 (1973).
39) Mourou, G., Denariez-Roberge, M. M.: IEEE J. Quantum Electron. *QE-9*, 787 (1973).
40) Eisenthal, K. B., Drexhage, K. H.: J. Chem. Phys. *51*, 5720 (1969).
41) von der Linde, D., Rodgers, K. F.: IEEE J. Quantum Electron. *QE-9*, 960 (1973).
42) Shelton, J. W., Armstrong, J. A.: IEEE J. Quantum Electron. *QE-3*, 696 (1967).
43) Scarlet, R. I., Figueria, J. F., Mahr, H.: Appl. Phys. Letters *13*, 71 (1968).
44) Penzkofer, A., von der Linde, D., Laubereau, A.: Opt. Commun. *4*, 377 (1972).
45) Penzkofer, A., von der Linde, D., Laubereau, A., Kaiser, W.: Appl. Phys. Letters *20*, 351 (1972).
46) Gires, F.: J. Physique Radium *30*, 203 (1969).
47) Göppert-Mayer, M.: Ann. Physik *9*, 273 (1931).
48) Schäfer, F. P., Schmidt, W.: IEEE J. Quantum Electron. *QE-2*, 357 (1966).
49) Hermann, J. P., Ducuing, J.: Opt. Commun. *6*, 101 (1972).

[50] Kuhn, H.: Fortschr. Chem. Org. Naturstoffe *17*, 404 (1959).
[51] Bradley, D. J., New, G. H. C.: Proc. IEEE *62*, 313 (1974).
[52] Schmidt, W., Schäfer, F. P.: Phys. Letters *26A*, 558 (1968).
[53] Arthurs, E. G., Bradley, D. J., Roddie, A. G.: Appl. Phys. Letters *20*, 125 (1972).
[54] Hirth, A., Vollrath, K., Faure, J., Lougnot, D.: Opt. Commun. *7*, 339 (1973).
[55] Soffer, B. H., McFarland, B. B.: Appl. Phys. Letters *10*, 266 (1967).
[56] Karl, N.: Phys. Stat. Solid. (a) *13*, 651 (1972).
[57] Steyer, B., Schäfer, F. P.: Opt. Commun. 10, 219 (1974).
[58] Steyer, B., Schäfer, F. P.: Appl. Phys. *7*, 113 (1975).
[59] Smith, P. W., Liao, P. F., Shank, C. V. Gustafson, T. K., Lin, C., Maloney, P. J.: Appl. Phys. Letters *25*, 144 (1974).
[60] Smith, P. W., Liao, P. F., Shank, C. V., Lin, C., Maloney, P. J.: IEEE J. Quantum Electron. QE-11, 84 (1975).
[61] Borisevich, N. A., Kalosha, I. I., Tolkachev, V. A.: Zh. Prikl. Spektrosk., *19*, 1108 (1973).
[62] Ippen, E. P., Shank, C. V., Dienes, A.: IEEE J. Quantum Electron. *QE-7*, 178 (1971).
[63] Kato, D., Sugimura, A.: Opt. Commun. *10*, 327 (1974).
[64] Winters, B. H., Mandelberg, H. I., Mohr, W. B.: Appl. Phys. Letters *25*, 723 (1974).
[65] Rustagi, K. C., Ducuing, J.: Opt. Commun. *10*, 258 (1974).
[66] Schweig, A.: Chem. Phys. Letters *1*, 195 (1967).
[67] Bey, P. P., Giuliani, J. F., Rabin, H.: IEEE J. Quantum Electron. *QE-4*, 932 (1968).
[68] Bey, P. P., Giuliani, J. F., Rabin, H.: IEEE J. Quantum Electron. *QE-7*, 86 (1971).
[69] Diels, J. C., Schäfer, F. P.: Appl. Phys. *5*, 197 (1974).
[70] Hermann, J.-P.: Opt. Commun. *12*, 102 (1974).

Reaction of Excited Dye Molecules at Electrodes

Prof. Dr. Heinz Gerischer and Dr. Frank Willig

Fritz-Haber-Institut der Max-Planck-Gesellschaft, D-1000 Berlin-Dahlem, Faradayweg 4—6

Contens

I. Introduction

Excited molecules which are usually generated by light absorption have a lowered ionisation energy and an increased electron affinity. The result is a higher reduction power for electron acceptors and an equally higher oxidation power for electron donors. This change of the redox properties in the excited state, compared to the ground state, is the driving force of many photochemical reactions in solution. Photosensitized redox reactions are especially well known in electrolytes [1,2]. The same reaction behaviour is found for excited dye molecules in contact with electrodes where the electrode takes over the function of the electron acceptor or donor. Electron transfer is the prominent reaction of excited molecules at electrodes [3,4]. The reaction probability of such redox reactions in the excited state depends mainly on the lifetime of the excited state and on the coupling intensity with the reaction partner, in our case the electrode surface. The lifetime can to a great extent be influenced by quenching processes like energy transfer. The coupling efficiency depends on electronic and structural properties of the molecules and the solid.

The net result of a photochemical redox reaction often gives very little information on the quantum yield of the primary electron transfer reaction since this is in many cases compensated by reverse electron transfer between the primary reaction products. This is equally so in homogeneous as well as in heterogeneous reactions. While the reverse process in homogeneous reactions can only by suppressed by consecutive irreversible chemical steps, one has a chance of preventing the reverse reaction in heterogeneous electron transfer processes by applying suitable electric fields. We shall see that this can best be done with semiconductor or insulator electrodes and that there it is possible to study photochemical primary processes with the help of such electrochemical techniques [5,6,7].

The reactions which will be discussed here are basic in the application of dyes as sensitizer for photographic materials like silver halides, zinc oxide and others. Model experiments can be performed at electrodes of such materials which help to understand the mechanism of spectral sensitization in photography.

In the following we shall first discuss the theoretical basis for redox reactions of excited molecules at electrodes in comparison with such reactions in the ground state. We shall then present and discuss some typical examples for the best studied types of reactions in the case of semiconductor and insulator electrodes. Since the properties of these two materials are sufficiently different to need different techniques for the investigation and rather distinct models for the theoretical interpretation, we shall deal with reactions in the case of semiconductors and insulators in separate chapters.
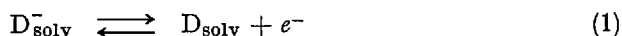
II. Redox Properties of Excited Molecules

1. Thermodynamics

Dye molecules in electrolytes behave at electrodes like other organic molecules and can either be reduced or oxidized. This can occur even more easily in the electronic excited state. Such redox reactions can produce stable or instable
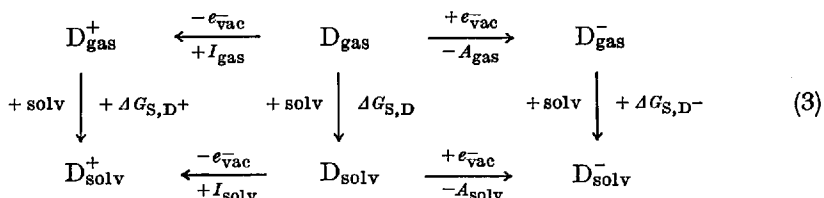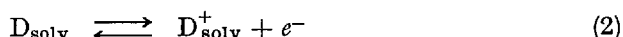
products and can behave reversibly or irreversibly. The term irreversibly has as usual only a relative meaning and depends on the reaction rate in comparison with the time scale of the measurement. The equilibrium properties of the two components of a redox system with respect to electron transfer are characterized by a standard redox potential. This can be defined even in such systems where one of the components is an intermediate with only a very limited lifetime. We shall at first discuss the redox properties of organic molecules in solution in general before we proceed to excited molecules.

1.1. Redox Reactions in the Ground State

Since we have pointed out that an excited molecule D* can either be oxidized or reduced, we have to consider also for the unexcited dye molecule D two redox potentials, one, $^0E_{(D/D+)'}$ for oxidation, the other, $^0E_{(D/D-)'}$ for reduction. For a better understanding we want to relate the redox potential for both reactions to molecular properties in the gas phase and in the electrolyte. The following scheme gives the cycles from which free energy correlations can be derived for the two reactions:

$$D_{solv}^- \rightleftarrows D_{solv} + e^- \tag{1}$$

and

$$D_{solv} \rightleftarrows D_{solv}^+ + e^- \tag{2}$$

$$
\begin{array}{ccccc}
D_{gas}^+ & \xleftarrow[+I_{gas}]{-e_{vac}^-} & D_{gas} & \xrightarrow[-A_{gas}]{+e_{vac}^-} & D_{gas}^- \\
+\text{solv} \downarrow +\varDelta G_{S,D^+} & & +\text{solv} \downarrow \varDelta G_{S,D} & & +\text{solv} \downarrow +\varDelta G_{S,D^-} \\
D_{solv}^+ & \xleftarrow[+I_{solv}]{-e_{vac}^-} & D_{solv} & \xrightarrow[-A_{solv}]{+e_{vac}^-} & D_{solv}^-
\end{array}
\tag{3}
$$

I represents the ionisation energy of D_{gas} or D_{solv}, A the respective electron affinity and $\varDelta G_S$ the free energy of solvation, including the electric terms when charged specimen pass the surface of the solvent.

The balance of the free energy for the reactions (1) and (2) shall be calculated with the reacting electrons at the vacuum level as the standard state for its free energy, neglecting any entropy term for the electron in vacuum, and for equal concentration of the redox components D^+ and D, or D and D^- respectively, in the gas phase as well as in solution. The resulting free energy changes $\varDelta^0G_{redox}$ are for reaction (1a), $D_{solv} \rightarrow D_{solv}^- + e_{vac}^-$

$$\varDelta^0G_{(D/D^-)solv} = +A_{solv} = +A_{gas} + \varDelta G_{S,D} - \varDelta G_{S,D^-} \tag{4}$$

and for reaction (2a), $D_{solv} \rightarrow D_{solv}^+ + e_{vac}^-$

$$\varDelta^0G_{(D^+/D)solv} = +I_{solv} = +I_{gas} + \varDelta G_{S,D^+} - \varDelta G_{S,D} . \tag{5}$$

The absolute redox potentials for these reactions are defined by a compensation of the free energy change ΔG_{redox} by the free energy of the reacting electrons. Therefore, at equilibrium conditions, the electrons have not to be at the vacuum level but at the energy level $^0E_{\text{redox}}$

$$^0E_{\text{redox}} = -\Delta^0 G_{\text{redox}} . \tag{6}$$

In the above formulation of the reaction, $\Delta^0 G_{\text{redox}}$ will have the positive sign for all reactions of interest here. Consequently, the electron free energy in this absolute redox potential scale has always negative values.

The equilibrium situation can be achieved with the reacting electrons coming from the Fermi level E_{F} of a metal electrode in contact with the solution of the redox couple. The free energy change in the respective redox reaction is then zero.

$$D_{\text{solv}}^- \;\underset{\longleftarrow}{\longrightarrow}\; D_{\text{solv}} + e^-(E_{\text{F}}); \;\; \Delta G = 0 \tag{7}$$
$$\text{if } E_{\text{F}} = {}^0E_{\text{D/D}^-}$$

$$D_{\text{solv}} \;\underset{\longleftarrow}{\longrightarrow}\; D_{\text{sdlv}}^+ + e^-(E_{\text{F}}); \;\; \Delta G = 0 \tag{8}$$
$$\text{if } E_{\text{F}} = {}^0E_{\text{D}^+/\text{D}} .$$
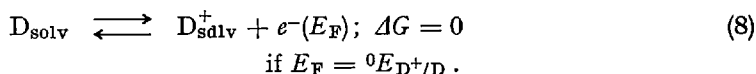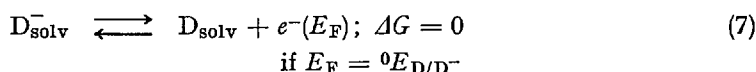
We can define therefore the standard redox potentials $^0E_{\text{redox}}$ as the Fermi energies of the redox systems [6] and obtain for the reactions (1) and (2),

$$^0E_{\text{D/D}^-} = -A_{\text{gas}} + \Delta G_{\text{S,D}^-} - \Delta G_{\text{S,D}} \tag{9}$$

$$^0E_{\text{D}^+/\text{D}} = -I_{\text{gas}} - \Delta G_{\text{S,D}^+} + \Delta G_{\text{S,D}} . \tag{10}$$

1.2. Absolute and Conventional Redox Potential Scale

The practical way of measuring redox potentials is not performed with electrons in vacuum as the reference state. It is done in a galvanic cell with a standard reference electrode, like the hydrogen electrode or calomel electrode, as counter electrode. But an electron at the Fermi level of the metal in such a reference electrode has an exactly defined free energy difference ΔE_{ref}, relative to the energy of the free electron in vacuum. The absolute energy scale of the redox systems is therefore fully parallel to the conventional scale referred to as reference electrode and only shifted against the latter by the free energy difference ΔE_{ref}. Let us denote the electrode potential in the conventional scale with U. The relation between the two scales is then,

$$E = \Delta E_{\text{ref}} - Ue_0 \tag{11}$$

where e_0 is the elementary charge.

The negative sign of U in this equation is caused by the convention on the potential scale for galvanic cells while we consider in the absolute scale electron

energies. ΔE_{ref} has a negative value because electrons are strongly bound in matter with electronic conduction or in redox systems of electrolytes. Its value has been calculated by Lohmann [8] for the N-hydrogen electrode to be in the order of

$$\Delta E_{ref} = -4.5 \text{ eV} \tag{11}$$

1.3. Redox Reactions in the Excited State

The analogous cycle can be formulated for the redox reactions of the excited molecule D*. We have to distinguish the two reactions,
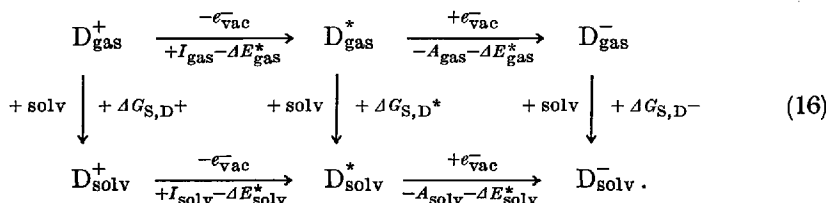
$$D_{solv}^- \; \xrightleftharpoons \; D_{solv}^* + e^- \tag{12}$$

$$D_{solv}^* \; \xrightleftharpoons \; D_{solv}^+ + e^- . \tag{13}$$
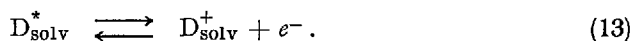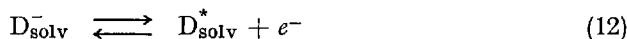
The equilibrium is again obtained if the electrons are located at the respective Fermi energies for these redox reactions,

$$^0E_{D*/D^-} = -\Delta^0G_{(D*/D^-)solv} \tag{14}$$

$$^0E_{D^+/D*} = -\Delta^0G_{(D^+/D*)solv} \tag{15}$$

The respective reaction cycle is as follows, with ΔE^* representing the energy of electronic excitation in the molecule D which has always a positive sign, but will be somewhat different in the gas phase and in solution,

$$
\begin{array}{ccccc}
D_{gas}^+ & \xrightarrow[+I_{gas}-\Delta E_{gas}^*]{-e_{vac}^-} & D_{gas}^* & \xrightarrow[-A_{gas}-\Delta E_{gas}^*]{+e_{vac}^-} & D_{gas}^- \\[2mm]
+\text{solv} \downarrow +\Delta G_{S,D^+} & & +\text{solv} \downarrow +\Delta G_{S,D^*} & & +\text{solv} \downarrow +\Delta G_{S,D^-} \\[2mm]
D_{solv}^+ & \xrightarrow[+I_{solv}-\Delta E_{solv}^*]{-e_{vac}^-} & D_{solv}^* & \xrightarrow[-A_{solv}-\Delta E_{solv}^*]{+e_{vac}^-} & D_{solv}^- .
\end{array}
\tag{16}
$$

The results are,

$$^0E_{D*/D^-} = -A_{solv} - \Delta E_{solv}^* = -A_{gas} + \Delta G_{S,D^-} - \Delta G_{S,D*} - \Delta E_{gas}^* \tag{17}$$

$$^0E_{D^+/D*} = -I_{solv} + \Delta E_{solv}^* = -I_{gas} - \Delta G_{S,D*} + \Delta G_{S,D} + \Delta E_{gas}^* \tag{18}$$

The consequences are obvious. The redox reaction with reduction of D* has at equilibrium a much lower Fermi energy, that means a more positive redox potential, the redox reaction with oxidation of D* has a much higher Fermi energy, that is a more negative redox potential than in the ground state. This is schematically demonstrated in Fig. 1.

The definition of ΔE^* in Eqs. (16)−(18) needs some comment. We are discussing here equilibrium conditions, and therefore, ΔE^* describes the excitation
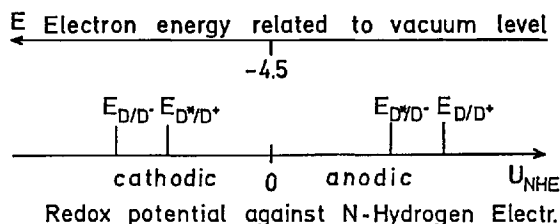
Fig. 1. Correlations between redox potentials of the excited and unexcited dye molecule, acting as electron acceptor or electron donor, in absolute (E) and conventional (U_{NHE}) scale

energy stored in an excited molecule with an equilibrium distribution of all vibrational and rotational states and at equilibrium of the interaction with the surrounding medium. The reference state is a nonexcited molecule in such an equilibrium ground state. ΔE^* is therefore not identical with the energy of spectral absorption and also not identical with the energy of fluorescence because these transitions are restricted by the Franck-Condon conditions and contain excess energies or energy deficiencies from the excitation of vibrational and rotational states and differences in the interaction energies with the surroundings. In vacuum, ΔE^* is represented by the 0—0-transition of the electronic spectra; in a medium with a difference in the interaction energy of the ground and excited state there will be a slight difference from the 0—0-transition energy of the absorption spectrum but this is not significant for our discussion.

One further complication has to be mentioned. Many organic molecules have triplet states with a long lifetime which cannot be reached by a direct optical transition but are often formed from the excited singlet state by intersystem crossing. Due to their long lifetime such triplet states play a very important role in photochemical reactions, and the same has to be expected for electrode reactions of excited molecules. Therefore, we shall later distinguish in some systems between excited singlet and triplet state energies denoted by $\Delta^1 E^*$, $\Delta^3 E^*$.

We can conclude from these thermodynamic considerations that it is possible to estimate the redox potentials of excited molecules, if we know the equilibrium redox potentials for the molecules in the ground state, as well for reduction as for oxidation, and add or subtract from these redox potentials the excitation energy ΔE^* of the lowest singlet or triplet state. For most dye molecules the reduction redox potential is experimentally more easily accessible than the oxidation redox potential. In such cases we have found that an estimation can be made by assuming that the ionisation energy of the dye molecule in crystalline state is similar to the ionisation energy in a polar solvent and gives an approximate value for the absolute redox potential. Such estimations are especially useful for a comparison of molecules with similar structure.

1.4. Rhodamine B as an Example

We shall discuss now the redox properties of the dye molecule rhodamine B which is often used in photosensitization experiments.

The structural formula for rhodamine B is the following:
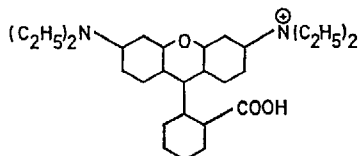
At pH $= 7$ rhodamine B is a cation, since the carboxy-phenyl group dissociates with pK $= 9$ [2]. In the following text we will refer to this cation as the singlet ground state dye molecule $^1D_0$. Due to steric conditions the carboxy-phenyl group remains almost perpendicular to the plane of the chromophore. The carboxy-phenyl group is not part of the chromophore as can be seen from an almost identical absorption spectrum for pyronin G which is an analogous dye molecule to rhodamine B but lacking the carboxy-phenyl group [9]. The lowest excited singlet state $^1D^*$ is separated by 2.13 eV from the ground state $^2D_0$, and the triplet state is separated by 1.86 eV [10], that means $\Delta^1E^* = 2.13$ eV and $\Delta^3E^* = 1.86$ eV. The fluorescence yield is high about 0.97 in ethanol and the intersystem crossing correspondingly small [11]. The lifetime of the excited singlet state is 3.2 ns [12].

In aqueous alkaline solution the ground state of rhodamine B takes up an electron from a metal electrode at -0.75 V (NHE) forming the reduced dye $^2D^-$ [13]. This corresponds to an electron affinity of about 3.75 eV in absolute scale [8] or $^0E_{D/D^-} = -3.75$ in our nomenclature. The reduced molecule is a semiquinone with pK $= 5.5$ for the uptake of a proton [2]. The neutral semiquinone has an absorption maximum at 425 nm whereas its protonated form is colourless [2]. The oxidation potential estimate, as pointed out before, can be obtained from the ionisation energy for crystalline rhodamine B which is 5.3 eV [14]. This would mean $^0E_{D/D^+} \approx -5.3$ eV or $^0U \approx +0.8$ V (NHE). The reduction and oxidation potentials of the excited states of rhodamine B can be obtained by adding or substracting the respective excitation energy from the values for the ground state yielding an estimated $^0E_{1D^*/D^-} \approx -5.88$ eV for the excited singlet state and $^0E_{3D^*/D^-} \approx 5.61$ eV for the excited triplet state.

The most probable electron transfer term of the excited dye as an acceptor is shifted by L_{reorg} into positive directions as explained later (p. 41). With an estimated L_{reorg} of 0.4 eV this would give $_0E_{1D^*_{acc}} \approx -5.48$ eV and $_0E_{3D^*_{acc}} \approx -5.21$ eV. The crude estimate based on the ionisation energy of crystalline rhodamine B yields for $^0E_{1D^*/D^+} \approx -3.17$ eV for the excited singlet state and $^0E_{3D^*/D^+} \approx -3.44$ eV for the excited triplet state. This value gives for the electron transfer terms of D* as a donor the values $_0E_{1D^*_{don}} \approx -3.57$ eV and $_0E_{3D^*_{don}} \approx -3.84$ eV. Such estimates are only valid when in first approximation proton addition can be neglected e.g., for the reduction of rhodamine B at a pH, where proton attachment during the lifetime of the excited state is negligible.

2. Kinetics

The theory of electron transfer to electrodes has been worked out by various authors [15–19]. The basic assumption in all theories is that electron transfer occurs like an electronic transition in spectroscopy under the restrictions of the

Franck-Condon principle. That means in other words that the time for electron transfer from a molecule to an electrode is short compared with the time of atomic movements in vibrations or rotations. This has the consequence that for electron transfer reactions the energy terms E of the electrons in the donors or acceptors are different from the thermodynamic energy levels ^0E which we have discussed in the preceding section.

2.1. Electron Transfer Energy Levels in Redox Species

We discuss this with help of Fig. 2 for a cyclic electron transfer from a molecule in the ground state to the vacuum level, and back to the ionized molecule. After each electron transfer we leave enough time for relaxation of the solvent to reach the new equilibrium state of interaction in which electrostatic forces play a prom-
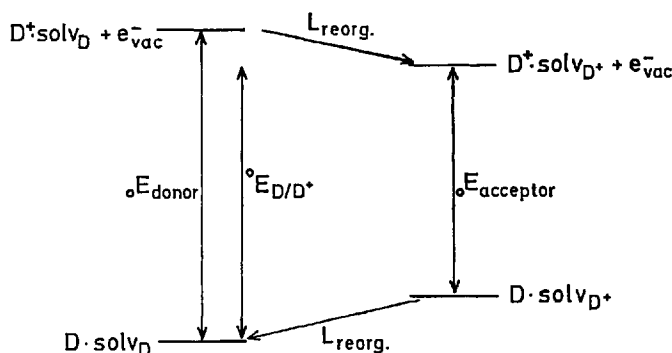

Fig. 2. Energy cycle for electron transfer under Franck-Condon conditions ($_0E$) in relation to electron transfer at thermal equilibrium (^0E) for redox species in solution

inent role. Here we see clearly the difference between the Franck-Condon energy levels, $_0E_{acc}$ and $_0E_{don}$ and the thermodynamic energy levels, ^0E, controlling the redox potentials. We see further that the electron transfer energy level $_0E_{don}$ of the molecule in its reduced state acting as an electron donor is in principal lower than the equivalent energy level $_0E_{acc}$ of the same molecule in its oxidized state acting as an electron acceptor. Although it is the same electron orbital which takes part in the electron exchange the energies are different due to the different interaction with the surroundings in different states of oxidation. In electron transfer under Franck-Condon conditions, the electron leaves behind an oxidized molecule in a surrounding which has minimized the free energy for the unoxidized state. It has, therefore, a higher free energy than in the equilibrium state minimized for this new situation. This excess energy is released after electron transfer by reorganisation of the molecule itself and its surroundings. If, on the other hand, an electron is added to an oxidized species, it has to enter surroundings which do not fit the reduced state. Therefore, less energy is gained in the electron transfer step, but the difference is afterwards added during adjustment of the solvent to the new situation.

In this discussion we have assumed that electron transfer would only occur in the optimally adjusted state of interaction with the surroundings. However, there is in reality not only one single Franck-Condon energy level which can be attributed to a molecule in solution. Due to thermal fluctuations in the interaction with the surroundings and due to thermal excitation of vibrations and rotations, the Franck-Condon energy levels of a single molecule fluctuate over quite a range of energies which can be described by a Gaussian distribution around the most probable energy levels $_0E_{don}$ and $_0E_{acc}$ of Fig. 2. This fluctuation of the energy levels for electron exchange tends in both directions from the most probable energy level because the initial state can become more or less similar to the optimum of interaction in the final state [19].

The same situation is to be expected for the excited states with the only difference that now the most probable energy states are shifted by the stored excitation energy upwards or downwards depending on whether the excited molecule acts as a donor or as an acceptor [20]. These energy distribution functions for a molecule in the ground state and in the excited state are represented in Fig. 3. They can be described by the following equations:
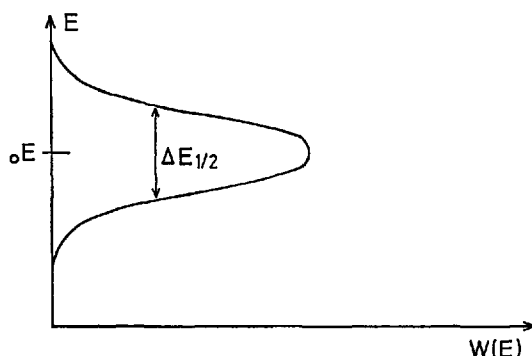
Fig. 3. Distribution function for electron transfer energy levels of a redox species in an electrolyte. $\Delta E_{1/2} = 3.35 \cdot (k \cdot T \cdot L_{reorg})^{\frac{1}{2}} \cdot eV$

For the electron levels of a molecule acting as a donor, the distribution function is

$$W_{don}(E) = A_{don} \cdot \exp\left(-\frac{(E - {_0E_{don}})^2}{4kTL_{don}}\right) \tag{19}$$

A_{don} is a normalizing factor, making $W(E)dE = 1$

$$A_{don} = \left(\frac{1}{4\pi kTL_{don}}\right)^{1/2} \tag{20}$$

L_{don} is the reorganization energy of the ion-solvent interaction after electron transfer.

We have in our system 3 species which can act as a donor, D, D^-, and D^*. For each of them we have different characteristic energies $_0E$ and different reorganization energies L, therefore also different A values. However, the reorganization energies of D and D^* as donor will be so similar that we can use the same value for both, as long as we have no special reason to expect a large deviation.

For the electron terms of the acceptor molecules we obtain an analogous distribution function,

$$W_{\mathrm{acc}}(E) = A_{\mathrm{acc}} \cdot \exp\left(-\frac{(E - {}_0E_{\mathrm{acc}})^2}{4\,kT\,L_{\mathrm{acc}}}\right) \tag{21}$$

with

$$A_{\mathrm{acc}} = \left(\frac{1}{4\,\pi kT\,L_{\mathrm{acc}}}\right) \tag{22}$$

Again, we have 3 acceptor species in our system, D, D^+, and D^* with different $_0E$ and L values. For D and D^* we shall equally assume that their reorganization energies are equal.

Further there are some other correlations between the characteristic energy terms $_0E$, the equilibrium redox energy levels ^0E and the reorganization energies L which read as follows:

$$^0E_{\mathrm{D/D^+}} - {}_0E_{\mathrm{D_{don}}} = L_{\mathrm{D_{don}}} \tag{23}$$

$$_0E_{\mathrm{D^+}} - {}^0E_{\mathrm{D/D^+}} = L_{\mathrm{D^+}} \approx L_{\mathrm{D_{don}}} \tag{24}$$

$$^0E_{\mathrm{D^*/D^+}} - {}_0E_{\mathrm{D^*_{don}}} = L_{\mathrm{D^*_{don}}} \approx L_{\mathrm{D_{don}}} \tag{25}$$

$$^0E_{\mathrm{D/D^-}} - {}_0E_{\mathrm{D^-}} = L_{\mathrm{D^-}} \approx L_{\mathrm{D_{acc}}} \tag{26}$$

$$_0E_{\mathrm{D_{acc}}} - {}^0E_{\mathrm{D/D^-}} = L_{\mathrm{D_{acc}}} \tag{27}$$

$$_0E_{\mathrm{D^*_{acc}}} - {}^0E_{\mathrm{D^*/D^-}} = L_{\mathrm{D^*_{acc}}} \approx L_{\mathrm{D_{acc}}} \tag{28}$$

2.2. Rate of Electron Transfer

We can now treat electron transfer kinetics with the simplest model, based on the assumption that an electron transfer can only occur between two electronic energy states having equal energy, one being occupied, the other vacant. That means we can describe the rate of electron transfer by the following equations:

Electron transfer from an electron donor to the electrode, equivalent to an anodic current,

$$j^+ = j_{\mathrm{don}} = B_{\mathrm{don}} \cdot c_{\mathrm{don}} \int_{-\infty}^{\infty} \varkappa_{\mathrm{don}}(E) \cdot W_{\mathrm{don}}(E) \cdot D_{\mathrm{vac}}(E)\, dE \tag{29}$$

electron transfer from the electrode to an electron acceptor, equivalent to a cathodic current,

$$j^- = j_{acc} = B_{acc} \cdot c_{acc} \int_{-\infty}^{\infty} \varkappa_{acc}(E) \cdot W_{acc}(E) \cdot D_{occ}(E) \, dE \,. \qquad (30)$$

In B all factors are collected which are independent of the momentary energetic state of the reactants, like collision numbers, geometrical and also normalizing factors [*e.g.* A from Eqs. (20, 22)] etc. The $\varkappa(E)$ in the integrals represent the transition probability for electrons in case the condition of energy conservation is fulfilled ($E_{initial} = E_{final}$). The $D(E)$ functions denote the densities of vacant or occupied electron states in the electrode.

2.3. Metal Electrodes

In the case of a metal electrode we can use the approximation that all electron quantum states above the Fermi level E_F are vacant and below the Fermi level are occupied, since the energy range around E_F, where vacant and occupied levels are simultaneously present, is uninteresting for electron transfer in the excited state. The current at a metal electrode is therefore controlled by the relative correlation between the Fermi level of the metal electrons to the position of the vacant and occupied energy states of the redox system in the electrolyte. Assuming that we have an equal concentration of electron donors and electron acceptors in the electrolyte, three characteristic situations can be expected for the contact between a metal electrode and a redox system which are shown in Fig. 4. They represent the equilibrium situation, the situation of anodic polarisation and of cathodic polarisation. The differences are caused by the differences in the position of the Fermi level in the metal relative to the Fermi energy of the redox system which depends on the voltage drop in the double layer at the electrode/electrolyte interface and is therefore controlled by the applied electrode potential, given in Fig. 4 as overvoltage η.

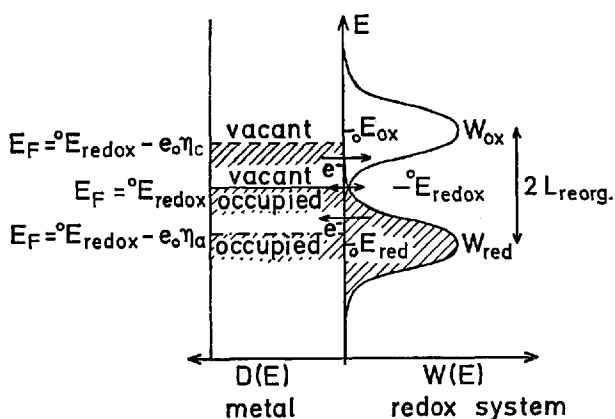

Fig. 4. Correlations between electron transfer energy levels in metal electrode and in redox species. At equilibrium ($E_F = {}^0E_{redox}$), for anodic ($\eta_a > 0$) and cathodic ($\eta_c < 0$) polarisation ($E_F = {}^0E_{redox} - e_0 \cdot \eta$). The arrows indicate the direction of electron transfer

2.3.1. Electron Transfer in the Excited State of a Molecule D*. We consider now electron transfer in the excited state of a molecule D^* which may be able to act as an electron donor with an energy level distribution around the characteristic energy level ${}_0E_{D^*_{don}}$ and an electron acceptor with energy levels around the energy level ${}_0E_{D^*_{acc}}$ where ${}_0E_{D^*_{don}}$ is far below ${}_0E_{D^*_{acc}}$. We assume that a metal electrode in contact with the solution of D is brought to a potential where D is neither oxidized nor reduced. This situation is represented in Fig. 5. If now light is absorbed by D, new electron transfer levels are generated, the states of D^*_{don} and of D^*_{acc} of Fig. 5. With these excited states electron transfer to and from the metal is possible, since they are located in an energy range where the corresponding electron states in the metal are either vacant or respectively occupied. However, the two photocurrents in the excited state of D have opposite directions and will compensate each other to some extent, if not one process has a large preference.
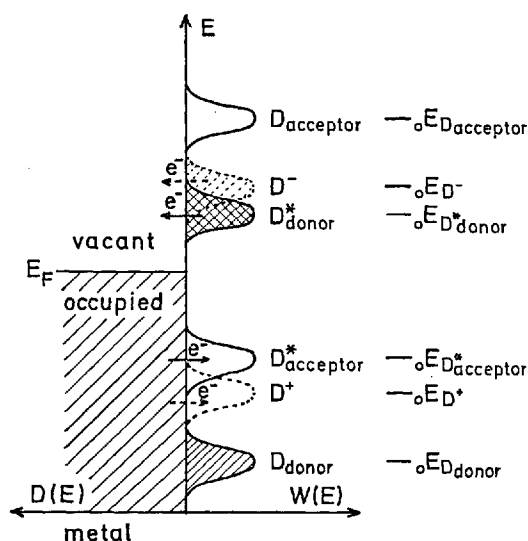

Fig. 5. Correlations between electron transfer terms of dye molecules in all possible oxidation states and in the excited state related to E_F of a metal electrode where neither oxidation nor reduction of the unexcited dye is possible

There is another compensating effect at a metal electrode as a consequence of such an electron transfer in the excited state. The species D^+ and D^- which are generated have acceptor or donor levels below or above the Fermi level of the metal where a reverse electron transfer is now possible. In the steady state reached within the lifetime of the products D^+ and D^- at the electrode the photocurrents are compensated by the reverse electron transition from the products. Only if a fast consecutive reaction brings one of the products to an energy state where no reverse electron transfer is possible a net photocurrent can be observed at a metal electrode. It is not clear whether up to now any reaction has been found which

produces a photocurrent by this mechanism. In all more thoroughly investigated systems the photocurrents seem to be caused by homogeneous photochemical reactions, the products of which have a redox potential different from the mother substances and therefore give a different contribution to the current at the electrode potential applied [21].

Further there is another very effective process which prevents a direct generation of photocurrents by excited molecules at a metal electrode, this is quenching of the excitation by energy transfer to the metal. According to the dipol-dipol interaction mechanism as postulated by Förster [22], the rate of energy transfer is given by a rate constant:

$$k_{qu} \sim \frac{1}{r^6} \int\limits_{-\infty}^{\infty} f_{don}(\nu) \cdot f_{acc}(\nu) \frac{d\nu}{\nu^4} \tag{34}$$

where r is the distance between donor and acceptor, ν the frequency and $f(\nu)$ the oscillator strength for the particular frequencies. A metal as energy acceptor is much more efficient than a single molecule since one has to integrate over the full volume of the metal. This has been done far a monolayer as acceptor [23] and for a compact metal [23,24,25]. These results show that the lifetime of the excited molecule drops with decreasing distance from the metal surface at short distances by

$$\frac{\tau}{\tau_\infty} \sim \left(\frac{d}{d_0}\right)^3, \ d < d_0 \tag{35}$$

where d_0 contains all the individual properties of the spectra and system. The metal has a continuous spectrum which fully overlaps with the fluorescence spectrum of all dye molecules, the rate constant for energy transfer from an adsorbed excited dye molecule to a metal is therefore extremely high. A rough estimation based on these formulas gives a reduction in lifetime of an excited dye molecule in a few Å distances from the surface by a factor of $10^{-3} - 10^{-4}$ due to energy transfer. In reality the lifetime in the adsorbed state will even be shorter since energy transfer by other mechanisms as exchange interaction has not been taken into account in this calculation. A similar calculation for excited species approaching from solution by diffusion has been made by Hale [26]. We see that there are enough reasons to make the chance of finding photocurrents at metals by direct electron transfer from excited molecules extremely low.

2.4. Semiconductor and Insulator Electrodes

The situation is utterly different for semiconductors or insulators with a wide enough band gap [5,6,27,28]. If the band gap exceeds the energy range of the fluorescence spectrum of the dye, energy transfer is either prevented or at least reduced to a very small rate which is controlled by the number of electronic energy levels within the band gap of the semiconductor or insulator. Such states are usually localized and can be caused by impurities or structural defects and represent optical transitions with a low oscillator strength. With a suitable position of the

band edge energies in relation to the electron transfer energy levels of the dye molecule, the reverse electron transfer steps can also be prevented. Therefore, one can often find conditions where only one type of electron transfer from the excited molecule to the electrode is possible. Such situations are shown in Figs. 6 and 7 for electron transfer from the excited molecule as donor to the electrode and for the reverse process with the excited molecule as acceptor. The quantum efficiency per excited molecule can be very high in such situations, since only the internal desactivation processes compete then with the electron transfer step. However, the overall quantum efficience calculated for the incident light is in all cases restricted by the limited light absorption of a monomolecular dye layer on an electrode which scarcely can exceed 2%. In multilayers of dyes the quenching probability increases and an ohmic resistance for electron transfer is formed which prevents fast removal of electric charge from the dye layer. Therefore,
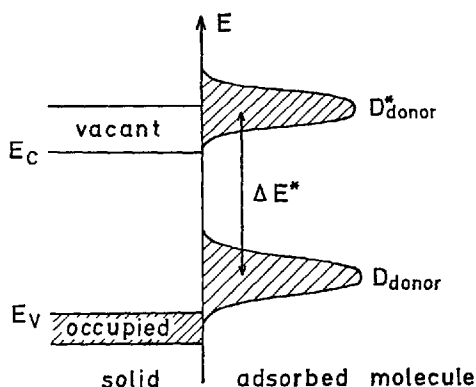

Fig. 6. Typical electron energy correlation for electron injection from excited dye into a semiconductor or insulator
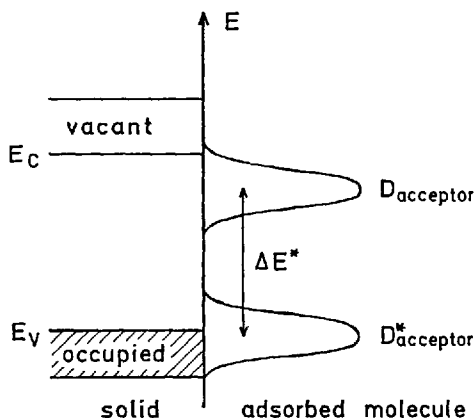

Fig. 7. Typical electron energy correlation for hole injection from excited dye into a semiconductor or insulator

45

not much can be gained in absolute quantum efficiency by multiple dye films. In the following we shall concentrate our discussion on reactions of adsorbed dye molecules in the excited state being adsorbed on semiconductor or insulator electrodes in monolayer amount.

III. Reactions at Semiconductors

There is no sharp distinction between a semiconductor and an insulator. Both can have such a wide band gap that the conductivity of the intrinsic materials is negligible. In this chapter, however, we shall discuss only such solids which by doping can be made conductive to such an extent that ohmic voltage drops in the bulk remain small for the size of currents which can be generated by excited molecules. The other extreme, where the conductivity is only caused by the injected charge carriers, will be treated in the next chapter.

1. Measuring Device

Semiconductor electrodes can be used in galvanic cells like metal electrodes and a controlled electrode potential can be applied by means of a potentiostat, if the electrode can be contacted with a suitable metal without formation of a barrier layer (ohmic contact). Suitable techniques for ohmic contacts have been worked out in connection with semiconductor electronics. Surface treatment is important for the properties of semiconductor electrodes in all kind of charge transfer processes and especially in the photoresponse. Mechanical polishing generates a great number of new electronic states underneath the surface [29] which can act as quenchers for excited molecules at the interface. Therefore, sufficient etching is imperative for studying photocurrents caused by excited dyes.

The cell arrangement is otherwise quite normal. The cell only has to contain a window in front of the electrode for illumination [30]. For dye-sensitization studies it is most favorable if the electrode can be used in the form of thin plates with an ohmic contact around the side parts so that the light can be lead through the electrode from the back. It is in this way filtered for all wave lengths which are absorbed by the semiconductor and could thereby generate photocurrents at the electrode-electrolyte interface [31]. However, this can often not be achieved. The photoresponse is at best separated from dark currents by modulation techniques and can be detected with great sensitivity by lock-in amplifiers. Fig. 8 gives the principle scheme of most arrangements for the measurement of photocurrents at semiconductors with direct illumination of the electrode.

The dye should be added to the solution by such an amount that the electrode surface was nearly covered with an adsorbed monolayer. Though most inorganic semiconductors exhibit only a low tendency for the adsorption of large organic molecules, the formation of an adsorbed layer is largely favoured by the salting-out effect of concentrated electrolytic solutions. It is sufficient therefore to use solutions of $1 - 3 \cdot 10^{-5} M$ in dye concentration. Such low concentrations in the solution are necessary to avoid larger losses in light intensity at transmission of the light beam between window and electrode surface.
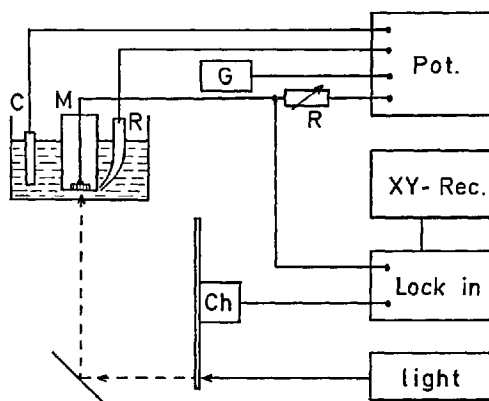
Fig. 8. Experimental set-up for the measurement of photocurrents. M = semiconductor electrode, C = counter electrode, R = reference electrode, Pot = potentiostat, G = voltage generator, Ch = chopper

2. Energy Correlations

In doped semiconductors of high enough conductivity, electrode potentials in the electrochemical sense have the same meaning as for metal electrodes, namely defining the position of the Fermi level in the bulk of the semiconductor relative to the Fermi level of a reference electrode in contact with the same electrolyte. The main difference is, however, that the electric potential drop between the bulk of the semiconductor and the electrolyte extends over a space charge layer underneath the semiconductor surface, in full correspondence with the diffuse part of the double layer in the electrolyte. Besides this we have a sharp potential jump in the Helmholtz double layer at the semiconductur/electrolyte interface which is in the absence of surface states (ideal semiconductor electrode) mainly controlled by the chemical composition of the electrolyte and only to a very small, often negligible part, by the voltage applied to the electrode [20,28,32]. If surface states are present we can have any intermediate situation between a metal and an ideal semiconductor electrode depending on the concentration of surface states. The difference in potential distribution between a metal and a semiconductor electrode with none or few surface states is demonstrated in Fig. 9. The potential drop in the Helmholtz double layer region is due to an unsymmetric distribution of ionic charge between the surface and the electrolyte caused by ion adsorption from the electrolyte or ionic dissociation from the semiconductor surface [28,33]. This charge distribution is little affected by the applied voltage and will in the following be assumed as only being controlled by the chemical composition of the electrode and the electrolyte.

The situation where the excess electric charge in the bulk of the semiconductor is zero has a particular importance because this can often be obtained experimentally. This state is called "flat band situation" and the respective electrode potential, "flat band potential" because in the absence of electric fields inside the semiconductor the position of the band edge energies runs flat from the interior to the surface [20]. This energy pattern at the semiconductor-electrolyte contact is shown in Fig. 10 for the flat band situation, i. e. an anodic and a cathodic
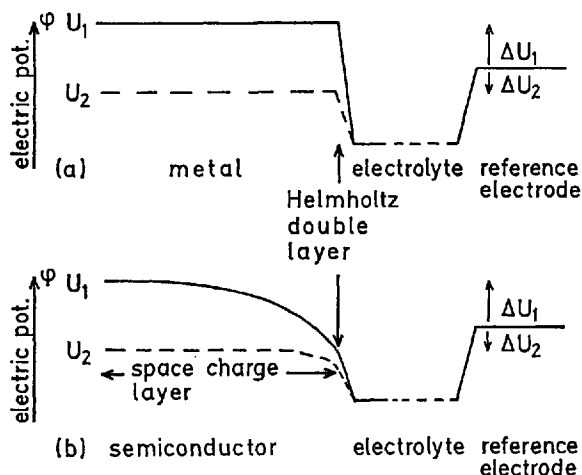
Fig. 9. Distribution of the electric potential φ in galvanic cell with (a) metal and (b) semiconductor electrode
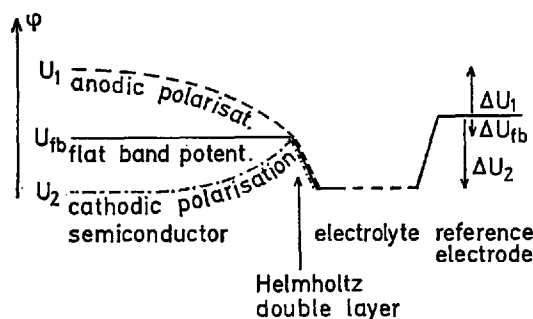

Fig. 10. Electric potential in semiconductor electrode at flat band situation and at anodic or cathodic polarization relative to the flat band potential

potential. The flat band potential can often be derived from capacity [34,35,36,37] or from surface-photovoltage [38,39] measurements depending on the electrode potential that allows to calculate the position of the band edges in terms of the electrode potential scale against a reference electrode. For this calculation one needs to know besides the flat band potential the energy distance between the Fermi level in the bulk of the semiconductor and the band edges which is given by the following

$$
\begin{aligned}
E_c - E_F &= \frac{kT}{e_0} \ln \frac{N_c}{n} \\
E_F - E_v &= \frac{kT}{e_0} \ln \frac{N_v}{p}
\end{aligned}
\tag{36}
$$

where N_c, N_v are the effective densities of states in the conduction and valence band and n, p are the bulk concentrations of electrons and holes. With this in-

formation one can construct the solid state part of Fig. 6 and 7 in the electro-chemical energy scale and one knows also in which potential range a positive or negative space charge exists in the semiconductor.

The presence of a space charge layer with an excess of positive or negative electric charge is very important for studying the electrode reactions of excited dye molecules. With the right sign of the excess charge, the electric field in the space charge layer removes the injected charge carriers from the surface to the bulk and prevents in this way recapturing of injected charge carriers by the ionised dye molecules. This is explained in Fig. 11. If the excited dye molecule acts as electron donor corresponding to a situation of Fig. 6, we need a positive space charge to remove the injected electrons from the interface. Such a situation where the electron concentration in the surface is reduced to a negligible amount can be obtained with n-type semiconductors if they are anodically polarised relative to the flat band situation and form a depletion layer. If the excited mole-cule acts as an electron acceptor, as in Fig. 7, we need a negative space charge with negligible hole concentration in the surface as shown in Fig. 11 b what can be reached with p-type semiconductors. The injected holes are then removed to the bulk and have no chance to be recaptured. In both cases the reverse reactions are prevented and the electron transfer from or to the excited molecule can be ob-served with 100% yield as a photocurrent.
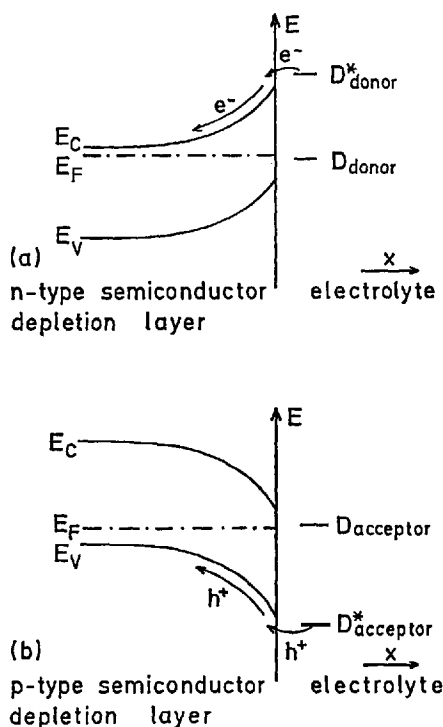

Fig. 11. Position of electron energies at the band edges of conduction (E_c) and valence (E_v) band in depletion layer of (a) n-type and (b) p-type semiconductor electrode

In Fig. 12 we have collected the position of the band edges for various inorganic semiconductors in contact with aqueous electrolytes as derived from flat band potential measurements [40-46]. The pH of the electrolyte has a great influence on the position of the band edges. The reason is that most of these semiconductors react with water to form an oxide or hydroxide monolayer at their surface which can exchange protons with the electrolyte. Other ions which are strongly adsorbed on the surface can also change the position of the band edges which is therefore dependent on electrolyte composition and must be controlled in the experiments individually.
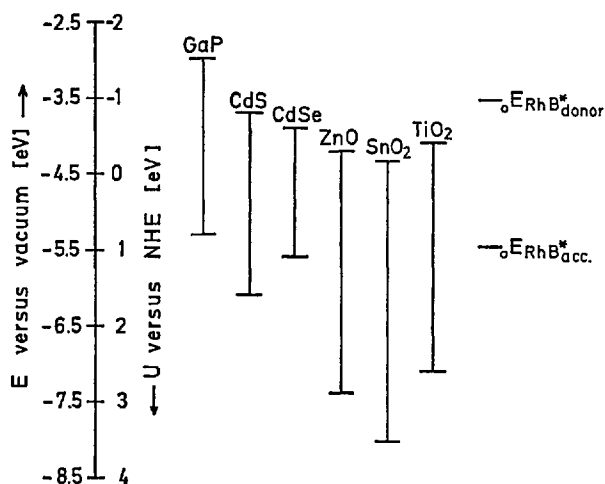

Fig. 12. Position of the band edges of various semiconductors in absolute and conventional electrode potential scale at pH = 7 GaP (40). CdSe (41), CdS (42), ZnO (43), TiO$_2$ (44, 45), SnO$_2$ (46) and the electron transfer terms of the excited rhodamine B in solution

3. Electron Injection

Most of the available inorganic semiconductors with wide enough band gap to prevent energy transfer have n-type character. The conditions for studying electron injection from excited dye molecules are therefore most favourable with these materials since a depletion layer (compare Fig. 11) can easily be formed by anodic polarisation. This barrier layer prevents electronic currents in the absence of illumination (or keeps the dark current at least very small) and makes the system most sensitive for photocurrents.

ZnO-electrodes (band gap 3.2 eV) have in this connection been studied in great detail [30,31,47,48,49]. We give here a few typical examples of the experimental results. Fig. 13 shows the dependence of the photocurrent on electrode potential for the dye rhodamine B adsorbed at a ZnO-electrode with illumination in the wave length range of the absorption maximum of the dye ($\lambda = 570$ nm). The photocurrent reaches a saturation above a critical voltage which is about 0.25—0.4 V positive above the flat band potential. This means that for a barrier height
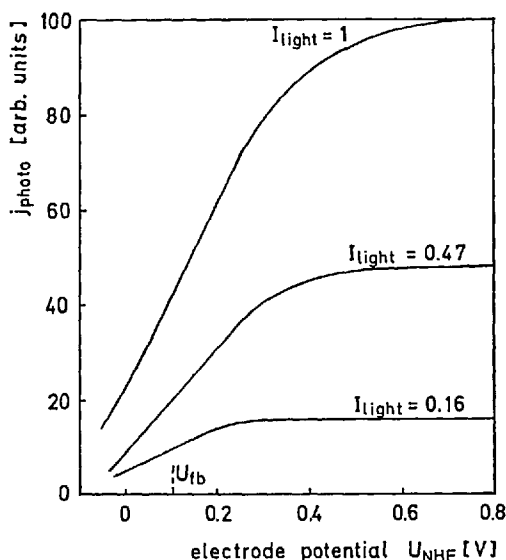
Fig. 13. Photocurrent versus voltage curves for n-ZnO-electrode with adsorbed rhodamine B at pH $= 5$ under illumination with different light intensities ($\lambda = 570$ nm)

of 0.25 eV in the depletion layer back-capturing of electrons by oxidized dye molecules is negligible. The photocurrent increases linearly with light intensity as is expected for a one-quantum, monomolecular process.

The photocurrent spectrum corresponds in this case almost fully to the absorption spectrum of the dye in solution. This is shown in Fig. 14 where we see the photocurrent, measured in the potential range of current saturation of Fig. 13, depending on the wavenumber. The current has been corrected for constant quantum flux from the light source (a Xenon lamp with monochromator). The picture contains also the absorption spectrum of the dye in solution in a normalized scale to coincide at the absorption maximum with the photocurrent maximum. One sees a slight shift of the photocurrent spectrum to longer wavelengths which must be attributed to an adsorption interaction being stronger in the excited state than in the ground state [4]. Clearly, sensitized photocurrents can only be measured in spectral ranges where the basic photocurrent of the semiconductor is relatively small.

The close correspondence between the absorption spectrum in solution and the photocurrent spectrum of the adsorbed dye is by no means found in all cases. The adsorbed state can be different in structure from the solution state which is seen in a different photocurrent spectrum. It has been found e. g. that polymers are formed in the adsorbed state. This is a well known phenomenon for cyanine dyes [50,51] where polymer bands are found in the absorption spectrum of the adsorbed molecules. An example is given in the photocurrent spectra of Fig. 15. One sees that with increasing amount of adsorbed dye — no equilibrium adsorption was reached during this experiment — the polymer absorption band appears in the photocurrent.
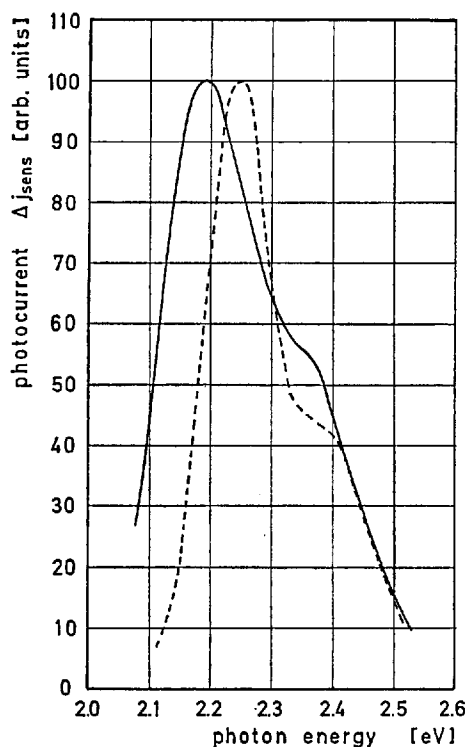
Fig. 14. Photocurrent spectrum at $U_{NHE} = +0.5$ V for system of Fig. 13 in comparison with absorption spectrum of the dye in solution (dashed curve)

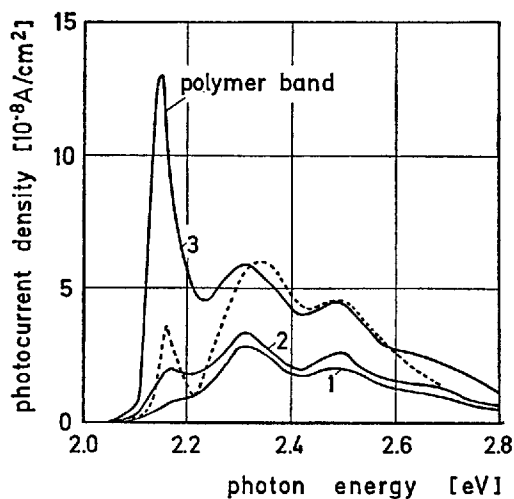Fig. 15. Photocurrent spectra for n-ZnO-electrode (at pH $= 5$) with different amounts of adsorbed cyanine dye, increasing in concentration from 1 to 3. For comparison the light absorption spectrum of the adsorbed dye on ZnO (dashed curve)

It is unlikely in such cases where different species exist on the surface that the photocurrent spectrum coincides with the absorption spectrum, since the efficiency of charge transfer will be different for different species. Memming [52] has concluded that for a cyanine dye adsorbed on a SnO_2-electrode the monomer seems to be more effective for charge injection than the dimer or higher aggregates. Hauffe and co-worker [53] have found that chelating dyes are especially efficient for sensitized electron injection into ZnO-electrodes which is seen in the variation of the photocurrent spectrum.

Electron injection from excited dye molecules has been also observed with SnO_2- [7,52], TiO_2- [45], and CdS-electrodes [54,55]. The position of the conduction band edges of these materials in a solution of pH 7 (compare Fig. 12) is below or around the estimated energy level of the excited rhodamine B (or cyanine-dyes) (see p. 50), when acting as a donor, but the energy level for the excited molecule acting as an acceptor is above the valence band edges of these semiconductors. The energy levels $_0E_{D^*_{don}}$ and $_0E_{D^*_{acc}}$ for rhodamine B are indicated in Fig. 11. One sees that the experiments agree well with the theoretical conditions derived in the first chapter.

Dye sensitization plays an important role in photography. The sensitization mechanism for ZnO-materials as used in electro-photography is obviously in complete correspondence with these electrochemical experiments as shown for single crystals under high vacuum conditions by Heiland [56] and for imbedded ZnO-particles by Hauffe [57]. Even for silver halides where electron injection as sensitization mechanism has been questioned by the energy transfer mechanism [58] electrochemical experiments have shown that the electron injection mechanism is at least energetically possible in contact with electrolytes [59]. Silver halides behave as mixed conductors with predominance of ionic conductivity at room temperature. These results will therefore not be discussed here in any detail since such electrodes are quite inconvenient for the study of excited dye molecules.

4. Hole Injection

According to our energy conditions of Fig. 7, materials suitable for hole injection must have a relative high energy position of the valence band edge. From Fig. 12 we learn that this is the case for GaP, and CdSe. CdS could be a candidate but it is not available as p-type material. Besides p-GaP only p-SiC (band gap 3 eV) [7] has been used for the study of hole injection from excited dye molecules.

In Fig. 16 we show a current-voltage curve for p-type GaP in the presence of a dye in the dark and at illumination with light being only absorbed by the dye. We see again a saturation current, now however, in cathodic direction. The photocurrent spectrum is represented in Fig. 17. It corresponds fully with the absorption spectrum of the adsorbed dye. One sees a saturation current at a polarisation of more than 0.35 eV negative of the flat band potential. Some special features at GaP-electrodes seem to be caused by the existence of surface states with energies in the range of the band gap. It has been assumed that these surface states can
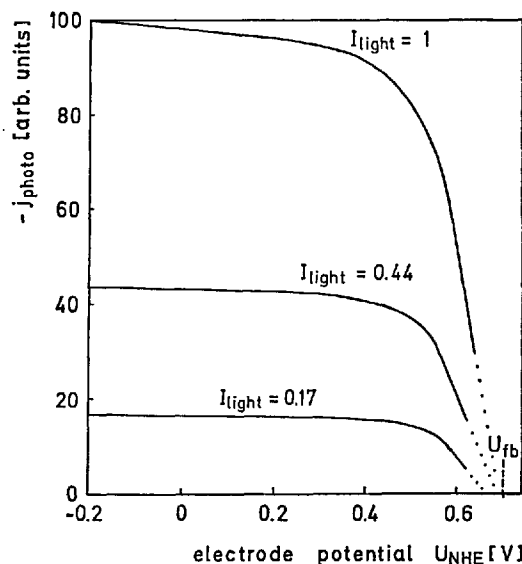
Fig. 16. Photocurrent-voltage curves for p-GaP in contact with crystalviolet containing electrolyte (pH = 2) for various illumination intensities (λ = 580 nm)
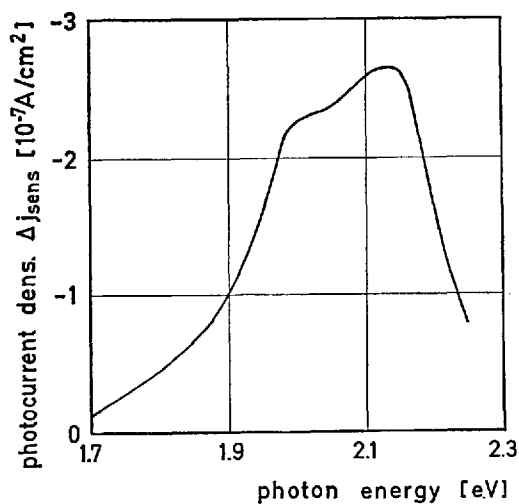
Fig. 17. Photocurrent spectrum for system of Fig. 16. $U_{NHE} = -0.45$ V

act as energy acceptors and quench the sensitized photocurrent by energy transfer with consecutive desactivation without charge separation [60]. It is, however, not yet clear whether this interpretation is correct since the derivation from the experiments included the unlikely assumption that energy transfer occurred prior to vibrational relaxation of the excited state.

5. Relaxation Phenomena and Supersensitization

All photocurrents described in the previous sections have been measured under steady state conditions. Since photo-oxidation or photo-reduction of the dye causes chemical change a steady state can only be reached when the consumed dye molecules can be restored either by exchange of the products with dye molecules from solution or by an inverse redox reaction with some component of the solution. Both processes need some time to reach the steady state. Exchange of adsorbed molecules with fresh dye molecules from solution is usually a very ineffective and slow process. One reason is that the products often do not desorb from the electrode surface, another that the dye concentration in solution is usually kept very small to avoid light absorption by the solution. In most experimental arrangements it is necessary to illuminate the electrode through the solution. Only in a few systems semiconductors are available in such sizes that the transparency of the materials in the wavelength range of sensitization can be used for illumination through the electrode [31,48].

It has further tacitly been assumed that photocurrents can only be induced by excited dye molecules in the absorbed state on the electrode surface. Although one would expect that excited dye molecules in solution should be able to exchange electrons with the electrode by approach from the solution [26], the lifetime of excited molecules is too short and the excess of adsorbed molecules over the amount of dissolved ones in a layer of $\sqrt{D\tau} \approx 10^{-7}$ cm thickness is too high as to detect charge injection from dissolved molecules, besides that from adsorbed ones.

In most cases the photocurrent decreases with time according to a consumption of the dye. In the absence of any supply from the solution one can use this for a kind of coulometric titration of the amount of adsorbed dye molecules. The decrease can be avoided by addition of a redox couple which regenerates the oxidized or reduced dye molecules directly in its adsorbed state [31].

The redox potential of this regenerating couple has to be either more negative than the oxidative redox potential of the dye ($^0E_{D/D^+}$) in the case of electron injection from D^*, or more positive than the reductive redox potential ($^0E_{D/D^-}$) in the case of hole injection from D*. A simple "term scheme" of such a charge injection with regeneration of the reaction products is given in Fig. 18. Such a

a)
$D^* \rightarrow D^+ + e^-$
$D^+ + R_{donor} \rightarrow D + R^+$

b)
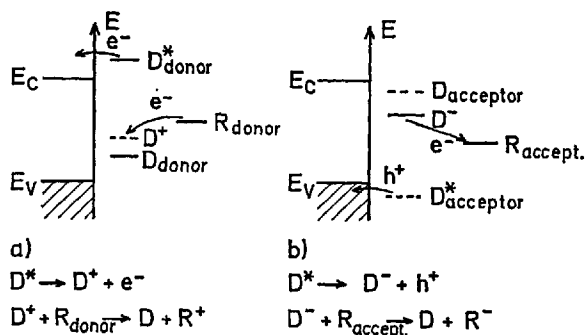$D^* \rightarrow D^- + h^+$
$D^- + R_{accept.} \rightarrow D + R^-$

Fig. 18. Electron energy correlations for regeneration of dyes after electron transfer in the excited state by redox reactions with electron donors or acceptors

behaviour may often be mixed up with supersensitization since it grants the highest possible efficiency of the adsorbed dyes and a repetitive action of the same molecules. However, it does not really change the sensitization behaviour of the dye.

The relaxation behaviour of the sensitized photocurrent at a ZnO-electrode during a light pulse in the absence and in the presence of a regenerative redox system is shown in Fig. 19. One sees that the current decreases exponentially with time if no regeneration of the oxidized dye molecule is possible, while in presence of such a regenerator the current reaches a steady state after a short period [61]. The initial current is smaller in the presence of the regenerating redox system, in this case this is caused by a competitive adsorption of the hydrochinone used as regenerator which decreases the adsorbed amount of the dye. It is not a general effect.
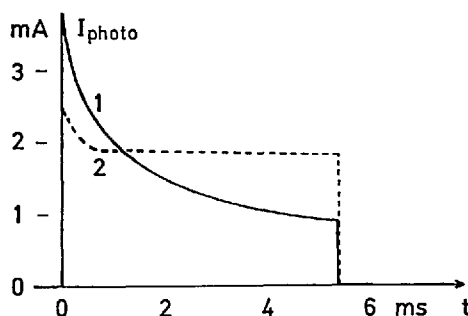

Fig. 19. Photocurrent during light pulse (Ar-Laser, 514 nm, 1 W) at moderately doped ZnO_2 electrode ($N_D \approx 10^{17}$ cm^{-3}) with rhodamine B, in absence of hydrochinon (1) , in presence of 10^{-3} M hydrochinon (2)

There is another possible mechanism which really deserves the name super-sensitization because the charge injection becomes either only just possible or is largely increased by the interaction between dye molecule and supersensitizer. This is the case if the excited dye molecule reacts at first with the supersensitizer and reaches in this way a state where it can inject an electric charge even in the ground state. The "term scheme" for this mechanism is shown in Fig. 20. The assumption here is that the excited state of the molecule as a donor cannot inject an electron into the conduction band or can do this only very ineffectively. It can, however, act as an electron acceptor against the supersensitizer.

The electron energy term of the reduced dye may then be so energetic that direct electron injection is possible as indicated in Fig. 20a. The energy conditions for the inverse mechanism with hole injection by the oxidized dye (which reacts in the excited state primarily with an oxidizing supersensitizer) are shown in Fig. 20b.

It is characteristic for the above mechanism that the photocurrent spectrum is not changed by the presence of the supersensitizer. A change in the spectrum is only to be expected if the interaction between the dye molecule and the super-sensitizer has already occurred in the ground state. Though this possibility has
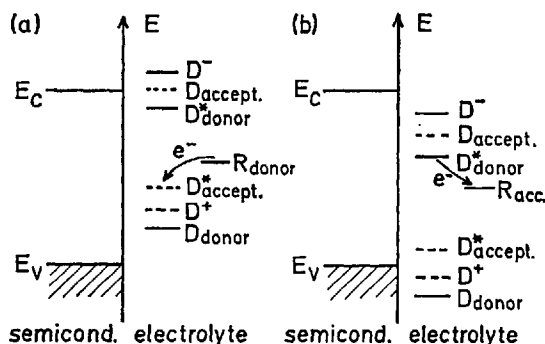
Fig. 20. Energy correlations for a mechanism of supersensitization by photoreduction (a) or photooxidation (b) of the excited dye prior to electron transfer

been discussed frequently in photographic systems [62], an unquestionable example for this mechanism has not yet been found in the electrode reactions of excited dye molecules.

Coming back now to the relaxation processes during dye sensitized charge injection we want to discuss a special case where the oxidation and regeneration of the dye molecules could be directly followed in the current. This is possible if the regeneration occurs also by an electric current of the electrode. One needs for this purpose a very highly doped semiconductor electrode at which the barrier layer of the space charge is so thin that the reverse electron transfer after charge injection is possible by tunnelling. This can be reached with ZnO- and SnO$_2$-electrodes [46,61,63].

In such systems the current relaxation curves look different from those of Fig. 20. After the termination of the light pulse an inverse current can be observed as shown in Fig. 21 [61]. This reverse current is caused by reduction of photo-
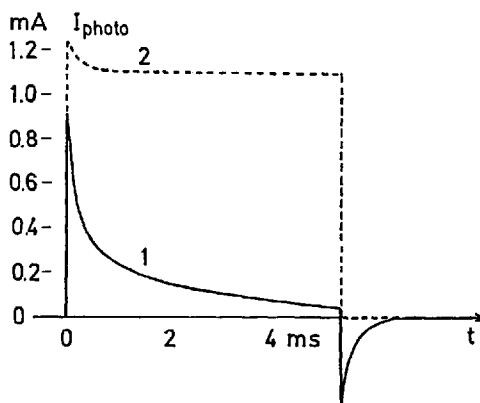

Fig. 21. Photocurrent during light pulse as in Fig. 19 at highly doped ZnO electrode ($N_D \approx 10^{20}$ cm^{-3}) (1) no hydrochinon (2) 10^{-3} M hydrochinon

oxidized dye molecules through electrons which can tunnel back from the conduction band through the barrier layer. The regeneration by a redox system in solution, however, is much more efficient as indicated by the absence of the reverse current in presence of the regenerator.

It is striking to note in Fig. 21 that in contrast to the results shown in Fig. 19 even the initial current is higher in the presence of the regenerator. This has been interpreted [61] as a competition between energy transfer and photoreduction of the excited dye molecule prior to electron injection. Energy transfer is possible from the excited dye molecule to the electrons in the conduction band which are close enough to the surface in such a thin space charge barrier. This reduces the photocurrent by electron injection from the excited dye. On the other hand, a photoreduction of the excited dye can cause electron injection from the reduced dye molecule according to the mechanism of Fig. 19 a. The net results depend on the particular rate constants. The different reactions which seem to occur simultaneously in the system of Fig. 21 are summarized in Fig. 22. We learn from these experiments that the mechanism of supersensitization can be quite complex and also that relaxation experiments where they can be applied give much more information than steady state measurements.
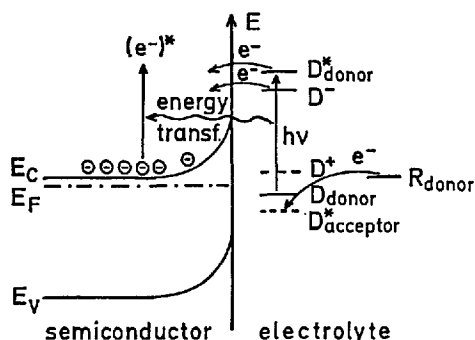
Fig. 22. Energy scheme for reactions at highly doped semiconductor with very small depletion barrier.

Reactions:

$$D \xrightarrow{h\nu} D^*$$

$$D^*_{don} \longrightarrow D^+ + e^- \text{ (injection)}$$

$$D^*_{aac} + R_{don} \longrightarrow D^- + R^+ \text{ (photoreduction)}$$

$$D^- \longrightarrow D + e^- \text{ (injection)}$$

$$D^* \longrightarrow D + (e^-)^* \text{ (quenching)}$$

$$D^+ + e^- \longrightarrow D \text{ (reverse electron transfer by tunnelling)}$$
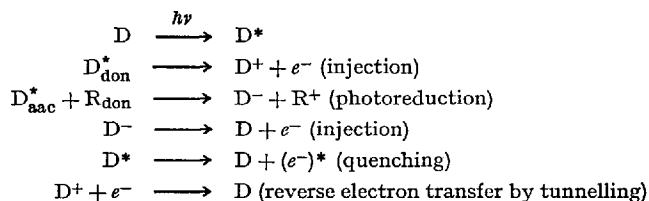
Summarizing the results obtained up to now with semiconductor electrodes and excited dye molecules one can say that it is possible by using different semiconductors to get an approximate information on the energy position of the electron exchange orbitals of excited molecules in solution. In future it should become possible to study photochemical reactions with other reactants by competition with the electrode reaction (quenching for instance) and to analyse in this way

mechanisms of more complicated photoreactions. Proceeding to non-aqueous solvents may be especially useful because a much greater variety of photoreactions will then become accessible.

IV. Reactions at Organic Insulator Crystals

1. Measuring Device

Before describing dye sensitized electron transfer reactions at the surface of organic crystals a few remarks shall be made concerning experimental peculiarities of the system.

Firstly, organic crystals are insulators with a wide band gap (> 3 eV [64]) and narrow conduction and valence bands (a few kT wide [65]). Correspondingly the current voltage curve is that for charge injection into a dielectric medium [66]. The injection current can saturate at higher voltages when it is limited by charge generation and destruction at the crystal surface. Some more details of the process are explained in Section 5 below. To obtain the desired direct correspondence between the rate of charge generation at the crystal surface and the magnitude of the injection current flowing through the crystal bulk a large voltage has to be applied far beyond the space charge limited range of the current voltage curve. The thickness of the crystals has to be kept $\leqslant 50\ \mu$ in order to allow for the measurement of a current versus applied field strength curve extending up to 10^6 V/cm (limited by electric breakdown [67]). This way an unambiguous determination of the contact controlled injection current is ensured, provided the other two conditions are met concerning the contact formation and the composition of the electrolytic contact.

Charge carriers at the crystal surface undergo slow side reactions with solvent molecules (*e.g.* holes with OH$^-$) thereby changing the chemical nature of the crystal surface. Mechanical polishing cannot be carried out since the next crystal planes adjacent to the surface can be damaged easily through such a procedure on such fragile crystals. Therefore, to exclude the deteriorating effect of side reactions prior and during the measurement of the injection current a freshly grown crystal surface has to be used for each experiment and a specific technique of contact formation has been developed [68] which is seen in Fig. 23. Furthermore, the electrolytic contact has to be composed in such a way that the destruction of charge carriers through solute molecules can be neglected or at least its effect can be corrected through an independent measurement [69].

The solution of the charge injecting species is dropped from a pipette on the virgin crystal surface with the opposite crystal surface already in contact with an electrolyte suitable for discharging the charge carriers to be injected and connected through a platinum wire to the second pole of the voltage supply. The falling droplet of the charge injecting solution first touches the other platinum wire connected to the first pole of the voltage supply before reaching the virgin crystal surface and thereby switches the voltage across the crystal bulk.

The above procedure ensures a low density of injected charge carriers at the crystal surface and only about 3 ms elapse (due to the spreading of the solution over the crystal surface) before the current reading is obtained [68]. When charge
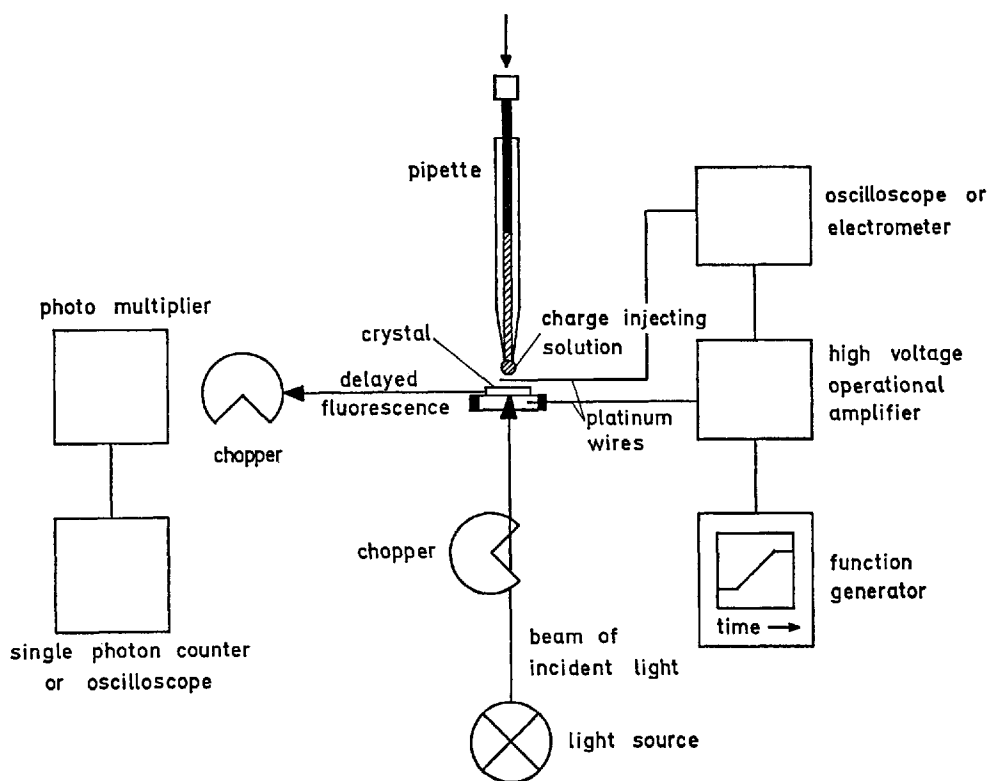
Fig. 23. Experimental set-up for the measurement of dye sensitized charge injection in organic crystals and of dye sensitized delayed fluorescence of the crystal

injection occurs only through light absorption corresponding precautions have to be taken *e.g.* the light is switched on only after the voltage has been applied to the crystal. The light intensity should be as low as possible and the measuring time should not exceed more than *e.g.* 5 minutes.

An experimental set-up suitable for measuring dye sensitized injection currents and dye sensitized delayed fluorescence of the crystal is shown in Fig. 23. To shield the photomultiplier (detection of the fluorescence) from the incident light beam the two light choppers in Fig. 23 are rotating with a corresponding phase shift.

2. Energy Correlations

The organic single crystals considered here for hole injection are composed of aromatic molecules with the following structural formulas:
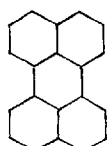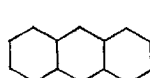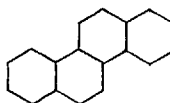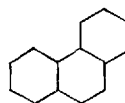
perylene   anthracene   chrysene   phenanthrene

The elementary cell of the single crystals is monoclinic with 4 or 2 molecules per unit cell for α-perylene and chrysene or anthracene and phenanthrene respectively [70,71,72,73]. Until now the sensitized hole generation has only been studied at the 001 plane of these crystals. The planar area of the organic molecules is turned away by a large angle from the 001 plane. The molecules in the crystal are facing the adsorbed dye molecule with their rims. Thus, no sandwich arrangement can be formed between the dye molecule and a crystal molecule at the ideal 001 surface of the crystal as shown later in Fig. 30.
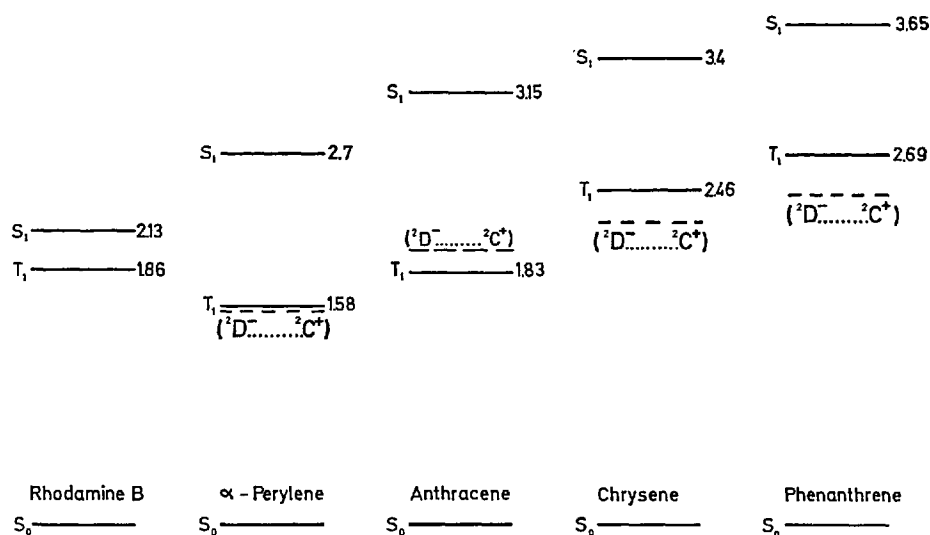
Fig. 24. Energy of the excited singlet state S_1 and triplet state T_1 of rhodamine B [10] ($S_1 = {}^1D^*$, $T_1 = {}^3D^*$) and of the organic crystals ($S_1 = {}^1C^*$, $T_1 = {}^3C^*$) [74–78]. The energy of the reduced dye-hole pair ($^2D^- \ldots {}^2C^+$) is also shown as derived from the experimental yield curve (compare Figs. 31 and 32)

The excited singlet and triplet states of these crystals [74–78], are shown together with those of rhodamine B in Fig. 24. Obviously, the excited singlet state of rhodamine B can be reached without exciting the singlet state in the crystals. Even for very thick crystals (μm to mm) the absorption $\varepsilon d < 10^{-4}$ of the triplet state in the crystal is negligible compared to the absorption of the singlet state of the adsorbed dye molecules even at small coverage of the crystal surface (see below). Therefore, the adsorbed dye molecules can be illuminated with a beam passing through the crystal bulk. This way there is no correction necessary for light absorption by dye molecules in the solution. However, the triplet state of the crystal can be populated by an indirect reaction path after excitation of the excited singlet state of rhodamine B and consecutive formation of the "reduced dye-hole pair" ($^2D^- \ldots {}^2C^+$) with an energy obtained from the experiments as shown in Fig. 24 (see Section 7).

Sensitized hole generation in the organic crystals involves the ionisation energies at the surface of the organic crystals shown in Table 1 which have been derived from thermally activated electron transfer to redox ions [79].

Table 1. Ionisation energies I_c of the organic crystals in eV

	α-Perylene	Anthracene	Chrysene	Phenanthrene
Crystal	5.33	5.8	5.98	6.19
Molecule [80]	7.00	7.47	7.60	7.86

Going from α-perylene to phenanthrene the ionisation energy is increased by 0.86 eV. We see from the ionisation energies of the organic crystals in Table 1 and the above estimated reduction potential $^0E^1_{D*/D-} = -5.88$ eV (electron affinity) for the excited singlet state of rhodamine B that for hole injection the free energy change ΔG^0 should go from a large negative value at perylene through zero at about anthracene and finally to a large positive value at phenanthrene. As will be seen later such an energy correlation is indeed borne out by the experimentally determined quantum yield for sensitized hole generation at these different organic crystals. Since rhodamine B has been used in most of the investigations of sensitized charge generation at organic crystals we will also consider it as our typical dye molecule. The effect of different properties of other dye molecules on the reaction paths shall be mentioned in the respective place in the discussion.

The above ionisation energies of these organic crystals together with their band gap > 3 eV yield positions of their conduction band < 2.3 eV [64]. Since the oxidation potential (ionisation energy) for the excited singlet state of rhodamine B is expected around $^0E^1_{D*/D+} = -3.17$ eV (see above) we can neglect direct sensitized electron injection implying an "uphill" electron transfer with a free energy change $\Delta G^0 > 1$ eV for rhodamine B at these organic crystals. A suitably large electron affinity, *i.e.* a low enough empty conduction band for sensitized electron injection can be attained only by introducing electron attracting atoms instead of hydrogen. The electron affinity of the chloranil crystal has been found around 4 eV [81] which is sufficiently large to allow for direct electron injection through the excited rhodamine B molecule with an ionisation energy estimated around 3.2 eV. The choranil molecule has the following structural formula:
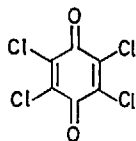
The ionisation energy of the chloranil crystal is expected to be so large that sensitized hole injection through excited rhodamine B can be neglected.

3. Survey of the Main Observations

3.1. Hole Injection

Hole injection in the fully occupied valence band of anthracene through excited rhodamine B molecules adsorbed at the crystal surface has been discovered in 1963 by Steketee and deJonge [82]. Mulder has investigated this effect for a number of dyes at anthracene and perylene crystals [83]. Mulder and deJonge have found that the excited singlet state of adsorbed dye molecules can be populated more effectively by energy transfer from mobile singlet excitons produced in a strong $S_0 - S_1$ transition in the surface layer of the organic crystal than by direct absorption of the incident photons [84]. The energy transfer from the crystal to the dye allows for a thicker absorbing layer in the crystal than the approximately monomolecular layer of the adsorbed dye molecules. Thus, a larger quantum efficiency for sensitized hole injection is reached referring to the number of incident photons per unit time. Gerischer, Michel-Beyerle, and Rebentrost have pointed out the necessity to reoxidize the reduced dye molecules through redox ions in order to obtain a stationary current flow [85]. Nickel, Staerck and Weller have found delayed fluorescence of the anthracene crystal stemming from excited rhodamine B molecules at the crystal surface [86]. This observation of dye sensitized delayed fluorescence of the crystal gave definite proof for yet another reaction path besides hole injection. Nickel showed that sensitized delayed fluorescence of the crystal can originate from intersystem crossing in the adsorbed dye molecule and consecutive energy transfer or from voltage dependent recombination of the injected hole with the reduced dye molecule [87]. Willig and Michel-Beyerle compared the quantum yield of rhodamine B sensitized hole injection with the difference between the ionisation energies of organic crystals and the electron affinity of the excited dye molecule [88]. The estimated free energy correlation between rhodamine B and the organic crystals has been confirmed recently through measurements at phenanthrene [89] (see also Section 7). Groff, Suna, Avakian, and Merrifield have observed a decrease in the rhodamine B sensitized delayed fluorescence in anthracene in the presence of a small magnetic field and have presented a quantitative model explaining the formation of the triplet state in the reduced dye-hole pair produced through the reaction of the singlet state of the excited dye and the singlet ground state of the organic crystal [90,91]. For this triplet formation from singlet states to occur, spin randomization is not required but an asymmetric spin Hamiltonian due to a stronger hyperfine interaction of one of the two particles either the hole in the organic crystal or the electron at the reduced dye as will be discussed below.

Before looking at the complete reaction scheme emerging from these observations we list the principal events leading to the stationary dye sensitized hole current in organic crystals.

1) Excitation of the adsorbed dye molecule symbolized as $(^1D_0 \ldots {}^1C_0)$ with photons of energy $h\nu_D = \Delta^1E^*$ e.g. yellow light in the case of rhodamine B.

$$(^1D_0 \ldots {}^1C_0) + h\nu_D \longrightarrow (^1D^* \ldots {}^1C_0)$$

2) Generation of a defect-electron $\oplus$ which contributes to the current flow:

$$(^1D \ldots *^1C_0) \longrightarrow (^2D^- \ldots {}^1C_0) + \quad \oplus$$
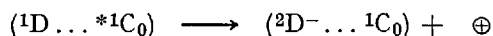
The occurrence of processes 1) and 2) is at once evident from the observation of the sensitized hole current in an organic crystal with an excitation spectrum closely resembling the absorption spectrum of the dye and with a linear dependence on the light intensity. Fig. 25 shows the identity (except for a slight red shift) of the absorption spectrum ε of the rhodamine B monomer with the excitation spectrum of the corresponding sensitized current j of a 10^{-6} M solution at phenanthrene.
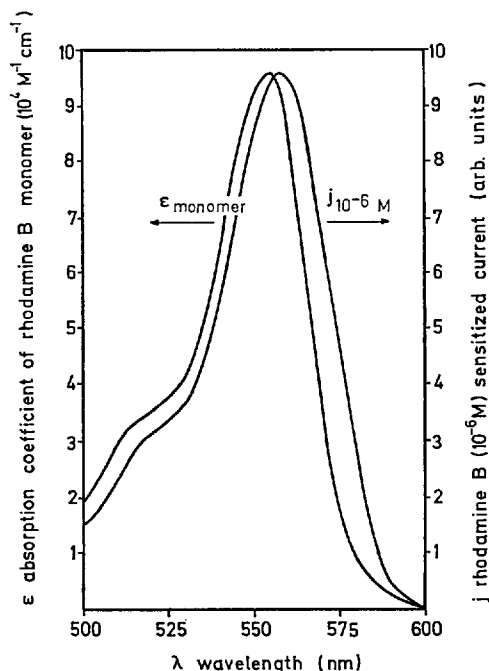
Fig. 25. Comparison between the excitation spectrum of the rhodamine B sensitized current J_M in phenanthrene (dye coverage $\theta = 0.4$ for 10^{-6} M rhodamine B in aqueous solution at pH $= 7$) with the absorption coefficient $\varepsilon_{monomer}$ of the rhodamine B monomer in aqueous solution at pH $= 7$

3) To observe a stationary current flow it is necessary to reoxidize the reduced dye molecule by an electron acceptor Ox:

$$(^2D^- \ldots {}^1C_0) + Ox \longrightarrow (^1D_0 \ldots {}^1C_0) + Ox^-$$
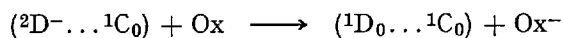
Reaction (3) completes the cycle and we can start again with reaction (1). Besides reactions (1), (2), and (3) side reactions also occur. The most interesting

example is the population of the triplet state of the organic crystal and possibly also of the adsorbed dye. The triplet state of the crystal can be populated *e.g.* via recombination of the reduced dye-hole pair in the triplet spin state [87,90]. This way the excitation of the singlet state of rhodamine B with energy $h\nu_D$ renders triplet excitons in an anthracene crystal (first line in process 4). Two triplet excitons can form a singlet excition (second line in process 4) which finally decays by emitting the blue fluorescence of the anthracene crystal with energy $h\nu_c > h\nu_D$ (third line in process 4).

4)
$$(^1D^* \ldots {}^1C_0) \longrightarrow (^1D_0 \ldots {}^3C^*)$$
$$^3C^* + {}^3C^* \longrightarrow {}^1C^* + {}^1C_0$$
$$^1C^* \longrightarrow {}^1C_0 + h\nu_C$$
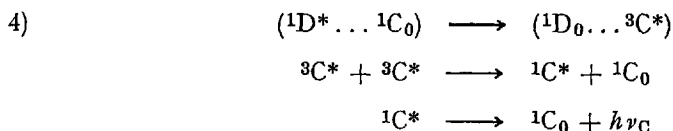
The overall rate constants and yield expressions for processes 2) to 4) can be split up into rate constants for individual reaction steps using the reaction scheme shown below (Fig. 26).
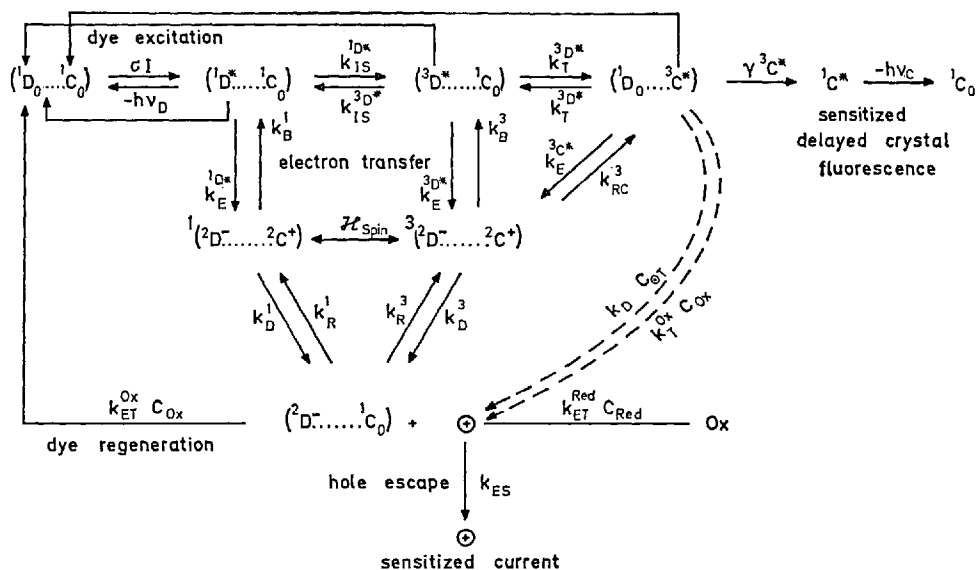
Fig. 26. General reaction scheme for dye sensitized hole injection in organic crystals. The scheme shows the excitation of the adsorbed dye ($^1D_0 \ldots {}^1C_0$) in the first row at the left hand side. Through electron transfer the "reduced dye-hole pair" ($^2D^- \ldots {}^2C^+$) is generated with its singlet and triplet spin state (2. row). The dissociated "reduced dye-hole pair" is shown in the third row, and finally the hole $\oplus$ contributing to the injection current in the fourth row. The regeneration of the dye molecules can be seen on the left hand side of the third row and the generation of sensitized delayed crystal fluorescence in the first row on the right hand side. Details are explained in Section IV 4 of the text

3.2. Electron Injection

Dye sensitized electron injection in the empty conduction band of chloranil has been described by Michel-Beyerle and Brickl [92]. The principal events listed in points 1) to 3) for hole injection also apply in the corresponding formulation to sensitized electron injection. The detailed formulation of a reaction scheme, however, is more complicated for sensitized electron injection at chloranil since protons also can take part in the formation of the reduced hydrochinone form of the reduced chloranil molecule.

In the next 4 sections we shall give a more detailed account of the individual reaction paths connected with hole injection when an excited dye molecule is formed at the surface of an organic crystal.

4. Reaction Scheme for Hole Injection

The reaction scheme in Fig. 26 gives a detailed picture of the main reactions initiated by the excitation of the dye molecule at the surface of an organic crystal. The rate constants connecting the reactants with the products are given in the dimensions s^{-1} for monomolecular reactions and in the dimensions $cm^3 \, s^{-1}$ for biomolecular reactions. Going from left to right in the first line σJ describes the excitation of an adsorbed dye molecule ($^1D_0---^1C_0$) to its ecited singlet state ($^1D^*---^1C_0$), $\sigma =$ absorption cross section for a photon, $J =$ light intensity. $k_{IS} =$ intersystem crossing to the triplet state of the dye ($^3D^*---^1C_0$). $k_T^{3D^*} =$ energy transfer to the triplet state of the crystal ($^1D_0 \ldots {}^3C^*$). $\gamma {}^3C^* =$ bimolecular reaction of two triplet excitons yielding the excited singlet state of the crystal $^1C^*$ which finally emits a photo $h\nu_c$ yielding the ground state $^1C_0$. Thus, all forward reactions in the first line finally yield the sensitized delayed fluorescence of the crystal via energy transfer from the triplet state of the dye to that of the crystal. The meaning of the reverse reactions is obvious.

In the second line the singlet and the triplet configurations of the "reduced dye-hole pair" are symbolized by $^1(^2D^- \ldots {}^2C^+)$ and $^3(^2D^- \ldots {}^2C^+)$. The range of the dipole interaction between the spins of the hole in the organic crystal and the electron at the dye has been estimated as 15 Å [90] implying on average (see below) the hole at 5 equivalent next neighbour positions to the reduced dye in the ab plane of the organic crystal. From the species in the first line of Fig. 26 rate constants k_E for the activation of the electron transfer reactions lead to the reduced dye-hole pair in the second line. Such activation involves changes in the distance between the reactants, changes in bond-lengths and bond-angles and also changes in the solvent- and ionic-environment [16-19,93]. The rate constant for activation of electron transfer also depends on the free energy barrier ΔG^0 of the reaction, *i.e.* the difference between the ionisation energy of the crystal and the electron affinity of the excited dye corrected for the interaction in the reactant and product state [16-19,93]. The change of the spin in the electron-hole pair produced from the excited singlet state of the dye and the singlet ground state of the crystal is brought about through a spin Hamiltonian $\mathcal{H}_{spin}$ which is asymmetric in the hyperfine coupling of one of the particles (either electron or hole) [90,91]. Thus,

even though intersystem crossing is small in the individual reactants *e.g.* the rhodamine B molecule and the anthracene crystal, the triplet state can be effectively populated in the reduced dye-hole pair. Details will be discussed in section 8 below.

For the discussion in Section 8 it is meaningful to formulate in the third line separately the dissociated reduced dye-hole pair with the hole still remaining at the crystal surface but separated from the reduced parent dye molecule $(^2D^-\dots{}^1C_0)$ by more than 1 molecular diameter. The final escape of the hole is characterized by k_{ES} = reciprocal escape time for the hole to reach a position in the crystal bulk where the applied field dominates over the attraction due to its counter and image charge in the solution. Thus, this rate constant k_{ES} implies the field assisted Brownian motion of the hole (including the time spent in traps) leading out of the potential well at the crystal surface [79]. The reduced dye molecule $(^2D^-\dots{}^1C_0)$ is oxidized (regeneration) with a rate $C_{Ox}k_{ET}^{Ox}$, C_{Ox} = concentration of the oxidized redox ions, yielding again the adsorbed dye molecule in the ground state $(^1D_0\dots{}^1C_0)$. Hole-generation through sidepaths is also indicated, mainly detrapping of holes in surface traps with concentration $n_{\oplus T}$ through photons and triplet excitions [94] and possibly electron transfer from the triplet exciton to the oxidized redox ion with rate constant k_T^{Ox} [95].

5. Sensitized Hole Currents in Organic Crystals

The generation of a hole at the surface of the organic crystal is measured as current flow through the bulk of the organic crystal. Electron exchange with excited dye molecules leads to the formation of a stationary positive space charge in the organic insulator crystal. When an external voltage is applied to the crystal a space charge limited current flows through the crystal bulk which rises steeply with increasing voltage (dashed curve in Fig. 27). It is controlled by bulk properties of the organic crystal [96]. When a sufficiently large voltage is applied, the current is controlled by contact properties, *i.e.* the generation and destruction of holes at the crystal surface. In the present context only the latter range of the current voltage curve is of interest to us.

In spite of the Coulombic attraction between the injected hole and the reduced dye molecule the hole can dissociate from the electron at the dye with the rate constant k_D in the reaction scheme (Fig. 26). Other ions in the solution then can take over the role of the negative counter charge for the injected hole and only after a number of encounters with the crystal surface (including the time spent in traps) the hole finally can escape over the potential barrier with rate constant k_{ES}. The form of the potential barrier is somewhat time dependent due to several relaxation times in the system. The hole spends an overalll time of *e.g.* about 10^{-8} s at the surface of our perylene crystals at an external field strength of 10^5 V/cm [79]. A competition with the escape of the hole from its counter and image charge in the solution arises from its recombination with the parent reduced dye molecule (rate constants k_R and k_B) or with other electron donors with rate constant k_{ET}^{Red} C_{Red}. The rate constants k_B and k_{ET}^{Red} depend on the respective activation times for electron transfer to the hole which can be derived from the free energy plots for the generation reactions (see Section 7). A recombination with other reduced
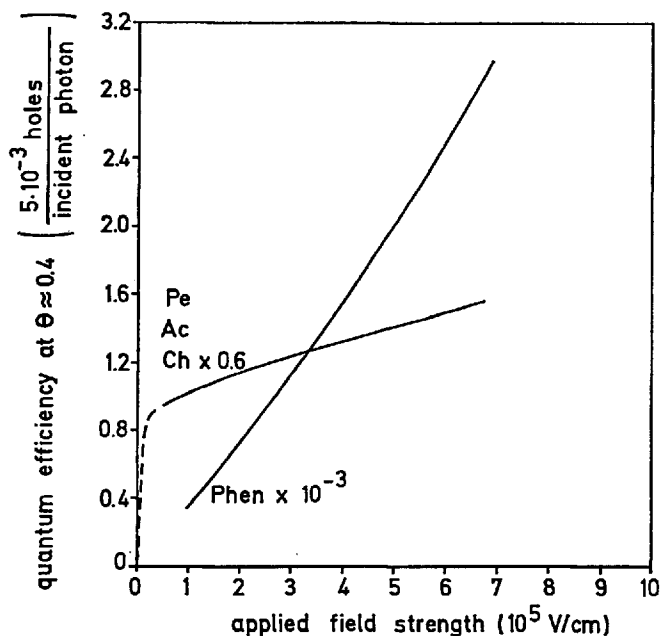
Fig. 27. Quantum efficiency of sensitized hole injection in organic crystals (injected holes per incident photon) versus applied field strength (ratio of voltage to crystal thickness) Pe = perylene, Ar = anthracene, Ch = chrysene, Phen = phenanthrene

dye molecules can be prevented by using low light intensity and a sufficiently fast regeneration reaction $k_{\text{ET}}^{\text{Ox}} C_{\text{Ox}}$ for the reduced dye molecule.

According to Fig. 26 the probability P_{es} for the hole to escape from the crystal surface can be written as follows:

$$P_{\text{es}} = P_{\text{es}}^{\text{g}} \frac{k_{\text{ES}}}{k_{\text{ES}} + k_{\text{ET}}^{\text{RED}} C_{\text{Red}}} \tag{37}$$

With P_{es}^{g} = probability for the excape of the hole from its parent reduced dye molecule.

Through the external field strength the depth and width of the potential well for the hole is decreased and thus the escape probability is enhanced. For a small concentration of the electron donors C_{Red} and with a large external field strength $\geqslant 10^5$ V/cm the overall excape time for the hole at perylene, anthracene and chrysene is sufficiently short compared to the time necessary for electron capture at the crystal surface to yield an escape probability $P_{\text{es}} \approx 1$ for every hole generated at the crystal surface.

The corresponding injection currents for sensitized hole generation are almost independent of the applied voltage. The remaining increase in the quantum efficiency (holes per incident photon) with rising external field strength (Fig. 27) corresponds to a relative linear increase of the current with a coefficient of 10^{-6} $\frac{\text{cm}}{\text{V}}$ also observed for saturation currents in the dark [68]. Since this influence of the external field is not observed for diffusion controlled hole injection [68] it is ten-

tatively attributed to a decrease in electron hole recombination k_R taking place before the hole leaves the immediate vicinity of the still activated electron acceptor. Except for this small effect the sentisized injection currents at perylene, anthracene and chrysene are saturation currents for sensitized hole generation.

In contrast with phenanthrene the rhodamine B sensitized injection current remains smaller by a factor of about 10^{-3} and rises steeply with increasing external field strength as shown in Fig. 27 independent of the light intensity [89]. This strong influence of the external field indicates a fast recombination reaction taking place during the encounters between the hole and the parent reduced dye molecule after their first dissociation. For donating the electron back to the hole the reduced dye molecule at phenanthrene needs a very short activation time τ_E^b (corresponding to rate constants k_B in Fig. 26) compared to the time the hole spends in the immediate vicinity of the reduced dye molecule [79]. As will be shown in Section 7 such a short activation time is indeed expected at phenanthrene from the free energy plot for the reverse electron transfer reaction k_B^1 leading back to the excited singlet state of rhodamine B.

The quantum efficiencies shown in Fig. 27 have been determined with the 568.2 nm beam of a Krypton laser (compare Fig. 25) attenuated to $3 \cdot 10^{14}$ photons/ cm^2 s. The field dependence has been measured 4 minutes after contact formation between the dye solution and the virgin crystal surface when the dye adsorption has attained virtually its equilibrium value. The estimate for the dye coverage $\theta = 0.4$ indicated at the ordinate of Fig. 27 will be explained below. We have added 10^{-2} N $Fe(CN)_6^{3-}$ to a solution of 10^{-6} M rhodamine B at pH 7 for regeneration of the dye in a 1 electron step as has been formulated in Section 3 above.

Another reactant 10^{-1} M Na_2SO_3 has also been used to regenerate the dye [87, 90]. This species is less suitable since besides being a complicated electron acceptor it is at the same time an electron donor [97] for the injected holes which brings about $P_{es} < 1$ at large concentrations e.g. 10^{-1} M Na_2SO_3 in the solution. A stationary measurement at anthracene with 3×10^{14} photons/cm^2 s and 10^{-6} M rhodamine B but with 10^{-1} M Na_2SO_3 instead of 10^{-2} N $K_3Fe(CN)_6$ yields a steeply voltage dependent (i.e. recombination controlled) injection current with a 30 times smaller quantum efficiency than shown in Fig. 27 at an external field strength of 10^5 V/cm [89].

6. Interaction between Dye and Organic Crystals

To obtain from the measured quantum efficiency the quantum yield for an individual excited dye molecule to inject a hole, we have to know the number of dye molecules excited per unit time at the crystal surface. For the number of adsorbed dye molecules a rough estimate can be obtained from the surface coverage θ and from the area occupied by one adsorbed rhodamine B molecule which is estimated at 200 $Å^2$. This yields the density of adsorbed rhodamine B molecules:

$$n_{1D0} = \theta \cdot 5 \times 10^{13}/cm^2 . \tag{38}$$

The interaction leading to the adsorption of rhodamine B at the surface of organic crystals and also the dye coverage θ can be deduced from properties of

injection currents in the presence of dye molecules in the solution. The lower curve in Fig. 28 shows the time dependence of the rhodamine B sensitized current (10^{-6} M rhodamine B in the presence of 10^{-2} N $K_3Fe(CN)_6^{3-}$ at pH 7) at anthracene after the solution has been dropped on the virgin crystal surface. The contact formation has switched on an external field strength of 1×10^5 V/cm in the saturation range of the current voltage plot. Three minutes later the external field has been increased continuously yielding within 1 minute Fig. 27. The time dependence of the rhodamine B sensitized current after contact formation stems from the adsorption of the dye molecules at the crystal surface. It is the same with the different organic crystals. When a saturation current for hole injection of the same solution is measured at perylene in the dark the upper curve in Fig. 28 is obtained. At perylene hole injection through 10^{-2} N $K_3Fe(CN)_6$ in the dark corresponds to a rate constant of 3×10^5 cm/s whereas it is already negligible in the case of anthracene and chrysene [98]. The adsorbed rhodamine B molecules prevent the access of the redox ions $Fe(CN)_6^{3-}$ to the crystal surface. Thus the decrease in the upper curve of Fig. 28 indicates the increasing area of the crystal surface which is covered by dye molecules. The lower curve is proportional to the dye coverage θ and is normalized according to the upper curve. The equilibrium coverage for the 10^{-6} M rhodamine B solution according to Fig. 28 is $\theta = 0.4$. The complete adsorption curve i.e. dye coverage θ versus dye concentration in the solution has been obtained through such measurements [88]. With perylene the rhodamine B sensitized

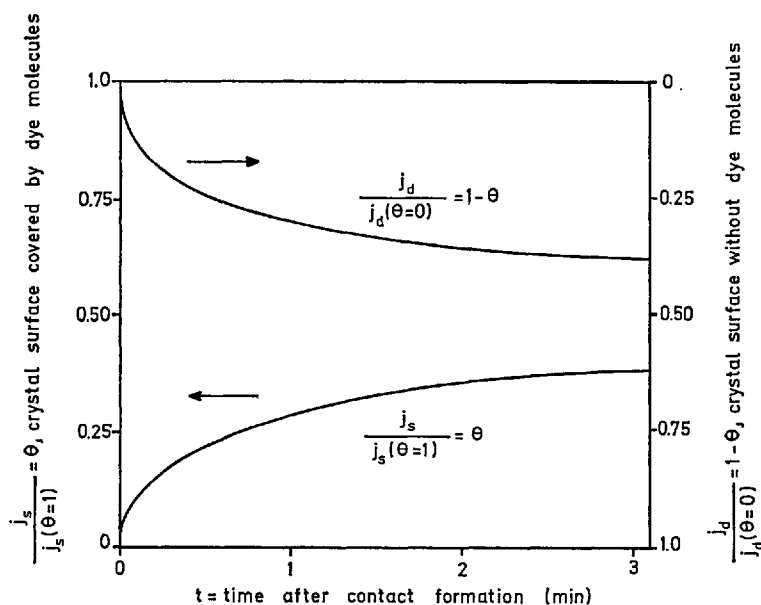Fig. 28. Time dependence of the rhodamine B sensitized injection current indicating the dye coverage θ (lower curve) and of a dark current indicating the crystal area without dye molecules $1 - \theta$ (upper curve). The time at the abcissa is measured from the moment of contact formation between the organic crystal and the solution containing 10^{-2} $Fe(CN)_6^{3-}$ and 10^{-6} M rhodamine B at pH $= 7$

current reaches about half of its maximum value with 10^{-6} M rhodamine B in the solution and levels off at higher dye concentrations. Thus, the absorption constant for rhodamine B at organic crystals is $K_{ad} = 10^6$ M^{-1} implying with about 1 M concentration at the crystal surface an about 10^6 times larger rate constant for adsorption than desorption. For comparison, the association constant for the formation of rhodamine B dimers in aqueous solution is $K_{as} = 1.5 \times 10^3$ M^{-1} [99]. The adsorption at the surface of organic crystals therefore is 10^3 times stronger than dimer formation in the solution. In aqueous solution rhodamine B adsorbed at the surface of organic crystals does not form dimers or even polymer islands.

Indeed, the excitation spectrum of the sensitized current j in Fig. 29 resembles the absorption spectrum of the dye monomer even when 70% of the dye molecules form dimers in a 10^{-3} M solution of rhodamine B for which the very different absorption coefficient ε is shown also in Fig. 29. The red-shift and broadening of the j curve in Fig. 29 as compared to the absorption ε of the dye nomomer in Fig. 25 is due to the influence of the environment, mainly neighbouring dye molecules. Fig. 29 refers to phenanthrene but holds good also for the other crystals [88]. Fig. 29 also shows the absorption spectrum (A) obtained after the 10^{-3} M rhodamine B solution has been dried up at the crystal surface through contact with a paper cloth. The remaining rhodamine B molecules form dimers and even a polymer as can be seen from the narrow absorption peak appearing at the long wavelength side of the spectrum [99]. Since there is no decrease but even a slight increase in the sensitized current at perylene up to 10^{-3} M rhodamine B the excitation
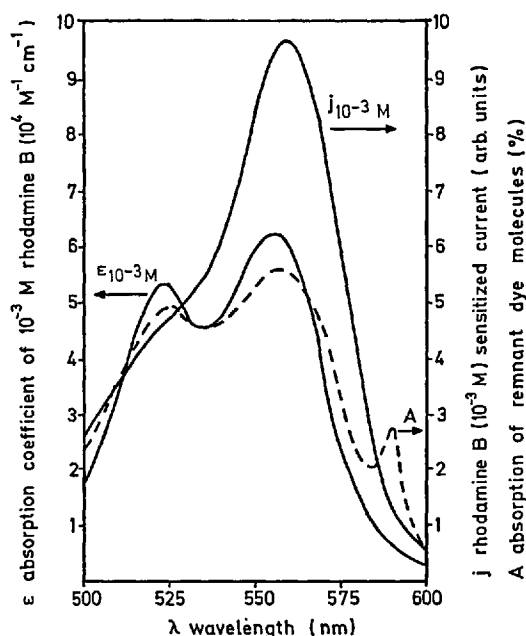

Fig. 29. Comparison between the excitation spectrum of the sensitized current J and of the absorption coefficient of a 10^{-3} M rhodamine B solution containing also 10^{-2} Fe(CN)$_6^{3-}$ at pH = 7. The absorption A is that of the dye molecules when the same solution is dried up at the crystal surface

spectrum of the current indeed indicates the dye species adsorbed at the crystal surface. Through a suitable procedure one can obtain the excitation spectrum of the sensitized current corresponding to a dye polymer on the same crystal [85].

Since dimerisation of Xanthene dyes does not occur in organic solvents and shows an increase in aqueous solution with the number and size of the alcylic substituents at the dye molecule, Drexhage recently has attributed dimerisation to hydrophobic interaction of the dye molecules [9]. It is at hand to attribute the even stronger adsorption of rhodamine B molecules at the surface of organic crystals also to hydrophobic interaction. The adsorption is thus brought about by an entropic gain due to a decrease in the number of hydrogen bonds in the water environment otherwise ordered in the presence of the alcylic groups of the dye [100]. Simple electrostatic arguments would predict even a repulsion of the cationic dye at the boundary of a medium with a smaller dielectric constant. Thus, we expect that the hydrophobic diethyl-amino groups of rhodamine B are closely attached to the surface molecules of the organic crystal. One of the possible arrangements of the rhodamine B molecule at the 001 surface of anthracene is shown in Fig. 30. Nikel has found at the same crystal surface different orientations for the dyes erythrosin and pyronin G which have different alcylic substituents [101].
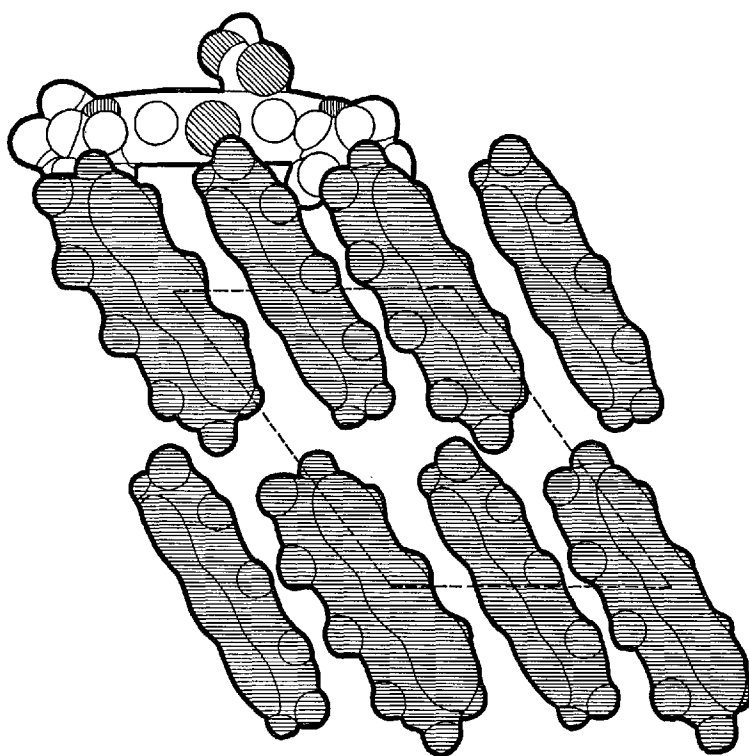

Fig. 30. One of the possible adsorption sites for rhodamine B (molecule at the top) at the 001 surface of anthracene. The projection of the *a* and *c* vectors of the unit cell are shown as dashed lines

To obtain a better control over the number of dye molecules at the crystal surface, sensitized current measurements have been carried out with dye molecules incorporated into a fatty acid layer deposited at the surface of an organic crystal and in contact with an eletrolytic solution at the other side [102]. However, the experimental technique which alllows for the reproduction of known experimental results for fatty acid layers deposited on glass slides and on aluminium-oxide [103,104] does not yield a satisfactory preparation of such layers at the hydrophobic surface of organic crystals [105].

Absorption measurements, however, on such fatty acid layers mixed with dye molecules which are deposited on glass slides can be used for estimating light absorption in the layer of dye molecules at the crystal surface. A monomolecular layer of dye molecules with an absorption coefficient of 10^5 M^{-1} cm^{-1} as for rhodamine B yields the percentage of absorbed photons $\frac{J_a}{J} = n_{1_{D_0}} \cdot \sigma = 0.02$ implying for an individual dye molecule the cross section for photon absorption $\sigma = 3 \times 10^{-16}$ cm^2. According to this estimate the quantum efficiency Y obtained with perylene and anthracene with a rhodamine B coverage of $\theta = 0.4$ (Fig. 28) corresponds to a quantum yield close to 1 indicating that about every excited rhodamine B molecule at the crystal surface injects a hole. For this to occur the electronic interaction between the chromophore of the dye and the organic crystal can be weak and electron exchange can need thermal activation. A weak electronic interaction is suggested by the excitation spectrum of the sensitized current which resembles closely the absorption spectrum of the dye monomer in solution independent of the ionisation energy of the organic crystal (compare Fig. 25).

7. Free Energy of the Reduced Dye-Hole Pair

We can now discuss the quantum yield W for sensitized hole generation. With sufficient regeneration of the dye $C_{Ox} k_{ET}^{Ox} > \sigma J W$ we can write for the sensitized current:

$$j = e_0 \, J \, \sigma n_{1_{D_0}} \, W \, P_{es} . \tag{39}$$

W = probability of an individual excited dye molecule for generating a hole, *i.e.* the quantum yield of sensitized hole generation. When P_{es} is known W can be determined from the sensitized current j using the above estimate (38) for the number of photons absorbed per unit time in the adsorbed dye layer.

When the regeneration of the dye is insufficient the stationary sensitized current depends on quantities characterizing the oxidation of the reduced dye and becomes simply the diffusion controlled current of the oxidizing redox ion at a very high light intensity.

A rather lengthy expression for W can be obtained in terms of the individual rate constants in the reaction scheme (Fig. 26). The conditions for $W = 1$ are at once obvious. The effective lifetime of the excited dye $^1D^*$ shoud be ldetermined by the electron transfer reaction $k_E^{1D^*}$ and the effective lifetime of the reduced dye hole pair in the second line should be controlled by the dissociation reactions k_D^1 and k_D^3. We have shown already that $P_{es} = 1$ can be realized for some of the systems in the actual experiment.

In Fig. 31 the yield $W = j/e_0 J \, n_{1_{D_0}}$ is shown for constant coverage $\theta = 0.4$ of rhodamine B at various organic crystals relative to the yield at perylene (compare Fig. 27). The yield remains constant when the ionisation energy (lower abcissa in Fig. 31) is increased by 0.6 eV from perylene to chrysene. The drop by less than a factor 2 at chrysene will not be considered here. As already seen in Fig. 27 the yield drops considerably at phenanthrene for a further increase in the ionisation energy by only 0.21 eV (Table 1). Since the sensitized current at phenanthrene is recombination controlled (compare Fig. 27) we have to consider the highest efficiency obtained at an external field strength of 6.7×10^5 V/cm as a lower boundary for the quantum yield of hole generation at this crystal relative to perylene or anthracene. The possible range of the yield for hole generation at phenanthrene is indicated by a wiggled line with an attached arrow, leading upward from the point indicating in Fig. 31 the maximum measured efficiency at phenanthrene ($P_{es} < 1$). The range of the wiggled line has been estimated by comparing
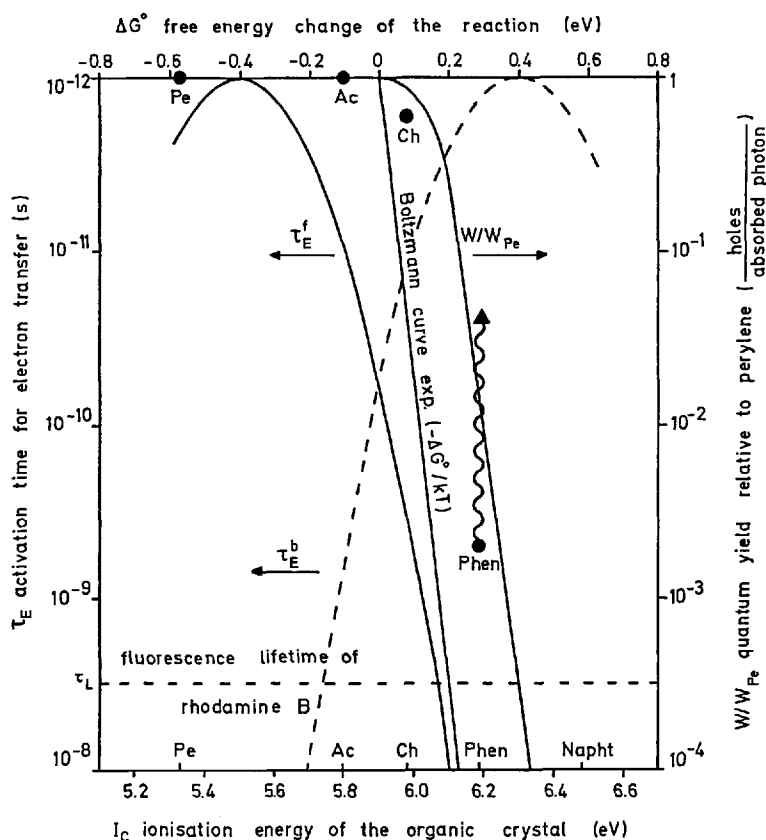
Fig. 31. Quantum yield (filled circles) of rhodamine B sensitized hole generation at the surface of organic crystals relative to perylene W/W_{Pe} versus the ionisation energies I_c of the organic crystals (lower abcissa). The range of the estimate for the value at phenanthrene is indicated by the wiggled arrow. The activation times for electron transfer τ_E^f and back electron transfer τ_E^b are also shown (compare Section IV 7)

74

the current versus field strength curve with known recombination controlled currents which have been followed up to the saturation range [79]. We can draw now the yield curve W/W_{Pe} according to this estimate as shown in Fig. 31. From this yield curve we derive the free energy plot $\tau_E^f(\Delta G^0)$ for the electron transfer reaction of the excited singlet rhodamine B molecule. We assume that the difference in yield at crystals with different ionisation energies I_C (compare Table 1) is determined by different activation times for electron transfer τ_E^f (*i.e.* the time to reach the activated state for electron transfer). Thus, we can write for the yield curve with τ_L the lifetime of all the other desactivation channels:

$$W = W_{\max} \frac{\tau_L}{\tau_L + \tau_E^f} \tag{40}$$

The free energy plot of the electron transfer reaction can be obtained from the measured yield curve by making an assumption about the dependence of τ_E^f on the free energy change ΔG^0 and also about the lifetime τ_L. From the preceding discussion we can obtain some idea about the electron transfer activation time τ_E^f. Firstly, the excitation spectrum for hole injection is that of the S_0—S_1 transition in the dye molecule (Fig. 25), and it remains unchanged when the electron donating valence band in the organic crystal is shifted from a position in perylene above the electron accepting level of the excited dye molecule to a position in phenanthrene well below that level (p. 62). Secondly, the apparent strong adsorption of rhodamine B at the crystal surface appears to be caused by an entropy gain (hydrophobic interaction) and not by the formation of a bond. These two points lead us to the assumption that in this system electron transfer requires in general also the reorganisation of solvent molecules and of bonds in the reactants and that electronic overlap necessary for electron transfer is switched on and off with a characteristic frequency for which a reasonable guess appears to be $\nu_0 = 10^{12} s^{-1}$. For the activation process we use formula (21) with $\Delta G^0 = I_C - \left| {}^0E_{1D}{}^*/{}_{2D^-} \right| - E_w$ and we set $L_{reorg} = 0.4$ eV. E_w is the difference in interaction energy between reactants and products [93].

$$\tau_E^f = \frac{1}{\nu_0} \exp \left[\frac{L_{reorg}}{4\,kT} \left(1 + \frac{\Delta G^0}{L_{reorg}} \right)^2 \right] \tag{41}$$

and setting in formula (40) $\tau_L = \tau_{Fl} = 3.2$ ns (τ_{Fl} fluorescence lifetime of rhodamine B) we obtain the plot of the activation time for electron transfer in dependence on the free energy change of the reaction ΔG^0 as shown in Fig. 31. For comparison in Fig. 31 is also drawn the straight line of a simple Boltzmann curve for activation.

According to our yield curve the electron transfer reaction of the excited singlet state of rhodamine B corresponds to a zero free energy change $\Delta G^0 = 0$ at an organic crystal with the effective ionisation energy of $I_c = 5.9$ eV at the crystal surface. Since at $\Delta G^0 = 0$ the free energy of the reactants with equilibrium positions of their slow components is the same as that for the products of the electron transfer reaction, *i.e.* the reduced dye molecule with the hole in the organic crystal we know that at $\Delta G^0 = 0$ the excitation energy of the excited singlet state

of rhodamine B (2.13 eV) is stored in the reduced dye-hole pair at the crystal surface. Thus, from Fig. 31 we obtain the free energies of the reduced dye-hole pairs at the surface of the different organic crystals relative to the energies of the electronic transitions in the individual reactants as shown in Fig. 24.

The same relationship is plotted in Fig. 32 in a way which is more customary than Fig. 24 for a discussion of reactions at electrodes. The reduction potential of the excited singlet state of rhodamine B $^0E_{1_D*/2_D-}$ has been fixed according to Fig. 31 relative to the valence bands (ionisation energies) at the surface of the organic crystals. The distribution curve for the empty and occupied excited singlet state of rhodamine B is also drawn according to Fig. 31. A comparison with the above estimated value of

$$\left|{}^0E_{1_D*/D-}\right| = 5.88 \text{ eV}$$

yields excellent aggreement. At least the precision of this result appears fortuitous since it implies an exact value for $^0E_{D/D-}$ and a cancellation of the correction terms contributing to E_w.
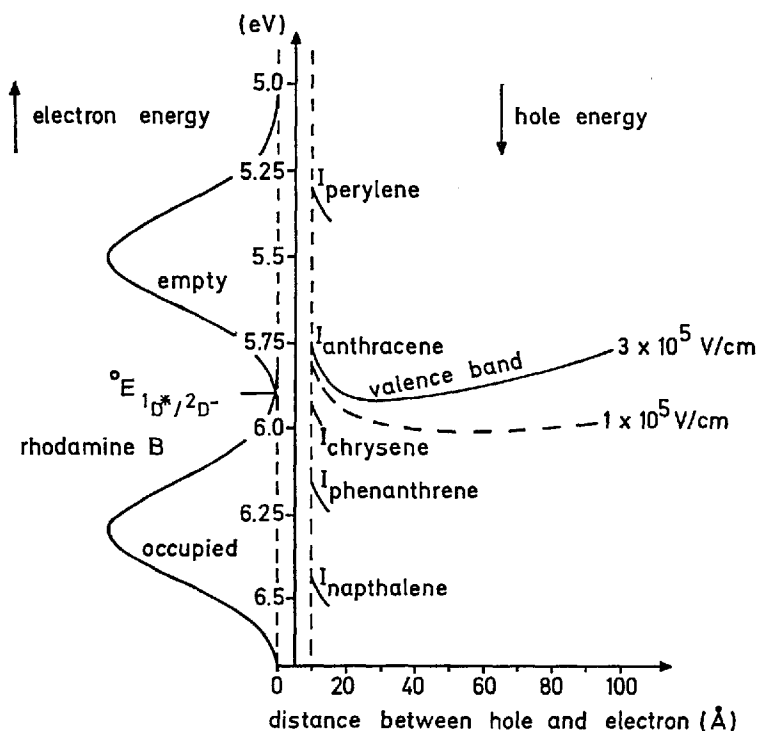

Fig. 32. The relationship between the reduction potential $^0E_{1_D*/D^-}$ of the excited singlet state of rhodamine B and the ionisation energies I_c at the surface of the organic crystals as derived from the yield for hole generation at the different crystals (Fig. 31). As an example at anthracene the potential curve (valence band) is shown for the hole moving into the crystal bulk at two different external field strengths 3×10^5 V/cm (solid curve) and 1×10^5 V/cm (dashed curve)

For anthracene the bending of the valence band is shown for the hole moving away from the crystal surface at two different external field strengths. This bending of the valence band has been explained in Section 5 and should not be confused with the effect of a space charge. It is due to the attraction of the hole through its counter charge (*e.g.* the electron at the reduced dye molecule) and its image charge in the solution [79].

In Figs. 31 and 32 it should be noticed that even when the electron transfer reaction requires thermal activation at anthracene and chrysene, it can still occur with almost certainty within the lifetime of the excited rhodamine B molecule. Thus thermal activation does not necessarily bring about a decrease in the quantum yield for sensitized charge generation as compared to the near activation less electron transfer reaction taking place at perylene[a]. However, a drop in the yield of sensitized charge generation occurs at phenanthrene when the time necessary for thermal activation of the electron transfer reaction is longer than the fluorescence lifetime of the rhodamine B molecule. Obviously, the gauge for ΔG^0 derived from the drop in the yield curve in Fig. 31 does not depend critically on the assumption $L_{reorg} = 0.4$ eV but would decrease by about 0.1 eV when the lifetime of the excited rhodamine B molecule at the crystal surface in the absence of electron transfer is shorter by one order of magnitude than has been assumed. We have used the fluorescence lifetime $\tau_{Fl} = 3.2 \cdot 10^{-9}$ s as an estimate at smaller dye concentrations in the solution $\leqslant 10^{-6}$ M. At large dye concentrations ($\geqslant 10^{-5}$ M) energy transfer quenching and possibly enhanced intersystem crossing due to neighbouring dye molecules can lead to a decrease in the effective lifetime τ_L. According to Figs. 31 and 32 a corresponding decrease in the yield is expected to occur with higher dye concentrations for anthracene, chrysene and phenanthrene but not for perylene with a much shorter activation time for electron transfer. Such a difference in the yield at high dye concentration has indeed been observed for perylene and anthracene [88] or phenanthrene [89].

8. Spin Orientation and Recombination in the Reduced Dye-Hole Pair

For the excited singlet state of rhodamine B as product state the free energy plot of the reverse electron transfer from the reduced dye to the hole (dashed curve τ_E^b in Fig. 31) is a mirror image to the free energy plot of the forward reaction relative to $\Delta G^0 = 0$. We immediately see from Figs. 31 and 32 that this reverse reaction is very fast at phenanthrene and slower at chrysene. It is still slower at anthracene and extremely slow at perylene. At phenanthrene this reverse reaction can compete with the dissociation of the hole from the reduced dye as is borne out by the recombination controlled current in this system (Fig. 27).

When in addition the singlet spin state is not preserved even though the reduced dye-hole pair is formed from the two singlet states $^1D^*$ and $^1C_0$ we have to consider similar free energy plots for the reverse electron transfer reactions lead-

---

[a] We like to remind the reader that a hole needs activation for moving "downhill" in the customary energy scheme (Fig. 32) which refers to the transfer of the electron.

ing to excited triplets as product states. Such plots yield a very fast reverse electron transfer at anthracene for the formation of the triplet state of the crystal and also of the dye rhodamine B. The formation of the triplet dye should also be a fast reaction at chrysene. At perylene all the possible reverse electron transfer reactions should be slow. Processes leading to a triplet spin in the electron hole pair have been studied at anthracene. Before discussing this very interesting point we like to mention again that the large quantum yield $W \approx 1$ observed at anthracene and at chrysene for the complete injection of the hole suggests that the dissociation reaction (k_D^1 and k_D^3) determines predominantly the lifetime of the reduced dye-hole pair at these crystals.

The population of the triplet state of anthracene through the recombination of the defect electron with the reduced rhodamine B molecule has been shown by Nickel through a 50% decrease of the sensitized delayed fluorescence with increasing applied voltage [87]. From the above discussion of the escape probability P_{es} it is evident that such an observation indicates $P_{es} < 1$ and the expected steep rise of the sensitized current with increasing voltage has indeed been observed simultaneously [87]. A similar result has been confirmed recently [106]. If e.g. through spin lattice relaxation the spin orientation of the electron hole pair is randomized the recombination reaction should yield 3 triplet states for 1 singlet state. Thus, randomization of the spin orientation in the reduced dye-hole pair would render a qualitative explanation for this observation.

However, in the same system consisting of rhodamine B and anthracene in the presence of 10^{-1} M Na_2SO_3 Groff et al. have observed a decrease in the sensitized delayed fluorescence by about 50% when a small external magnetic field (200 Gauß) was applied (Fig. 33 [90]). This observation has been explained by the authors in a quantitative model. Electron transfer between the singlet excited rhodamine B $^1D^*$ and the singlet ground state of the crystal $^1C_0$ leads to an elec-
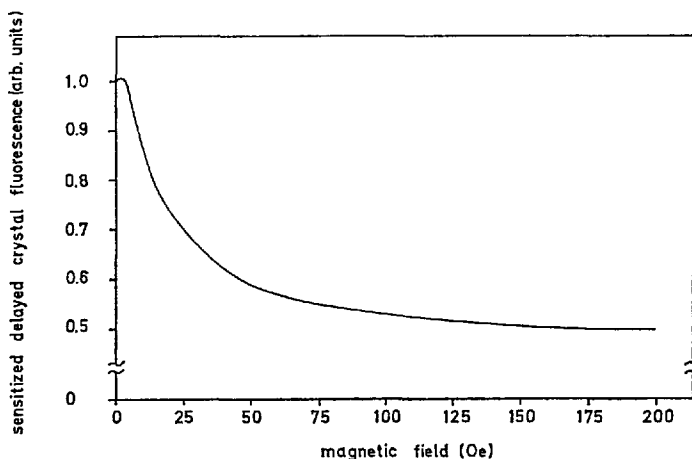

Fig. 33. Dependence of the rhodamine B sensitized delayed fluorescence in anthracene on the magnetic field oriented parallel to the 001 surface of anthracene. (2×10^{-7} M rhodamine B and 10^{-1} NaHSO$_3$ in aqueous solution) [90]

tron-hole pair *i.e.* the electron at the reduced dye and the hole in the organic crystal. The motion of the total spin of this electron hole pair is governed by a spin Hamiltonian $\mathscr{H}_{spin}$ (Fig. 26) which is asymmetric with respect to an exchange of the spins between electron and hole due to a different hyperfine interaction with their nuclear spin environment. To account for this asymmetric hyperfine interaction in a simple model the authors have introduced the hyperfine interaction only for the hole with just one additional nuclear spin. The important feature of this asymmetric spin Hamiltonian is the mixing of singlet and triplet configurations of the electron-hole pair through the hyperfine interaction. Such triplet configurations now allow for a reverse electron transfer reaction with the triplet of the crystal or the dye as product state. Since the Zeemann effect renders a symmetric part in the spin Hamiltonian $\mathscr{H}_{spin}$ which is larger than the asymmetric hyperfine interaction at *e.g.* 200 Gauß it yields virtually pure triplet configurations for the $m = \pm 1$, triplet levels of the electron-hole pair which therefore cannot be populated any more via the electron transfer reaction of the two singlet states $^1D^*$ and $^1C_0$ in the presence of this magnetic field. This way the total number of triplet configurations as regards the electron-hole pair is reduced through the magnetic field and a decrease in sensitized delayed fluorescence of the anthracene crystal is observed (compare process 4 in Sections 3 and 4). A suitable branching ratio between the overall rate constant for destruction of the electron-hole pair and the hyperfine interaction yields the modulation curve obtained in the experiment. The success of this model in explaining the experimental observation also proves that sensitized electron transfer at anthracene occurs predominantly from the excited singlet state of the rhodamine B molecule. Apparently the model proposed by Groff *et al.* does not require the dissociation of the electron-hole pair for the formation of the triplet state (these authors therefore call the reduced dye-hole pair a charge transfer complex [90]). If this holds good the formation of the triplet state in the originally generated electron-hole pair should depend very little on the external electric field.

However, the effect of the small magnetic field on the sensitized delayed fluorescence should even occur when in addition the hole moves about in the vicinity of the reduced parent dye molecule with its spin orientation remaining the same, when returning to the reduced dye. The probability for a return of the hole from a larger distance to its reduced parent dye now should decrease with increasing external electric field as long as an escape probability 1 is not reached. Thus in the latter case the decrease in the sensitized delayed fluorescence with increasing electric field should remain together with the same relative decrease occurring in the presence of the magnetic field. The above assumption of the hole moving about in the vicinity of the reduced parent dye is perhaps suggested by the observation of a 50% decrease in the sensitized delayed fluorescence due to an external magnetic field [90] under similar experimental conditions for which also a 50% decrease has been observed due to an external electric field [87]. We like to stress that the effect of the magnetic field would not occur for a recombination reaction with randomized spin orientation in the electron-hole pair where always 3 out of 4 recombination reactions should yield a triplet state. In this case the sensitized delayed fluorescence should not depend on the magnetic field but can still depend on the electric field.

It has been suggested that for erythrosine with a large intersystem crossing from $^1D*$ to $^3D*$ the delayed sensitized fluorescence of the crystal is mainly produced by energy transfer from the triplet of the dye to the triplet of the crystal [87]. The observed dependence of the sensitized delayed fluorescence on the light intensity agrees in all cases with the assumption of a source for triplet excitons at the crystal surface [107,108]. Even for erythrosine the quantum yield of sensitized hole injection can still be high when the lifetime of the triplet state $^3D*$ is mainly determined by the electron transfer reaction k_E^{3D*}.

Summing up we can state that by now considerable insight has been gained into the reactions of excited dye molecules at the surface of organic crystals. The models emerging from these systems should be useful in the discussion of related reactions *e.g.* also in biological systems. Since the relevant energy levels (Figs. 24 and 32) can be varied systematically over a wide range further investigations concerning their influence on the dominant reaction paths in different systems appear worthwhile. By a combined variation of the electric and magnetic field in each system more details should emerge concerning the influence of various reaction paths on the sensitized delayed fluorescence and on the sensitized hole injection.

V. List of Symbols

A	electron affinity
C	surface molecule of the organic crystal in the ground state
C*	surface molecule of the organic crystal in the excited state
$^2C^+$	hole in the organic crystal (doublet state)
c	concentration of reactants
D	dye molecule in the ground state
D^+, D^-	oxidized and reduced dye molecule
D*	dye molecule in the excited state
$D(E)$	density of electron quantum states in the electrode per unit volume
E	electron free energy in absolute scale
$^0E_{D/D^+}$	standard redox potential for oxidation in absolute scale
$^0E_{D/D^-}$	standard redox potential for reduction in absolute scale
E_F	Fermi energy in electrode (metal or semiconductor)
$\Delta E*$	energy of electronic excitation in the molecule D*
ΔE_{ref}	free energy difference between the Fermi energy of the electrons in the reference electrode and at the vacuum level
$_0E_{don}, _0E_{acc}$	electron energy terms of redox species with highest probability
$f(\nu)$	oscillator strength
ΔG_S	free energy of solvation
ΔG_{redox}	free energy of redox reaction, $Red_{solv} = Ox_{solv}^+ + e_{vac}^-$
$\mathscr{H}_{spin}$	Spin Hamiltonian of the reduced dye-hole pair
I	ionisation energy
j	current

j_0	exchange current
j^+, j^-	anodic or cathodic partial currents
J	light intensity
k_{ET}^{Ox}	rate constant for oxidizing the reduced dye
k_E, τ_E^f	rate constant and activation time for electron transfer from the organic crystal to the reduced dye
k_B, τ_E^b	rate constant and activation time for electron transfer from the reduced dye to the hole at the surface of the organic crystal
k_{Es}	reciprocal escape time of a hole from the crystal surface
L_{reorg}	reorganisation energy
N_c	effective density of states in conduction band
N_v	effective density of states in valence band
n	electron concentration in conduction band
n_{1D_0}	number of dye molecules adsorbed per unit area at the crystal surface
Ox	oxidized redox ion
P_{es}	overall excape probability for a generated hole
P_{es}^g	escape probability for a hole from geminate recombination with the reduced parent dye molecule
p	hole concentration in valence band
U_{NHE}	electrode or redox potential in conventional scale against Normal Hydrogen Electrode (NHE) as reference
$W(E)$	distribution function (normalized)
W	quantum yield of sensitized hole generation referring to one excited dye molecule
Y	quantum efficiency of sensitized hole injection referring to incident photons
ε	absorption coefficient
η	overvoltage
θ	dye coverage
$\varkappa(E)$	transition probability factor for electrons between energy levels with equal E
λ	wavelength of light
ν	frequency of light
σ	absorption cross section
τ	lifetime
τ_L	lifetime of an excited dye molecule due to all activation channels at the crystal surface except electron transfer

VI. References

[1] Weller, A.: In: Fast reactions and primary processes in chemical kinetics (Cleasson, ed.), p. 413. Stockholm: Almquist and Wiksell 1967.
[2] Stevens, B., Sharpe, R. R., Bingham, W. S. W.: Photochem. Photobiol. *6*, 83 (1967).
[3] Gerischer, H., Michel-Beyerle, M. E., Rebenstrost, F., Tributsch, H.: Electrochim. Acta *13*, 1509 (1968).
[4] Gerischer, H.: Faraday Discussions *58*, 219 (1974).
[5] Gerischer, H.: Ber. Bunsenges. Physik. Chem. *77*, 771 (1973).
[6] Gerischer, H.: Z. Physik. Chem. (Frankfurt) *26*, 223 (1960).
[7] Memming, R.: Photochem. Photobiol. *16*, 325 (1972).
[8] Lohmann, F.: Z. Naturforsch. *22a*, 813 (1967).
[9] Drexhage, K. H.: In: Topics in applied physics (Schäfer, ed.), Vol. 1, p. 145. Berlin—Heidelberg—New York: Springer 1973.
[10] Chambers, R. W., Kearns, D. R.: Photochem. Photobiol. *10*, 1215 (1969).
[11] Weber, G., Teale, F. W. J.: Trans. Faraday Soc. *53*, 646 (1957).
[12] Berlman, J. B.: Handbook of fluorescence spectra of aromatic molecules. New York: Academic Press 1971.
[13] Tani, T., Kikudu, S.: Report of the Institute of Industrial Science, The University of Tokyo, 1968.
[14] Gerischer, H., Ranke, W.: Z. Naturforsch. *24a*, 463 (1969) and unpublished results.
[15] Gurney, R. W.: Ions in solution. Cambridge: University Press 1936.
[16] Marcus, R. A.: Can. J. Chem. *37*, 138 (1959). — In: Trans. symp. electrode processes (Yeager, ed.), p. 239. New York: Wiley 1961. — Ann. Rev. Phys. Chem. *15*, 155 (1964).
[17] Levich, V. G.: In: Advances in electrochem. and electrochem. engineering (Delahay, Tobias, eds.), Vol. 4, p. 249. New York: Interscience 1966. — In: Physical chemistry (Eyring, Henderson, Jost, eds.), Vol. IX B, p. 985. New York: Academic Press 1970.
[18] Dogonadze, R. R.: In: Reactions of molecules at electrodes (Hush, ed.), p. 135. New York: Wiley-Interscience 1971.
[19] Gerischer, H.: Z. Phys. Chem. (Frankfurt) *26*, 223, 325 (1960); *27*, 48 (1961).
[20] Gerischer, H.: In: Physical chemistry (Eyring, Henderson, Jost, eds.), Vol. IXA, p. 463. New York: Academic Press 1970.
[21] Memming, R., Kirsten, G.: Ber. Bunsenges. Phys. Chem. *76*, 4 (1972).
[22] Förster, Th.: Ann. Phys. *2*, 55 (1948); Z. Elektrochem. *53*, 93 (1949).
[23] Kuhn, H.: J. Chem. Phys. *53*, 101 (1970).
[24] Tews, K. H.: Ann. Phys. *29*, 97 (1973).
[25] Chance, R. R., Prock, A., Silbey, R.: J. Chem. Phys. *60*, 2744 (1974).
[26] Hale, J. M.: J. Phys. Chem. *73*, 3196 (1969).
[27] Gerischer, H.: Photochem. Photobiol. *16*, 243 (1972).
[28] Gerischer, H.: In: Advances in electrochem. and electrochem. engineering (Delahay, Tobias, eds.), Vol. 1, p. 139. New York: Interscience 1961.
[29] Gerischer, H., Hein, F., Lübke, M., Meyer, E., Pettinger, B., Schöppel, H. R.: Ber. Bunsenges. Phys. Chem. *77*, 284 (1973).
[30] Gerischer, H., Tributsch, H.: Ber. Bunsenges. Phys. Chem. *72*, 437 (1968).
[31] Tributsch, H., Gerischer, H.: Ber. Bunsenges. Phys. Chem. *73*, 251 (1969).
[32] Myamlin, V. A., Pleskov, Yu. V.: Electrochem. of semiconductors. New York: Plenum Press 1967.
[33] Hofman-Perez, M., Gerischer, H.: Ber. Bunsenges. Phys. Chem. *65*, 771 (1961).
[34] Mott, N. F.: Proc. Roy. Soc. (London) *A 171*, 27 (1939).
[35] Schottky, W.: Z. Physik *113*, 367 (1939).
[36] Dewald, J. F.: Bell System Tech. J. *39*, 615 (1960).
[37] Boddy, P. J.: J. Electroanal. Chem. *10*, 199 (1965).
[38] Brattain, W. H., Garrett, C. G. B.: Bell System Tech. J. *34*, 129 (1955).
[39] Boddy, P. J., Brattain, W. M.: Ann. N. Y. Acad. Sci. *101*, 683 (1963).
[40] Memming, R.: J. Electrochem. Soc. *116*, 785 (1969).
[41] Tyagai, V. A., Kolbasov, G. Ya.: Surface Sci. *28*, 423 (1971).
[42] Haberkorn, R.: Dissertation T. H. München 1967.

43) Lohmann, F.: Ber. Bunsenges. Phys. Chem. *70*, 428 (1966).
44) Boddy, P. J.: J. Electrochem. Soc. *115*, 199 (1968).
45) Fujishima, A., Hayashitani, E., Honda, K.: J. Institute of Industr. Sci., University of Tokyo (Seisan Kenkyo) *23*, 363 (1971).
46) Möllers, F., Memming, R.: Ber. Bunsenges. Phys. Chem. *76*, 469 (1972).
47) Hauffe, K., Range, J.: Z. Naturforsch. *23b*, 736 (1968).
48) Hauffe, K., Pusch, M., Range, J.: Z. Physik. Chem. (Frankfurt) *64*, 122 (1969).
49) Hauffe, K., Danzmann, H. J., Pusch, H., Range, J., Volz, H.: J. Electrochem. Soc. *117*, 933 (1970).
50) Scheibe, G.: Angew. Chem. *52*, 633 (1939).
51) Fry, D. J.: In: Dye sensitization (Berg, Mazzucato, Meier, Semerano, eds.), p. 44, London: The Focal Press 1970.
52) Memming, R.: Faraday Discussions *58*, 261 (1974).
53) Danzmann, H. J., Hauffe, K.: Ber. Bunsenges. Phys. Chem. *79*, 438 (1975).
54) Tributsch, H., Gerischer, H.: Ber. Bunsenges. Phys. Chem. *73*, 850 (1969).
55) Fujishima, A., Wanatabe, T., Tatsuoki, O., Honda, K.: Chem. Letters *1*, 13 (1975).
56) Heiland, G., Bauer, W., Neuhaus, M.: Photochem. Photobiol. *16*, 315 (1972).
57) Hauffe, K., Martinez, V., Range, J., Schmidt, R.: Phot. Korr. *104*, 113 (1968).
58) Terenin, A., Akimov, I.: J. Phys. Chem. *69*, 730 (1965).
59) Gerischer, H., Selzle, H.: Electrochim. Acta *18*, 799 (1973).
60) Memming, R., Tributsch, H.: J. Phys. Chem. *75*, 562 (1971).
61) Pettinger, B., Schöppel, H.-R., Gerischer, H.: Ber. Bunsenges. Phys. Chem. *77*, 963 (1973).
62) Pietsch, H., Jäkel, D., Schneider, W., Treue, D.: In: Dye sensitization (Berg. Mazzucato, Meier, Semerano, eds.) p. 178. London: The Focal Press 1970.
63) Boddy, P. J.: J. Electrochem. Soc. *115*, 199 (1968).
64) Karl, N.: In: Advances in solid state phys. (Queisser, ed.), Vol. XIV, p. 261. Braunschweig: Vieweg 1974.
65) Munn, R. W., Siebrand, W.: J. Chem. Phys. *52*, 6391 (1970).
66) Wright, G. T.: Solid State Electronics *2*, 165 (1961).
67) Rothämel, W., Willig, F.: unpublished results.
68) Willig, F., Scherer, G., Rothämel, W.: Z. Naturforsch. *29a*, 131 (1974).
69) Willig, F., Scherer, G.: to be published.
70) Sinclair, V.C., Robertson, J. M., McL. Mathieson, A.: Acta Cryst. *3*, 251 (1950).
71) Donaldson, D. M., Robertson, J. M., White, J. G.: Proc. Roy. Soc. (London) *220*, 311 (1953).
72) Iball, J.: Proc. Roy. Soc. (London) *164A*, 140 (1934).
73) Trotter, J.: Acta Cryst. *16*, 605 (1963).
74) Birks, J. B.: Photophysics of aromatic molecules. London: Wiley 1970.
75) Tanaka, J.: Bull. Chem. Soc. Japan *36*, 1237 (1963); *38*, 86 (1965).
76) Nakada. I.: J. Phys. Soc. Japan *20*, 346 (1965).
77) Mc.Clure, D. S.: J. Chem. Phys. *25*, 481 (1956).
78) Pope, M., Burgos, J., Gianchino, J.: J. Chem. Phys. *43*, 3368 (1965).
79) Scherer, G., Willig, F.: to be published.
80) Boschi, R., Clar, E., Schmidt, W.: J. Chem. Phys. *60*, 4406 (1974).
81) Michel-Beyerle, M. E., Willig, F.: Solid State Commun. *7*, 913 (1967).
82) Steketee, J. W., deJonge, J.: Proc. Koninkl. Ned. Akad. Wetenschap. *B 66*, 76 (1963).
83) Mulder, B. J.: Philips Res. Rept. *22*, 553 (1967).
84) Mulder, B. J., deJonge, J.: Proc. Koninkl. Ned. Akad. Wetenschap. *B 66*, 303 (1963).
85) Gerischer, H., Michel-Beyerle, M. E., Rebentrost, F.: In: Dye sensitization (Berg, Mazzucato, Meier, Semerano, eds.), p. 140. London: The Focal Press 1970.
86) Nickel, B., Staerk, H., Weller, A.: Chem. Phys. Letters *4*, 27 (1969).
87) Nickel, B.: Mol. Cryst. Liqu. Cryst. *18*, 227 (1972).
88) Willig, F., Michel-Beyerle, M. E.: Photochem. Photobiol. *16*, 371 (1972).
89) Willig, F., Müller, N.: to be published.
90) Groff, R. P., Suna, A., Avakian, P., Merrifield, R. E.: Phys. Rev. *B 9*, 2655 (1974).
91) Groff, R. P., Merrifield, R. E., Suna, A., Avakian, P.: Phys. Rev. Letters *29*, 429 (1972).

92) Michel-Beyerle, M. E., Brickl, R.: Third International Conference on Photosensitization in Solids, Sarlat, France, 1971.
93) Marcus, R. A.: J. Chem. Phys. *43*, 679 (1965).
94) Willig, F., Korsch, B., Scherer, G., Gährs, H. J.: to be published.
95) Michel-Beyerle, M. E., Willig, F.: Chem. Phys. Letters *5*, 281 (1970).
96) Mark, P., Helfrich, W.: J. Appl. Phys. *33*, 205 (1962).
97) Charlot, G.: Oxydo-reduction potentials, p. 28. London: Pergamon Press 1958.
98) Willig, F., Scherer, G., Rothämel, W.: Ber. Bunsenges. Physik. Chem. *77*, 921 (1973).
99) Förster, Th., König, E.: Z. Elektrochem. *61*, 344 (1957).
100) Rattee, I. D., Breuer, M. M.: The physical chemistry of dye adsorption. London: Academic Press 1974.
101) Nickel, B.: Ber. Bunsenges. Phys. Chem. *75*, 795 (1971).
102) Michel-Beyerle, M. E., Haberkorn, R.: Z. Naturforsch. *27a*, 1496 (1972).
103) Kuhn, H., Möbius, D.: Angew. Chem. *83*, 672 (1971).
104) Mann, B., Kuhn, H.: J. Appl. Phys. *42*, 4398 (1971).
105) Gaehrs, H. J., Willig, F.: unpublished results.
106) Michel-Beyerle, M. E., Bube, W., Haberkorn, R.: Z. Naturforsch. *30a*, 506 (1975).
107) Nickel, B.: Mol. Cryst. Liqu. Cryst. *18*, 263 (1972).
108) Willig, F.: Naturforsch. *27a*, 368 (1972).

Application of the Semiconductor Properties of Dyes Possibilities and Problems

Prof. Dr. Hans Meier

Staatliches Forschungsinstitut für Geochemie, D-8600 Bamberg, Postfach 4041

Contents

I. Introduction

The electronic conductivity of organic dyes was established for the first time and has been investigated mainly in experiments aimed at elucidating the mechanism of spectral sensitization [1-6]. These experiments, which began in the early 1950's, can be considered as the starting point of the development of a new class of semiconductors covering the large field of organic compounds.

The significance of the semiconductivity of organic dyes and other classes of organic solids, such as charge-transfer complexes, which behave in some ways like metals [7] or polymers [8,9], is to day beyond doubt. The possible industrial applications of this new class of semiconductors are, however, still in the discussion stage.

The present position as regards the industrial application of the dark- and photoconductor properties of organic dyes is outlined in this paper.

II. Mechanism of Dark- and Photoconductivity

1. General Remarks

The dark- and photoconductivity of organic compounds has long been regarded as a sort of side-effect arising from impurities, ionic carriers, or traces of adsorbed water.

It is now known that dark- and photoconductivity is connected with the structure of organic compounds [10]. The conductivity of organic dyes and other organic compounds, like that of inorganic semiconductors, is attributable to electronic charge carriers, $i.e.$ electrons and positive holes. The dark conductivity σ_D can generally be described by

$$\sigma_D = e(n\,\mu_n + p\,\mu_p) \tag{1}$$

and the photoconductivity σ_{phot} by

$$\sigma_{phot} = e\,(\Delta n\,\mu_n + \Delta p\,\mu_p) \tag{2}$$

where n, p are the concentrations of electrons and holes, respectively, in the unilluminated solid; μ_n, μ_p are the mobilities of electrons and holes, and Δn, Δp steady-state electron and hole concentrations on illumination.

It must be stressed that the conductivity of organic systems is the combined result of several processes, $i.e.$ the generation, transport, and recombination of charge carriers [11,12].

2. Elementary Processes of Conductivity

A. Generation Process

Electrons and holes can be generated by several different processes. For dyes with a difference of less than 2 eV between the ground state and the first excited singlet state, it is often possible to assume an intrinsic excitation process, as in the

case of inorganic intrinsic semiconductors. In this process charge carriers are formed by thermal or optical transfer of an electron from the ground state to the excited state. This can be derived from the agreement of

(a) the thermal activation energy ΔE, obtained from measurements of the temperature dependence of the dark conductivity [Eq. (7)] and the optical excitation energy,

(b) the photoconduction and absorption spectra, and

(c) the thermal activation energy ΔE and the optical activation energy ΔE_{opt} deduced from the long-wave limit of photoconductivity.

Examples: for Cu-phthalocyanine $\Delta E = 1.7$ eV and $\Delta E_{opt} = 1.63$ eV; for pinacyanol $\Delta E = 1.8$ eV and $\Delta E_{opt} = 1.77$ eV. Further examples are given in [3,10,13-15].

In addition, particularly in compounds with a gap of more than 2 eV between the ground state and the excited state, charge carriers may be generated in the unilluminated dye by thermal excitation of defects (impurities such as adsorbed gases, disturbed counterions in ionic dyes, etc.) or by injection from electrodes. Excitation with high light intensities can produce a detectable concentration of electrons or holes by ionization of excitons [16,17]. In special cases, e.g. in simple polymer systems, at irradiation wavelengths in the ultraviolet region a photoemission from the electrode can also contribute to photoconductivity [18].

B. Transport of Charge Carriers

Several mechanisms are proposed to explain the transport through the organic solid of electronic carriers produced in primary or secondary processes [10,11].

a) Tunneling Mechanism. This mechanism postulates that migration of electrons results from the fact that an excited electron (e.g. in the singlet state) can reach a vacant term of the neighboring molecules by tunneling through the potential barrier with a probability ($k_T \approx 10^{11}$—10^{14} sec^{-1}) greater than the probability of its returning to the ground state ($k_d \approx 10^8$—10^9 sec^{-1}). This mechanism seems to be in agreement with such observations as the anisotropy of the conductivity or the compensation rule [19]. However, the observation that mobility decreases with increasing temperature does not support this mechanism [20,21].

b) Hopping Mechanism. In solids with broad intermolecular barriers (>10 Å) that cannot be crossed by tunneling, electrons can migrate by a "hopping" mechanism from a molecule to its neighboring molecules. There seems no doubt that this kind of carrier transport, characterized by low mobility ($\mu < 0.1$ [cm^2/V sec]) and increasing with decreasing temperature, does occur in various organic compounds, e.g. polymers or solid radicals [22]. However, low mobility increasing with temperature can also be observed in the case of band conduction due to multiple trapping. Such cases can be distinguished by their different frequency dependence on the conductivity [23]. In the case of band conduction, σ decreases with increasing frequency; with the hopping mechanism, σ increases with increasing frequency.

In discussing low temperature-dependent mobility, we should mention charge transport by polarons, an intermolecular phonon-assisted hopping process [24,25]. Polarons (charge carriers trapped in their polarization field) arise from a strong electron–phonon interaction where there is a weak overlap of wave functions of

molecular states; on the other hand, formation of localized states in the forbidden gap may also produce phonon-assisted hopping in noncrystalline materials with disturbed long-range order.

c) Band Model. As intermolecular distances decrease, the hopping mechanism is replaced by a carrier transport described by the band model. This model [26] postulates that narrow energy bands allow quasifree transport of the electrons and holes generated by the discrete energy levels of the molecules due to electronic interaction. A number of theoretical and experimental results confirm the existence of this mechanism in many organic solids. Full details are given in [10,11], so here we mention only that (1) quantum-mechanical calculations give band widths of the order of kT [16], as are characteristic of the narrow-band type, mobilities of 0.1 to 10 [cm²/Vs], and free paths corresponding to the various lattice constants (*e.g.* 18—80 Å for metal-free phthalocyanine [27]); (2) there is experimental confirmation of electron and hole mobilities ranging from 0.1 to more than 100 [cm²/Vs] for photocurrent transients [21,28,29], thermoelectric effects [30] or the Hall effect [31-34], a decrease in mobility with increasing temperature, as is typical of lattice scattering in a band [20,21,35,36], and other observations [37,38]. Because of this behavior, which is analogous to that of inorganic semiconductors and insulators in an organic solid, a valence band (energy E_v) and a conduction band (energy E_c) separated by a forbidden gap can generally be defined [26]. When there is predominantly migration of electrons in the conduction band, *n*-type conduction is produced; where holes in the valence band predominate, we have *p*-type conduction. If the electrons and holes are equal in concentration and mobility, we call it intrinsic conductivity.

Fermi statistics can be used to calculate the distribution of charge carriers between the different states of organic solids. For example, it is possible to describe the distribution of electrons between the conduction band and traps, *i.e.* localized states where electrons (holes) will be thermally reexcited into the conduction (valence) band with a higher probability then that they will be captured by a hole (electron) of the valence (conduction) band [38]. Hence, we can also postulate Fermi energies E_F in organic solids as the limit of the energy levels up to which a filling with electrons occurs. Again as in inorganic semiconductors, the steady-state Fermi energy of *n*-type dyes has been observed to lie close to the conduction band and that of *p*-type dyes close to the valence band [39,40].

C. Recombination of Charge Carriers

The recombination of electrons and holes is a rather complicated process. We have to distinguish between (a) the direct recombination of electrons and holes, occurring in particular at high concentrations of charge carriers; (b) recombination via defect states which depends, among other factors, on the densities and capture cross-sections of the defects (recombination centers) located in the bulk of the solid or on its surface.

Process (b) is characterized by two steps: (1) electrons or holes are captured at the corresponding recombination centers; (2) the captured electrons or holes recombine with holes of the valence band or with electrons of the conduction band before their thermal reexcitation. The parameters of the recombination centers

responsible for these reactions are determined by structural effects and chemical purity. For instance, the densities of these centers may range from 10^{12} to 10^{19} cm^{-3}, and the capture cross-sections from 10^{-12} to 10^{-21} cm^2 [41].

The significance of the interplay of the elementary processes (generation, transport, and recombination) for dark- and photoconductivity is discussed below.

3. Dark Conductivity

Most monomeric organic dyes have a conductivity of the order of 10^{-10} to 10^{-14} ohm^{-1}cm^{-1} because the relatively broad forbidden gap between the valence and conduction bands limits the generation rate z to low values:

$$z = \alpha \exp\left(-\Delta E/kT\right) . \tag{3}$$

If we think of dyes as intrinsic semiconductors, each excitation gives an electron–hole pair $(n = p)$ so that in the case of a bimolecular recombination process

$$r = k_r \, n \, p \tag{4}$$

(k_r = recombination coefficient) at equilibrium we have

$$\alpha \exp\left(-\Delta E/kT\right) = k_r \, n \, p \tag{5}$$

or

$$n(=p) = \sqrt{\frac{\alpha}{k_r}} \exp\left(-\Delta E/2\,kT\right) . \tag{6}$$

Then, with $\sigma = e \, n \, \mu$, we obtain for intrinsic-dye semiconductors as we do for organic semiconductors

$$\sigma = \sigma_0 \exp\left(-\Delta E/2\,kT\right) \tag{7}$$

where $\sigma_0 = e \left(\mu_n + \mu_p\right) \sqrt{\alpha/k_r}$
or by application of Fermi statistics

$$\sigma_0 = e \left(\mu_n + \mu_p\right) \sqrt{N_c N_v} . \tag{8}$$

N_c, N_v are the effective density of states in the conduction band and valence band, respectively.

In the case of extrinsic conduction, ΔE may be replaced by ΔE_D and ΔE_A, the values of donors and acceptors [10].

As mentioned above, with broad forbidden gaps a carrier injection from the electrodes may contribute to the dark current. Because the energetic conditions are

for hole injection $$\Phi_H^+ = E_v - \Phi_M \tag{9}$$

and for electron injection $$\Phi_H^- = \Phi_M - E_c , \tag{10}$$

where Φ_M is the metal work function and Φ_H the barrier height [eV], it is possible to observe ΔE values smaller than the forbidden gap. Moreover, using Eqs. (9) and (10), we see that with low Φ_H values the electrodes are injecting or Ohmic contacts which inject holes ($\Phi_M \approx E_v$) or electrons ($\Phi_M \approx E_c$) into the solid. With high values of Φ_H^+ or Φ_H^-, blocking contacts are formed and no charge carriers are injected into the solid.

As soon as the concentration of free carriers (n_i) injected from Ohmic contacts exceeds the concentration of carriers (n_0) produced by intrinsic or extrinsic excitation, space-charge-limited currents (SCLC) appear. In this case the Ohmic current

$$I_{\text{Ohm}} = n\, e\, \mu\, U/L \qquad (11)$$

passes over in a space-charge-limited current

$$I_{\text{SCL}} \simeq \varepsilon\, \varepsilon_0\, U^2/L^3 \qquad (12)$$

where ε_0 is the permittivity of free space, ε the dielectric constant, U the voltage, and L the length of the specimen. It is important to note that the theory of space-charge-limited currents may help to explain the I–U interdependence in organic materials and the influence of traps. For example, in the presence that of trapping levels a proportion of the injected carriers is going into the traps so a higher voltage is necessary to obtain the SCLC condition $n_t > n_0$. Therefore, the ratio of free to trapped carriers can be derived from the Ohmic/SCLC transition voltage; see e.g. [10,14,16,41–44].

The existence of Ohmic and blocking contacts have a great influence on the properties of a photoconductor [41,45,46].

4. Photoconductivity

A. General Relationships

If the generation process is characterized by the primary quantum efficiency η, the transport properties by the mobility μ, and the recombination by the free-carrier lifetime τ, the steady-state photoelectric current can in the case of mobile electrons and immobile holes generally be described by Eq. (13) [14]:

$$I_{\text{phot}} = e\, \eta\, I_A\, V\, \mu\, \tau\, E/L \qquad (13)$$

where e is the magnitude of the electronic charge, I_A the quanta absorbed per cm^3 and per sec, V the volume of the sample, E the field strength, and L the distance between the electrodes. Now, the photocurrent is strongly dependent on the carrier lifetime τ and the mobility μ, yet these parameters are relatively small in organic materials. Thus, photocurrents can often be detected in these materials only at very small electrode spacings ($L < 0.1$ mm). Moreover, in discussing photoconduction it must be remembered that the generation rate g

$$g = \eta\, I_A \qquad (14)$$

(number of excitations per cm³ and sec) or, to be precise, the quantum efficiency of carrier generation, depends upon the applied electric field because only higher fields can *separate* generated carriers before mutual Coulomb interaction causes geminate recombination [44,47-49].

With the steady-state density of photogenerated electrons

$$\Delta n = g\,\tau \tag{15}$$

and the transit time T that a carrier requires to travel from one electrode to the other

$$T = L/\mu\,E\;, \tag{16}$$

we obtain from Eq. (13)

$$I_{\text{phot}} = e\,\Delta n\,V\,\mu\,E/L \tag{17}$$

$$I_{\text{phot}} = e\,\Delta n\,V/T\;. \tag{18}$$

For a photoconductor with mobile electrons and holes generated at the generation rate g per unit volume, the photocurrent density is given by

$$j_{\text{phot}} = e\,(\Delta n\,\mu_n + \Delta p\,\mu_p)\,E \tag{19}$$

and the photoconductivity by

$$\sigma_{\text{phot}} = e\,(\Delta n\,\mu_n + \Delta p\,\mu_p) \tag{20}$$

where μ_n, μ_p = mobility of electrons and holes, respectively, and Δ_p the steady-state density of holes.

B. Photoconductivity Gain

The photoconductive gain G, defined as the number of charge carriers passing through the sample per absorbed photon, can be derived from Eq. (13):

$$G = \frac{I_{\text{phot}}/e}{I_A V} = \eta\,\mu\,\tau\,E/L\;. \tag{21}$$

If $\eta = 1$, substitution of the transit time T [Eq. (16)] gives

$$G = \frac{\tau}{T}\;. \tag{22}$$

For a comparison of different photoconductors, a knowledge of their photo-electric gains is very important. However, it should not be forgotten that G depends, among other factors, on the mean lifetime τ. Since the parameters responsible for the mean carrier lifetime depend considerably on structural effects

and on chemical purity, G can vary within wide limits (up to a factor of 10^{10}) in different samples of one and the same compound.

a) Influence of Blocking Contacts. When photoconductors such as dyes are insulated with blocking contacts at both electrodes, an increase of the field can only give a maximum gain $G = 1$. The current–voltage curve becomes saturated for these "primary" photocurrents at high voltages if all photogenerated carriers characterized by a Schubweg $w = \mu \tau E$ reach the electrodes (*i.e.* $w = L$ and $\tau = T$) and are extracted. In the case of mobile electrons and holes, the photoconductive gain is then given by

$$G = (\mu_n \tau_n + \mu_p \tau_p) \frac{E}{L} \tag{23}$$

$$G = \left(\frac{\tau_n}{T_n}\right) + \left(\frac{\tau_p}{T_p}\right) = \frac{W_n + W_p}{L} \tag{24}$$

The photoconductive gain G as measured from saturated current–voltage curves is of the order of unity in several dyes [3,50,51], *e.g.* in malachite green $G = 0.2$, pinacyanol $G = 0.37$ and merocyanine A 10 *1* $G = 0.6$.
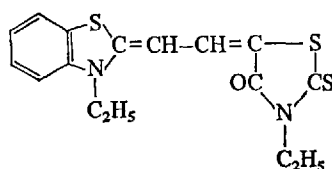
1

Moreover, in agreement with the given relationships, the photoconductive gain G increases considerably with decreasing electrode spacing at constant field strength and layer thickness (cf. Table 1 [50]).

Table 1. Relation between G and L for crystal violet ($\lambda = 5870$ Å; $E = 7000$ V/cm; layer thickness 3×10^{-6} cm)

L [cm]	G
0.08	0.0009
0.042	0.0012
0.02	0.0026
0.01	0.0052
0.003	0.014

b) Influence of Ohmic Contacts. In photoconductors with Ohmic contacts G values may exceed unity because the primarily excited carriers after extraction from the sample by the electric field can be replenished by a carrier supply from an injecting contact. Moreover, because of the formation of space charges, these "secondary" photocurrents generally saturate at high fields so that maximum gain is obtained. For example, in the voltage-induced transition from Ohmic conduction

to space-charge limited conduction [*i.e.*, the voltages in Eqs. (11) and (12) become equal: U_{SCL}] the photoconductive gain is determined by the fact that the transit time becomes equal to the dielectric relaxation time τ_{rel} [$= \varepsilon\varepsilon_0/\sigma = 10^{-12}\varepsilon/4\pi\sigma$ (sec)]:

$$\frac{L^2}{\mu\, U_{\text{SCL}}} = \frac{\varepsilon\varepsilon_0}{n\, e\, \mu} \quad \text{or} \quad T = \tau_{\text{rel}} \,. \tag{25}$$

Without traps the response times τ_0 of photoconductors are equal to the mean lifetime τ; therefore we obtain for the maximum gain instead of Eq. (22)

$$G = \frac{\tau_0}{\tau_{\text{rel}}} \,. \tag{26}$$

This relation also holds in the presence of shallow traps since the ratio of trapped (n_t) to free carriers (n) $(n_t \gg n)$ influences both the response time (τ_0)

$$\tau_0 \simeq \left(\frac{n_t}{n}\right)\tau \tag{27}$$

and the transit time

$$T = \frac{1}{(n_t/n)}\,\tau_{\text{rel}} \,; \tag{28}$$

We obtain Eq. (26) by introducing τ and T from Eqs. (27) and (28) into Eq. (22).

From these relationships it can be seen that, *e.g.* in low-resistivity photo-conductors with equal response times, or by introduction of deep traps that increase the transition voltage U_{SCL}, photoconductive gains greater than unity may be obtained. For example, in merocyanine dyes doped with electron-acceptor compounds a quantum yield $G = 2.3$ has been measured [14,53].

The situation is more complicated in photoconductors with Ohmic and blocking contacts and different types of carriers. However, with the aid of the concepts discussed above, the photoconductive behavior of such systems may also be understood.

5. Photovoltaic Effects

As in inorganic photoconductors, with organic dyes and other organic compounds, too, photocurrents and photovoltages may be observed without the application of auxiliary voltages. The following effects may be mentioned.

A. Dember Effect

This effect is characterized by light-induced formation of a photo-emf in boundary layer-free systems [3,10]. It is necessary for the generation of the Dember emf to have (a) the formation of a concentration gradient of charge carriers resulting from non-uniform illumination, and (b), electrons and holes of different mobilities:

$$E_{\text{phot}} = \frac{kT}{e}\left[\frac{(\mu_n/\mu_p)-1}{(\mu_n/\mu_p)+1}\right]\ln\frac{\sigma_1}{\sigma_d} \tag{29}$$

where σ_1, σ_d represent the conductivity of specimen in illuminated and dark parts, respectively. The photo-emf is generally of the order of 0.01—0.1 mV.

B. Barrier Layer Photopotentials

The formation of space-charge layers at contacts or at the surface of a semiconductor may lead to the generation of photovoltages. This type of photo-emf results from the separation of electron–hole pairs under the influence of the electric field in the contact or surface space-charge region.

Note that a surface charge compensated by a space charge below the surface may be formed.

(a) as a result of differences in the work functions of metal and photoconductor;

(b) due to the presence of localized states for majority carriers on the surface of the semiconductor.

Where there is depletion of majority carriers, we have in both cases a depletion layer, that is characterized in the band diagram by a bending of the bands, as shown in Fig. 1.
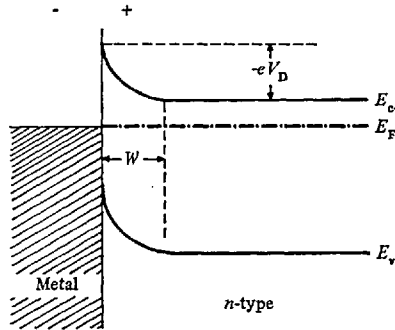
Fig. 1. Scheme of the band diagram for the contact metal/n-type semiconductor

The diffusion voltage V_D and the barrier width W depend on the influence of diffusion and recombination (*i.e.* the Debye length $L_D = \sqrt{D \cdot \tau_{rel}}$, $D = \left(\dfrac{kT}{e}\right)\mu =$ diffusion coefficient) and are therefore given by

$$W = \sqrt{\frac{2\varepsilon\varepsilon_0 V_D}{e \cdot N_D}} \tag{30}$$

($N_D =$ donors per unit volume). Thus, we obtain for the electric field strength at the interface between metal (or surface states) and photoconductor

$$E_0 = -2 V_D/W . \tag{31}$$

The photovoltage across the barrier can be expressed [53] as

$$E_{\text{phot}} = \left(\frac{kT}{e}\right) \ln \left[1 + \frac{I_1}{I_0 \exp\left(-\Delta E/2\,kT\right)}\right] \tag{32}$$

where I_1 is the induced current under illumination and $I_0 \exp\left(-\Delta E/2kT\right)$ the current flow in the dark. With large I_1 we have

$$E_{\text{phot}} = \frac{\Delta E}{2e} + \left(\frac{kT}{e}\right) \ln \frac{I_1}{I_0} \simeq \frac{\Delta E}{2e} \tag{33}$$

as condition for the maximum photovoltage. For small I_1 the photo-emf is

$$E_{\text{phot}} = \left(\frac{kT}{e}\right) \left(\frac{I_1}{I_0}\right) \exp\left[\frac{\Delta E}{2\,kT}\right]. \tag{34}$$

In the early 1950's it first became possible to determine the photoelectric sensitivity of dyes of different classes (phthalocyanines, cyanines, etc.) by measuring barrier-layer photopotentials in cases where barriers were strongly affected by carriers trapped in the surface states of adsorbed gases [54-56]. In agreement with the theory of inorganic surface-barrier rectifiers, asymmetric current–voltage curves were also observed.

Therefore, we can assume that at surfaces or contacts of organic solids in the equilibrium state diffusion currents $(=eD\,dn/dx)$ and field currents $(=en\mu E)$ may cancel each other out, i.e.

$$j = n\,e\,\mu\,E + e\,D\,dn/dx = 0. \tag{35}$$

Moreover, it is probable that, as with the space-charge layers of inorganic semiconductors, the following relationships can be considered for organic systems:

(a) When a voltage which adds to the diffusion potential of a contact is applied, the barrier width W increases and a weak field current exceeds the diffusion current because the concentration gradient is slight;

(b) When, the reverse voltage is applied, the width W decreases, the concentration gradient becomes steeper and a high diffusion current outweighs the field current [57].

The photopotentials of dye–gas–metal systems have reached an order of 0.1 mV [55] and those of alkali metal–aromatic junctions 0.2 to 1.0 V [53]. Whereas the photo-emf of noble metal–aromatic junctions were of the order 1—15 mV [53], thin tetracene films sandwiched between two different evaporated metal electrodes (Au, Al) showed photovoltaic effects with an open-circuit photovoltage up to 0.6 V [58]. This high photovoltage may be attributed either to a built-in voltage resulting from the difference in work functions of the two electrodes or to cooperation of two space-charge layers at the contacts.

C. P—N Junction Photovoltaic Devices

In p—n junctions a space-charge layer is formed in the transition region between an n-type and a p-type region by an exchange of charge carriers. This is a consequence of the overall tendency for the Fermi levels to become equal in height throughout the system (Fig. 2).
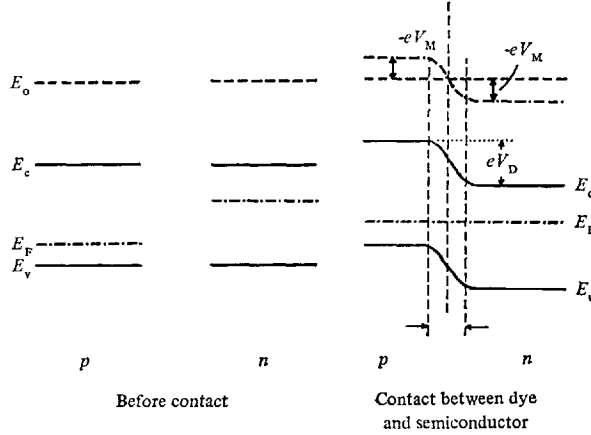
Fig. 2. Formation of diffusion voltage V_D in p—n junctions. Note: V_M = macropotential which results from macroscopic space charges, double layers etc. Any shifting of V_M caused by any kind of charge (positive charge in the n region and negative charge in the p region of p—n junctions) displaces the other energy levels in an analogous manner; see [61,62] for details

As with metal–semiconductor contacts, the electric field in the space charge, which is given by the diffusion voltage V_D and the width of the space-charge region W, separates optically generated electron–hole pairs. W is given by [41]:

$$W = \left[\frac{2\varepsilon\varepsilon_0}{e}\frac{N_A + N_D}{N_A N_D} V_D\right]^{1/2} \tag{36}$$

where N_A, N_D = concentration of acceptors on the p side and of donors on the n side. In systems in which $N_A \gg N_D$ (p^+—n junction) or $N_D \gg N_A$ (p—n^- junction), W is small as in space-charge layers at contacts [see Eq. (30)]. Therefore, the photocurrent will be carried mainly by minority carriers, which are generated in field-free regions and diffuse into the space-charge region [15,59–61].

For an understanding of photocurrent density and photovoltage (Fig. 3) it is necessary to take into account that in the dark there is diffusion of electrons from the n side to the p side and that this depends among other things on an external voltage V,

$$\dot{j}_{n(d)} = \frac{e \cdot n_p \cdot L_n}{\tau_n} \left[\exp\left(eV/kT\right) - 1\right], \tag{37}$$
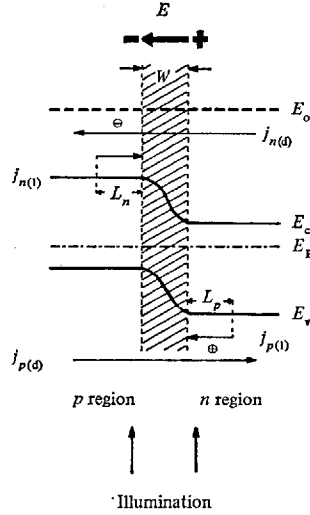
97

Fig. 3. Scheme for an explanation of the photovoltaic effect in p—n junction devices (see text)

whereas during illumination electrons photogenerated as minority carriers in the p region diffuse in the opposite direction to the barrier layer and are injected under the influence of the internal field into the n region:

$$j_{n(1)} = e \cdot g \cdot L_n \tag{38}$$

where L_n is the diffusion length of electrons, n_p the concentration of electrons in the p-zone, g the number of excitations per cm^3 and sec. Therefore, the whole electron current density during illumination is

$$j_n = e \cdot g \cdot L_n - \frac{e \cdot n_p \cdot L_n}{\tau_n} \left[\exp (eV/kT) - 1 \right]. \tag{39}$$

A similar expression can be written for holes, which diffuse in the dark from the p to the n region and during illumination act as minority carriers from the n side to the space-charge region and move from there under the influence of the field into the p region;

$$j_p = e \cdot g \cdot L_p - \frac{e \cdot p_n \cdot L_p}{\tau_p} \left[\exp (eV/kT) - 1 \right] \tag{40}$$

where L_p is the diffusion length of holes, and p_n the concentration of holes in the n zone.

In the n zone and the p zone outside the p—n space-charge layer the currents flow as field currents, i.e. $j_n = e \mu_n n_n E$ (if $n_n \gg p_n$) and $j_p = e \mu_p n_p E$ (if $p_p \gg n_p$). By addition of Eqs. (39) and (40) we obtain for the photocurrent density

$$j_{\text{phot}} = e \cdot g \left(L_n + L_p \right) - e \left(\frac{n_p \cdot L_n}{\tau_n} + \frac{p_n \cdot L_p}{\tau_p} \right) \left[\exp (eV/kT) - 1 \right]. \tag{41}$$

In the case of a short circuit $(V = 0)$, the photocurrent density can be given as

$$j_{phot} = e \cdot g \, (L_n + L_p) \tag{42}$$

or, taking into consideration the broad width of the space–charge region W and the area F of the p–n system,

$$I_{phot} = e \, F \, \eta \, I_A \, (L_n + L_p + W) \tag{43}$$

$[g = \eta I_A$ from Eq. (14)]. This means there is a linear relationship between short-circuit photocurrent and light intensity.

By inserting $j_{phot} = 0$ in Eq. (41) we can derive the photovoltage $E_{phot} \, (= V)$

$$E_{phot} = \frac{kT}{e} \ln \left[\frac{g \, (L_n + L_p)}{n_p \, L_n/\tau_n + p_n \, L_p/\tau_p} + 1 \right] \tag{44}$$

or

$$E_{phot} \simeq \frac{kT}{e} \ln \left(z \, \eta \, I_A + 1 \right) . \tag{45}$$

Hence, a logarithmic relation exists between the open-circuit photovoltage and light intensity (Fig. 4).
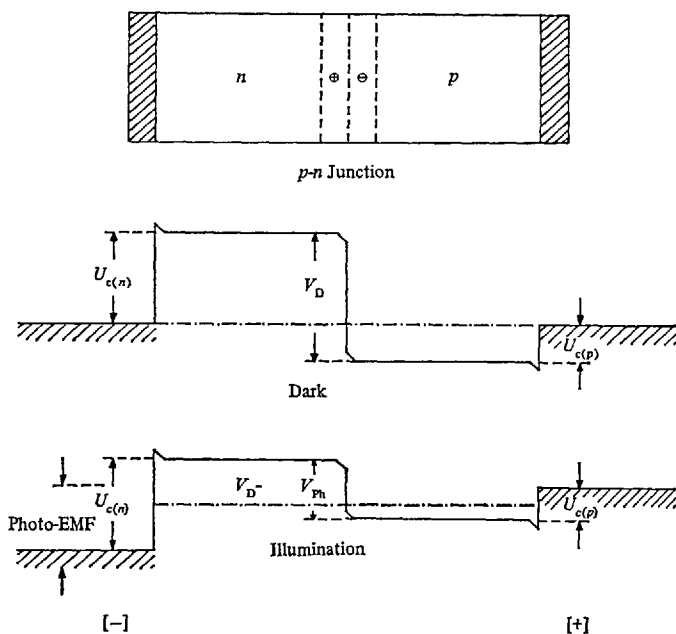
Fig. 4. Scheme of the p–n photoeffect (according to [59]) explaining the generation of photo-emf. Note: U_c = contact voltage between metal and photoconductor; V_D = diffusion voltage in the p–n junction; V_{ph} = reverse internal photovoltage (in relation to V_D)

In discussing the relations for the photocurrent and the photovoltage of p—n junctions it should not be forgotten that the sensitivity of these devices depends among other things (*e.g.* the primary quantum yield η) on the diffusion length L, *i.e.* on the mean distance a charge carrier travels before it recombines, This is given by

$$L = \sqrt{D\tau} \qquad (46)$$

with

$$D = \frac{kT}{e}\,\mu\,. \qquad (47)$$

Therefore, the values for the mobility and lifetime of electrons and holes are important for efficient p—n photovoltaic devices.

6. Conclusion

In conclusion it must be stressed that, for applications of the semiconductor properties of organic dyes and other compounds, the important factors besides the energy gap ΔE and the primary quantum efficiency η of the generation of electron–hole pairs are the characteristic parameters mobility μ and lifetime τ of electrons and holes.

If polymeric dyes are also taken into consideration, the energy gap ΔE can range from tenths of an eV to several eV. While the primary quantum efficiency η may reach values of the order of unity, we can also have weak field-dependent values.

Unlike inorganic semiconductors whose mobility ranges from a few cm²/Vsec up to $\mu_n = 77,000$ cm²/Vsec (in InSb), organic dyes because of the influence of the high density of traps and narrow energy bands have mobility values that lie between very low values ($< 10^{-4}$ cm²/Vsec) and values of 1—50 cm²/Vsec.

As with inorganic photoconductors, *e.g.* CdS [63], the lifetime τ of free carriers, which can be considered as a measure of photosensitivity, depends on the preparation of the compound. This is because of the great influence of defect states (impurities, lattice defects) in the forbidden zone. It is probable that the values of τ can range from 10^{-2} to 10^{-10} sec. When testing organic materials, it should be borne in mind that τ is not constant for a given compound. Therefore in the search for the optimum photoconductivity of a compound systematic variation of the conditions of preparation is essential. Lifetimes longer than 10^{-4} sec may be considered as a criterion for sensitive photoconductors. It would be useful to have systematic measurements of τ and the diffusion coefficient D, which are important in discussing the efficiency of photovoltaic devices. Some values are given in Table 2; see also [10,16].

Table 2. Electronic parameters of some dyes (from Ref. [15])

Dye	τ	$D\tau$	D
Pinacyanol	1.1×10^{-4} s	1.3×10^{-11} cm²	1.2×10^{-7} cm²/s
Trypaflavin	2×10^{-4} s	6.1×10^{-11} cm²	3×10^{-7} cm²/s

Attempts have recently been made to produce organic semiconductor components for industrial use without taking account of the characteristic parameters of semiconductivity of organic compounds. Nowadays, we know the need for a systematic study of these parameters because they can show us both the limits of application and the conditions which must be fulfilled for maximum use of the electrical and photoelectrical properties of dyes and other organic compounds.

III. Influence of the Structure of Organic Compounds on Their Electrical Behavior

The most important difference between organic and inorganic semiconductors arises from the fact that the molecules in the crystalline state are held together by small forces and are fixed at relatively long distances from each other (of the order of >3.4 Å). In many organic solids this restricts the intermolecular transport of charges, as discussed above. For applications of the semiconducting properties of organic solids it is necessary to have materials with low resistivities and photo-conductivities characterized by light-enhanced conductivity of several orders of magnitude. There are several possible ways of influencing conduction behavior through variations of the organic structure. However, much work is still necessary in this special field; see details in [10].

1. Dark Conductivity

As mentioned above, organic dyes generally have dark conductivity only below 10^{-10} ohm^{-1}cm^{-1}. However, higher conductivity can be achieved in dyes — and as in other organic solids — by the three methods described below.

1. The number of delocalizable π electrons can be increased. This is possible because the activation energy of the dark conduction, like the intramolecular excitation energy of the electrons, decreases with increasing number N of delocalizable electrons in agreement with the electron gas theory. Hence, if the relationship between ΔE and N for the open [Eq. (48)] and cyclic [Eq. (49)] π electron systems is represented graphically, the ΔE values obtained from conductivity measurements will generally lie between the two curves; see e.g. [13,64].

$$\Delta E = 19.2 \frac{N+1}{N^2} \tag{48}$$

$$\Delta E = 38 \frac{1}{N} \tag{49}$$

For instance, the value of $\Delta E = 1.7$ eV measured for single crystals of phthalocyanine, leads us to conclude that the 18-π-electron system is responsible for both light absorption and conduction.

On the other hand, the conductivity within a given class of organic semiconductors increases with decreasing activation energy according to Eq. (50) [10,65]:
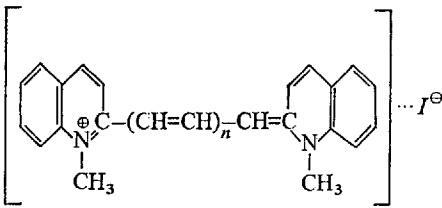
$$\varDelta E_n = -c' \log \sigma_n + \log X_0 \qquad (50)$$

where c' and X_0 are specific constants for a special class.

The correctness of these relationships can be seen from the values in Table 3, obtained for monomeric polymethine dyes.

Table 3. Relation between the number of π electrons N, thermal activation energy $\varDelta E$, and dark conductivity σ_D of polymethine dyes (after [66,67])

Dye	Structure	N	λ_{max} [nm]	$\varDelta E$ [eV]	σ_D [ohm^{-1}cm^{-1}]
Trimethinecyanine	2	8	605	1.8	2×10^{-13}
Pentamethinecyanine	3	10	710	1.3	10^{-11}
Heptamethinecyanine	4	12	817	0.69	1.3×10^{-8}

2 $n=1$ 3 $n=2$ 4 $n=3$

Polymeric dyes, such as the polymeric phthalocyanines, become more conducting as the degree of polymerization increases. This is demonstrated in Fig. 5 for polymeric Fe- and Co-polyphthalocyanines [65].
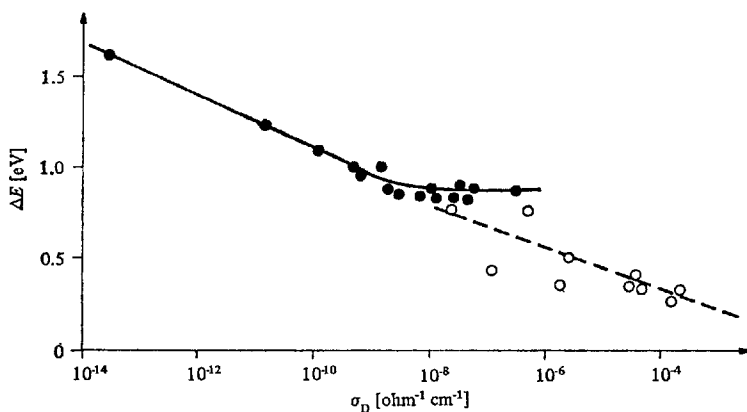
Fig. 5. Relationship between thermal activation energy and dark conductivity: $\varDelta E_n = f$ (log σ_D). ——— Fe-polyphthalocyanine; -------- Co-polyphthalocyanine

However, Fig. 5 also indicates that where there is disturbance of the delocalization of π electrons the ΔE_n values and the corresponding σ_n values [resulting from Eq. (50)] tend toward a limit. Thus, as in other organic semiconductors, we have to distinguish between rubiconjugated compounds (characterized by a disturbed delocalization as in Fe-polyphthalocyanines) and ekaconjugated compounds (characterized by an undisturbed delocalization of π electrons as in Cu-polyphthalocyanines).

It should be stressed here that the conductivities of e.g. polymers with phthalocyanine-type structure vary between 6.3×10^{-3} and 2.1×10^{-10} ohm^{-1}cm^{-1} with activation energies down to 0.04 eV [8,68,69]. The best conducting dye polymers showed a maximum of $\sigma_D = 0.3$ ohm^{-1}cm^{-1} [70].

2. Another way of increasing conductivity is to use special doping agents such as o-chloranil, tetracyanoethylene, or tetracyanoquinodimethane. This effect, first observed by Hoegl et al. [71,72] during photoconductivity experiments on electrophotographically interesting polymers and later on dyes [52,73], is characterized by a rapid increase of dark conductivity with concentration of doping agent according to Eq. (51) [74]:

$$\sigma_D = a\, C^{\beta} \qquad (51)$$

where C is concentration of the doping agent and a is a constant. For example, a β-value of 5.3 is found on doping phthalocyanines with o-chloranil, as shown in Fig. 6.
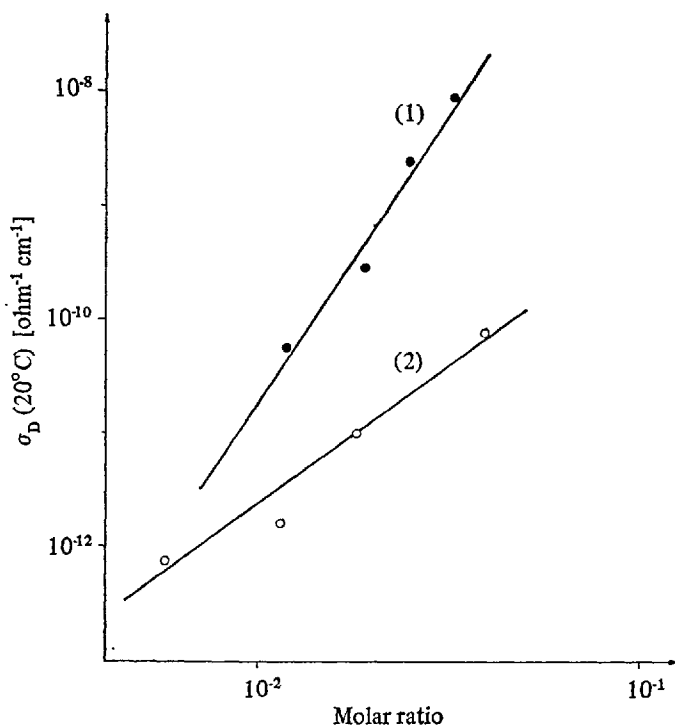
Fig. 6. Relation between dark conductivity and concentration of doping compounds: $\log \sigma_D = f$ ($\log n_{acceptor}/n_{dye}$). (1) phthalocyanine + o-chloranil; (2) poly-N-vinylcarbazole + o-chloranil

In discussing doping of organic compounds allowance must be made for the fact that activation energy decreases with concentration of doping compound (see Table 4).

Table 4. ΔE values of phthalocyanine doped with o-chloranil [74]

Molratio [chloranil/phthalocyanine]	ΔE [eV]
No doping	1.82
1.26×10^{-2}	0.87
1.84×10^{-2}	0.81
2.47×10^{-2}	0.78
3.12×10^{-2}	0.71

This observation may result from an usual acceptor effect according to which ΔE can be identified with the energetic position of acceptors in the forbidden gap. It should be mentioned here that, according to Lyons [75], ΔE is connected by Eqs. (52) and (53) with the electrostatic polarization energy P.

$$\Delta E = I_c - A_c = I_g - A_g - 2P \qquad (52)$$

$$E \cong I_c - 2P \qquad (53)$$

where I_c and A_c are the ionization energy and electron affinity in the solid state and I_g and A_g the ionization energy and electron affinity in the gaseous state.

Because P depends on the molecular polarizability α, the activation energy may change under the influence of the introduced charge-transfer dipoles between dye and acceptor.

Hence there exists a relationship between ΔE and the dielectric constant ε which is correlated with α by the Clausius-Mosotti equation:

$$\Delta E = I_g - \eta' \frac{\varepsilon - 1}{\varepsilon + 2} \qquad (54)$$

where η' is a term describing doping effectiveness (e.g. $\eta' = 10.2$), and $I_g = 7.90$ eV in phthalocyanines doped with iodine [76].

The important thing is that this decrease of ΔE obtained by doping may be accompanied by an enhancement of dark conductivity of several orders of magnitude.

3. In phthalocyanines, changing the central atom may cause the conductivity to differ between 10^{-16} and 10^{-2} ohm^{-1}cm^{-1} [10]. The highest conductivity of 4×10^{-2} ohm^{-1}cm^{-1} has been reported for Nd phthalocyanine [77].
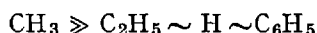
2. Photoconductivity

Traps and recombination centers which depend on purity, crystal defects and preparation, can exert an influence, and electrode contacts, carrier injections, and other factors can interfere with measurements. Yet there is no doubt that the photoconductive gain (quantum yield) G can be reproduced by different methods. As in the case of dark conductivity, the photoconductivity properties are related to the electronic and structural behavior of pure and doped organic compounds, also those in the polycrystalline state.

A. Relation between Molecular Structure and Photoconductivity

The chances of synthesizing good dye photoconductors for use in photoconductive devices can be deduced from certain structural relationships (details are discussed in [10].

1. In triphenylmethane dyes the degree of methylation of the amino groups is proportional to the photoconductivity and there is a decrease in sensitivity on replacement of a methyl group by other substituents; thus we have the order

$$CH_3 \gg C_2H_5 \sim H \sim C_6H_5$$

2. In cyanines and merocyanines there is an increase in the photoconductivity with the number of methine groups, $i.e.$ with the lengthening of the conjugated chain [61,78].

3. In pyrazines based on aceanthraquinoxaline 5

5
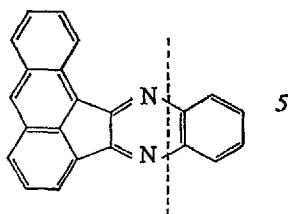
obtained by condensation of aceanthraquinone with 1,2-aromatic diamines, the photoconductive response depends on variation of the structure of part B of 5 according to the order [79]:

| (a) | (b) | (c) | (d) | (e) |
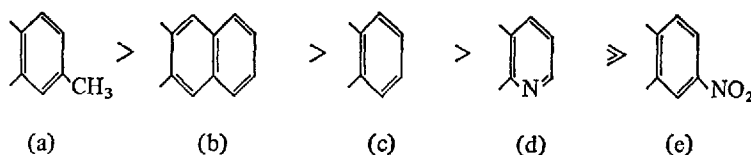
$5 \; a\text{-}e$

Table 5 illustrates this structural dependence by giving some values for I_{phot}/I_{dark}.

Table 5. Structural dependence of acean-
thraquinoxaline derivates (after Ref. [79])

Moiety B of 5	I_{phot}/I_{dark}
(a)	7×10^5
(b)	7.2×10^4
(c)	2.6×10^4
(d)	4×10^2

The fundamental influence of substituent groups on the photoconductivity within aceanthraquinoxaline derivatives is shown in Fig. 7 for two pyrazines that differ by a methyl group.
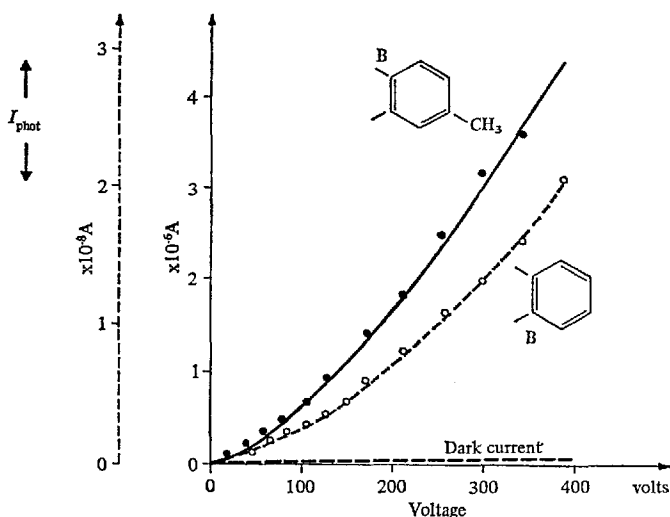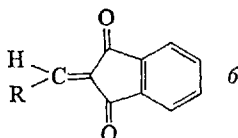

Fig. 7. Dependence of photoconductivity on structure for aceanthraquinoxaline 5 $I_{phot} = f$ (Voltage)

From these results it can be concluded that photoconductivity is closely connected with the number and degree of delocalization of the π-electrons. An increase in the number of aromatic rings or methyl substitution increases the photoelectric sensitivity. Conversely, the incorporation of electron-accepting groups or the reduction of the π-electron density in the ring system by replacing C-atoms by N-atoms causes photoconductivity to decrease.

In addition to this influence of the molecular structure, which correlates with the number and the delocalization of π-electrons, steric effects resulting from the internal molecular geometry and the nature of the substituents may play an important role in intermolecular charge transfer because of the packing of adjacent molecules in the solid [80]. For instance, the observation that the introduction

of a second benzene ring in the 2—3 position of 5 leads to $I_{phot}/I_{dark} = 7.2 \times 10^4$ whereas if it is in the 3—4 position I_{phot}/I_{dark} is 3.8×10^3 may be explained as due to a packing effect.

4. In 2-arylidene-1,3-indandiones 6, which can be considered as ethylene derivatives with two end-carbon atoms attached to 1,3-indandione and to electron-acceptor and electron-donor groups (R), respectively, photoconductivity depends on the substituents of the arylidene group [81].

This dependence is clear from some I_{phot}/I_{dark} values given in Table 6.

Table 6. Dependence of the photoconductivity of arylidene-1,3-indandiones on structure (after Ref. [81])

Group R	I_{phot}/I_{dark}	λ_{max} [nm]
4-Nitrophenyl	3.8	
3,4,5-Trimethoxyphenyl	26	
4-Diethylaminophenyl	1×10^3	546
4-Dimethylaminophenyl	1.2×10^5	582
1-Naphthyl	99	
3-Pyrenyl	2.5×10^3	570
3-N-ethylcarbazolyl	9.3×10^3	506

The maximum photoconductivity of the 4-dimethylaminoderivative is in good agreement with the high degree of delocalization of the π-electrons of this compound. Similarly, in other compounds with the same molecular framework there is good correlation between photoconductivity and delocalization of π-electrons; this correlation is enhanced by increasing the electron-donating power of the group R. For instance, in the 3-N-ethylcarbazolyl derivative we can assume intramolecular migration of the lone-pair electrons on the nitrogen, leading to a polar form of the excited state. When intramolecular electron transfer is inhibited, as in the anthracene derivative, the photoconductivity is weak.

5. In derivatives of 9-dicyanomethylene-2-nitrofluorene 7 the ratios of photocurrent to dark current range between 100 and 20.000 depending on the position of the introduced nitro groups [82].

The highest ratio is obtained in the 2,7-dinitro derivative. It is probable that the planarity of the nitro derivatives and the way the molecules are packed in the bulk play an important role in the photoelectric behavior. A self-complex type of structure may be formed, which favors charge transfer in the solid.

B. Doping

The addition of doping agents can increase the photoconductivity of dyes by several orders of magnitude [52,74]. Some examples are given in Table 7.
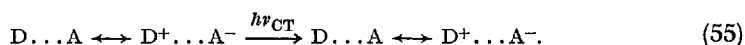
Table 7. Enhancement of photoconductivity on doping

Dye	Doping compound	$\dfrac{I_{phot}(\text{doped})}{I_{phot}(\text{undoped})}$	Ref.
Merocyanine A 10 *1*	o-Chloranil	60	[52]
	Iodine	1.7×10^3	
Merocyanine FX 79 *8*	p-Chloranil	6	[52]
	o-Chloranil	150	
Phthalocyanine	Tetracyanoethylene	400	[73,74]
	o-Chloranil	10^4	[73,74]

8
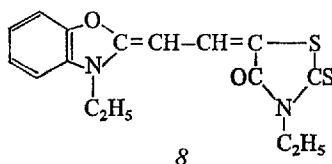
Like dark conductivity, photoconductivity increases rapidly with the concentration of the doping compound [see Eq. (51)]. Suitable doping agents can give photoconductive gains $G > 1$ [52].

In some compounds the doping effect may be the result of charge-carrier generation brought about by an intermolecular charge-transfer transition [72,83]

$$D\ldots A \longleftrightarrow D^+\ldots A^- \xrightarrow{h\nu_{CT}} D\ldots A \longleftrightarrow D^+\ldots A^-. \tag{55}$$

In systems in which the charge-transfer excitation band differs from the action spectrum of photoconductivity, the doping effect may be due to a change of recombination path that results in an enhancement of carrier lifetime (*e.g.* holes in merocyanines and phthalocyanines). (Details on the mechanism are given in [10,11,74].)

3. P- and N-Type Conductivity

A. Dark Conductivity

Like other organic compounds, dyes can be divided into *n*- and *p*-type conductors. This may be confirmed by measuring the influence of oxygen or hydrogen [3,14,84], the Hall effect [31,34,85] or the thermoelectric effect [66,86]. Moreover, in agreement

with the rules for extrinsic semiconductors, the Fermi levels are close to the energy bands.

For instance, the Fermi level of monomeric p-type phthalocyanine is close to the valence band and can be shifted nearer to this band by doping, as shown in Fig. 8.
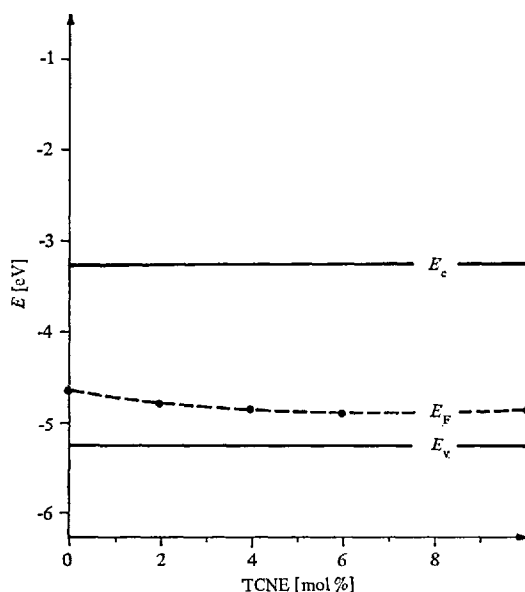

Fig. 8. Position of the Fermi level E_F in phthalocyanine doped with tetracyanoethylene (TCNE)

There seems no doubt that this effect results from an increase in the concentration of holes in the valence band, described by

$$E_F = E_v - kT \ln (p/N_v) \tag{56}$$

where N_v is the effective density of states in the valence band and $p \ll N_v$.

The fact that the thermoelectric-emf Q falls within polymeric homologs and is lowered by a transition from monomers to polymers (see Table 8 [65]) also confirms these results, because we have the relation between Q and p:

$$Q_p = \left(\frac{k}{e}\right) \log \frac{N_v}{p} . \tag{57}$$

In conclusion it can be stated that the p- and n-type dark conductivity of doped dyes and a number of undoped dyes is the result of differences in the densities of holes and electrons. Thus, in p-type dyes we have $p \gg n$, and in n-

109

Table 8. Relation between thermoelectric-emf and structure [65]

Phthalocyanine	Q [μV/^{0}C]	Type
Monomeric Fe Pc	1406	p
Polymeric Fe Pc	643	p
Monomeric Co Pc	1165	p
Polymeric Co Pc	555	p

type dyes $n \gg p$. However, it should not be overlooked that in the case of intrinsic dark conduction $p \approx n$. In such compounds the type of conduction may be determined by differences in the mobility of holes and electrons; the thermo-emf is therefore given by [87]

$$Q = \frac{k}{e} \frac{(b-1)}{(b+1)} \left[\frac{\Delta E}{2k\,T} + 2 \right] \tag{58}$$

$(b = \mu_n/\mu_p)$.

B. Photoconductivity

It has been shown in a series of experiments [3] that illuminated dyes can be classified into n- and p-type photoconductors. This classification correlates in many cases with the structure of the dyes.

1. Triphenylmethane derivatives, rhodamines, and nitro derivatives of 9-dicyanomethylene fluorene are characterized by n-type photoconductivity.

2. Merocyanines, phthalocyanines, pyrazines based on aceanthraquinoxalines, and several arylidine-1,3-indandiones exhibit p-type photoconductivity.

3. Small changes in the molecular structure — e.g. the replacement of a bridging carbon atom by a nitrogen atom — can change a p-type dye into an n-type dye. This effect is connected with changes in optical absorption and photographic behavior [10,40].

Whereas in good-conducting doped or polymeric dyes p-or n-type conductivity can be explained without difficulty by analogy with inorganic semiconductors, the p- and n-type photoconductivity in insulating (intrinsic) dye films cannot be explained in this manner. It is necessary to take into consideration the existence of defect states (lattice defects, dislocations, impurities etc.) distributed at different depths in the forbidden zone between valence and conduction band; these defect states are able to trap electrons and holes, respectively, with different probability [10,11,88].

In this connection it should be remembered that we can distinguish between recombination centers and traps. On the one hand, electron or hole traps can be considered as states from which trapped electrons or holes will with relatively high probability be reexcited thermally into the conduction or valence band.

On the other hand, electrons or holes trapped in recombination centers have a higher probability of capturing a free hole or electron in the valence or conduction band than of being reexcited. The distinction may in many cases be somewhat arbitrary [41]. However, there seems no doubt that, as in inorganic semiconductors and insulators in organic photoconductors, a high density of recombination centers and traps with densities ranging from 10^{12} cm^{-3} to 10^{19} cm^{-3} can be assumed in the forbidden gap. Moreover, in polycrystalline and particularly in amorphous samples these defect states are distributed at different energy levels throughout this zone.

Therefore, we are able to discuss the existence of defect states (recombination centers and traps) in the forbidden gap of solid organic dyes characterized by different trapping probabilities (ranging from 10^{-12} cm^2 to 10^{-20} cm^2) for electrons and holes. Hence, asymmetric trapping of electrons and holes leading to n- and p-photoconductivity is very probable.

(a) With a large number of trapping centers for holes (*e.g.* traps filled with electrons from donating centers or from injecting contacts by an applied electric field) the holes of excited electron–hole pairs would be rapidly trapped and therefore to a great extent immobilized. The electrons, however, are distributed between the conduction band and high-lying shallow traps so that the solid is characterized by n-type photoconductivity.

(b) On the other hand, if only low-lying trapping states are filled, a large number of empty defect states will be ready to trap electrons. Such a dye film would be characterized by p-type photoconductivity.

According to this concept of asymmetric trapping — which is also discussed for inorganic photoconductors by Rose [63,89] — the chemical potential of electrons (*i.e.* the Fermi potential) should be situated close to the conduction band (in n-type photoconductors) and valence band (in p-type photoconductors), respectively, as illustrated in Fig. 9.
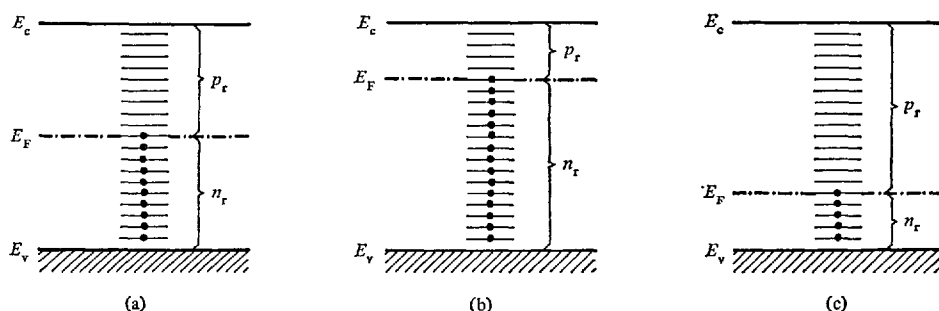
Fig. 9. Dependence of n-type or p-type organic photoconductors on trapping. (a) Symmetric trapping; (b) Asymmetric trapping: n-type; (c) Asymmetric trapping: p-type; p_r, n_r = empty and filled centers, respectively; E_F = Fermi energy

These differences in the location of the Fermi energies of p- and n-type dyes have been experimentally confirmed [11,40]. It was also shown by experiment that, in accordance with the model given, the Fermi energy of illuminated dyes

E_{F}^{*} is situated above the Fermi energy of nonilluminated dyes E_{F} because of the excitation of electrons into the conduction band [90]. Therefore we have

$$E_{\mathrm{F}}^{*} - E_{\mathrm{F}} = kT\, ln\ (n_{\mathrm{L}}/n_{\mathrm{D}}) \tag{59}$$

(n_{L}, n_{D} = density of free electrons in the light and dark, respectively).

Quantitatively, it should be possible to describe the p- and n-type conductivity of dye films with known densities of empty and filled centers (p_{r}, n_{r}) by capture cross-sections of these centers for free electrons and free holes (s_n, s_p), because the free-carrier lifetime (τ_n, τ_p) of electrons and holes is given by

$$\tau_n = \frac{1}{p_{\mathrm{r}}\, s_n\, v_{\mathrm{th}}} \qquad \tau_p = \frac{1}{n_{\mathrm{r}}\, s_p\, v_{\mathrm{th}}} \tag{60}$$

(v_{th} = thermal velocity). The steady-state density of electrons ($\varDelta n$) and holes ($\varDelta p$) is given according to Eq. (15) by

$$\varDelta n = g\, \tau_n \qquad \varDelta p = g\, \tau_p \tag{61}$$

(g = number of excitation/cm^3 sec). It therefore follows from Eqs. (60) and (61) that

$$\frac{\varDelta n}{\varDelta p} = \frac{n_{\mathrm{r}}\, s_p}{p_{\mathrm{r}}\, s_n}\ . \tag{62}$$

The photoconductivity can be described by

$$\sigma_{\mathrm{phot}} = e\,(\varDelta n\, \mu_n + \varDelta p\, \mu_p) \tag{20}$$

so that from Eq. (62) the conditions for n- or p-type conductivity can be derived as follows (if $\mu_n \sim \mu_p$):

$$n\text{-type}\ (\varDelta n > \varDelta p)\ n_{\mathrm{r}}\, s_{\mathrm{p}} > p_{\mathrm{r}}\, s_n \tag{63}$$

$$p\text{-type}\ (\varDelta p > \varDelta n)\ p_{\mathrm{r}}\, s_n > n_{\mathrm{r}}\, s_{\mathrm{p}}\ . \tag{64}$$

In systems with $s_p \approx s_n$ these conditions are

$$n\text{-type}\ n_{\mathrm{r}} > p_{\mathrm{r}} \tag{65}$$

$$p\text{-type}\ p_{\mathrm{r}} > n_{\mathrm{r}}\ , \tag{66}$$

in accordance with the scheme illustrated in Fig. 9. With this hypothesis we can explain the classification of dyes into n- and p-type photoconductors. For example, n-type photoconductivity of cationic triphenylmethane dyes may be the result of the influence of anions operating as defects according to Eq. (63), whereas the p-type photoconductivity of anionic dyes such as fluoresceins may result from cationic defect states [Eq. (64)]. Moreover, intramolecular electron accepting or donating sites, impurities, or dislocations could operate in a similar way.

IV. Connections between the Electrical Properties of Dyes and Industrial Processes

1. Lightfastness

In discussing the use of photoconduction measurements for testing the photobleaching process, it is important to recognize that the photoconduction of dyes is due to the formation and migration of electronic charge carriers and not to impurities of photochemical decomposition. However, the following facts should not be overlooked [91].

(a) The start of the photochemical decomposition of the dye may be recorded, since it is associated with a decrease in conductivity. For example, it was found that the conductivity of the triphenylmethane dyes used as standards in the ISO lightfastness test [91] decreases with the photochemically induced transition of dyes into the leuco form [92].

(b) The negative photoelectric effects (details are given in [93,10]) of colored fibers, may well be correlated with their lightfastness [94,95]. However, more measurements should be made.

(c) A relation has been found between lightfastness and thermal activation energy of photoconductivity (ΔE_{phot}) as determined from Eq. (67):

$$\sigma_{phot} = \sigma_0' \exp\left(-\Delta E_{phot}/kT\right).$$ (67)

ΔE_{phot} increases with lightfastness [92] as shown for the standard dyes CI Acid Blue 104 *9*, 109 and 83; see Table 9.

Table 9. Relation between ΔE_{phot} and time t_B to the beginning of bleaching (after Ref. [92])

Dye	t_B [min]	ΔE_{phot} [eV]
CI acid blue 104 *9*	9	0.39
CI acid blue 109	25	0.48
CI acid blue 83	60	0.58
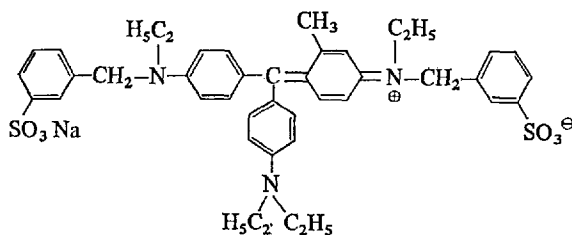
9

The relationship between t_B and ΔE_{phot} holds only for dyes of similar chemical structure, so that *e.g.* there is no connection between ΔE_{phot} and t_B of copperphthalocyanine.

However, small changes in structure, *i.e.* an increase in the electrophilic nature of the susbtituents in the side-chain, resulting in a stronger localization of the positive charge on the central carbon atom or on the nitrogen atom of triphenylmethane, influence both photoconductivity and lightfastness. The explanation is probably that electrons and holes generated by the absorption of light are trapped with different efficiency. Because of the very efficient trapping of holes and the low mobility of these positive charge carriers in triphenylmethane dyes, the quantum efficiency of photoconduction and the value of ΔE_{phot} will depend on the mobility and concentration of electrons, *i.e.* on the trapping of electrons by single dye molecules etc., and therefore on the localization of the positive charge in the molecule. The trapping influence increases with increasing localization, as may be seen from the high activation energies ΔE_{phot} and the low values of quantum efficiency. On the other hand, this trapping of electrons causes uniradicals to form and these, owing to the disproportion between short-lived uniradicals, produce a biradical and a molecule of the leuco dye. The probability that this reaction will occur in the solid state depends on the probability of the formation of such species close to one another, and this probability increases with increasing diffusion (mobility) of the electrons through the layer.

Further experiments are necessary to confirm this hypothesis [91]. However, it seems possible that further work may establish relationships such as that between ΔE_{phot} and fading grades, from which perhaps methods for grading fastness ratings can be derived.

2. Spectral Sensitization

In the process of spectral sensitization, the energy absorbed by a dye in contact with a solid is transferred to the solid, causing it to show photoelectric or chemical effects. Not only is this of overwhelming importance in silver halide photography, it is also an important phenomenon in electrophotography, because of the need to extend the spectral response of various inorganic semiconductors of electrophotographic interest through the visible spectrum. For instance, as in silver halide photography, dye sensitization is a prerequisite for the practical application of the zinc oxide Electrofax system.

Surveys of these problems and of the mechanism are given in [3,40,88,90,96-98]. Therefore only a few facts are mentioned here. Measurements of electronic conductivity can be used on the one hand for the determination of data and properties of dye layers (*e.g.* the absolute position of energy levels) that are important for an understanding of spectral sensitization, and on the other hand they could explain the electron-transfer mechanism of spectral sensitization, especially the "driving force" that transfers the charge from dye layers to inorganic photoconductors. According to this *p-n* or *n-n'* mechanism of spectral sensitization [40,99-105], two effects may act together: (1) in the dark, the build-up of an electrostatic field is brought about by electron exchange between dye and photoconductor as a consequence of the overall tendency for the electrochemical potential of electrons (*i.e.* Fermi energies) to be equal on both sides of each boundary; (2) during illumination, the separation of optically formed electron–hole pairs is effected by the internal electrical field.

The photovoltaic effects found in model arrangements of sensitized systems support this mechanism [40,90,101,106]. Moreover, measurements of the Dember effect [103-105] — an increase of zinc oxide resistance by low coverages [102] — and other observations [107] confirm this mechanism. Therefore, we can assume a correlation between the semiconductivity and sensitizing behavior of dyes, according to which the sensitizing behavior of dyes depends upon

(a) the photoelectric sensitivity of the dye, *i.e.* the photoelectric parameters η, τ and μ;

(b) the *n*- or *p*-type conductivity and the electrochemical (or Fermi) potential of the dye, respectively;

(c) the relative position of the conduction or valence band between the inorganic semiconductor and the dye after the equalizing of the Fermi levels.

The possibilities of utilizing these findings for the production of particularly effective sensitizing dyes should be looked into.

3. Catalytic Effects

It can be concluded from various experiments that a correlation exists between electrical and catalytic data for organic solids, provided the catalytically active substances compared are very similar in their specific chemical and structural properties [10,108,109]. The following relationships should be mentioned:

(a) Between the catalytic activity K_a and the thermal activation energy of the dark conductivity ΔE_{therm} [obtained from Eq. (7)] there is the relation:

$$\log K_a \sim \frac{1}{\Delta E_{therm}} \tag{68}$$

Example: the oxidation of acetaldehyde ethylene acetal to ethylene glycol monoacetate with Fe—M-polyphthalocyanines (M: V, Cr, Cu, etc.) as catalysts [110].

(b) The catalytic activity of phthalocyanine samples for the decomposition of H_2O_2 increases with increasing conductivity (and decreasing activation energy) as shown in Table 10 for different Co-phthalocyanine samples.

Table 10. Relation between catalytic activity of H_2O_2 decomposition (given in time t_{50} [min] necessary for a decomposition of 50% H_2O_2) and dark conductivity of Co-polyphthalocyanines (from Ref. [65])

Co-Polyphthalo-cyanine [sample No]	H_2O_2-Decomposition t_{50} [min]	Conductivity σ_D [ohm^{-1}cm^{-1}]
17	>30.0	2.8×10^{-8}
1	30.0	2.7×10^{-8}
6	11.4	1.2×10^{-7}
2	10.2	5.3×10^{-7}
4	10.2	1.9×10^{-6}
13	6.5	4.1×10^{-5}
9	4.5	1.2×10^{-4}

Similar results have been obtained with Cu-phthalocyanine samples [111] and Fe-polyphthalocyanines [65].

(c) Catalytic activity increases on transition from the monomer to the polymer, which may be the results of the increase in conductivity connected with this transition. Example: the increase of the oxidation of cumene in the presence of Cu-phthalocyanine on transition from the monomer to the polymer [112].

(d) Catalytic activity may depend on the type of dark conductivity. For example, the decomposition of formic acid is catalyzed more strongly by n-conducting Cu-polyphthalocyanine than by p-conducting Cu-phthalocyanine [113].

(e) Moreover, the photocatalytic activity of dyes is also connected with their electronic conductivity. For example, in testing the photocatalytic activity of a series of triphenylmethane dyes in the oxidation of propanol (2), it was found that only fluorescing dyes of the p-type are active catalysts [114]. Moreover, dye photoconductors of the p-type (eosin, fluorescein, acridine, etc.) catalyze the photooxidation of isopropyl alcohol with O_2 to acetone, while dyes of the n-type (crystal violet, rhodamine, etc.) are either inactive or cause pinacol formation [115]. Thus, we have

$$(CH_3)_2CHOH \quad \begin{array}{c} \xrightarrow{\text{p-type}} \quad CH_3\,CO\,CH_3 \\ \xrightarrow{\text{n-type}} \quad (CH_3)_2C(OH)C(OH)(CH_3)_2 \end{array}$$
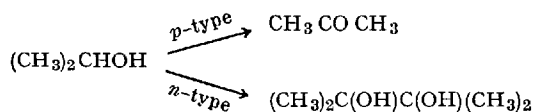
From this reaction it can be seen that high selectivity is an important characteristic of organic catalysts.

4. Electrocatalytic Effects in Fuel Cells

The relations between structure, conductivity, and catalytic activity are of particular interest in connection with the use of organic dyes for the reduction of oxygen in fuel cells. Since Jasinsky's discovery [116] that Co-phthalocyanine can be used instead of platinum for the reduction of oxygen in fuel-cell cathodes, several investigations have been concerned with this question [117–119]. There no longer seems any doubt that the electrocatalysis of oxygen reduction is activated on the largest scale by those polymers of the Fe- or Co-phthalocyanine type that are characterized by the highest conductivity. This can be seen from the examples given in Table 11.

Moreover, the conductivity, and hence the catalytic decomposition of hydrogen peroxide, has been observed to influence the stability of the oxygen electrode. The stability of phthalocyanine catalysts is a decisive factor for the practical applicability of organic catalysts in fuel cells operating in an acid medium. This is therefore a very important observation. The observed disturbance of the delocalization of the π electrons (rubiconjugation) in Fe-polyphthalocyanines, in addition to the correlation between conductivity on the one hand, and electrocatalysis and catalytic decomposition of hydrogen peroxide on the other, leads to a special model of the electroreduction of oxygen on phthalocyanines. The model

Table 11. Relation between electrocatalytic activity (given in the potential ψ_{20} measured at a current density of 20 mA/cm^2) and conductivity in Fe-polyphthalocyanine samples (from Ref. [65])

Fe-polyphthalo-cyanine [sample No]	Electrocatalytic activity ψ_{20} [mV]	Dark conductivity σ_D [ohm^{-1}cm^{-1}]
43	530	8×10^{-12}
33	645	1.5×10^{-11}
57	640	6.5×10^{-10}
51	700	3.6×10^{-10}
40	720	1×10^{-9}
58	705	4.7×10^{-9}
25	795	2.4×10^{-9}

shows that high electrocatalytic activity and stability in electrocatalysts are associated with a combination of

(1) donor states for oxygen reduction

$$O_2 + e^- \rightleftharpoons O_2^-$$
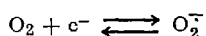
(2) acceptor states for the decomposition of hydrogen peroxide, because

$$Pc \oplus + {}^-OOH \rightleftharpoons \langle Pc....OOH \rangle$$
$$\langle Pc....OOH \rangle + H_2O_2 \longrightarrow H_2O + O_2 + OH^- + Pc .$$
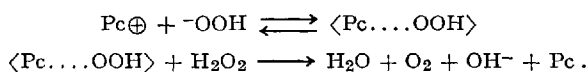
The high electrocatalytic activity of Fe-polyphthalocyanines is explained by this model; see [65,120] for details. It should be mentioned that these results, obtained in a systematic study of a large number of different polymeric phthalocyanines, allow an optimistic prediction regarding the possibility of using fuel cells with high-conducting dye catalysts, e.g. in heart pacemakers [121] and perhaps also in metal–air high-energy batteries [122)a)].

V. Potential Applications of the Electrical Properties of Dyes

In the course of experiments on the dark- and photoconductivity of dyes a series of industrially interesting effects have been noted. Some examples are given below; for further details, see [10,12,88]; for the fundamentals of the different effects, see Section II.

1. Dark Conductivity

A. Rectifiers

As discussed in Section III.3, some dyes can be considered as p- or n-semiconductors in the unilluminated state, particularly in the doped form. The use of organic dyes for the production of rectifiers therefore seems attractive.

There are two possibilities:

(1) The formation of p—n rectifiers by contact between n- and p-conducting systems. Example: layers of p-conducting Cu-phthalocyanine and n-conducting Cl—In-chlorophthalocyanine that are pressed together [123].

(2) The formation of barrier layers at point contacts of organic crystals. Example: arrays of silver/phthalocyanine mixed crystal/Al point contacts with a forward/backward current ratio of 3000:1 can rectify alternating currents up to 10^4 Hz [124]; see Fig. 10.
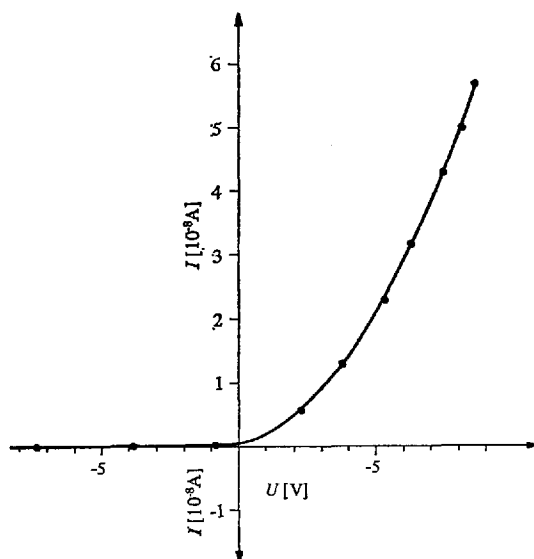
Fig. 10. Rectifier effect in the system Ag/phthalocyanine mixed crystal/Al (after Ref. [124])

Inorganic rectifiers are, of course, still superior to organic systems. However the experiments show that p—n junctions and space-charge layers at contacts can be obtained with the help of organic solids. Further experiments should be made, especially with doped systems.

B. Microwave Generation

It is interesting to note that, with organic compounds, diodes with negative resistance characteristics were obtained [10]. These systems could become important in microwave generation. Example: β-carotene single crystals showed low-frequency current oscillations [125,126] having a certain analogy to Gunn oscillations.

C. Thermoelectric Devices

The discovery of thermovoltages that are high relative to inorganic semiconductors and can reach an order of 3 mV/°C for organic semiconductors [74] also suggests a possible application. In this context it should be recalled that under the influence of a temperature gradient charge carriers diffuse from the warm region into the cold one (Seebeck effect); on passage of a current cooling may be expected at one electrode and warming at the other (Peltier effect). The practical possibility of using the Seebeck effect for thermoelectric energy production or the Peltier effect in refrigeration is favored by

(1) the high value of the differential thermo-emf Q [μV/deg]

(2) high conductivity [ohm^{-1}cm^{-1}]

(3) low thermal conductivity $\varkappa$ [W/cm deg].

Table 12 shows the quality factors or thermoelectric effectivities G_T

$$G_T = \frac{\sigma \cdot Q^2}{\varkappa} \; [\text{deg}^{-1}] \tag{69}$$

of some systems.

Table 12. Thermoelectric effectivities G_T of various systems

System	σ [ohm^{-1}cm^{-1}]	Q [μV/deg]	$\varkappa$ [W/cm · deg]	G_T [deg^{-1}]	Ref.
Refrigeration				6×10^{-3}	[127]
Bi$_2$Te$_3$	1000	200	1.6×10^{-2}	2×10^{-3}	[127]
Pyromellitonitrile		-150	5×10^{-3}	$10^{-12} \times 10^{-8}$	[128]
Phthalocyanine (doped)	10^{-7}	1000	5×10^{-3}	10^{-10}	[129]
Cu-polyphthalo-cyanine	0.3	3100	5×10^{-3}	5×10^{-4}	[130]

It can be seen from Table 12 that, in spite of a thermo-emf of up to 1 mV/degree, the G_T factor of pure phthalocyanines is very low because of their low conductivity. However, the conductivity of some compounds can be increased by polymerization [130] or doping [74,131] without an excessive fall in thermo-emf. For example, as can be seen from figure 11, although conductivity increases by several orders of magnitude, thermo-emfs of up to 1 mV/degree are still obtained in doped systems.

Yet it will be necessary to look for systems having higher conductivities, since a Peltier refrigerator, for example, would become competitive in its power consumption only above an effectivity of $G_T = 6 \times 10^{-3}$ deg^{-1}. It is probable that this aim will be reached. Table 12 shows a Cu-polyphthalocyanine sample with a remarkably favorable G_T value of about 5×10^{-4} deg^{-1}.
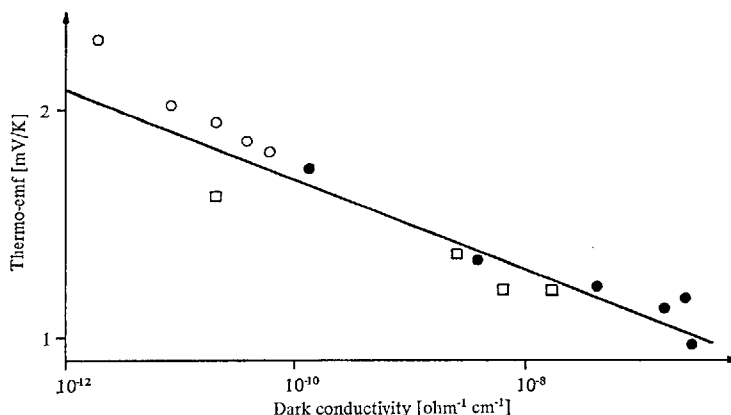
Fig. 11. Relation between thermo-emf Q and conductivity. Plot: $Q = C - (k/e \log e) \log \sigma$.
● : iodine/phthalocyanine; □ : TCNE/phthalocyanine; ○ : o-chloranil/poly-N-vinylcarbazole

D. Gas Detectors

Not only oxygen and hydrogen [3,84,132] but also a number of gases [133–135] have characteristic reversible effects on dark (and photo-) conductivity. The use of dyes as gas detectors has therefore been discussed. It is interesting to note that organic semiconductors are as sensitive to adsorbed gases as inorganic ones, *e.g.* ZnO [136]. As can be seen from Table 13, the conductivity changes in certain systems, *e.g.* β-carotene [134,137,138], range over six orders of magnitude. The response can also be highly specific, as is the case with metal-free phthalocyanine [135].

Table 13. Dependence of the dark conductivity of β-carotene on the nature of the adsorbed gas (after Ref. [134])

Gas	$\sigma_{gas}/\sigma_{vacuum}$
NO	2
Butanol	7
Methylacetate	10
Oxygen	10^2
SO_2	10^3
Acetone	10^4
Ethanol	10^5
NH_3	10^5
Methanol	10^6
NO_2	10^6

If we consider the influence of gases on conductivity, we can understand how Rosenberg [139] succeeded in separating of odorous substances by means of a device containing β-carotene. The detection contaminating gases in the atmosphere by organic semiconductors is also a possibility.

E. Electrets

The electronic charge carriers injected into organic solids from ohmic contacts can build up a stable space charge by trapping in deep traps; thus some dyes assume the properties of electrets on application of an electric field in the dark. According to Euler *et al.* [140], this effect can be utilized for the storage of electrical energy.

Example: with nigrosine paste and silver electrodes, a storage of 1.5 mAh/cm³ and, at a mean voltage of 0.9 V with a discharge time of about 11 min, a volumetric storage capacity of 1.3 mWh/cm³ were measured. The corresponding capacity of a lead starter battery is 11 mAh/cm³ or 15 mWh/cm³.

F. Pressure Indicators

The dark conductivity of a number of organic solids increases reversibly with increasing pressure; details are given in [10]. Because these changes range over several orders of magnitude, the possibility of using them to measure pressure should be tested. For the pressure effect in Cu-phthalocyanine and polymeric phthalocyanines, see [8,141,142].

G. Organic Superconductors

As a final example, let us mention that Little [143,144] has discussed the possibility of obtaining organic superconductors that operate at high temperature. The first superconductive model compound to be proposed was a polymethine chain connected with highly "polarizable" sensitizing cyanine dyes (see *e.g.* Table 3). The first report on superconducting fluctuations in tetrathiafulvalene-tetra-cyanochinodimethane crystals appeared recently [145].

2. Photoconductivity

A. Photoresistors

In principle, it is possible to use organic dyes in photoresistance cells designed either as surface cells (electric field normal to the direction of the light) or sandwich cells (electric field parallel to the direction of the light). This possibility is supported in particular by the fact that the characteristic dependence of photocurrents on light intensity, voltage, etc. largely agrees with that of the photocurrents of inorganic photoconductors. Moreover, the high photoelectric gains found for doped dyes ($G > 1$) and the high values of the photocurrent/dark current ratio (see Section III. 2) also suggest that a systematic testing of this possibility would be worthwhile.

With merocyanine dyes it proved possible to make photoresistance cells that gave photocurrents of up to 10^{-4} A with an external voltage of 100 V and a light intensity of 1 mW/cm² [3].

As discussed in Section II.4, it is necessary to use photoelectric devices with small electrode spacings

(a) to obtain high photocurrents despite low mobilities [cf. Eq. (13)];

(b) to reduce the influence of traps on the response time τ_0 of rise and decay of photocurrents because, according to Eq. (27), τ_0 depends on the population (n_t) of traps [3,10].

The enhancement of the photoconductive gain G (Eq. [(22)] with decreasing layer thickness, as shown in Table 14 [50,90], should also be mentioned here.

Table 14. Effect of dye thickness on photoconductive gain G

Dye	Layer thickness [Å]	G
Pinacyanol	7500	0.03
	1800	0.13
	750	0.3
Crystal violet	1000	0.06
	700	0.13
	300	0.33

Because G, as given by Eq. (22), is

$$G = \frac{\tau}{T}, \tag{22}$$

the enhancement is explained by

(a) a decrease in the transit time T given by $T = L^2/\mu V$ according to Eq. (16);

(b) a reduction in the number N_r of recombination and trapping centers which, because of the relationship

$$\tau = \frac{1}{N_r \cdot s \cdot v_{\text{th}}}, \tag{70}$$

leads to an increase in the free-carrier lifetime τ.

Hence, the highest photoelectric sensitivity of dyes can be obtained in (sandwich-type) photoresistor cells in which very thin dye layers ($L < 1$ mm) are sandwiched between semitransparent electrodes.

B. Photovoltaic Devices

The photoelectric sensitivity of dyes in conjunction with their n- and p-conduction makes it possible to apply dyes in photovoltaic devices that give photocurrents and photovoltages without the use of auxiliary voltages. There seems no doubt that the photoelectric behavior of organic p—n photovoltaic devices can be explained by the theory given in Section II.5.C. The properties: order of photovoltaic effect, additional efficiency as photodiodes, dependence of photocurrents and photovoltages on light intensity, and the polarity of photovoltages and the direction of the photocurrents, respectively, are all in good agreement with the barrier-layer or p—n junction theory [14,40,90]. Therefore, the photovoltaic effect

is due to a p—n junction between the contacted compounds, and the devices described below should not be overlooked in seeking to develop efficient solar cells:

1. heterojunctions consisting of two organic photoconductors of n- and p-type. Examples of these photovoltaic systems, as first described in [146,147], are combinations of n-conducting dyes, such as malachite green or Rhodamine B, and p-conducting dyes, such as a phthalocyanine or a merocyanine dye. The dependence of short-circuit photocurrents on light intensity can be seen from Fig. 12.
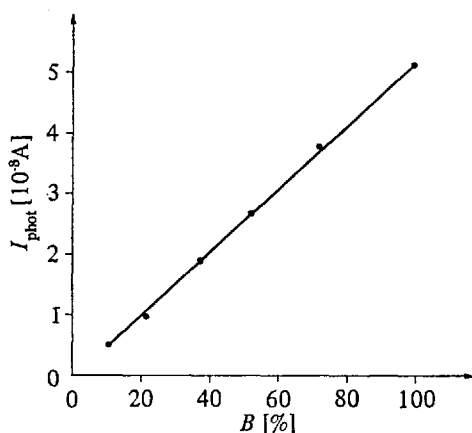
Fig. 12. Relation between the short-circuit photocurrent in the system malachite green (n) + merocyanine FX 79 (p) 8 and light intensity: $I_{phot} = f(B)$. Note: $\lambda = 6200$ Å. B = 100% corresponds to $3.7 \cdot 10^{15}$ quanta/cm² sec; Cell dimensions: $L \approx 10^{-4}$ cm; illuminated area 1 cm²

2. heterojunctions consisting of an organic and an inorganic photoconductor. An important example of these p—n photovoltaic devices, first described in [148, 149], is the combination of n-type CdS and a p-type dye (e.g. phthalocyanine, merocyanine). Fig. 13 shows the dependence of the effect on light intensity, which is in good agreement with Eqs. (43) and (45).

Table 15 gives the outputs obtained so far for some organic p—n photocells of both classes (organic–organic; organic–inorganic).

The technologically developed inorganic photodiodes and photovoltaic cells are, of course, superior to devices with organic photoconductors, but the design of heterojunction devices has not yet reached its optimum. Moreover, the photocurrent and photovoltages can be enhanced by doping [40,154] because the lifetime, i.e. the diffusion length of the carriers [see Eqs. (41) and (44)], is prolonged and the diffusion voltage V_D increased. Furthermore, one can envisage that the formation of p—n junctions in homogeneous solids could further enhance the photovoltaic effect [155]. Further experiments should be undertaken, aimed at improving the outputs N_{max} of organic, and especially organic–inorganic photovoltaic cells.
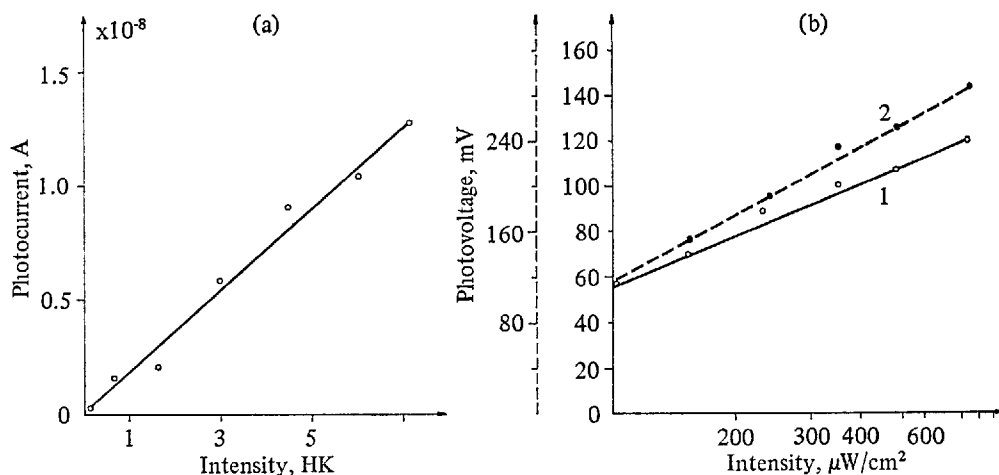
Fig. 13. Dependence of the p—n photovoltaic effect of dye/inorganic photoconductor systems on light intensity. (a) Short-circuit photocurrent of the system CdS/merocyanine A 10 *1*; $\lambda = 5580$ Å; 1 HK (Hefner unit) $= 94.7$ μW/cm^2; (b) Photovoltages of the systems 1. CdS/merocyanine A 10 *1*; $\lambda = 5580$ Å 2. AgI/rhodamine B; $\lambda = 6000$ Å

Table 15. Outputs N_{max} of organic p—n photoelectric cells ($I_0 =$ short-circuit current; $U_{\infty} =$ photovoltage)

System		U_{∞} [mV]	I_0 [A]	N_{max} [W]	Ref.
n-Type	p-Type				
Malachite green	Phthalocyanine	100	10^{-8}	10^{-9}	[14]
CdS	Phthalocyanine	300	10^{-8}	3×10^{-9}	[148]
CdS	Cu-phthalocyanine	200[1]	3×10^{-6} [2]	6×10^{-7}	[150]
Triphenylmethane dyes	Phthaleins	100	0.5×10^{-9}	6×10^{-10}	[151]
Ion exchange membrane	Thionin/ascorbic acid	15	1.6×10^{-6}	2×10^{-8}	[152]
Tetramethyl-p-phenylenediamine	Mg-Phthalocyanine	200		3×10^{-12}	[153]

[1] Under illumination of 10^4 lx.
[2] Integral sensitivity in the photodiode region: 2 mA/lm.

C. Vidicon Television Pickup Tubes

Because of their photoelectric sensitivity and frequently high I_{phot}/I_{dark} ratio, organic dyes of various classes (mercocyanines, phthalocyanines, etc.) can be used as targets in vidicon television pickup tubes for image reproduction [156-159].

In principle, the dye is arranged in these camera tubes as in a sandwich-type cell (see Fig. 14). In the vidicon, however, one electrode is replaced by a scanning electron beam which brings the dye layer to the potential of the cathode. Since the transparent electrode supporting the thin dye layer ($L < 1$ μm) is positively biased, a photocurrent is produced on illumination of the dye.
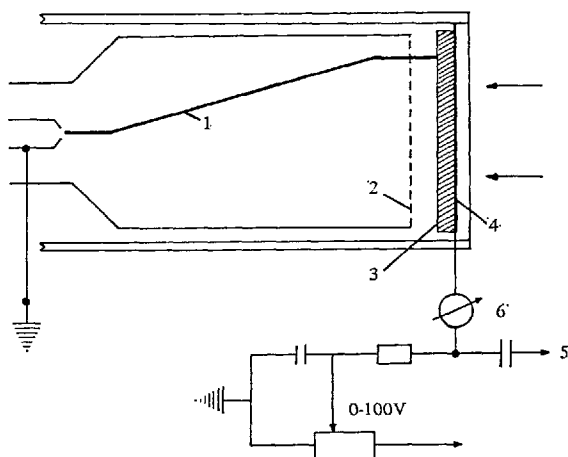
Fig. 14. Scheme of the vidicon tube. (1) Scanning beam (cathode potential $V = 0$ volt); (2) gauze; (3) dye film; (4) transparent supporting electrode (potential $V \approx +30$ volt); (5) amplifier; (6) galvanometer

The photocurrent can be measured with a galvanometer or recorded on the television screen.

Some characteristics of organic vidicons are given below.

(a) Their photoelectric sensitivity is about 10—100 μA/lm (or 100 nA/lx), which extends to the order of magnitude of inorganic vidicons.

(b) The photocurrent depends on voltage, light intensity, and scanning electron beam, as observed in vidicons with inorganic targets. This agreement is shown in Fig. 15 for the case of the intensity dependence of the vidicon photocurrents measured with phthalocyanine and Sb_2S_3 as targets.
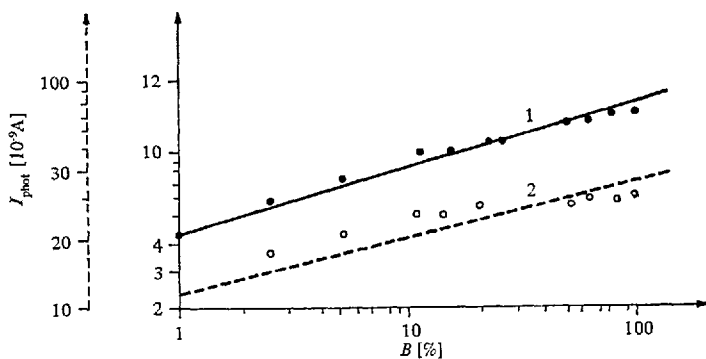
Fig. 15. Dependence of photocurrents (measured in the vidicon arrangement) on light intensity:$\log I_{phot} = f$ (B). (1) Sb_2S_3; (2) phthalocyanine ($\lambda = 5500$ Å)

125

(c) There is a fundamental possibility that several colors could be reproduced with a single target containing photoconductor points that absorb in different wavelength regions.

(d) Layers characterized by a high density of deep traps have appreciable storage capacity.

(e) The action spectra of photoconductive polymers (*e.g.* poly-N-vinylcarbazole) can be sensitized by different dyes and by the addition of dye/acceptor admixtures [160,161].

The results obtained hitherto are of interest *e.g.* for color television, for medically important IR vidicons [3], and for the construction of storage vidicons. Further systematic studies should test as many dyes as possible for possible use in television image reproduction[b].

D. Spectrally Sensitive Detectors

The photoelectric currents of dye–metal contacts, which reach an order of only 10^{-10} A/cm^2, in some cases show a dependence of direction on wavelength. Examples are systems consisting of Orthochrom T [14,56] and β-carotene [162], which change the sign of photocurrents and photovoltages on transition from short to long wavelengths. The approximate wavelength of the exciting light may therefore be registered from the direction of the photoelectric current. It would be of practical use if the sensitivity of the spectrally sensitive effect could be increased.

For the mechanism of this effect, we refer to Refs. [60,163].

E. Possible Use in the Activation of Electro-Optic Effects in Liquid Crystals

Besides the direct electrical induction of electro-optical effects in liquid crystals, their activation by illumination of photoconductors could be of great technical interest. This method might well permit the electro-optical properties of nematic liquid crystals to be used on a larger scale, because photoconductor activation may eventually be applied to light amplification, optical data processing, and projection display systems, or used for recording phase-type holograms.

It has recently been shown that organic photoconductor–liquid crystal sandwich cells can in theory act as dynamic scattering devices [164] and the technical possibilities ought to be tested. In this context, it should be noted that dyes can be used in two-layer photocondensers (consisting *e.g.* of phthalocyanine and a ferroelectric ceramic), which are very sensitive to light and have a response time of 10^{-4} to 10^{-3} sec [165].

F. Use in Reprography

It is certain that organic photoconductors will be used on an industrial scale in the near future in methods of reproduction based on photoelectric and electrostatic processes (reviews are given in [10,166]).

The photoconductivity of organic dyes, especially phthalocyanine pigments, could be utilized to provide reusable or non-reusable electrophotographic plates having sensitivities that extend over the entire visible spectrum and produce high-contrast images [167,168]. Microcrystalline dispersions of metal-free phthalocyanine in suitable binders have a white-light sensitivity equal to that of selenium [169] and can be incorporated into coated papers and drums.

Photoconducting polymers having a phthalocyanine structure are easily applied to a substrate and have been proved to be usable in electrophotographic processes [170]. The feasibility of using photoconducting leuco bases of triarylmethane dyes as components of transparent electrophotographic recording materials, which would allow e.g. the electrophotographic production of microfilms, has also been described [171].

There seems no doubt that organic photoconductor systems will permit the development of new reproduction processes based on the electrophotographic principle [10]. Dyes play an important role in this development: on the one hand they act as spectral sensitizers of the organic photoconductors (e.g. poly-N-vinylcarbazole [161]) and on the other hand, the photoelectric effects of dyes are important for

(a) use of the memory effect (persistent photoconductivity [172–174]) which allows several copies of equal quality to be obtained from one original after exposure to light without a corona discharge;

(b) use of the photoelectric sensitivity of dyes in a polychromatic photoelectrophoretic image-reproduction process [175–176].

VI. Conclusion

In summary, we see that there are many cases where industrial applications of the dark- and photoconductivity of organic dyes can be envisaged. Of course, inorganic materials which are technologically well understood are still superior in most fields. However, we should not forget that organic semiconductors are in the development stage and that we are only beginning to understand the mechanism of dark- and photoconductivity in organic solids and to recognize the fundamental correlations between electronic conductivity and the structure of the organic compounds. Much remains to be done, but the potential due to the variety of organic compounds available and their observed effects is clear. The search for practical applications of the dark- and photoconductive properties of dyes and other organic compounds looks very promising.

VII. References

1) Noddack, W., Eckert, G., Meier, H.: Z. Elektrochem. *56*, 735 (1952).
2) Noddack, W., Meier, H.: Z. Elektrochem. *57*, 691 (1953).
3) Meier, H.: Die Photochemie der organischen Farbstoffe. Berlin–Göttingen–Heidelberg: Springer 1963.
4) Nelson, R. C.: J. Chem. Phys. *20*, 1327 (1952); *23*, 1550 (1955).
5) Wartanjan, A. T.: Izv. Akad. Nauk SSSR, Ser. Fiz. *16*, 169 (1952).
6) Weigl, J. W.: J. Chem. Phys. *24*, 883 (1956).
7) Metz, W. D.: Science *180*, 1041 (1973).
8) Härtel, M., Kossmehl, G., Manecke, G., Wille, W., Wöhrle, D., Zerpner, D.: Angew. Makromol. Chem. *29/30*, 307 (1973).
9) Rembaum, A.: J. Polymer Sci. C *29*, 157 (1970).
10) Meier, H.: Organic Semiconductors: dark- and photoconductivity of organic solids. Weinheim: Verlag Chemie 1975.
11) Meier, H.: Chimia *27*, 263 (1973).
12) Meier, H., Albrecht, W., Tschirwitz, U.: Angew. Chem. *84*, 1077 (1972); Angew. Chem. Intern. Ed. Engl. *11*, 1051 (1972).
13) Meier, H.: Z. Physik. Chem. (Leipzig) *208*, 325 (1958).
14) Meier, H.:Angew. Chem. *77*, 633 (1965); Angew. Chem. Intern. Ed. Engl. *4*, 619 (1965).
15) Rexer, E.: Organische Halbleiter, Berlin: Akademie Verlag 1966.
16) Gutmann, F., Lyons, L. E.: Organic semiconductors. New York–London–Sidney: J. Wiley & Sons 1967.
17) Bauser, H., Ruf, H. H.: Phys. Status Solidi *32*, 135 (1969).
18) Binks, A. E., Campbell, A. G., Sharples, A.: J. Polymer Sci. A-2, *8*, 529 (1970).
19) Hänsel, H.: Ann. Physik *24*, 147 (1970).
20) Kepler, R. G.: Phys. Rev. *119*, 1226 (1960). In: Organic semiconductors, pp. 1. New York: Macmillan & Co. 1962.
21) Meier, H., Albrecht, W.: Z. Naturforsch. *24a*, 257 (1969).
22) Boguslavskii, L. I., Vannikov, A. V.: Organic semiconductors and biopolymers (Transl. from Russian by B. J. Hazzard). New York: Plenum Press 1970.
23) Pohl, H. A.: J. Polymer. Sci. C *17*, 23 (1967).
24) Holstein, T.: Ann. Physik. *8*, 343 (1959).
25) Spear, W. E.: Annu. Rep., Conf. on Electrical Insulation and Dielectric Phenomena, Nat. Acad. Sciences, pp. 1. Washington 1971.
26) Meier, H.: Dissertation, pp. 107. Universität Mainz 1954.
27) Sukigara, M., Nelson, R. C.: Mol. Phys. *17*, 387 (1969).
28) Williams, W. G.: Discussions Faraday Soc. *51*, 61 (1971).
29) Cox, G. A., Knight, P. C.: J. Phys. C: Solid State Phys. *7*, 146 (1974).
30) Hamann, C., Starke, M.: Phys. Status Solidi *4*, 509 (1964).
31) Heilmeier, G. H., Harrison, S. E.: Phys. Rev. *132*, 2010 (1963).
32) Eley, D. D., Pethig, R.: Proc. 2. Int. Conf. on Conduction in Low-Mobility Materials, Eilat, Israel, 1971, pp. 397.
33) Pethig, R., Morgan, K.: Phys. Status Solidi (b) *43*, K 119 (1971).
34) Dresner, J.: J. Chem. Phys. *52*, 6343 (1970).
35) Mey, W., Hermann, A. M.: Phys. Rev. *B 7*, 1652 (1973).
36) Pethig, R., Morgan, K.: Nature *214*, 266 (1967).
37) Le Blanc, O. H.: J. Chem. Phys. *39*, 2395 (1963).
38) Schmillen, A., Falter, W. W.: Z. Physik *218*, 401 (1969).
39) Meier, H., Albrecht, W.: Ber. Bunsenges. Physik. Chem. *69*, 917 (1965).
40) Meier, H.: Spectral sensitization. London–New York: Focal Press 1968.
41) Sadasiv, G.: Photoelectronic devices, Vol. 1, pp. 111. New York: Plenum Press 1971.
42) Lampert, M. A.: Rept. Progr. Phys. *27*, 329 (1964).
43) Helfrich, W.: In: Physics and chemistry of the organic solid state (eds. D. Fox, M. Labes and A. Weissberger), Chap. 1. New York: Interscience 1967.
44) Pope, M., Kallmann, H.: Discussions Faraday Soc. *51*, 7 (1971).

45) Ruppel, W.: In: Semiconductors and semimetals, Vol. 6, pp. 315. New York–London: Academic Press 1970.

46) Stöckmann, F.. Phys. Status Solidi (a) *15*, 381 (1973).

47) Batt, R. H., Braun, C. L., Hornig, J. F.: J. Chem. Phys. *49*, 1967 (1968); Appl. Optics, Suppl. 3: Electrophotography 20 (1969).

48) Stockmann, D. L.: In: Current problems in electrophotography (eds. W. F. Berg and K. Hauffe), pp. 202. Berlin–New York: W. de Gruyter 1972.

49) Killesreiter, H., Baessler, H.: Phys. Status Solidi (5) *53*, 193 (1972).

50) Noddack, W., Meier, H., Haus, A.: Z. Physik. Chem. *212*, 55 (1959).

51) Meier, H.: Phot. Sci. Eng. *6*, 235 (1962).

52) Meier, H., Albrecht, W.: Z. Physik. Chem. [N.F.] *39*, 249 (1963).

53) Inokuchi, H., Maruyama, Y., Akamatu, H.: In: Electrical conductivity in organic solids, pp. 69, New York–London: J. Wiley & Sons 1961.

54) Noddack, W., Meier, H.: Z. Elektrochem. *57*, 691 (1953).

55) Meier, H.: Z. Elektrochem. *59*, 1029 (1955).

56) Meier, H.: Z. Wiss. Phot., Photophysik, Photochem. *50*, II, 301 (1955).

57) Madelung, O.: In: Physical chemistry, Vol. 10, p. 367. New York: Academic Press 1970.

58) Ghosh, A. K., Feng, T.: J. Appl. Phys. *44*, 2781 (1973).

59) Wiesner, R.: In: Halbleiterprobleme III (Hrsg. W. Schottky), S. 59. Braunschweig: Vieweg 1956.

60) Ruppel, W.: Phys. Status. Solidi *5*, 657 (1964).

61) Meier, H.: Spectral sensitization, pp. 188. London-New York: Focal Press 1968.

62) Spenke, E.: Elektronische Halbleiter, 2. Aufl., S. 501. Berlin-Heidelberg-New York: Springer 1965.

63) Rose, A.: Concepts in photoconductivity and allied problems. New York-London: Interscience Publ. 1963.

64) Eley, D. D., Parfitt, G. D.: Trans. Faraday Soc. *51*, 1529 (1955).

65) Meier, H., Albrecht, W., Tschirwitz, U., Zimmerhackl, E.: Ber. Bunsenges. Physik. Chem. *77*, 843 (1973).

66) Heider, M., Lochon, P., Neél, J.: Compt. Rend. Acad. Sci. Paris *267 C*, 797 (1968).

67) Heider, M., Neél, J.: J. Chim. Phys. *3*, 547, 553 (1973).

68) Manecke, G., Wöhrle, D.: Makromol. Chem. *120*, 176 (1968).

69) Manecke, G., Wöhrle, D.: Makromol. Chem. *120*, 192 (1968).

70) Epstein, A., Wildi, B. S.: In: Electrical conductivity in organic solids (eds. H. Kallmann and M. Silver), pp. 337. New York: Interscience 1961.

71) Hoegl, H., Süs, O., Neugebauer, W.: Kalle AG 1957/1967. DP 1068115.

72) Hoegl, H.: J. Phys. Chem. *69*, 755 (1965).

73) Kearns, D. R., Tollin, G., Calvin, M.: J. Chem. Phys. *32*, 1020 (1960).

74) Meier, H., Albrecht, W., Tschirwitz, U.: Ber. Bunsenges. Physik. Chem. *73*, 795 (1969).

75) Lyons, L. E.: Proc. Royal Austr. Inst. *37*, 329 (1970).

76) Aoyagi, Y., Masuda, K., Namba, S.: J. Phys. Soc. Japan *31*, 524 (1971).

77) Kirin, I. S., Moskalev, P. N.: Russ. J. Phys. Chem. (English Transl.) *41*, 251 (1967).

78) Albrecht, W.: Dissertation, Universität Erlangen-Nürnberg, 1964.

79) Golubovic, A.: J. Phys. Chem. *73*, 1352 (1969).

80) Yannoni, N. F., Hanscom, L. G.: Sol. Cells, p. 175. Proc. Int. Colloq. 1970 (Publ. 1970).

81) Dimond, N. A., Mukherjee, T. K.: Discussions Faraday Soc. *51*, 1 (1971).

82) Mukherjee, T. K.: J. Phys. Chem. *70*, 3848 (1966).

83) Löhr, B., Arneth, R., Winkelmann, D.: In: Current problems in electrophotography (eds. W. F. Berg and K. Hauffe), pp. 219. Berlin-New York: W. de Gruyter 1972.

84) Meier, H.: Z. Wiss. Phot., Photophysik, Photochem. *53*, 1 (1958).

85) Delacote, M., Schott, M.: Phys. Status Solidi *2*, 1460 (1962).

86) Tschirwitz, U.: Dissertation, Universität Erlangen-Nürnberg, 1970.

87) Kan, K., Matsunaga, Y.: Bull. Chem. Soc. Japan *45*, 2096 (1972).

88) Meier, H., Albrecht, W., Tschirwitz, U.: Phot. Sci. Eng. *18*, 276 (1974).

89) Rose, A.: RCA Review *12*, 362 (1951).

90) Meier, H.: Photochem. Photobiol. *16*, 219 (1972).

91) Meier, H.: In: Photochemistry of Dyes, in the chemistry of synthetic dyes, (ed. K. Venkataraman), Vol. 4, pp. 389. New York: Academic Press 1971.

92) Patterson, D., Pilling, B.: Trans. Faraday Soc. *62*, 1976 (1966).

93) Meier, H.: Z. Wiss. Phot., Photophysik, Photochem. *53*, 117 (1959).

94) Moncrieff, R. W.: Textile Mfr. *92*, 462 (1966).

95) Fedotov, I. P., Yavorskii, B. M.: Izv. Vysshikh Uchebn. Zavedenii Tekhnol. Tekstil'n Prom. *2*, 115 (1966).

96) Berg, W. F., Mazzucato, U., Meier, H., Semerano, G.: Dye Sensitization — Symposium Bressanone. London-New York: Focal Press 1970.

97) Dörr, F.: In: Grundlagen der Photographischen Prozesse mit Silberhalogeniden (Hrsg. H. Frieser, G. Haase, E. Klein), S. 603. Frankfurt/M.: Akad. Verlagsges. 1968.

98) West, W.: Phot. Sci. Eng. *18*, 35 (1974).

99) Meier, H.: Chimia *18*, 170 (1964).

100) Meier, H.: J. Phys. Chem. *69*, 719 (1965).

101) Meier, H., Albrecht, W.: Ber. Bunsenges. Physik. Chem. *69*, 160 (1965).

102) Grossweiner, L. I., Brennan, W. D.: J. Phot. Sci. *17*, 189 (1969).

103) Levy, B., Lindsey, M.: Phot. Sci. Eng. *16*, 389 (1972).

104) Levy, B., Lindsey, M., Dickson, C. R.: Phot. Sci. Eng. *17*, 115 (1973).

105) Levy, B.: Phot. Sci. Eng. *18*, 347 (1974).

106) Meier, H., Albrecht, W.: Ber. Bunsenges. Physik. Chem. *68*, 64 (1964).

107) Inoue, E.: In: Current problems in electrophotography (eds. W. F. Berg and K. Hauffe), pp. 146. Berlin-New York: W. de Gruyter 1972.

108) Hanke, W.: Z. Chem. *9*, 1 (1969).

109) Roginskii, S. Z., Sakharov, M. M.: Russ. J. Phys. Chem. (English Transl.) *42*, 696 (1968).

110) Inoue, H., Kida, Y., Imoto, E.: Bull. Chem. Soc. Japan *41*, 684 (1968).

111) Roginski, S. Z., Berlin, A. A., Galovina, D. A., Dokukina, E. S., Sakharov, M. M., Cherkashina, L. G.: Kinetika i Kataliz *4*, 431 (1963).

112) Hanke, W.: Z. Anorg. Allgem. Chem. *347*, 67 (1966).

113) Hanke, W., Karsch, W.: Monatsber. Deut. Akad. Wiss. Berlin *9*, 323 (1967).

114) Steinbach, F., Binding, D.: Z. Physik. Chem. [N. F.] *81*, 135 (1972).

115) Inoue, H., Hayashi, S., Imoto, E.: Bull. Chem. Soc. Japan *37*, 326 (1964).

116) Jasinski, R.: Nature *201*, 1212 (1964); J. Elektrochem. Soc. *112*, 526 (1965).

117) Jahnke, H.: Ber. Bunsenges. Physik. Chem. *72*, 1053 (1968).

118) Jahnke, H., Schönborn, M.: Proc. Joint Int. Etud. Piles Combust, p. 60. Brussels 1969.

119) Siemens AG, French Pat. 1591825 (1970).

120) Meier, H., Zimmerhackl, E., Albrecht, W., Tschirwitz, U.: In: Katalyse an phthalocyaninen (eds. H. Kropf and F. Steinbach), pp. 104. Stuttgart: G. Thieme Verlag 1973.

121) Schaldach, M.: Umschau *70*, 857 (1970).

122) Kordesch, K. V.: Ber. Bunsenges. Physik. Chem. *77*, 755 (1973).

123) Hamann, C., Storbeck, I.: cited in 124).

124) Hamann, C.: Phys. Status Solidi. *4*, K 97 (1964).

125) Madjid, A. H., Vaala, A. R.: Phys. Status Solidi (a) *7*, 211 (1971).

126) Madjid, A. H., Anderson, W. F., Roeckel, M. W., Vaala, A. R.: Phys. Status Solidi (a) *3*, 209 (1970).

127) Birkholz, U.: In: Halbleiterprobleme VI (Hrsg. F. Sauter), S. 206. Braunschweig: Vieweg 1961.

128) Katon, J. E., Wildi, B. S.: J. Chem. Phys. *40*, 2977 (1964).

129) Meier, H., Albrecht, W., Tschirwitz, U.: Ber. Bunsenges. Physik. Chem. *74*, 938 (1970).

130) Kossmehl, G.: Umschau *67*, 636 (1967).

131) Tschirwitz, U.: Dissertation, Universität Erlangen-Nürnberg, 1970.

132) Meier, H.: Z. Physik. Chem. (Leipzig) *212*, 73 (1959).

133) Vartanyan, A. T.: Soviet J. Opt. Techn. *38*, 763 (1971).

134) Rosenberg, B., Misra, T., Switzer, R.: Nature *217*, 423 (1968).

135) van Oirschot, Th. G., van Leeuwen, D., Medema, J.: Electroanal. Chem. Interfac. Electrochem. *37*, 373 (1972).

136) Seiyama, T., Kagawa, S.: Anal. Chem. *38*, 1069 (1966).

137) Cherry, R. J., Chapman, D.: Nature *215*, 956 (1967).

[138] Misra, T., Rosenberg, B., Switzer, R.: J. Chem. Phys. *48*, 2096 (1968).

[139] Williams, J. O., Rosenberg, B.: Umschau *69*, 348 (1969).

[140] Euler, K. J., Ryhiner, G., Scholz, F.: Z. Angew. Phys. *24*, 32 (1967).

[141] Vaišnys, J. R., Kirk, R. S.: Phys. Rev. *141*, 642 (1966).

[142] Manecke, G., Wöhrle, D.: Makromol. Chem. *120*, 176 (1968).

[143] Little, W. A.: Phys. Rev. *134*, A 1416 (1964).

[144] Little, W. A.: Proceedings of the International Conference on Organic Superconductors, New York-London: Interscience Publ. 1970.

[145] Heeger, A., Garito, A., Coleman, L. B., Cohen, M. J., Sandman, D. J., Yamagishi, F. G.: Chem. Week *112*, 30 (1973).

[146] Meier, H., Haus, A.: Angew. Chem. *72*, 631 (1960).

[147] Noddack, W., Meier, H., Haus, A.: Z. Wiss. Phot., Photophysik, Photochem. *55*, 7 (1961).

[148] Meier, H., Albrecht, W.: Ber. Bunsenges. Physik. Chem. *68*, 64 (1964).

[149] Meier, H., Albrecht, W.: Ber. Bunsenges. Physik. Chem. *69*, 160 (1965).

[150] Vertsimakha, Ya. I., Kurik, M. V.: Mikroelektronika *1*, 275 (1972).

[151] Kostelec, J.: US-Pat. 3009006 (1961).

[152] Yoshida, M.: Bull. Kobayashi Inst. Phys. Res. *13*, 109 (1963).

[153] Calvin, M., Kearns, D. R.: US-Pat. 3057947 (1962).

[154] Meier, H., Albrecht, W., Tschirwitz, U.: In: Current problems in electrophotography (eds. W. F. Berg and K. Hauffe), pp. 256. Berlin-New York: W. de Gruyter 1972.

[155] Krikorian, E.: U. S. Clearinghouse Fed. Sci. Tech. Inform. AD 1968, AD-679601.

[156] Meier, H., Albrecht, W.: Ber. Bunsenges. Physik. Chem. *73*, 86 (1969).

[157] Meier, H., Albrecht, W.: Ger. Offenlegungsschrift 1762283, 17.5.1968.

[158] Morozov, G. A., Antonova-Afanas'eva, I. V., Popov, Yu. A., Markova, I. Y. A.: USSR, 335740, 11.4.1972; from Chem. Abstr. *77*, no. 6 (40634f) (1972).

[159] Demirchoglyan, G. G., Lyubin, V. M.: USSR 384156, 23.5.1973; from Chem. Abstr. 79, no. 22 (1973).

[160] Meier, H., Albrecht, W., Tschirwitz, U.: Photochem. Photobiol. *16*, 353 (1972).

[161] Meier, H., Albrecht, W., Tschirwitz, U.: In: Current problems in electrophotography (eds. W. F. Berg and K. Hauffe), pp. 163. Berlin-New York: W. de Gruyter 1972.

[162] Rosenberg, B., Heck, R. J., Aziz, K.: J. Opt. Soc. Am. *54*, 1018 (1964).

[163] Stöckmann, F.: Acta Phys. Austriaca *19*, 71 (1965).

[164] Meier, H., Albrecht, W., Tschirwitz, U.: Paper given at 73. Hauptversammlung der Deutschen Bunsengesellschaft für Physikalische Chemie, Kassel, Mai 1974.

[165] Vivadi, Yu. A., Rozenshtein, L. D., Chistyakov, E. A.: Soviet Phys.-Semicond. *1*, 1049 (1968).

[166] Dessauer, J. H., Clark, H. E.: Xerography and related processes. London-New York: Focal Press 1965.

[167] Mammino, J., Ferguson, R. M.: US-Pat. 3640710, Feb. 8, 1972.

[168] Gerace, P. L., Wolff, N. E.: Ger. Offenlegungsschrift 2062900, 21.12.1970.

[169] Weigl, J. W., Mammino, J., Whittacker, G. L., Radler, R. W., Byrne, J. F.: In: Current problems in electrophotography (eds. W. F. Berg and K. Hauffe), pp. 287. Berlin-New York: W. de Gruyter 1972.

[170] Kramm, D. E., Light, L., Light, J. F.: US-Pat. 3498784, March 3, 1970.

[171] Wilson, C. V.: DBP 1237900, October 19, 1967.

[172] Meier, H.: Z. Physik. Chem. (Leipzig) *208*, 340 (1958).

[173] Hayashi, Y., Kuroda, M., Inami, A.: Bull. Chem. Soc. Japan *39*, 1660 (1966).

[174] Cassiers, P. M.: J. Phot. Sci. *10*, 57 (1962).

[175] Weinberger, L.: US-Pat. 3442781, January 6, 1966.

[176] Weigl, J. W.: Ger. Offenlegungsschrift 1947105 (1970).

Organic Dyestuffs as Catalysts for Fuel Cells

Dr. Horst Jahnke, Dr. Manfred Schönborn and Dr. Georg Zimmermann

Robert Bosch GmbH, Research Centre, Gerlingen-Schillerhöhe

Contents

Electrocatalysis in fuel cells requires as well substances capable of catalyzing the anodic oxidation of fuels as catalysts for the cathodic reduction of oxygen. Several dyestuffs that catalyze oxygen reduction are known, but up to now only one has been described as active in anodic reactions. All these dyestuffs are N_4-chelates.

Comparative studies have shown that chelates with other types of coordination, in particular N_2O_2-, O_4-, N_2S_2- and S_4-chelates, are able to catalyze the reduction of oxygen, though they are considerably less active than the N_4-compounds. With a given type of coordination, the nature of the central atom has a decisive influence on the catalytic activity of the dyestuff, whereas substitution on the organic skeleton has only a slight effect. Thermal pretreatment of the N_4-chelates can considerably increase their stability in electrolytes containing sulfuric acid.

All the experimental results point to the conclusion that, with electrocatalysts, as with natural oxygen carriers, the interaction essential for catalysis takes place between the oxygen and the central metal ion. Various assumptions may be made as to the nature of the rate-determining step. The cathodic reduction of oxygen can be regarded as redox catalysis, or it can be considered from the standpoint of molecular orbital theory. The *models* hitherto suggested for the mechanism of oxygen reduction are tested against the experimental results and a modified model based on MO theory is put forward.

1. Introduction

There are many organic dyestuffs but only one class, that of the metal chelates, has been found to be active in electrocatalysis. The first compounds described were the phthalocyanines [1-4], which are similar in structure to the heme in the blood pigment, hemoglobin; in both, the metal atom is surrounded by four nitrogen ligands.

The ability of phthalocyanines to transport oxygen and to accelerate oxidation reactions in the same way as heme was discovered soon after their molecular structure had been established [5,6]. The property of catalyzing chemical reactions seemed to offer promising practical applications [7].

The structural similarity with heme was likewise the starting point for more recent work on the electrocatalytic properties of phthalocyanines [3,4], which showed the influence of the nature of the central atom and of the substituents on the electrocatalytic activity for the reduction of oxygen. Shortly after this further N_4-metal chelates were found to be active for the same reaction [8,9].

With a single exception, all the compounds described catalyze only cathodic reactions. CoTAA is the only chelate capable of catalyzing the anodic oxidation of several fuels as well.

2. Electrochemical Aspects

2.1. Fuel Cells and Electrocatalysis

2.1.1. Electrochemistry of Fuel Cells

The chief potential for the application of dyestuffs with electrocatalytic action lies in fuel cells. A fuel cell is an electrochemical device in which the chemical energy of the fuels is converted *directly* into electrical energy, *i.e.* without first being transformed into heat energy. To this end, the oxidizing agent, in practically every case oxygen, is led to an electrode. By virtue of the reaction

$$O_2 + 4e^- + 4\,H^+ \longrightarrow 2\,H_2O \tag{1}$$
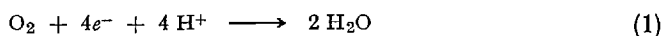
taking place there, the electrode functions as a cathode. The construction of a fuel cell is shown schematically in Fig. 1. If a gaseous fuel (usually hydrogen or carbon monoxide) is used in the cell, it is led to the anode in the same way as oxy-
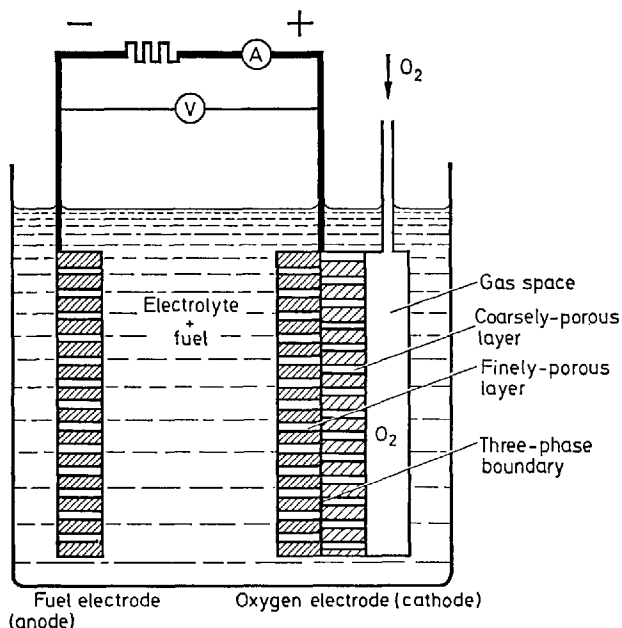
Fig. 1. Schematic diagram of a fuel cell for fuel soluble in electrolyte

gen to the cathode. A simpler construction of the anode may be achieved by using a liquid fuel miscible with the electrolyte, *e.g.* methanol, hydrazine, or formic acid. Such an anode is shown schematically on the left of Fig. 1. The methanol dissolved in the electrolyte is oxidized:

$$CH_3OH + H_2O \longrightarrow CO_2 + 6e^- + 6\,H^+. \tag{2}$$
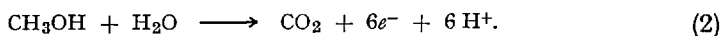
The overall reaction

$$CH_3OH + 1^1/_2 O_2 \longrightarrow CO_2 + 2 H_2O \tag{3}$$
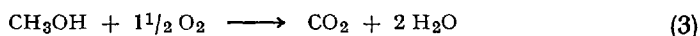
that takes place in this fuel cell corresponds exactly to the reaction of direct combustion of methanol. In the fuel cell, in contrast to energy transformation in a heat engine, the available free enthalpy can, in principle, be completely transformed into electrical energy.

The electrons liberated in the reaction at the anode flow through the external metallic conductor to the cathode and can in doing so perform work in an electrical load.

The electrolyte within the cell can be acid or alkaline. When carbonaceous fuels are used, continuous operation of the cell requires acid electrolytes because alkaline electrolytes form carbonates with the carbon dioxide produced by the cell reaction. The necessity of working with acid electrolytes, however, brings considerable disadvantages, as many materials are less stable in an acid than in an alkaline medium; they corrode or decompose.

The cell voltages for a fuel cell, as calculated from thermodynamic data, lie a little above one volt. In practice, they are considerably lower and fall still lower as the cell load increases. Figure 2 shows the relationship between cell voltage and current density, and the influences that reduce the cell voltage.
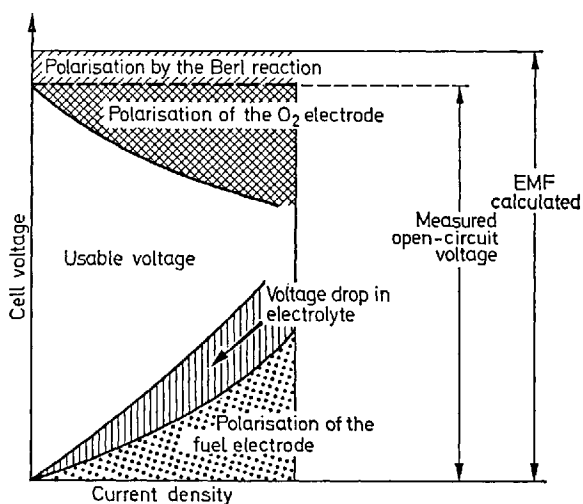
Fig. 2. Schematic current/voltage characteristic of a fuel cell

a) Polarization occurs at both electrodes as the electrode reactions are inhibited particularly at high current densities. Inhibition can be caused either by obstruction of electron transfer between the electrode and the reacting molecule (transfer polarization), or by a marked drop in the concentration of the reactants at the

electrode surface, or by an increase in the concentration of the reaction products (concentration polarization).

b) An additional voltage drop can occur at electrodes of certain types, even on open circuit, and always at the oxygen electrode. This happens because electrochemical splitting of the O_2 molecule is strongly impeded by the high stability of the $O=O$ double bond, so that H_2O_2 is formed as an intermediate product (Berl's reaction).

c) The electrical resistance of the electrolyte produces a voltage drop proportional to the cell current.

To obtain a useful fuel cell, polarization must therefore be kept as slight as possible. This can be done by choosing an electrolyte of good conductivity and above all by accelerating the electrode reactions. In low-temperature cells, that operate with aqueous electrolytes the reactions at both cathode and anode can be considerably accelerated by the addition of very active catalysts. These materials are incorporated in the appropriate electrode, so that the electrode not only conducts the current but in addition catalyzes the reaction. The rest of this paper is devoted exclusively to cells of this type.

2.1.2. Catalysts for Low-Temperature Fuel Cells

Which is the best catalyst for accelerating the reaction depends on the nature of the working materials. For the reaction of hydrogen or oxygen in potassium hydroxide solution, nickel or silver is suitable; for carbonaceous fuels as well as for the reaction of oxygen in acid electrolytes platinum metals were up to the middle '60s, the only known catalysts. Precious metals are ruled out by price for wide application in fuel cells, and the search for cheaper catalysts has been actively pursued in many research laboratories. Many classes of inorganic substances (carbides, nitrides, oxides, sulfides, phosphides, etc.) have been investigated and, in particular, several chelates.

The first chelate found to be electrocatalytic was cobalt phthalocyanine [1], which functions as an oxygen catalyst in alkaline electrolytes. Soon afterwards we were able to show [3,4,10,11] that several phthalocyanines are also active in commercially important, sulfuric acid containing media. A comparison of various central atoms showed that activity increased in the order $Cu \approx Ni < Co < Fe$. The influence of substituents, on activity was also demonstrated in several examples. In the electrocatalysis of the reduction of oxygen on iron phthalocyanine, the nature of the carbon substrate plays a very important part: FePc is more active on a carbon substrate with basic surface groups than on one with acid surface groups [3]. This property is however specific to phthalocyanines (Pc).

At the beginning of the '70s Beck and co-workers discovered the electrocatalytic activity of dihydro-dibenzo-tetra-aza-annulene [8,12], and Binder, Sandstede and co-workers that of tetraphenylporphyrine and its tetramethoxy derivative [9,13–15].

Parallel to this work, catalysts for the anodic oxidation of several fuels were established [10]. Up to now, however, only one chelate is known to catalyze anodic reactions: the cobalt complex of dihydro-dibenzo-tetra-aza-annulene.

138

Under operating conditions, however, all chelates have only a limited working life, the length of which varies with the compound in question; their working life can be increased by previous heat treatment, as discussed in Section 4. The activity of the catalyst is not impaired by this treatment; in some cases it is even considerably enhanced.

2.2. Methods for Testing Electrocatalysts

The values obtained in different laboratories for the activity of various electro-catalysts are not directly comparable. The reduction of oxygen — for which data have been published by various groups — proceeds at the three-phase boundary where gas, liquid, and solid meet. This boundary is affected by such macroscopic properties of the catalyst as particle size, density, surface tension, and porosity.

All chelates discussed here are bad conductors of electricity. In order to study their electrocatalytic properties, it is therefore essential to maintain a very low ohmic resistance between the reaction site and the circuit connection. This is generally done by mixing the catalyst with an inert conductor such as powdered charcoal or powdered gold. Differences in the quantity and nature of the substance mixed with the catalyst further complicate comparison of the activity values obtained in different laboratories. The various groups have hitherto used different processes for testing chelates.

2.2.1. Testing in Compact Electrodes

The test substance is mixed with a conducting substance and usually with a binder (polyethylene or PTFE) and a pore producing compound, pressed and, if necessary, sintered. Compact electrodes are obtained, many with a large content of the test material, which can be used without much modification in operating cells. The measure of the activity is the current density in mA/cm^2. Despite the close simulation of operating conditions, this test method is unsuitable for the comparison of different substances. A relatively large quantity of catalyst is required, and the soft, hydrophobic binder can enclose the catalyst particles.

2.2.2. Testing in Electrodes without Binder

2.2.2.1. Supported electrodes. The mixture of catalyst and charcoal is poured into the space between two mechanically rigid walls, with asbestos paper as support and a graphite felt or metal sheet as current collector. No binder is necessary. With such electrodes, both liquid and gaseous working materials can be studied. For the experiments with dissolved fuels described in Section 4.2, we used modified electrodes of this type: 6 mg chelate was mixed with 6 mg soot and poured between two graphite felt discs.

2.2.2.2. Painted-on electrodes likewise need no binder. This is the type best suited for comparing various catalysts when working with gaseous reactants. The thin layer of the material and the direct contact between the catalyst particle and the gas phase at the hydrophobic covering layer ensures maximum utilization

of the catalyst. The electrodes are prepared by mixing equal quantities of the catalyst and charcoal, making the mixture into a paste with methanol, and painting this on to a sheet of porous PTFE. It is particularly advantageous to use acetylene black in place of powdered charcoal because of the low intrinsic activity of this material. The surface density of the chelate is about 2.5 mg/cm². The coated PTFE sheet, of 2 cm² area, is built in to a Perspex holder, as shown in Fig. 3. The catalyst layer is covered with a sheet of graphite felt and with a perforated metal sheet, to improve the electrical conductivity. Gas is passed through the arrangement from behind, *i.e.* from the PTFE side.
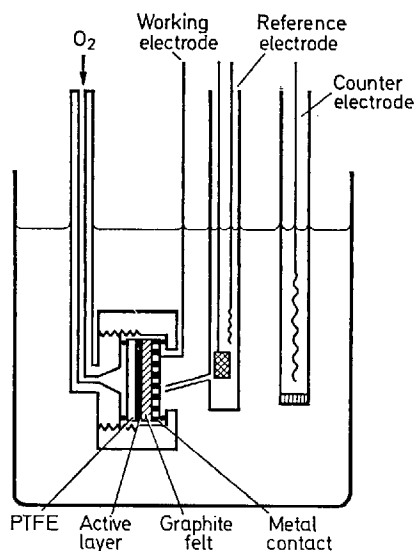
Fig. 3. Measuring system (measurements with felt holder and PTFE)

We used painted-on electrodes for all experiments with gaseous working materials.

2.2.2.3. Testing in suspension. The electrode structure is completely abandoned and the catalyst is suspended in the electrolyte [16,17]. Figure 4 is a diagrammatic view of an electrochemical measuring cell for catalyst suspensions. By vigorous stirring, the catalyst particles are thrown against the inert current-collecting electrode at which charge transfer occurs. Gaseous working materials are blown into the electrolyte as fine bubbles; liquid fuels are mixed with the electrolyte.

This method has revealed the activity of many metal chelates, but it is less suitable for the quantitative comparison of different dyestuffs because only materials of the same density and particle size are directly comparable [18].

In all measurements, the reference electrode was the autogenous hydrogen electrode. Most of the experiments were carried out in H_2SO_4 electrolyte, but in some cases KOH or carbonate/bicarbonate buffer electrolyte (pH 9.3) was used.
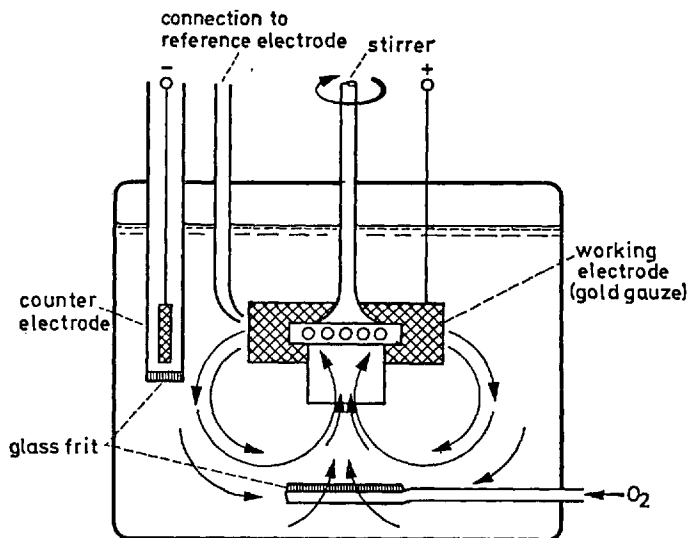
Fig. 4. Diagrammatic view of the electrochemical measuring cell for catalyst suspensions [22]

3. Dyestuffs with Electrocatalytic Properties

3.1. Principles of Selection

In accordance with the model concepts discussed in more detail in Section 5, dyestuffs selected for trial of their electrocatalytic properties had a central atom (metal ion) forming a plane square complex with an organic ligand. The central metal atom must possess unoccupied d levels for further attachment of the reactants. We tested only chelates with N_4-, N_2O_2-, N_2S_2-, O_4- and S_4-coordination, investigating some representatives of each type with various central atoms, mostly Fe, Co, Ni and Cu. In addition, we studied the effect on the electrocatalytic activity of the complex of altering the external organic skeleton: substituents, introduction of hetero-atoms, enlargement of the π-electron system, e.g. by polymerization.

Many complexes are unstable in 4.5 N H_2SO_4, which is used as electrolyte in the fuel cell, even at room temperature. Where this was the case, measurements were carried out in potassium carbonate/potassium bicarbonate buffer solution (pH 9.3). We were thus able to determine the reactivity of a wide range of substances, in particular for the catalytic reduction of oxygen.

3.2. Test Substances

All chelates tested for electrocatalytic activity are listed in Table 1.

For ease of reference, the substances are arranged in groups and numbered serially, as follows:

Nos. 1—12 = N_4-complexes
Nos. 13—16 = N_2O_2-complexes
Nos. 17—18 = N_2S_2-complexes

Nos. 19—22 = O_4-complexes
Nos. 23—24 = S_4-complexes

In addition to the structure and the systematic name of each compound, some of the more frequently occurring complexes are given special names. The table also contains information as to the nature of the central atom and literature references.

Table 1. Substances studied
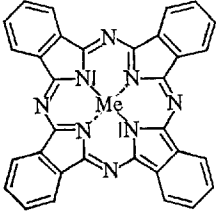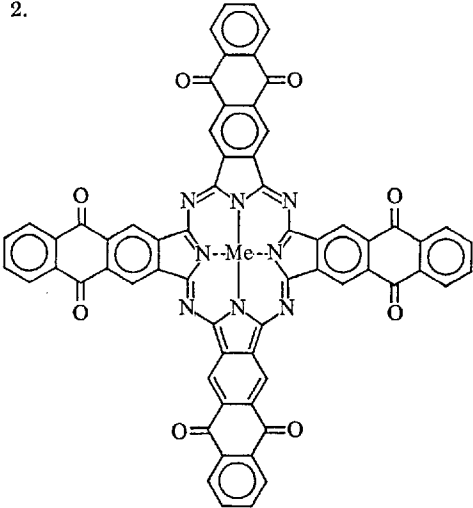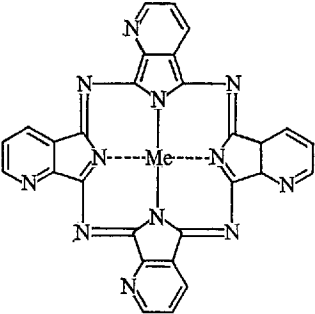
No. Structure and name		Abbre-viation	Me
1.	Phthalocyanine [1–4,10,11,19]	Pc	Fe Co Ni Cu
2.	Anthrachinocyanine [20]	ACC	Fe
3.	Tetrapyridino-tetraazaporphyrin [11,19]	TPAP	Fe Co Ni

142

Table 1 (continued)
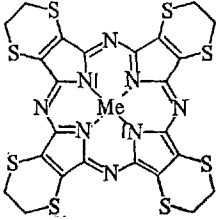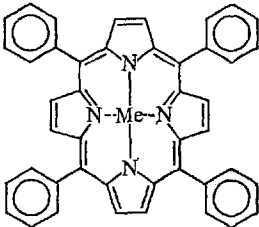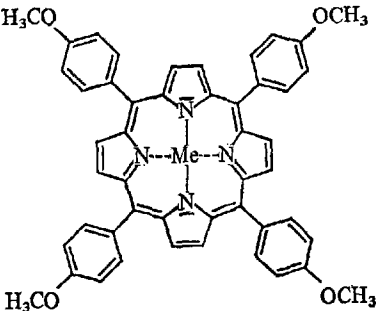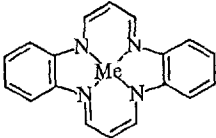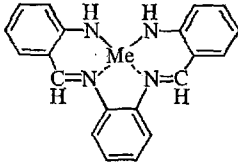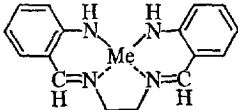
No.	Structure and name	Abbre-viation	Me
4.	Tetradithiacyclohexeno-tetraazaporphyrin [11,19]	TDAP	Fe Co Ni
5.	Tetraphenylporphyrin [21,22]	TPP	Fe Co
6.	Tetramethoxyphenyl-porphyrine [21,22]	TMPP	Co
7.	Dihydrodibenzotetraaza-annulene [8,23,24]	TAA	Co Ni Cu
8.	Metal complex of Schiff's base made from o-aminobenzaldehyde and o-phenylenediamine		Co Cu Ni
9.	Metal complex of Schiff's base made from o-aminobenzaldehyde and ethylenediamine		Co Cu Ni

Table 1 (continued)
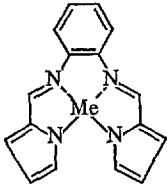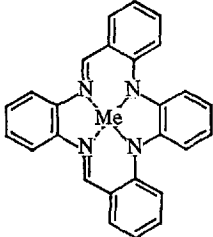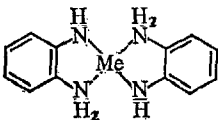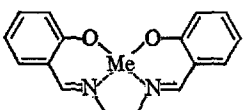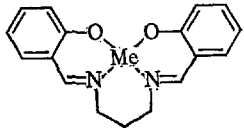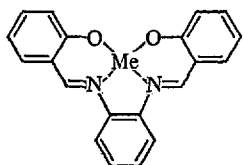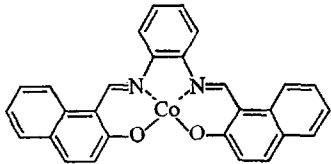
No.	Structure and name	Abbre-viation	Me
10.	Metal complex of Schiff's base made from pyrolaldehyde and o-phenylenediamine		Co Cu Ni
11.	Metal complex of Schiff's base made from salicylaldehyde and o-phenylenediamine		Co Cu Ni
12.	o-Phenylenediamine complex		Co Ni
13.	Pfeiffer complex made from salicylaldehyde and diaminoethane		Co Ni Cu Mn
14.	Pfeiffer complex made from salicylaldehyde and diaminopropane		Co Ni Cu Mn
15.	Pfeiffer complex made from salicylaldehyde and o-phenylenediamine		Fe Co Ni Cu
16.	Pfeiffer complex made from 2-hydroxy-1-naphthaldehyde and o-phenylenediamine		Co

Table 1 (continued)
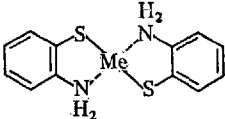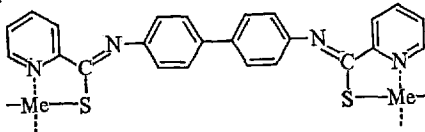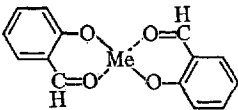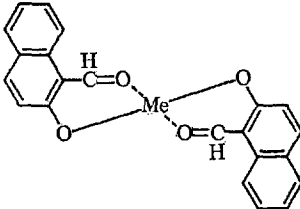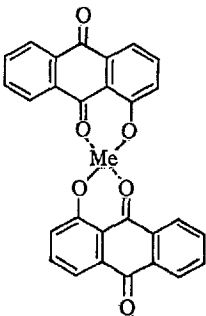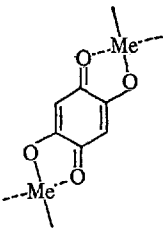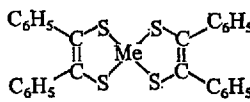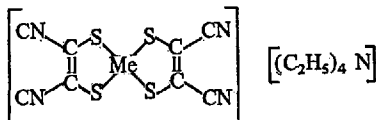
No.	Structure and name	Abbre-viation	Me
17.	N_2S_2 complex made from o-aminothiophenol		Co
18.	Metal complex of Schiff's base made from pyridine-2-mercapto-aldehyde and benzidine		Fe Co Cu Ni
19.	O_4 complex made from salicylaldehyde		Co Ni Cu
20.	O_4 complex made from 2-hydroxy-1-naphthaldehyde		Co Ni Cu
21.	O_4 complex made from 4-hydroxyanthrachinone		Co Ni Cu
22.	O_4 complex made from 2.5-dihydroxybenzochinone		Co Ni Cu

Table 1 (continued)

No.	Structure and name	Abbre-viation	Me
23.			Fe Co Ni
24.			Fe Co Cu

4. Experimental Results

4.1. Investigation of Cathodic O_2 Reduction on Metal Chelates

4.1.1. Previous Work

This section presents a short survey of the results published by various groups working on organic electrocatalysts for the cathodic reduction of oxygen. Widely differing experimental techniques have been used. The difficulty of quantitative comparison of the activities of different catalysts has been mentioned (Section 2.2).

4.1.1.1. Cobalt phthalocyanine as catalyst in alkaline electrolyte. Jasinski [1,2] was the first to show that CoPc in alkaline solution showed a pronounced activity for the cathodic reduction of oxygen. The compound was mixed with powdered nickel in a ratio of 1:10 w/w and pressed into a stainless steel tube (geometrical surface of the electrode 0.5 cm^2). The tube served for both current conduction and gas supply.

The results of half-cell measurements on such electrodes in 25% KOH at room temperature are summarized in Table 2. For comparison, the values obtained on

Table 2. Cathodic half-cell voltage for a cobalt phthalocyanine electrode [1-2]

Current density	Half-cell voltage (vs. H_2/H^+)	
(mA/cm^2)	Ni powder blank (mV)	CoPc (mV)
0	+ 870	+ 870
19.3	+ 720	+ 740
38.7	+ 540	+ 640
99.0	+ 440	+ 570
116.2	+ 290	+ 500

pure nickel powder are also shown. The increase effected in the load capacity of the nickel electrode by the CoPc catalyst can clearly be seen, even though in this series of experiments, as was later established, conditions were far from optimal.

The impregnation of porous nickel discs with CoPc was difficult because of the limited solubility of the chelate in the usual solvents. CoPc cathodes with carbon as substrate were therefore prepared for use in H_2/O_2 fuel cells. A mixture of 72 mg CoPc and 48 mg acetylene black, with PTFE as binder, was pressed into a nickel mesh of area 5 cm^2. Electrodes of this type were tested in an H_2/O_2 fuel cell with 35% KOH electrolyte in an asbestos matrix at 80° C. Figure 5 compares the current/voltage characteristics of CoPc cathodes (14 mg/cm^2) with those of other catalysts, including platinum (9 mg/cm^2), silver (40 mg/cm^2), and pure acetylene black (20 mg/cm^2). An hydrogen electrode (9 mg Pt/cm^2) was used as the anode in all tests. To facilitate comparison of the activity of different cathodes, the pure ohmic internal resistance of the cells (of the order of 0.02 ohm) was eliminated.
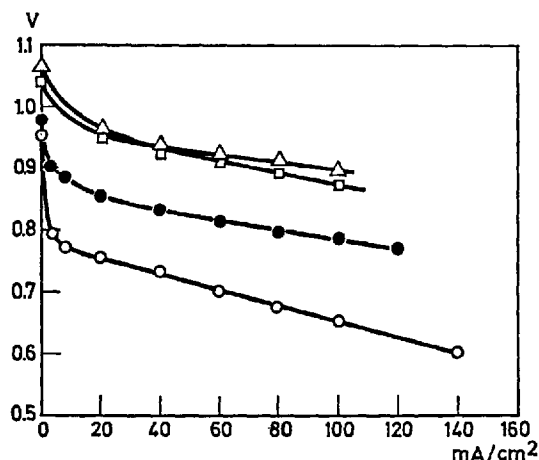

Fig. 5. H_2/O_2 fuel cells operating at 80 °C with 35% KOH, and a platinum black anode. The cathodes are: platinum (□); silver (Δ); CoPc (●); and acetylene black (O)[2]

4.1.1.2. Transition-metal phthalocyanines as catalysts in acid medium. To prevent carbonate formation by the carbon dioxide in the air or that produced by oxidation of carbonaceous fuels, an acid electrolyte is necessary; hence it is important to find electrocatalysts for an acid medium. Independently of Jasinski, we were soon able to show [3,4] that under certain conditions the reduction of oxygen in dilute sulfuric acid proceeded better with phthalocyanines on suitable substrates than with platinum metal. The purified phthalocyanines were dissolved in concentrated sulfuric acid and precipitated on to the carbon substrate by addition of water. This coated powder was made into porous electrodes bound with polyethylene and having a geometrical surface of 5 cm^2 (cf. Section 2.2.2.1.). The results obtained with compact electrodes of this type are shown in Fig. 6.

H. Jahnke, M. Schönborn, and G. Zimmermann

They comprise a comparison of the activities of polymeric phthalocyanines with various central atoms. The monomers always showed lower activity than the corresponding polymers. The nature of the substrate has a decisive influence on the catalytic properties of the chelate. Electrodes with gold substrate showed only very slight activity.
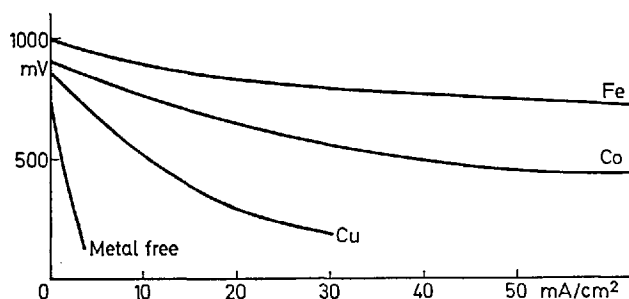

Fig. 6. Activity of polymeric phthalocyanines with various central atoms [4]

Table 3 shows the suitability of various types of carbon as substrate materials. The specific surface and the electrical conductivity play only a minor part. It is the nature of the oxygen-containing groups on the carbon surface that counts: alkaline surface groups must be present if the phthalocyanine is to have a catalytic effect [a].

Table 3. Physical properties and catalytic activity of various carbon supports [4]

Substances	Current density [mA cm^{-2}] at 700 mV with FePc	Specific resistance [Ω cm]	Specific surface area [m^2 g^{-1}]	Nature of surface groups
Acetylene black	51	0.069	57.5	Basic
Norit BRX	31	0.116	1740	Basic
Vulkan 3H	24	0.063	89.9	Basic
Corax 6	21	0.066	105	Basic
Corax A	21	0.053	44.7	Basic
Thermax	—	0.26	8.1	Basic
CK 3	—	0.905	76.2	Acid
Durex O	—	0.040	19.0	Acid
E_0 (graphite)	—	0.012	4.3	Acid
$S+E$ (graphite)	—	0.013	17.5	Acid

[a] This is sustained by more recently measurements [58] of Mössbauer spectra which showed the intimate interaction between FePc and the alcaline surface groups. A similar behaviour for the catalysis under non electrochemical conditions has been reported recently, too [59].

148

It is further important to note that all the current/voltage characteristics depicted in Fig. 6 are unchanged by the presence of liquid fuels such as methanol, formaldehyde, formic acid, or hydrazine. The phthalocyanine electrode remains completely inert toward such substances. For this reason, no mixed potential can be formed at a phthalocyanine electrode, as for example can occur at a platinum electrode, when it is used as cathode in a methanol cell containing sulfuric acid. This is shown by a comparison (see Fig. 7) of the stationary characteristics of the platinum alloy we found to be the most active in the presence of methanol, namely a Raney ruthenium–rhodium electrode, with an iron phthalocyanine electrode, both measured in 4.5 N $H_2SO_4 + 2M$ CH_3OH.
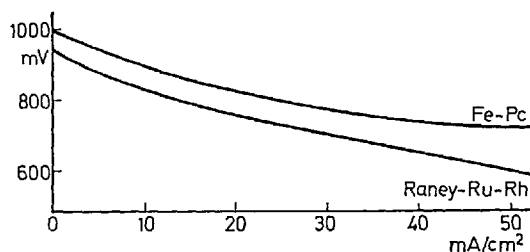
Fig. 7. Activity of phthalocyanine- and platinum metal electrodes for the cathodic reduction of oxygen in 4.5 N H_2SO_4 + 3 M CH_3OH at 25 °C [4]

Investigations by Savy and co-workers [35] on monomeric and polymeric phthalocyanines gave qualitatively the same results as were obtained in our work, despite considerable differences in the experimental method. Monomeric phthalocyanines were deposited in a very thin film on gold substrates by vacuum evaporation. This process could not be used with the polymeric compounds. These were therefore first deposited on an acetylene-black carrier and small quantities of this phthalocyanine-black catalyst were then electrophoretically deposited on an inert graphite electrode. The quasi-stationary potentiodynamic current/voltage characteristics reproduced in Fig. 8 were obtained in 0.2M H_3PO_4 (pH 1.3) at room temperature with a potential change of 0.16 mV/sec. The rest potentials with various metal atoms are marked by strokes on the abscissa (potential in mV against a saturated calomel electrode). The strong influence of the central atom on the activity of the chelate is clearly visible. The rapid decline in activity in the sequence Fe, Co, Ni, Cu agrees exactly with our results.

In a more recent publication [43] Savy and co-workers have studied the influence on oxygen activity of the conditions of preparation of iron phthalocyanine in the presence of carbon. They have also discussed a possible mechanism of reaction.

4.1.1.3. Substituted cobalt porphyrins as catalysts in sulfuric acid. Further very active chelates for the reduction of oxygen in acids discovered in the early '70s were CoTPP by Sandstede and co-workers [9,13–15] and CoTAA and FeACC by Beck and co-workers [8,12]. Sandstede *et al.* determined the activities of their chelate catalysts by the suspension method briefly explained in Section 2.2.2.3.
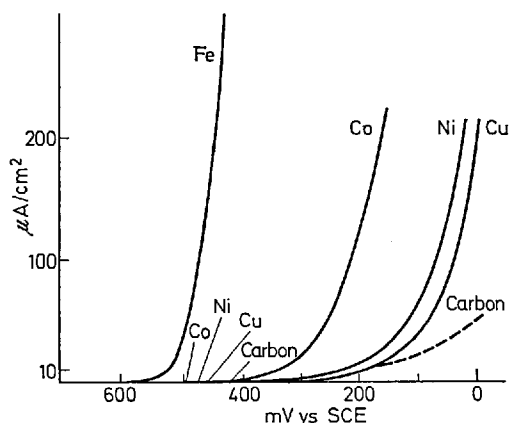
Fig. 8. Activity of polymeric phthalocyanines [35]

Figure 9 shows the results obtained by Sandstede [15] with tetra-(p-methoxy-phenyl)porphyrins on activated carbon in suspension. The activity decreases in the order $Co > Fe > Ni \approx Cu$. The same sequence of central atoms is observed with tetra-aza-annulene.
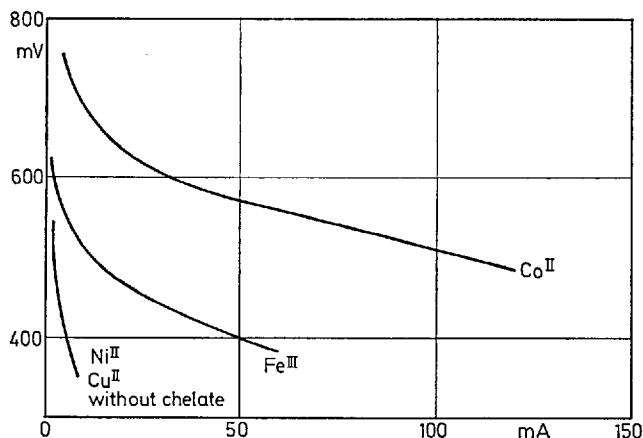

Fig. 9. Potentiodymanic current/voltage curves for oxygen reduction at metal porphyrine catalysts in 3 N H_2SO_4 at 30 °C. Sweep rate 40 mV/min [15]

Particularly important for the activity of CoTPP is the substituent in the p-position of the phenyl group (cf. Fig. 10). The donor groups $-OCH_3$ or $-C_6H_5$ increase the activity of the CoTPP roughly fivefold. Although the $-SCH_3$ group has the strongest donor property, its influence on the activity is slight. This is probably due to oxidation of the sulfur, so that $-SOCH_3$ or $-SO_2CH_3$ groups
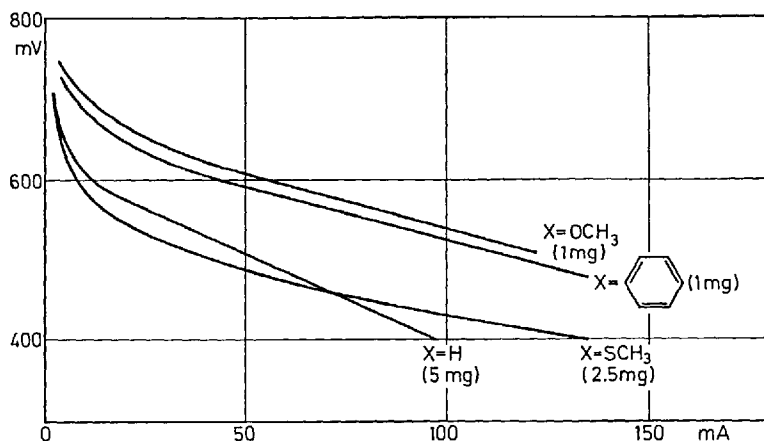
Fig. 10. Potentiodynamic current/voltage curves for oxygen reduction in 3 N H_2SO_4 at 30 °C at Co(II)(tetraaryl)porphyrins; effect of the ligand (X) in p-position. Sweep rate 40 mV/min[15]

are present. These groups tend rather to function as electron acceptors, so that practically no substituent effect can be observed. The activity of CoTMPP itself can be considerably enhanced by thermal pretreatment (Fig. 11).
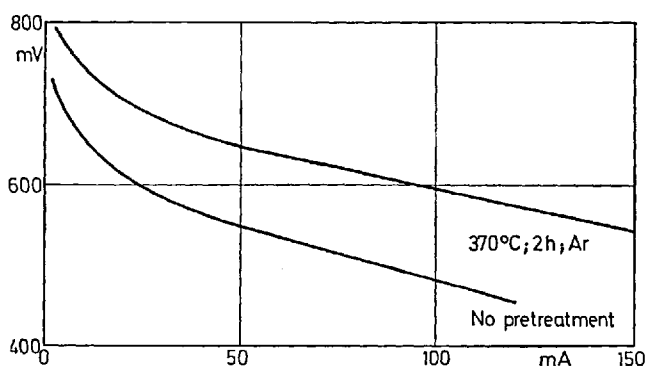

Fig. 11. Potentiodynamic current/voltage curves for oxygen reduction in 3 N H_2SO_4 at 30 °C, effect of pretreatment on the activity of the chelate catalyst. Sweep rate 40 mV/min [15]

Long-term tests on CoTMPP carbon electrodes with polyethylene as binder showed a drop in potential of about 5 mV per day, even after several hundred hours' operation.

4.1.1.4. Oxygen reduction on TAA *catalysts.* Beck and co-workers [23] also performed investigations on organic electrocatalysts, likewise using a suspension arrangement. To supplement this work, he plotted the polarographic current/voltage characteristics for pigments dissolved in conc. sulfuric acid, using the mercury dropping electrode or the rotating-platinum-disc electrode. The present summary is concerned only with the results of the suspension measurements.
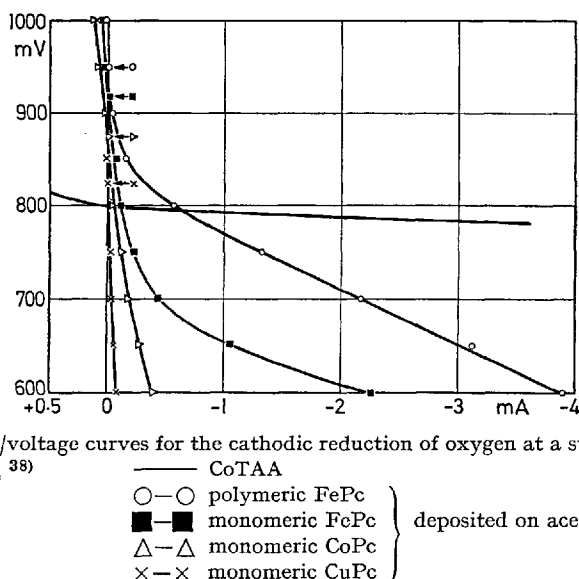
151

Fig. 12. Current/voltage curves for the cathodic reduction of oxygen at a suspension electrode in 4.5 N H_2SO_4 [38]   ———— CoTAA

O—O   polymeric FePc
■—■   monomeric FePc   } deposited on acetylene black
△—△   monomeric CoPc
×—×   monomeric CuPc

To prepare the standardized dispersion electrode, a mixture of 100 mg soot, 100 g 97% sulfuric acid and 100 mg pigment was stirred direct into the dilute sulfuric acid of the measuring vessel, so that the concentration of sulfuric acid in the electrolyte after stirring in was about 4.5 N. The current collector electrode was a gold–platinum mesh (90/10) of about 4.5 cm² area. The current/voltage characteristics shown in Fig. 12 make it possible to compare CoTAA with various phthalocyanines.

In contrast to the phthalocyanines, whose curves are relatively steep as they pass through the rest potential, the curve for CoTAA shows a very flat slope in this region. This result was confirmed by us (cf. Section 4.1.2.1.1.). Table 4 summarizes the most important results. Both the rest potential and the current at

Table 4. Rest potential and current/voltage values for the cathodic reduction of oxygen on pigment-catalyst dispersions at 25 °C in 4.5 N H_2SO_4 °C [38]

Chelate	Rest potential $°U_H$ [mV]	Cathodic current [mA] at $U_H = 600$ mV
Monomeric FePc	920	2.4
Polymeric FePc	955	3.9
Monomeric CoPc	880	0.32
Polymeric CoPc	780	0.25
Monomeric NiPc	800	0.2
Monomeric CuPc	860	0.1
Monomeric CoTAA	800	28.0
Monomeric FeTAA	860	2.9
Monomeric MnTAA	805	8.2
Monomeric NiTAA	750	1.2
Monomeric CuTAA	730	0.5
Acetylene black	800	0.2

600 mV are given as measures for the activity. $U_H = 0.6$ V is the lawest limit for an useful range of potential for an oxygen cathode.

While the activity of the monomeric phthalocyanines decrease in the well-known sequence Fe > Co > Ni > Cu (MnPc is completely inactive), the TAA compounds give the following sequence: Co > Mn > Fe > Ni > Cu. This sequence, established in sulfuric acid, also holds for the same compounds in carbonate/bicarbonate buffer electrolyte (cf. Section 4.1.2.2.2.).

The dispersion method, while not suitable for long-term tests lasting several days, can be used for preliminary trials of electrochemical behavior over a period of several hours. As can be seen from Fig. 13, the activity of CoTAA falls off sharply even within a few hours, in contrast to that of polymeric FePc. The stability of the CoTAA catalyst can however be considerably increased by suitable thermal pretreatment (cf. Section 4.1.3.).
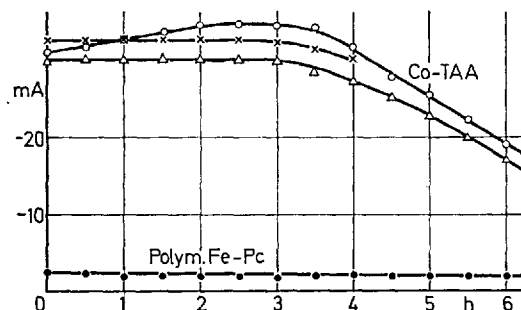

Fig. 13. Current/time characteristics of an oxygen suspension electrode with CoTAA- and FePc-catalyst at $U_H = 600$ mV [38]

4.1.1.5. Influence of catalase activity and electrical conductivity. Parallel to the determination of the oxygen activity, Beck and co-workers [38] investigated the activity for the decomposition of hydrogen peroxide by various chelates. In each case, 1 mg of freshly precipitated pigment was added to 1% hydrogen peroxide solution and the velocity of oxygen evolution was determined volumetrically. The results summarized in Table 5 show no correlation between electrocatalytic activity and catalase activity.

This result directly contradicts those of Meier and co-workers [25], though his group studied only phthalocyanines. The determination of both oxygen activity and activity in decomposing hydrogen peroxide was done on solid electrodes with a polyethylene binder containing the pigments precipitated on carbon (*e.g.* Norit BRX) always in the same proportions w/w. The oxygen activity was measured as the potential of the phthaloxyanine electrode under a load of 20 mA/cm². The catalase activity of the phthalocyanine was characterized by the time required for decomposition of 50% of the available quantity of H_2O_2. For further characterization of the various phthalocyanines, which were prepared and purified under various conditions, measurements of conductivity and thermoelectric voltage were carried out on the pure pigment powders. The most important results, those

153

Table 5. Activities of some metal chelates in the catalytic decomposition of hydrogen peroxide and in electrocatalysis with an oxygen cathode [38]

Metal chelate	$\left(\dfrac{\Delta V_{O_2}}{\Delta t}\right)$ ml/min	i_{600} [mA]	Ratio of values
FePc	30	2.4	0.08
Polym. FePc	0.5	3.9	7.8
CoTAA	0.3	28	94
CoPc	0.05	0.3	6
CuPc	0.02	0.1	5
NiPc	0.01	0.2	20

Table 6. Correlation between conductivity, catalase activity and electrocatalytic activity of polymeric FePc or CoPc [36]

p FePc No.	Catalase activity	φ_{20} [mV]	σ_D [Ohm^{-1} cm^{-1}]
43	25	530	$8 \cdot 10^{-12}$
33	23	645	$1.5 \cdot 10^{-11}$
57	20	640	$6.5 \cdot 10^{-10}$
51	5	700	$3.6 \cdot 10^{-10}$
40	3	720	$1 \cdot 10^{-9}$
58	1.7	705	$4.7 \cdot 10^{-9}$
25	0.6	795	$2.5 \cdot 10^{-8}$
p CoPc No.			
17	> 30	430	$2.8 \cdot 10^{-8}$
1	30	560	$2.7 \cdot 10^{-8}$
6	11.4	690	$1.2 \cdot 10^{-7}$
2	10.2	745	$5.3 \cdot 10^{-7}$
4	10.2	735	$1.9 \cdot 10^{-6}$
13	6.5	755	$4.1 \cdot 10^{-5}$
9	4.5	770	$1.2 \cdot 10^{-4}$

on polymeric FePc, and CoPc, are assembled in Table 6. Unfortunately, nothing is known as to the structure of the compounds.

A correlation between catalase activity, oxygen activity, and conductivity can be detected only within a series of phthalocyanines having the same central atom. The electrocatalytic activity increases considerably with increasing catalase activity and increasing conductivity of the chelate. A comparison of Fe- and Co-polyphthalocyanine fails to reveal any connection between oxygen activity and catalase activity. As polymeric CoPc has a high conductivity, it should be a better oxygen catalyst than polymeric FePc. An explanation of these effects is given by Meier [25]. The electrocatalytic properties are determined not only by the conductivity, but above all by the electron-donor action of the metal-containing polyphthalocyanine. The delocalization of the π-electrons of the polymeric com-

pounds is disturbed by the metal central atoms. This disturbance is connected with the different abilities of the respective metals to accommodate a higher change in valency. This property increases in the order Cu < Co < Fe, just like the activity.

4.1.2. Results of More Recent Experiments with Painted-on Electrodes

4.1.2.1. Activity of various metal chelates in sulfuric acid. Highly active and simultaneously stable catalysts in sulfuric acid are found only in the group of N_4-chelates. All other coordination complexes (N_2O_2, N_2S_2, O_4, S_4) could, for reasons of stability, be studied only in buffer solution ($KHCO_3/K_2CO_3$) and are discussed separately in Section *4.1.2.2.* All activities were determined by the same method of measurement, as already described in Section 2.2,. using painted-on electrodes. Departures from this procedure are expressly mentioned.

For graphical display of the results, we have chosen semilogarithmic curves with potential (measured against hydrogen in the same solution) as ordinate and current per unit mass of the test substance as abscissa.

The activity of the various chelates depends on:

— the nature of the central atome,

— the nature of the organic skeleton,

— the size of the π-electron system.

4.1.2.1.1. The influence of the *central atom* is shown in Fig. 14. In all the chelates we have studied, this influence is strong. The compounds with iron as central atom show the greatest activity, followed by cobalt, nickel and copper. This is shown by comparing monomeric Pc, TAA and TDAP. The activity of NiPc, CuPc and CuTAA is so small that potentials below 600 mV are measured even with a load of 30 mA/g catalyst. With TDAP, the Cu complex is more active than the Ni complex. The Fe complex of TAA, which would have been particularly interesting, was unfortunately not available. These observations indicate that oxygen reduction proceeds at the central atom of the chelate.

Comparing FePc and CoTAA, the differences in the slopes of the current/ voltage characteristic in the semilogarithmic representation is conspicuous. FePc has a slope of about 60 mV per decade of current, but CoTAA one of only about 30 mV. TAA behaves in this respect differently from all other chelates.

4.1.2.1.2. The influence of *different organic skeletons* with the same central atom is shown in Fig. 15. With cobalt as central atom, the activity decreases in the order TAA > TDAP > TMPP > Pc > TPAP > TPP. The last two of these classes of compounds are so inactive that their characteristic curves could not be shown in the same diagram (CoTPAP and CoTPP give potentials of 624 mV and 593 mV at 20 mA/g).

Substitution of the hydrogen atoms in the four benzene rings of Pc by chlorine produces only a slight change in the catalytic activity.

It is noteworthy that the introduction of heteroatoms (N or S) into the outer benzene rings of Pc can increase or reduce the activity.
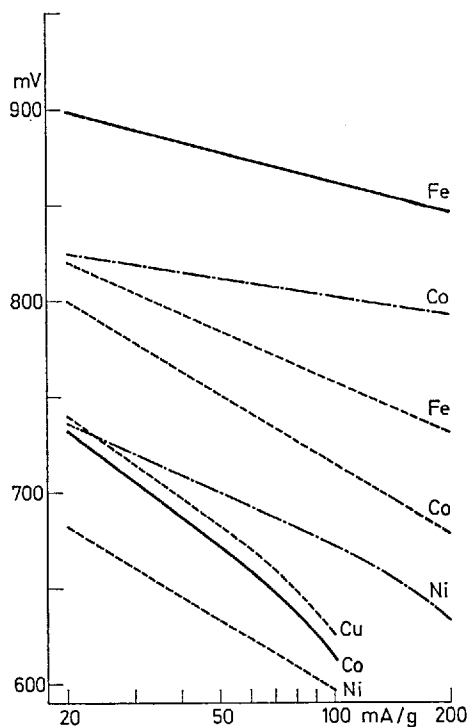
Fig. 14. Influence of the central atom in monomeric Pc (——), TAA (–·–·–) and TDAP (---) on the oxygen activity (Electrolyte: 4.5 N H_2SO_4)
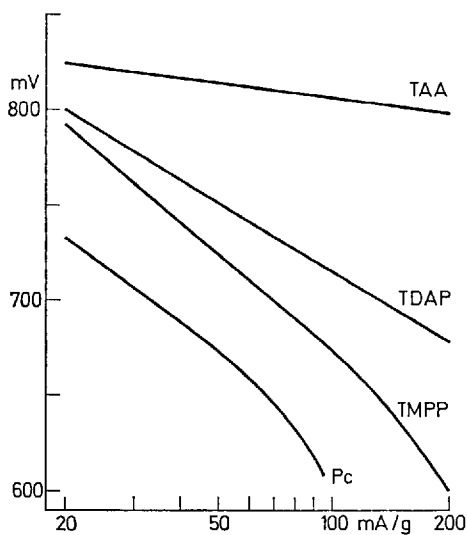

Fig. 15. Co complexes. Influence of various organic skeletons on the oxygen activity. (Electrolyte: 4.5 N H_2SO_4)

4.1.2.1.3. *Enlargement of the π-electron system.* Figure 16 shows the current/voltage characteristic curves of monomeric and polymeric phthalocyanines. With the same central atom, the polymeric compound is more than ten times as active as the monomer. Gel-chromatographic investigations have shown that the polymeric cobalt and iron phthalocanines we studied are built up from some 6 to 14 phthalocyanine ring systems. The conductivity of the Pc is increased by enlargement of the π-electron system. H. Meier [25] reports that the catalytic activity in oxygen reduction increases parallel to the conductivity of the polymeric Pc (with the same central atom). FeACC, discovered by Beck and Hiller [20], differs hardly at all in its activity from monomeric FePc.
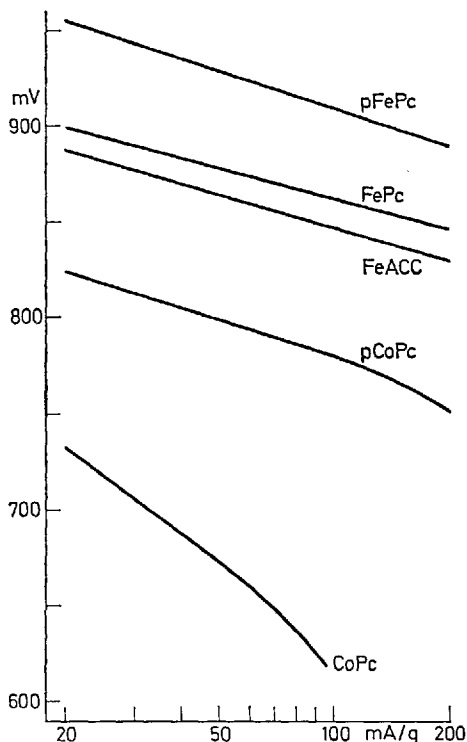

Fig. 16. Oxygen activity of monomeric and polymeric phthalocyanines. (Electrolyte: 4.5 N H_2SO_4)

4.1.2.1.4. Comparison of the *activity of various catalysts.* Figure 17 gives a survey of the activity of various catalysts usable for the cathodic reduction of oxygen in sulfuric acid. All the types of charcoal investigated (acetylene soot, BRX and RB 111) have only a slight activity. FePc is more active than CoPc and nearly as active as Raney platinum at the same coverage density. Platinum on the carbon substrate BRX with a content of 5% has 1/20th the activity of pure
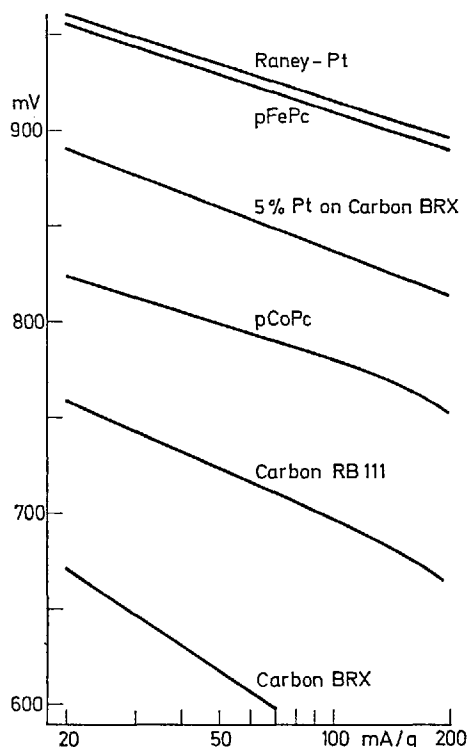
Fig. 17. Activity of various catalysts for the reduction of oxygen. (Electrolyte: 4.5 N H_2SO_4)

platinum, so that the activity is proportional to the quantity of platinum available. (Acetylene soot at 20 mA/g carbon gives a potential of less than 500 mV and could therefore not be shown in Fig. 17).

4.1.2.1.5. Summary of results on *activity in sulfuric acid*. Summing up the above results, it may be said, purely qualitatively, that the influence on the activity of a chelate is greater, the nearer to the centre the change is effected. Changing the central atom produces a considerable change in activity, changes in the inner coordination sphere do not have such a pronounced effect, and the substituents in the outer part of the molecule have least inflence. This decrease is parallel to the decrease of influence on the ligand field of the central atom.

4.1.2.2. *Activity of various metal chelates in oxygen reduction in carbonate/ bicarbonate buffer solution*. Experiments carried out in buffer solution (pH 9.3) have shown that not only N_4-chelates are able to catalyse O_2 reduction. The results confirm the statement above that changes in the centre of a complex influence the activity most strongly. The immediate neighbors of the central atom have as strong an influence as the central atom itself.

4.1.2.2.1. Influence of *coordination*. Figure 18a to d shows the activity of various coordinate complexes each figure part showing the complexes that occur with a particular central atom (Fe, Co, Cu, Ni). The broken line shows the control
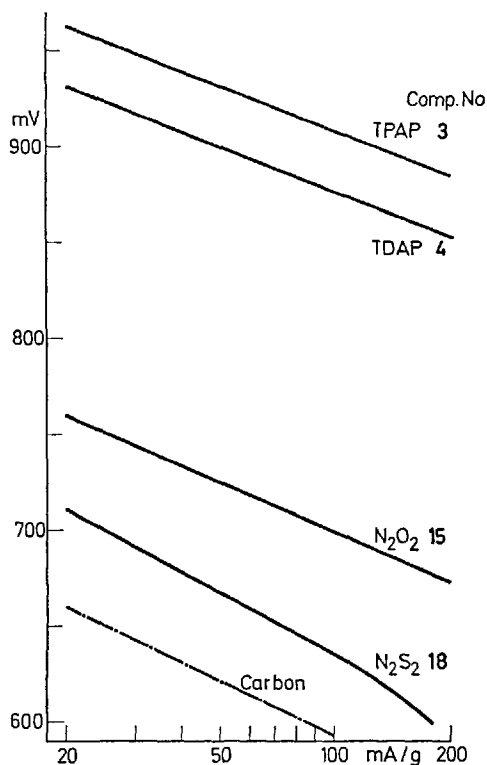
Fig. 18a. Fe complexes. Activities of variously coordinated metal chelates for the reduction of oxygen. (Electrolyte: Carbonate/bicarbonate buffer solution)

value, the activity of pure acetylene soot. The number next to the coordination symbol corresponds to the numbering in Table 1.

In the Fe complexes, activity decreases in the order

$N_4 > N_2O_2 > N_2S_2 > O_4 \approx S_4$ (inactive).

The Co complexes show a similar order, except that the first two complexes are interchanged:

$N_2O_2 > N_4 > N_2S_2 > O_4 \approx S_4.$

In the Cu complexes, which are all considerably less active, the order is

$N_4 > O_4 > N_2O_2 > N_2S_1 > S_4$ (inactive).

The Ni complexes, which are only feebly active, show the order

$O_4 > N_2O_2 > N_2S_2 > N_4.$

4.1.2.2.2. Influence of the *central atom*. With few exceptions, activity as a function of the metal ion of the central atom decreases in the order
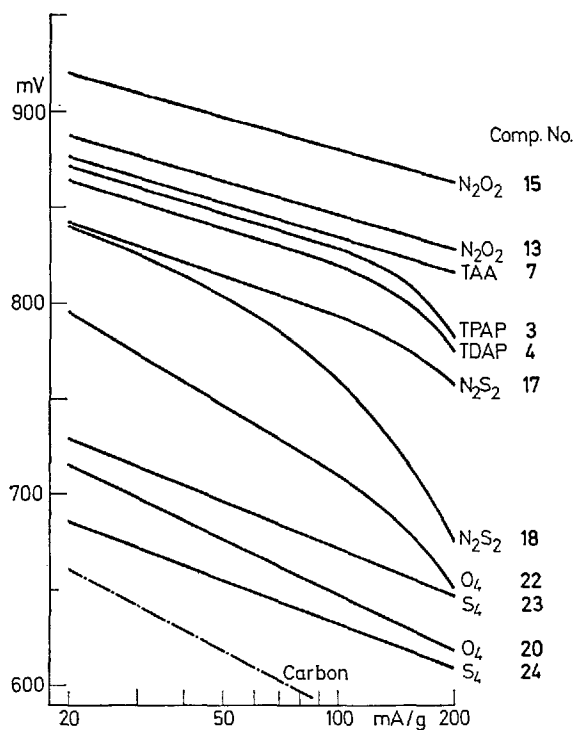
$Fe > Co > Ni \gtrsim Cu.$

Fig. 18b. Co complexes. Activities of variously coordinated metal chelates for the reduction of oxygen. (Electrolyte: Carbonate/bicarbonate buffer solution)
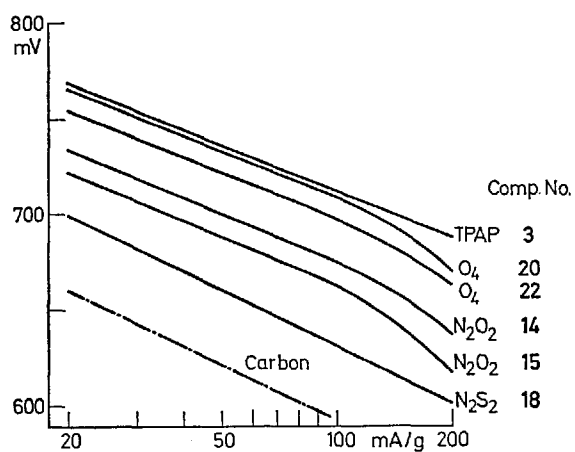

Fig. 18c. Cu complexes. Activities of variously coordinated metal chelates for the reduction of oxygen. (Electrolyte: Carbonate/bicarbonate buffer solution)
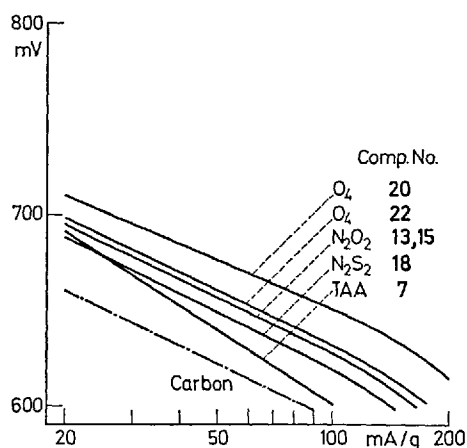
Fig. 18d. Ni complexes. Activities of variously coordinated metal chelates for the reduction of oxygen. (Electrolyte: Carbonate/bicarbonate buffer solution)

This is similar to the order reported above for complexes in sulfuric acid. Com parison of Fig. 18a to d shows that Fe and Co, and Ni and Cu, may change places.

Fig. 19 summarizes the results for the particularly interesting group of the Pfeiffer complexes (N_2O_2). The range of scatter shown corresponds to the in-
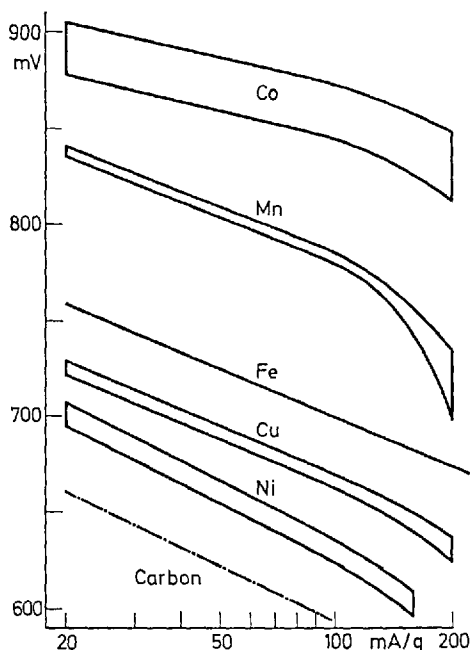

Fig. 19. Pfeiffer complexes. Influence of the central atom on the oxygen activity of the Pfeiffer complexes. (Electrolyte: Carbonate/bicarbonate buffer solution)

fluence of the organic skeleton (nos. 13–16). Of the Fe complexes, only compound no. 15 was available.

While *e. g.* MnPc is completely inactive in both sulfuric acid and buffer solution, the Pfeiffer complex of Mn shows even greater activity than the Fe compound. The activity decreases in the order

Co > Mn > Fe > Cu > Ni.

4.1.2.2.3. Influence of the *organic skeleton*. The example of the Pfeiffer complexes makes it clear that the influence of the organic skeleton is of subordinate importance. Figure 20 shows this influence for a number of Co—N_4 complexes. Here too, the differences in activity are much less than those produced by varying the central atom or the coordination.
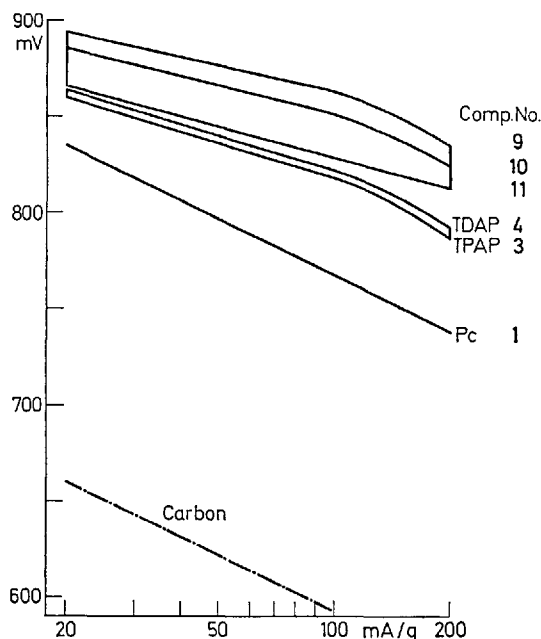

Fig. 20. Co-N_4-Complexes. Influence of the organic skeleton on the oxygen activity of various Co-N_4-complexes. (Electrolyte: Carbonate/bicarbonate buffer solution)

4.1.3. Improvement of Oxygen Activity by Thermal Pretreatment

The oxygen activity of various Co—N_4 complexes in sulfuric acid can be considerably improved by subjecting the carbon/chelate sample to thermal pretreatment in an atmosphere of a protective gas [57]. Such an effect is also reported by other authors for CoTMPP [22]. Figure 21 shows the influence of pretreatment on CoTMPP, pCoPc, and CoTAA. The given loadings (in mA/g catalyst) are all related to chelate plus carbon. The activity of CoTPP and CoTPAP is so low that,
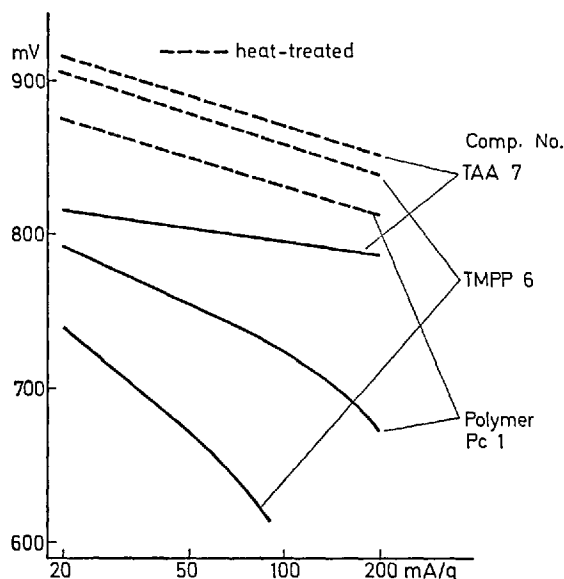
Fig. 21. Influence of thermal activation on the electrocatalytic activity of Co-N₄-complexes

in the untreated state, they give potentials at 20 mA/g of less than 600 mV, which cannot be shown in Fig. 21. After tempering, they attain the activity of tempered p CoPc. A tempering period of 1 h is sufficient. The best temperature range is 400 to 500 °C; at higher temperatures the activity of phthalocyanines and tetra-aza-porphyrins falls off sharply.

CoTAA plays a particular role here. The thermal activation of this compound is fully described in Section 4.2.4. in connection with its anodic formic-acid activity in sulfuric acid. Thermally pretreated mixtures of CoTAA and activated carbon BRX in the proportion of 1:2 w/w show their peak activity as oxygen-reduction catalysts as a function of treating temperature at about 600 °C (Fig. 22).
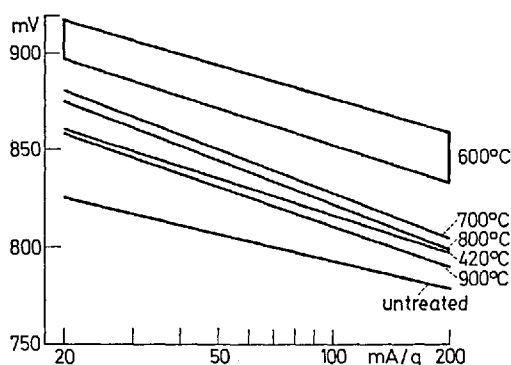

Fig. 22. Dependence of thermal activation on temperature. (Electrolyte: 4.5 N H_2SO_4)

Tempering at higher temperatures reduces the activity, but even after tempering at 900 °C the activity is still somewhat greater than that of the untreated substance. At the same time, however, the stability increases with increasing temperature. The most stable catalysts are obtained at 800 to 900 °C. Above 1000 °C, both stability and activity drop sharply.

4.1.4. Stability of Chelate Catalysts

Life tests have shown that all the chelate catalysts studied by us have only a limited operating life. Their life is restricted in some cases by direct chemical attack on the molecule, the central atom passing into solution as an ion. It depends very much on the nature of the central atom, degree of polymerization, and temperature. As shown in Fig. 23, acid attack is strongest in the case of polymeric FePc on soot
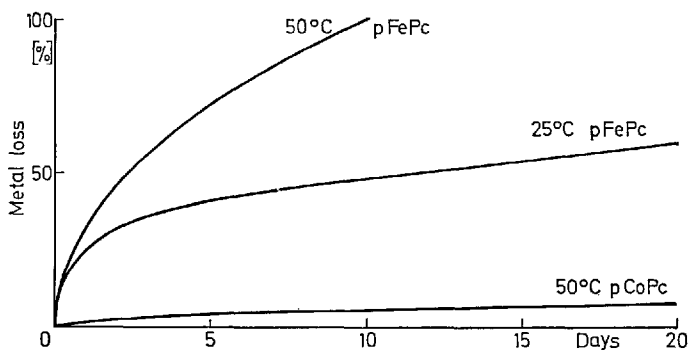

Fig. 23. Acid test of various Pc/soot samples in sulphuric acid

at elevated temperatures (50 °C), when the iron passes quantitatively into solution within 10 days. The less active polymeric CoPc is more stable by several orders of magnitude [b].

The conditions encountered in studying the stability of catalysts under electrochemical load are very complicated. Stability depends strongly on the potential and on the nature of the working substance. For example, pure CoTAA, when used as an oxygen catalyst at potentials of about 800 mV, is active only for a period of some hours. If, however, it is used in the anode for the oxidation of formic acid at 350 mV, it will give more than 6 months' (4000 hours') continuous service under the same conditions.

In Section 4.1.3. it was stated that the stability of CoTAA catalyst increases continuously on thermal pretreatment of mixtures with activated carbon (BRX) at temperatures of up to 900 °C, whereas the activity peaks below this level.

---

[b] As recently [58] shown by means of 59 Fe, there is no relation between the quantity of dissolved iron and the decrease in activity of FePc. Furthermore, FePc may show no decrease in activity over 3000 h at 60 m A/cm^2 when being prepared in the right manner [58].
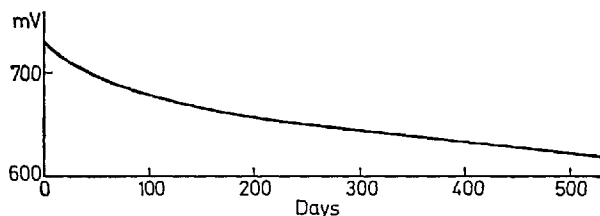
Fig. 24. Behaviour of heat-treated CoTAA in long-period tests. Conditions: 1A/g, 4.5 N H_2SO_4, room temperature

The most stable catalyst, in long-term tests lasting more than 500 days at room temperature under a constant load of 1 A/g, showed a mean potential decay of about 0.2 mV per day (Fig. 24). Under the same conditions, FePc and untempered CoTAA showed a potential decay of 100 to 200 mV/day. CoPc, although considerably more stable, cannot be subjected to so high a load.

4.2. Electrocatalysis of Anodic Reactions

4.2.1. Reaction of Various Fuels on CoTAA

Among the chelates active for the reduction of oxygen mentioned in Section 4.1, there is only one compound capable of catalyzing anodic reactions too. This is CoTAA, which, as Table 7 shows, is very active in acid solutions for the reaction of formic acid, oxalic acid and hydrazine, but less active for the reaction of formaldehyde and carbon monoxide [10].

Table 7. Activity of CoTAA complexes for the anodic oxidation of various fuels at 70 °C (from triangular voltage diagrams [11])

Catalyst	Electrolyte	Fuel	Activity (A/g catalyst) at 500 mV
Co-TAA monomer	2 N H_2SO_4	H_2	—
Co-TAA monomer	2 N H_2SO_4	CH_3OH	—
Co-TAA monomer	2 N H_2SO_4	CH_2O	0.2
Co-TAA monomer	2 N H_2SO_4	HCOOH	11.0
Co-TAA monomer	2 N H_2SO_4	Oxalic acid	10.5
Co-TAA monomer	2 N H_2SO_4	CH_3CHO	—
Co-TAA monomer	2 N H_2SO_4	CH_3COOH	—
Co-TAA monomer	2 N H_2SO_4	Ethylene glycol	—
Co-TAA monomer	2 N H_2SO_4	Glucose	—
Co-TAA monomer	2 N H_2SO_4	CO	0.15
Co-TAA monomer	2 N H_2SO_4	NH_3	—
Co-TAA monomer	2 N H_2SO_4	$N_2H_4 \cdot H_2O$	7.5
Co-TAA monomer	2 N H_2SO_4	Glycin	—
Co-TAA monomer	2 N KOH	HCOOH	—
Co-TAA monomer	2 N KOH	CO	0.7
Co-TAA "polymer"	2 N H_2SO_4	HCOOH	3.5

Formic acid does not react at all in alkaline solutions; carbon monoxide reacts better in alkaline than in acid solutions. Most surprisingly, no reaction at all can be produced with hydrogen, which under other conditions is readily oxidized. Hydrazine, which is present in acids almost exclusively as the corresponding hydrazonium salt, is very easily oxidized. This suggests that hydrazine reacts directly and not by the mechanism of previous separation of hydrogen.

The values for activity given in Table 7 are taken directly from the triangular voltage diagrams. They thus include the ohmic voltage drop, which is particularly large in this non-conductor. A measurement without this drop gives for the oxidation of formic acid at a potential of 350 mV an activity of 8 A/g; the value including the ohmic voltage drop at the same potential is 3.8 A/g.

"Polymeric" CoTAA [24] is produced by oxidizing the monomer in air and its structure is still obscure. It is likewise active for the oxidation of formic acid, but has only one third the activity of the monomer and is less stable.

4.2.2. Electrochemical Pretreatment of CoTAA

The most promising reaction is the oxidation of formic acid on monomeric CoTAA, which is thus considered here in greater detail.

If the activity of fresh CoTAA is measured at a fixed potential below 500 mV, the value obtained is low. Different results are obtained with the pretreated catalyst. This process can best be explained with reference to the potentiodynamic triangular voltage diagram.
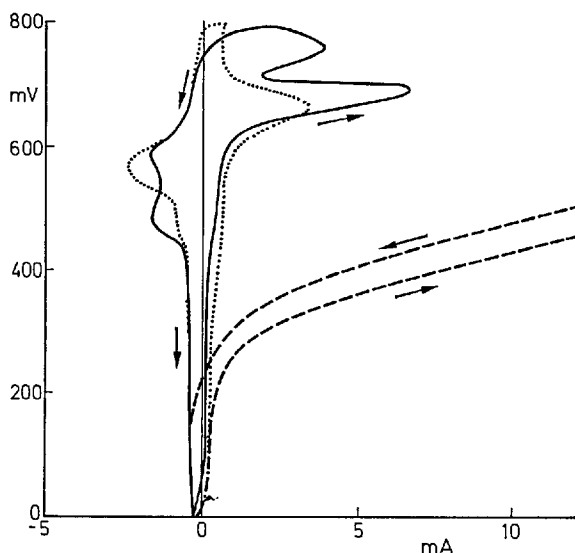

Fig. 25. Potentiodynamic current/voltage curves of monomeric cobalt tetra-aza-annulene. Conditions: 2 N H_2SO_4, 70 °C, sweep rate 50 mV/min.
— First Cycle under N_2
.. Steady-state curve under N_2
-- After adding HCOOH

The continuous curve in the triangular voltage diagram (Fig. 25) is the initial curve, obtained under nitrogen with a previously unused sample of catalyst. Two anodic peaks occur in the potential range betwen 650 and 800 mV. The quantities of charge transferred in the peaks between 600 and 450 mV in the cathodic process are considerably smaller than those corresponding to the anodic peaks.

After a few voltage cycles, the shape of the curve changes, and finally the "zero curve", shown dotted in the figure, is obtained. The areas under the anodic and cathodic peaks are here equal and correspond to the transfer of one electron per TAA molecule. We assume that these reproducible peaks, whose position is independent of the pH of the electrolyte, are caused by a change in valency of the central cobalt atom.

In the first cycle, there is superimposed on this change of valency an irreversible oxidation of the molecule, in which about two electrons are lost. This could, for example, involve the formation of a dication. It is obviously the species so formed that catalyzes so excellently the subsequent anodic oxidation of formic acid (broken curve, measured with 1 M HCOOH).

The anodic activation process described above proceeds similarly when operated under potentiostatic conditions. Experiments varying activation potential, temperature, and quantity of charge lost in activation have shown that optimal activation in 2 N H_2SO_4 takes place at 50 °C at a potential of 750 mV. The quantity of charge transferred must correspond to the loss of 3 electrons (change of valency of the Co central atom and irreversible oxidation).

In this way, using electrodes with the powdered substances between graphite discs (see Section 2.2.2.1.), we obtained an activity of 6 to 8 A/g (free from ohmic voltage drop) at 350 mV and 70 °C in 2 N $H_2SO_4 + 3M$ HCOOH. Unactivated CoTAA, on the other hand, gave a current of only 0.5 A/g under the same conditions. Stationary current/voltage curves for the anodic oxidation of HCOOH on electrochemically activated CoTAA at 50 °C and 70 °C are shown in Fig. 26. The reaction rate is strongly temperature-dependent, the activation energy being about 13 kcal/mol.
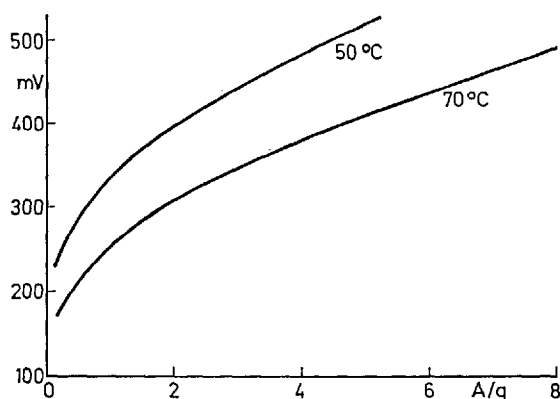

Fig. 26. Stationary U/I characteristic curves of the oxidation of 3 M formic acid on CoTAA in 2 N H_2SO_4

4.2.3. Chemical Activation of CoTAA

As oxidation of CoTAA obviously occurs in the electrochemical activation process described above, it should also be possible to improve the activity by the action of oxidizing agents. In fact, an active form of CoTAA can be obtained by bubbling air or oxygen through a suspension of CoTAA in $2N$ H_2SO_4 for about 15 h at room temperature. The activity of the black powder obtained in this way lies between 2 and 5 A/g. The wide spread of these results is chiefly due to the fact that conditions were not optimal for the action of oxygen, and probably not the same for all particles of catalyst. No attempt was made to refine this activation process because we found another method for increasing the activity of CoTAA, which appeared considerably more promising.

4.2.4. Thermal Activation of CoTAA

In the course of a series of experiments designed to investigate the possibility of activation of CoTAA by the action of very low concentrations of oxygen in the gas phase at higher temperatures, we established that, even in a pure nitrogen atmosphere, only a part of the chelate sample sublimates unchanged. At temperatures above 400 °C a grey-black residue is left; this is a very good catalyst for the oxidation of formic acid. The yield of this active residue is about 60 to 70% of the initial mass when the heat treatment is carried out under nitrogen in a beaker covered with a watch glass.

The most active catalysts are obtained by heating for about 4 h at 420 to 470 °C. They have almost the same activity as electrochemically activated CoTAA, and the slope of the current/voltage characteristic is also the same. Thermal treatment above 500 °C gives considerably less active catalysts. The activity of powder prepared at 600 °C is less than 1 A/g. Varying the period of tempering from 2 to 10 h has hardly any influence on the activity.

4.2.5. Attempts to Explain the Nature of Activated CoTAA

The samples of active CoTAA obtained by the three different activation methods are probably not identical, although they all show great similarity. Thus, all are greyblack or black powders, amorphous in X-ray diffraction analysis, hardly or not at all soluble in all usual solvents. The poor solubility indicates that the compounds are polymeric. This hypothesis could be confirmed in the case of a chemically activated sample of CoTAA, the activation consisting of exposure to air for 20 h at room temperature. Determination of the molecular weight of the component soluble in pyridine (about 10—30%) gave a value of 965. This is almost three times the molecular weight of monomeric CoTAA (345). The IR spectra also point to polymerization taking place in all activation processes. In all cases, in contrast to the spectrum of monomeric CoTAA, very poorly defined broad bands are obtained, probably due to the vibration capabilities of the structure being strongly reduced, in comparison to the monomer, by cross-linking in at least two dimensions. The spectra yielded no information as to the nature of the linkages.

This question was investigated more thoroughly with thermally activated CoTAA. Elementary analysis of the samples of active CoTAA obtained at various temperatures was very informative. According to these results, the powder obtained by heating to above 540 °C differs considerably in composition from CoTAA: the content of Co and C is much increased and that of H and N decreased. On the other hand, the particularly active catalysts obtained at temperatures between 420 and 500 °C show only a sudden drop in hydrogen content, corresponding to a change in the empirical formula from $C_{18}H_{14}N_4Co$, for pure CoTAA, to $C_{18}H_{11}N_4Co$. Furthermore, it was found by hot extraction that at 470 °C a quantity of elementary hydrogen is evolved, corresponding approximately to this change in the empirical formula. Polymerization with splitting off of H_2 and linkage of CoTAA monomer units by C—C bridges during thermal activation is thus very probable.

The CoTAA catalysts obtained by the three activation methods show different electrochemical behavior. This appears particularly clearly in the triangular voltage diagrams obtained under inert gas. The curve for chemically activated CoTAA (Fig. 27) is similar to the constant "zero curve" of electrochemically activated
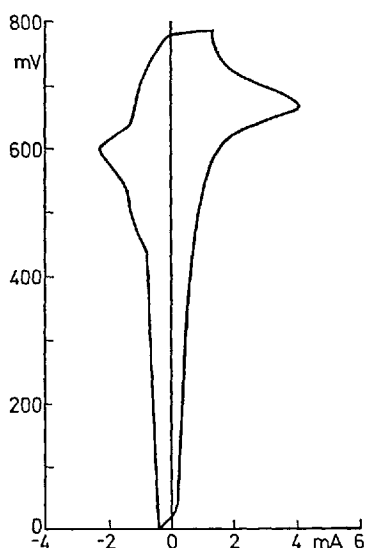

Fig. 27. Potentiodynamic current/voltage curves of chemically actived CoTAA

CoTAA (dotted curve in Fig. 25), though the peaks ascribed to the change in valency of the Co central atom are less pronounced. Thermally activated CoTAA, gives a completely different picture (Fig. 28). Here, the first cycle above about 600 mV gives an anodic current, which rapidly declines. This is obviously a corrosion current and it destroys the catalyst.
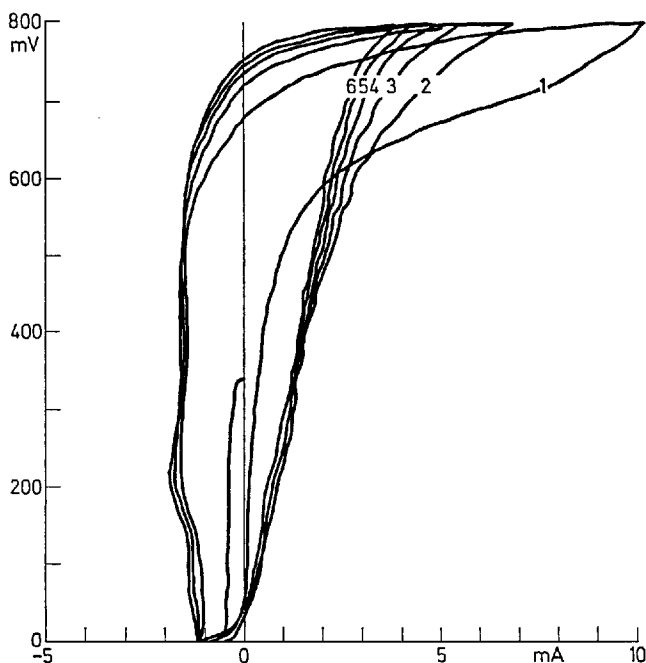
Fig. 28. Potentiodynamic current/voltage curves of thermally actived CoTAA in 2 N H_2SO_4 at 70 °C (activation temperature 500 °C)

4.2.6. Mechanism of Oxidation of Formic Acid

From the very good activity of thermally or electrochemically activated CoTAA for the reaction of CO one might deduce that the oxidation of formic or oxalic acid proceeds, not directly, but by way of a preliminary decarbonylization reaction. However, there is no evolution of gas from CoTAA in a solution of formic acid in dilute sulfuric acid, even at 70 °C. Such a reaction would have to occur on chemical decomposition of formic acid, with evolution of CO and H_2O, or CO_2 and H_2. It may thus be assumed that formic acid is oxidized directly.

4.2.7. Compact Electrodes with CoTAA as Catalyst

The modified supported powder electrodes used in the experiments hitherto described on the anodic activity of CoTAA are out of the question for practical application in fuel cells, as they do not have sufficient mechanical stability and their ohmic resistance is very high (about 1—2 ohm). For these reasons, compact electrodes with CoTAA were prepared by pressing or rolling a mixture of CoTAA, activated carbon, polyethylene, and PTFE powders in a metal gauze. The electrodes prepared in this way show different activities depending on the composition and the sintering conditions. Electrodes prepared under optimal conditions can be loaded up to about 40 mA/cm^2 at a potential of 350 mV at 70 °C in 3 M HCOOH, with relatively good catalyst utilization (about 5 A/g) and adequate stability.

The operating life of the electrodes is good: unter potentiostatic conditions at 350 mV, the current falls by about 6% over 2400 h continuous operation.

These properties make CoTAA a good catalyst for the anodic oxidation of formic acid. Economic application of this catalyst is, however, not anticipated because formic acid is not economically attractive as a fuel. It is certainly possible to prepare electrodes containing a mixture of tungsten carbide and CoTAA as catalyst, with the tungsten carbide catalyzing the first stage of the oxidation of CH_2O to $HCOOH$, and the CoTAA the further oxidation of $HCOOH$ to CO_2, but this possibility does not offer any more favorable prospects. Economic application of CoTAA will only come into question when cheap catalysts are available for the partial oxidization of methanol to formaldehyde or formic acid.

5. Theoretic Aspects

5.1. Influence of H_2O_2 on the Mechanism of Oxygen Reduction

In the fundamental reaction which proceeds at the cathode of a fuel cell with an acid electrolyte, the oxygen molecule gains a total of 4 electrons:

$$O_2 + 4\,H^+ + 4e^- \longrightarrow 2\,H_2O \tag{1}$$
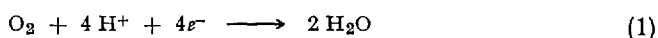
The mechanism of this strongly inhibited reaction has not yet been explained in detail, even with platinum, the most intensively studied of all catalysts [26]. The results obtained to date show that the course of the reaction is not the same on all catalysts and that other factors, such as oxygen absorption on platinum metal catalysts, play an important part. In most of the reaction mechanisms hitherto formulated and discussed H_2O_2 occurs as an intermediate stage [26]:

$$O_2 + 2\,H^+ + 2e^- \longrightarrow H_2O_2 \tag{4}$$
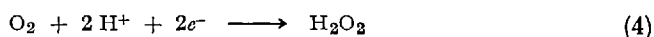
Absorbed species such as peroxide radicals or H_2O_2 are probably also formed as intermediates. The H_2O_2 formed in Reaction (4) could be experimentally detected in some cases [27-30].

Among the possible causes for the strong inhibition of the reduction of oxygen there must be mentioned the high overvoltage required for the further reduction of H_2O_2:

$$H_2O_2 + 2e^- + 2H^+ \longrightarrow 2H_2O \quad (^\circ U_H = 1.74\ \text{V}) \tag{5}$$

involving rupture of the O=O bond, and the first electron transfer involved in formation of the oxygen ionic radical:

$$O_2 + e^- \longrightarrow O_2^-. \tag{6}$$

Reaction (6) has been shown to exert a strong inhibiting effect, above all in acid electrolytes [31].

Kozawa, Zilionis and Brodd [32] have recently reported a 4-electron mechanism in the reduction of oxygen at a graphite electrode coated with iron phthalocyanine

171

in the pH range 6 to 7. The implication is that neither Reactions (5) or (6) nor any other intermediate step determines the reaction velocity, but rather that the reduction proceeds directly to water in accordance with Reaction (1). The limiting currents measured by these workers with the rotating disc-ring electrode correspond to a reaction of 4 electrons per O_2 molecule, but they could be interpreted differently. As H_2O_2 is also reduced in the potential range in which these limiting currents occur [33], it is more probable that what occurs is not a 4-electron step but a sequence of two 2-electron steps. A reaction mechanism such as that suggested by Breiter [34] for platinum

$$O_2 \longrightarrow H_2O_{2_{ad}} \longrightarrow H_2O_2$$
$$\downarrow \qquad\qquad\qquad\qquad (7)$$
$$H_2O$$
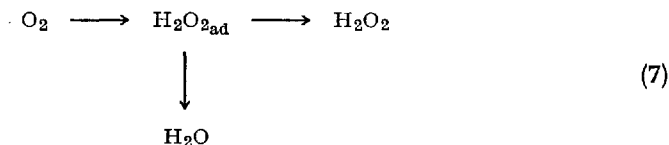
is also possible. The slope of the current/voltage characteristic curve, which has been measured for chelate catalysts (see Fig. 14), is about 60 mV per decade, and also corresponds rather to a 2-electron than to a 4-electron step.

If the velocity of reduction of oxygen is determined by Reaction (5), particularly high activity should be expected with catalysts possessing high catalase activity. The H_2O_2 formed could then at once react further according to the mechanism

$$2\,H_2O_2 \longrightarrow 2\,H_2O + O_2. \qquad\qquad (8)$$
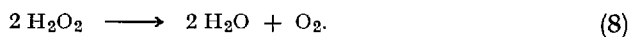
With phthalocyanines of the transition metals, for example, the activity for the decomposition of H_2O_2 should decrease in the same sequence as that for the reduction of oxygen, namely [4,35]

$$FePc > CoPc > NiPc \geqslant CuPc$$

Meier and co-workers [36] have reported such direct relationships in the case of phthalocyanine catalysts but their results could not be confirmed by Beck [37,38], who also studied CoTAA (see Table 5). The results obtained by Meier *et al.* do not in all cases confirm the expected relationship between catalase activity and electrochemical activity, too. Thus, for example, the phthalocyanines of Cd, Ti, Zr and Nb do indeed show good catalase activity, but they have not so far been found to possess any particular activity for the cathodic reduction of oxygen.
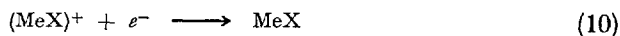
5.2. The Reduction of Oxygen as Redox Catalysis

Beck [23,37,38] carried out voltammetric investigations of chelates in solution (phthalocyanine and tetra-aza-annulene in 85—90% H_2SO_4). The particularly active electrocatalysts (FePc and CoTAA) showed very positive redox potentials and a pronounced positivization of the polarographic oxygen step in 85 % sulfuric acid. On the basis of these results, Beck proposed the following mechanism

for the reduction of oxygen, which he termed "redox-catalysis": the metal chelate MeX is transformed into the oxidized form by molecular oxygen according to

$$MeX + \tfrac{1}{4} O_2 + H^+ \longrightarrow (MeX)^+ + \tfrac{1}{2} H_2O. \tag{9}$$
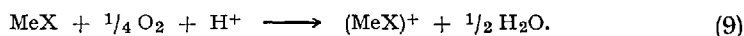
This is to be regarded as an overall reaction, and the individual steps are not discussed by Beck. The really potential-dependent reaction is then the electrochemical reduction of the oxidized metal chelate:

$$(MeX)^+ + e^- \longrightarrow MeX \tag{10}$$

by which the chelate is transformed back into its original form.

A similar mechanism could operate in the reduction of oxygen on chelate catalysts, as in the organic cathodes with air regeneration described by Alt, Binder, Köhling and Sandstede [13,40]. These cathodes contain a reversible insoluble quinone/hydroquinone system. The quinone, which is electrochemically reducible, can be obtained either by electrochemical oxidation or by purely chemical oxidation with H_2O_2 or oxygen (air). A cathodic current is observed in these systems only at potentials below the redox potential, and unusually hard current/voltage characteristic curves are obtained.

The reaction process in oxygen reduction on chelate catalysts however is less easily explained. A number of experimental results have been obtained which do not accord with Beck's mechanism of "redox catalysis".

1. Under operating conditions, in the absence of oxygen, a redox process in the potential range of interest for oxygen reduction is observed in only a few cases [11,41]. Consequently, there is no true correspondence between activity and redox potential.

2. With CoTAA, the stationary curve obtained in $2 N H_2SO_4$ under N_2 shows an anodic and a cathodic peak, which should probably be assigned to the change in valency of cobalt ($Co^{2+} \rightleftharpoons Co^{3+}$) [11]. The redox potential of this process lies at about 650 mV. The oxygen, contrary to Beck's suppositions, is reduced at CoTAA electrodes far above this potential, with relatively high current densities and in a potential region in which the reactions

$$Co^{3+} + e^- \longrightarrow Co^{2+} \qquad \text{or} \tag{11}$$

$$(CoTAA)^+ + e^- \longrightarrow CoTAA \tag{11a}$$
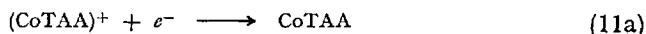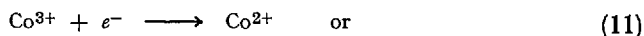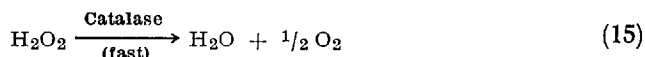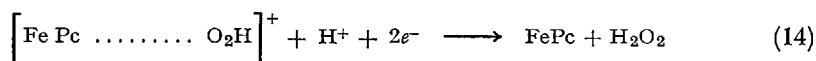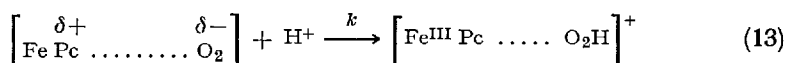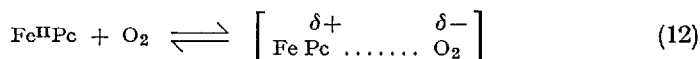
do not yet proceed.

3. The oxidation of hydroquinones with molecular oxygen is possible only in the presence of a catalyst, *i.e.* activated carbon. The velocity of oxidation decreases with increasing redox potential [13,14] (Duroquinone is formed more quickly than chloranil). For this reason, particularly with chelates that have a rather high redox potential, it cannot be assumed that oxidation in accordance with Reaction (9) proceeds with sufficient velocity.

4. The current/voltage characteristic curves for the reduction of O_2 on chelate catalysts mostly show a Tafel region with a slope of about 60 mV. This could

indicate the presence of a two-electron step, but Beck's mechanism allows only a one-electron step.

5. The substrate has been observed to exert an influence. This is not predicted by the mechanism of "redox catalysis".

According to Beck's more recent ideas [42], the observed discrepancies can all be resolved by a slight modification of the model of redox catalysis. In this modified model, the following reaction sequence takes place on FePc:

$$Fe^{II}Pc \; + \; O_2 \; \rightleftharpoons \; \left[\underset{Fe\,Pc}{\overset{\delta+}{}} \; \ldots \ldots \; \underset{}{\overset{\delta-}{O_2}} \right] \tag{12}$$

$$\left[\underset{Fe\,Pc}{\overset{\delta+}{}} \; \ldots \ldots \ldots \; \underset{}{\overset{\delta-}{O_2}} \right] + H^+ \; \xrightarrow{k} \; \left[Fe^{III}\,Pc \; \ldots \ldots \; O_2H \right]^+ \tag{13}$$

$$\left[Fe\,Pc \; \ldots \ldots \ldots \; O_2H \right]^+ + H^+ + 2e^- \; \longrightarrow \; FePc + H_2O_2 \tag{14}$$

$$H_2O_2 \; \xrightarrow[\text{(fast)}]{\text{Catalase}} \; H_2O \; + \; {}^1/_2\,O_2 \tag{15}$$

In this theory the essential electrochemical stage is no longer considered to be the reduction of the chemically oxidized chelate e.g. $[Fe^{III}\,Pc]^+$, but the reduction of the complex that arises through attachment of O_2 and H^+ to the chelate in accordance with Reactions (12) and (13). This modification would explain why

1. O_2 reduction proceeds at a potential far above the redox potential for the pure chelate;

2. a slope of 60 mV per decade is observed in the current/voltage characteristic curve;

3. the substrate exerts an influence through variation of the electron density at the central atom.

Whether the electrochemical step in Reaction (14) actually determines the velocity must, however, remain open. Alt, Binder and Sandstede [22] reached the opposite conclusion, as did Savy and co-workers [35], and Randin [44].

Randin, in a recently-published paper [44], investigated solely on the basis of results from the literature the relationship between electrocatalytic activity for O_2 reduction on the one hand, and oxidation potential, magnetic moment, and catalytic properties in gas-phase reactions on the other. It was found for the transition-metal phthalocyanines that magnetic moment and activity for the dehydrogenation of cyclohexanedione increase together with the activity of the phthalocyanines for O_2 reduction, while the oxidation potential becomes less. The last fact can be seen from Fig. 29, in which the first oxidation potentials in 1-chlornaphthalene, measured by Manassen and Bar-Ilan [45], are plotted against electrochemical activity. This result shows that the more easily an electron can
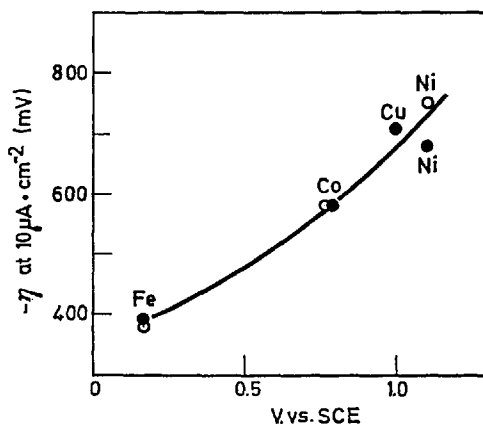
Fig. 29. Electrochemical activity for the oxygen reduction shown by Fe-, Co-, Ni- and CuPc in the work of Savy et al. [35] plotted against the first electrochemical oxidation of MePc taken from [45]. O monomeric McPc at pH 1.3, deposited on gold; ● polymeric MePc at pH 1.3, impregnated on graphite [44]

be detached from the Me—Pc electrode, the greater the electrocatalytic activity. Such an interpretation is acceptable only if, in contradiction to Beck's views [37,38], charge transfer from metal phthalocyanine to oxygen determines the velocity.

5.3. Interpretation of O_2 Reduction in the Light of MO Theory

5.3.1 Models Previously Suggested for the Mechanism of Oxygen Reduction

The chelate catalysts described in the literature as particularly active in the reduction of oxygen all have considerable structural similarity with the prophyrins [1-4, 11-13]. In these naturally occurring oxygen carriers the essential interaction takes place between the oxygen and the central metal ion; this is also the case in electrocatalysts on a chelate basis [2,4,13,32,35,46]. Investigations of gas-phase chemisorption on phthalocyanines by Contour, Lenfant and Vijh [47] have shown that oxygen is adsorbed molecularly and does not penetrate into the solid body. Therefore the nature of the central ion at the surface of the catalyst is probably of decisive importance for the activity of the catalysts. Savy, Andro, Bernard and Magner [35] as well as Alt, Binder and Sandstede [22] have accordingly interpreted the differences in activity on the basis of the electronic structure of the central ion. The energy partition of the d orbitals is not exactly known for transition metal chelates known to be electrocatalysts, so these authors used for their studies the electron states of the transition-metal ions in porphyrin complexes as calculated by Zerner and Gouterman [48]. The MO calculations give the distribution shown schematically in Fig. 30. The energy differences can be shown only qualitatively.

The decline of activity in the order

Co > Fe > Ni ≈ Cu

175
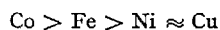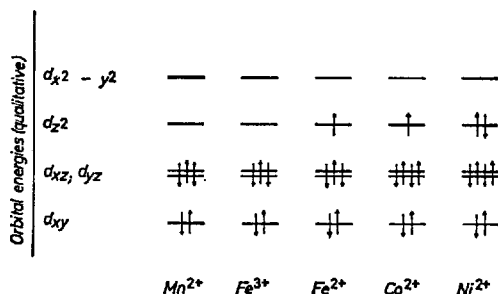
Fig. 30. Schematic occupation of the d-level of the metal ions in porphyrine

for the TMPP and TAA complexes can, according to Alt, Binder and Sandstede [22] be explained on the basis of the following assumptions:

1. Electrocatalysis takes place during the first step of O_2 reduction, H_2O_2 being formed in a two-electron step. The correctness of this assumption is supported by polarographic investigations of O_2 reduction in the presence of phthalocyanines [49].

2. The reduction of oxygen is favored by partial electron transition from the metal to the anti-bonding π orbitals of the oxygen during formation of the chelate–oxygen adsorption complex.

3. This partial electron transition is favored by filled d_{xz} and d_{yz} orbitals and empty d_{z^2} orbitals.

The formation of the adsorption complex, which is important for the electrochemical reduction of oxygen, then proceeds in close analogy to the formation of the ethylene–transition-metal complex as shown in Fig. 31.
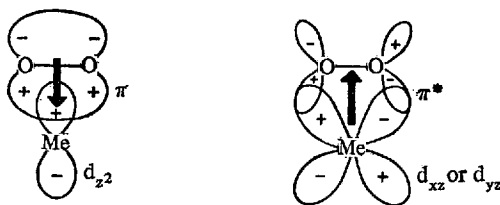
Fig. 31. Electron donation and back donation in oxygen-complexed transition metal bonding[22]

From this model it can be seen that electron transition from oxygen into the empty d_{z^2} orbitals proceeds first with formation of a σ bond. This lowers the energy of the anti-bonding π orbitals and raises that of the d_{xz} and d_{yz} orbitals, so permitting strong interaction between these two orbitals.

Savy et al. [35] reach practically the same conclusion concerning the electron transitions during formation of the activated complex but consider an edge-on arrangement of the oxygen above the plane of the chelate molecule more probable. Their studies relate only to the catalytic properties of the phthalocyanines for O_2 reduction. Their conclusion is that the conditions for optimal activation of oxygen

are best met in the series of phthalocyanines by monomeric or polymeric iron phthalocyanine. According to their work, catalytic activity should decrease in the order

Fe > Co > Ni > Cu [4,32,35,50].

This conclusion is qualitatively confirmed by experiment.

5.3.2. A Modified Model for Oxygen Reduction

The simple arguments according to which the energy partitions of the d levels calculated by Zerner and Gouterman [48] for porphyrins were assumed to hold for other N_4-chelates too, lead to the conclusion that the Fe and Co chelates fulfil the conditions for activation of oxygen. The experimental results show that, of the TAA and TPP complexes, those with Co are the most active, while in the phthalocyanines and the TDAP complexes the iron compounds show higher activity. To explain these facts, further assumptions are necessary. Alt, Binder and Sandstede [22] postulate the presence of Fe^{3+} in the TAA and TPP complexes and of Fe^{2+} in the phthalocyanines, the latter ion forming much more effectively activated complexes with the oxygen. We consider [57] the above model must be refined because

  1. the valency of the central atom at the working potential of the electrodes is not exactly known;

  2. any difference in the redox potential, for example in the various N_4-chelates of iron, is to be ascribed principally to the influence of the ligands.

A refined model is particularly necessary for interpretation of the differences in activation of the other chelates we have investigated.

  Not only does the central atom itself influence the activity of the chelate concerned but also its immediate neighbors. The activity of the symmetrical plane square Co and Fe complexes, like the ligand field strength, decreases according to the spectrochemical series of the donor atoms concerned in the order

N > O > S [51].

  In less symmetrical complexes, such as those with N_2O_2 or N_2S_2 groups, no such simple relationship holds, so that no conclusions as to the relative activity of the various complexes can be drawn from consideration of the ligand field strengths. The N_2O_2 complexes, however, include a series of Co complexes known to function as reversible O_2 carriers whose mode of action has been intensively studied [52]. This work gives some important indications as to the factors concerned in electrocatalytic O_2 reduction on similar chelates. The results that describe the influence of the occupation of the 5th coordination site of the central atom on the positions of the energy levels of the d orbitals are of the greatest interest. As can be seen from Fig. 32, the electron configuration that seems to constitute an essential condition for O_2 transfer [53,54] is found in square pyramidal complexes. It is characterized by the presence of filled d_{xz} and d_{yz} orbitals and empty d_{z^2} orbitals. This view is supported by ESR studies. The spectrum of Co(acacen)
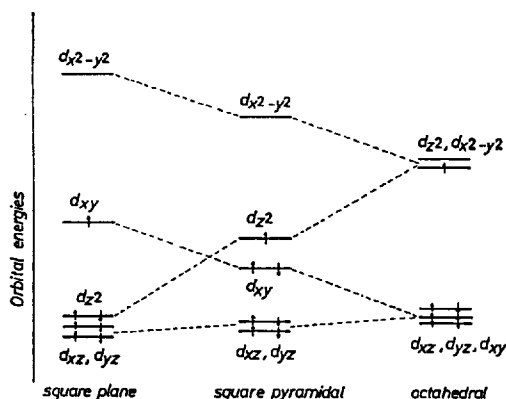
Fig. 32 [52]. Energy levels of the d-orbitals of cobalt in various surroundings

(see Fig. 33) in toluene accords best with the configuration $(d_{xz})^2 \, (d_{yz})^2 \, (d_{xy})$, as is to be expected for a square planar complex. A different spectrum is observed in the presence of a Lewis base: the signal of the pyridine-containing complex formed under these conditions, and which — in contrast to Co(acacen) — is capable of effecting O_2 transfer, is interpreted as meaning that the unpaired electron is assigned to the 3 d_{z^2} orbital [53,54].
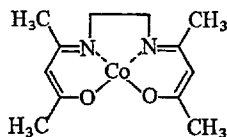
Fig. 33. Co(acacen)

From X-ray analysis and ESR measurements, it further appears that in the oxygenated pyridine-containing complex [Co(acacen)py O_2], the Co atom shows approximately octahedral coordination. In this complex, the O_2 molecule is linked to the central Co atom only by a σ bond at a single O atom, and the bond angle Co—O—O is 126°. The O—O distance is 1.26 Å, almost exactly the same as in the superoxide ion. This indicates a weakening of the O—O bond, which may be explained by a strong back-bonding component from an occupied Co-d orbital (t_{2g}) to the antibonding empty 1 π_g (p_x) orbital of the O_2.

Let us take the results briefly described above as our starting point. What new prospects do they offer for a better explanation of the experimental results obtained in O_2 reduction on chelate catalysts?

1. The presence of empty d_{z^2} orbitals should play a decisive part in the reduction of O_2, as they do in O_2 transmission. In the square planar complexes (cf. Fig. 32) investigated by us, this condition is fulfilled only by the attachment of a 5th ligand. We therefore assume that the surface groups of the carbon take effect as

strong 5th ligands. The extent to which the d_{z^2} orbitals are raised varies widely. For example, in the Fe(III)-porphyrin complexes, it increases in the order F < Cl < OH < CN [55]. Our experimental finding [3] that the activity of FePc in particular is considerably enhanced by certain types of carbon substrate, could thus be due to these surface groups exerting a particularly favorable effect on the raising of the d_{z^2} orbitals.

2. The differences effected in activity by the central atom with all the ligands studied can hardly be explained solely by the occupation scheme of the d level (Fig. 30) as calculated for the porphyrins. The influence of the 5th ligand is not taken into account in the above discussion. In addition, there is no information as to which of the two requirements for interaction with oxygen (empty d_{z^2} orbitals, or filled d_{xz} and d_{yz} orbitals) has the greater influence. For example, the requirement would be best fulfilled in the case of Fe(II) followed by Fe(III) if the d_{z^2} orbital were raised so far as to be no longer occupied. Where the orbitals lie close together, an occupation such as that shown in Fig. 30 will occur and the activity of Fe(II) should then be less than that of Co(II).

3. The influence of the ligand field strengths of the donor atoms is not sufficient to explain the result that, among cobalt complexes in buffer solution, those with N_2O_2 coordination are more active than the N_4 complexes. Perhaps this departure from the relationships observed in other cases [56] is due to non-integer electron occupation, which is usually arrived at on the basis of molecular-orbital considerations. A lower occupation of the d level might occur in the N_2O_2 complexes because of the greater electronegativity of oxygen (lower p_z level); this situation would approach conditions in a Co(III) complex. A lower occupation of the d_{z^2} orbital, and hence better possibilities for an interaction with O_2, would be obtained.

To sum up, it can be said that MO considerations can explain a number of experimental results in O_2 reduction on chelates, but they do not yet permit a quantitative explanation of the differences in activity.

5.4. Mechanism of the Anodic Activity of CoTAA

We are still further from being able to explain the anodic activity of the CoTAA complex. The cobalt phthalocyanine, which is structurally identical with CoTAA in the inner coordination sphere, is completely inactive in the catalysis of anodic reactions. It therefore looks as if the central region is not exclusively responsible for the anodic activity. On the other hand, the fact that CoTAA is inactive for the oxidation of H_2 points to π orbitals of the fuel participating in the formation of the chelate-fuel complex. A redox mechanism (cf. Section 5.2) can be ruled out because anodic oxidation proceeds only in the region below the redox potential of CoTAA (*i.e.* at about 600—650 mV).

179

H. Jahnke, M. Schönborn, and G. Zimmermann

6. References

[1] Jasinski, R.: Nature *201*, 1212 (1964).
[2] Jasinski, R.: J. Elektrochem. Soc. *112*, 526 (1965).
[3] Jahnke, H.: Ber. Bunsenges. Physik. Chem. *72*, 1053 (1968).
[4] Jahnke, H., Schönborn, M.: 3es Journées Int. d'Etude des Piles à Combustible, Bruxelles (1969), Comptes Rendus, 60.
[5] Cook, H. A.: J. Chem. Soc. London *1938*, 1761.
[6] Cook, H. A.: J. Chem. Soc. London *1938*, 1774.
[7] Hock, H., Kropf, H.: Ruhrchemie AG, DBP 1 041 960 (1954).
[8] Hiller, H., Polster, R., Beck, F., Guthke, H.: Deutsche Patentanmeldung Nr. P 2046354.1 vom 19.9.1970.
[9] Alt, H., Binder, H., Klempert, G., Köhling, A., Lindner, W., Sandstede, G.: Battelle Frankfurt, Informationsheft 11 (Juli 1971), S. 64.
[10] Haecker, W., Jahnke, H., Schönborn, M., Zimmermann, G.: Battelle Frankfurt, Informationsheft 11 (Juli 1971), S. 62.
[11] Jahnke, H., Schönborn, M., Zimmermann, G.: In: H. Kropf und F. Steinbach, Katalyse an phthalocyaninen, S. 71. Stuttgart: Georg Thieme Verlag 1973.
[12] Beck, F.: Symp. Appl. Electrochem., Wien 1971.
[13] Alt, H., Binder, H., Lindner, W., Sandstede, G.: In: G. Sandstede, From electrocatalysis to fuel cells. Seattle: Univ. of Washington Press 1971.
[14] Sandstede, G.: Chem.-Ing.-Tech. *43*, 495 (1971).
[15] Alt, H., Binder, H., Lindner, W., Sandstede, G.: J. Electroanal. Chem. Interfacial Electrochem. *31*, 19 (1971).
[16] Gerischer, H.: Ber. Bunsenges. Physik. Chem. *67*, 164 (1963).
[17] Held, J., Gerischer, H.: Ber. Bunsenges. Physik. Chem. *67*, 921 (1963).
[18] Behret, H., Binder, H., Köhling, A., Sandstede, G.: ISE-Meeting Stockholm, 1972, Extended Abstracts, p. 421.
[19] Jahnke, H., Schönborn, M., Zimmermann, G.: Bosch Technische Berichte *4*, 98 (1973).
[20] Hiller, H., Beck, F.: DOS 2125590 (1970).
[21] Binder, H., Alt, H., Lindner, W., Sandstede, G.: DOS 2049008 (1970).
[22] Alt, H., Binder, H., Sandstede, G.: J. Catal. *28*, 8 (1973).
[23] Beck, F.: Ber. Bunsenges. Physik. Chem. 77, 353 (1973).
[24] Hiller, H., Dimroth, P., Pfitzner, H.: Liebigs Ann. Chem. *717*, 137 (1968).
[25] Meier, H., Albrecht, W., Tschirwitz, U., Zimmerhackl, E.: Ber. Bunsenges. Physik. Chem. 77, 843 (1973).
[26] Breiter, M. W.: Electrochemical processes in fuel cells. Berlin-Heidelberg-New York: Springer 1969.
[27] Berl, G. N.: Trans. Electrochem. Soc. *83*, 253 (1943).
[28] Müller, L., Nekrassow, L.: Electrochim. Acta *9*, 1015 (1964).
[29] Bianchi, G., Mussini, T.: Electrochim. Acta *10*, 445 (1965).
[30] Winkelmann, D.: Z. Elektrochem. *60*, 731 (1956).
[31] Kastening, B., Kasemifard, G.: Ber. Bunsenges. Physik. Chem. *74*, 551 (1970).
[32] Kozawa, A., Zilionis, V. E., Brodd, R. J.: J. Electrochem. Soc. *118*, 1705 (1971).
[33] Kozawa, A., Zilionis, V. E., Brodd, R. J.: J. Electrochem. Soc. *117*, 1470 (1970).
[34] Breiter, M. W.: Electrochim. Acta *9*, 441 (1964).
[35] Savy, M., Andro, P., Bernard, C., Magner, G.: Electrochim. Acta *18*, 191 (1973).
[36] Meier, H., Zimmerhackl, E., Albrecht, W., Tschirwitz, U.: Ber. Bunsenges. Physik. Chem. *76*, 1104 (1972).
[37] Beck, F.: In: H. Kropf und F. Steinbach, Katalyse an phthalocyaninen, S. 53. Stuttgart: Georg Thieme Verlag 1973.
[38] Beck, F., Dannert, W., Heiß, J., Hiller, H., Polster, R.: Z. Naturforsch. *28a*, 1009 (1973),
[39] Meier, H., Zimmerhackl, E., Albrecht, W., Tschirwitz, U.: In: H. Kropf und F. Steinbach. Katalyse an phthalocyaninen, S. 104. Stuttgart: Georg Thieme Verlag 1973.
[40] Alt, H., Binder, H., Köhling, A., Sandstede, G.: Angew. Chem. *83*, 502 (1971).
[41] Jahnke, H., Schönborn, M.: Ber. Bunsenges. Physik. Chem. *74*, 944 (1970).
[42] Beck, F.: personal information of June, 6 (1974).

43) Savy, M., Andro, P., Bernard, C.: Electrochim. Acta *19*, 403 (1974).

44) Randin, J. P.: Electrochim. Acta *19*, 83 (1974).

45) Manassen, J., Bar-Ilan, A.: J. Catalysis *17*, 86 (1970).

46) Alt, J., Binder, H., Lindner, W., Sandstede, G.: J. Electroanal. Chem. Interfacial Electro-chem. *31*, App. 19 (1971).

47) Contour, J. P., Lenfant, P., Vijh, A. K.: J. Catalysis *29*, 8 (1973).

48) Zerner, M., Gouterman, M.: Theoret. Chim. Acta *4*, 44 (1966).

49) Beyer, W., v. Sturm, F.: Angew. Chem. *84*, 154 (1972).

50) Kozawa, A., Zilionis, V. E., Brodd, R. J.: J. Electrochem. Soc. *117*, 1474 (1970).

51) Schläfer, H. C., Gliemann, G.: Einführung in die Ligandenfeldtheorie. Frankfurt: Aka-demische Verlagsgesellschaft 1967.

52) Henrici-Olivè, G., Olivè, S.: Angew. Chem. *68*, 1 (1974).

53) Hoffmann, B. M., Diemente, D. L., Basolo, F.: J. Am. Chem. Soc. *92*, 61 (1970).

54) Ochiai, E. I.: J. Chem. Soc. Chem. Commun. *1972*, 489.

55) Zerner, M., Gouterman, M., Kobayaski, H.: Theoret. Chim. Acta *6*, 363 (1966).

56) Behret, H.: In: M. W. Breiter, Electrocatalysis, p. 319. Princeton: Electrochem. Soc. 1974.

57) Jahnke, H., Schönborn, M., Zimmermann, G.: In: M. W. Breiter, Electrocatalysis, p. 303. Princeton: Electrochem. Soc. 1974.

58) Meier, H., Albrecht, W., Tschirwitz, U., Zeitler, G., Zimmerhackl, E.: Paper, GDCh-Hauptversammlung Köln, 1975.

59) Wöhrle, D., Müller, R.: Paper, GDCh-Hauptversammlung Köln, 1975.